Synthesis and Characterisation of Initiators and Amphiphilic Miktoarm Star Polymers

BALSTER, RUSSELL

Synthesis and Characterisation of Initiators and Amphiphilic Miktoarm Star Polymers

A thesis submitted for the degree of

Doctor of Philosophy

by

Russell Balster

Department of Chemistry

Durham University

England

Abstract

This project involves the development of several novel heterofunctional initiators with a calix[4]arene centre that can facilitate a "core" first method for the synthesis of miktoarm star polymers.

Chapter 1 introduces main concepts on calixarenes, single electron transfer living radical polymerisation and the ring opening polymerisation of ε-caprolactone.

Chapter 2 describes the synthetic strategy employed for the synthesis of a novel A_2B_2 heterofunctional initiator that incorporated an alkyl halogen moiety and a primary hydroxyl. *p-tert*-butylcalix[4]arene was modified *via* a six step process to introduce the required functionality and was fully characterised at each stage using 1D and 2D NMR spectroscopy, ASAP MS and IR spectroscopy.

Chapter 3 describes how the A_2B_2 heterofunctional initiator was used to synthesise a novel 2-armed PCL polymer centred on a calixarene core. This was further used for copper(0) mediated polymerisation of 2-hydroxyethylacrylate due to the alkyl halide moieties remaining in the calixarene core, leading to the formation of several amphiphilic A_2B_2 miktoarm star polymers. Both polymers were fully characterised using 1D and 2D NMR spectroscopy, SEC, DSC, TGA and IR spectroscopy.

Chapter 4 describes the synthetic strategy employed for the synthesis of a novel A_4B_4 heterofunctional initiator that incorporated an alkyl halogen moiety and a primary hydroxyl. *p-tert*-butylcalix[4]arene was modified *via* a seven step process to introduce the required functionality and was fully characterised at each stage using 1D and 2D NMR spectroscopy, ASAP MS and IR spectroscopy.

Chapter 5 describes how the A_4B_4 heterofunctional initiator was used to synthesise a novel 4-armed star PCL polymer centred on a calixarene core. This was further used for copper(0) mediated polymerisation of 2-hydroxyethylacrylate due to the alkyl halide moieties remaining in the calixarene core, leading to the formation of several amphiphilic A_4B_4 miktoarm star polymers. Both polymers were fully characterised using 1D and 2D NMR spectroscopy, SEC, DSC, TGA and IR spectroscopy.

Chapter 6 described the self-assembly of A_2B_2 and A_4B_4 amphiphilic miktoarm star polymers **calixarene-A_2B_2starPCL$_{100}$PHEA$_m$**, **8-10**, where m = 75, 100 and 270,

respectively and **calixarene-A_4B_4starPCL_{20}PHEA_m**, **18**, **19** and **20** where m = 10, 25 and 48, respectively). The TEM analysis on polymer systems **8 - 10** and **18 - 20**, revealed spherical micelles, with the size of the micelle decreasing as the proportion of hydrophilic PHEA increased. The CMC determinations for polymers **8 – 10** revealed that the length of the hydrophilic chain does not appear to have a significant effect on the CMC. For polymers **18 – 20**, the CMC increases as the length of the hydrophilic polymer chain increases. For both polymeric systems **8 - 10** and **18 - 20**, low CMC values were calculated. This work showed the system has a potential in medical applications, with their ability to form micelles in the range of 5 to 110 nm and have the ability to encapsulate highly hydrophobic material, such as the fluorescent probe pyrene.

In chapter 7 general conclusions and future perspectives for the work are discussed.

Acknowledgements

Firstly I would like to thank my supervisor Dr. Ezat Khosravi for his support and great discussions over the past few years and also providing the opportunity to go to a conference in Thailand and Slovenia, which I enjoyed very much.

I would like to thank Catalytic Technologies LtD for the opportunity to undertake this research, and more specifically Dr. Alan Cooper and Dr. Richard Ward.

I would like to thank all of the Khosravi group and fellow colleagues who have made carrying out my PhD so enjoyable.

Special thanks go to my family for always being there.

Most importantly to me I would like to thank my wife, Lily Zhu, for providing much support and love.

Memorandum

The work reported in this thesis was carried out in the Department of Chemistry, Durham University, between October 2012 and December 2015. This work has not been submitted for any other degree in Durham and is the original work of the author except where acknowledged by means of appropriate reference.

Signed:_____ Date:_____

Statement of Copyright

Financial Support

I gratefully acknowledge Catalytic Technologies LtD for their funding for this research.

Contents

Abstract i

Acknowledgements iii

Memorandum iv

Statement of Copyright iv

Financial Support iv

Abbreviations ix

Chapter 1 1

Introduction 1

1.1. Calixarenes 2

1.2. Synthesis of Calixarenes 3

1.3. Conformations of calixarenes 5

1.4. pKa Values for Calix[4]arenes 7

1.5. Reactions of Calix[4]arenes 8

1.6. Application of Calixarenes 11

1.7. Calixarene-core Initiators for the Synthesis of Star Polymers 12

1.8. Controlled Radical Polymerisation 18

1.8.1. Single Electron Transfer-Living Radical Polymerisation (SET-LRP) 21

1.8.2. SET-LRP vs SARA-ATRP 24

1.8.1.1. Cu(0) or Cu(I) as the major activator 25

1.8.1.2. Disproportionation or comproportionation 27

1.8.1.3. OSET or ISET 29

1.9. Ring Opening Polymerisation of ε-caprolactone 31

1.9.1. Polycondensation 32

1.9.2. Ring Opening Polymerisation 32

1.9.2.1. Anionic ROP 33

1.9.2.2. Cationic ROP 33

1.9.2.3. Monomer Activated ROP 34

1.9.2.4. Coordination-insertion ROP 34

1.10. Aims 36

1.11. References. 37

Chapter 2 41

A2B2 Heterofunctional Initiator With Calix[4]arene Core 41

2.0. Introduction 42
2.1. Experimental 44
2.1.1. Materials 44
2.1.2. Instrumentation 44
2.1.3. Synthesis of calix[4]arene, **1** 46
2.1.4. Synthesis of 25,27-bis(prop-2-en-1-yloxy)calix[4]arene, **2** 47
2.1.5. Synthesis of 25,27-bis(prop-2-en-1-yloxy)-26,28-bis(ethyleneacetate)-calix[4]arene,**3** 50
2.1.6. Synthesis of 25,27-bis(prop-2-en-1-yloxy)-26,28-bis(ethanolxy)-calix[4]arene, **4** 49
2.1.7. Synthesis of 25,27-bis(prop-2-en-1-yloxy)-26,28-bis(ethoxyester-2-bromo-acetate)-calix[4]arene, **5** 50
2.1.8. Synthesis of 25,27-bis(3-(hydroxyethyl)thioether-propan-1-yloxy)-26,28-bis(ethoxyester-2-bromo-acetate)-calix[4]arene, **6** 52
2.0. Results and Discussion 53
2.2.1. Calix[4]arene, **1** 53
2.2.2. 25,27-bis(prop-2-en-1-yloxy)calix[4]arene, **2** 59
2.2.3. 25,27-bis(prop-2-en-1-yloxy)-26,28-bis(ethyleneacetate)-calix[4]arene, **3** 66
2.2.4. 25,27-bis(prop-2-en-1-yloxy)-26,28-bis(ethanoloxy)-calix[4]arene, **4** 76
2.2.5 25,27-bis(prop-2-en-1-yloxy)-26,28-bis(ethoxyester-2-bromo-acetate)-calix[4]arene, **5** 83
2.2.6. 25,27-bis(3-(hydroxyethyl)thioether-propan-1-yloxy)-26,28-bis(ethoxyester-2-bromo-acetate)-calix[4]arene, **6** 91
2.3. Conclusion 98
2.4. References 99

Chapter 3 100
Amphiphilic A2B2 Miktoarm Star Polymer with Calix[4]arene Core 100
3.0. Introduction 101
3.1 Experimental 103
3.1.1. Materials 103
3.1.2. Instrumentation 103
3.1.3. Synthesis of Calixarene-PCL100 macro-initiator, **7** 104
3.1.4. Synthesis of Calixarene-starPCL100PHEAm Miktoarm Star Polymer, **8-10** - Typical Polymerisation Procedure 106
3.2. Results and discussion 108
3.2.1. Calixarene-PCL_{100}, **7** 108
3.2.2. Amphiphilic Miktoarm Star polymer, **8-10** 117

3.3. Conclusion 127
3.4. References 129

Chapter 4 130
A4B4 Heterofunctional Initiator with Calix[4]arene Core 130
4.0. Introduction 131
4.1 Experimental 134
4.1.1. Materials 134
4.1.2. Instrumentation 134
4.1.3. Synthesis of 25,26,27,28-tetrakis(prop-2-en-1-yloxy)calix[4]arene, **11** 135
4.1.4. Synthesis of 5,11,17,23-tetrakis(prop-2-en-1-yloxy)-calix[4]arene, **12** 136
4.1.5. Synthesis of 5,11,17,23-tetrakis(prop-2-en-1-yloxy)-25,26,27,28-tetrakis(methyl acetateoxy)- calix[4]arene, **13** 137
4.1.6. Synthesis of 5,11,17,23-tetrakis(prop-2-en-1-yl)25,26,27,28-tetrakis(ethanoloxy)-calix[4]arene, **14** 139
4.1.7. Synthesis of 5,11,17,23-tetrakis(prop-2-en-1-yl)-25,26,27,28-tetrakis(ethoxyester-2-bromo-acetate)-calix[4]arene, **15** 140
4.1.8. Synthesis of 5,11,17,23-tetrakis(3-(hydroxyethyl)thioether-propanyl)-25,26,27,28-tetrakis(ethoxyester-2-bromo-propanoate)-calix[4]arene, **16** 141
4.2. Results and Discussion 143
4.2.1. 25,26,27,28-tetrakis(allyloxy)-calix[4]arene, **11** 143
4.2.2. 5,11,17,23-tetrakis(prop-2-en-1-yl)-calix[4]arene, **12** 149
4.2.3. 5,11,17,23- tetrakis(prop-2-en-1-yl)-25,26,27,28-tetrakis(methyl acetateoxy)-calix[4]arene, **13** 155
4.2.4. 5,11,17,23- tetrakis(prop-2-en-1-yl)-25,26,27,28-tetrakis(ethanoloxy)-calix[4]arene, **14** 161
4.2.5. 5,11,17,23- tetrakis(prop-2-en-1-yl)-25,26,27,28-tetrakis(ethoxyester-2-bromo-propanoate)-calix[4]arene, **15** 169
4.2.6 5,11,17,23-tetrakis(3-(hydroxyethyl)thioether-propanyl)-25,26,27,28-tetrakis(ethoxyester-2-bromo-propanoate)-calix[4]arene, **16** 178
4.3. Conclusion 186
4.4. References 187

Chapter 5 188
5.0. Introduction 189
5.1. Experimental 190
5.1.1. Materials 190
5.1.2. Instrumentation 190

5.1.3. Synthesis of Calixarene-starPCL$_{20}$, **17** 191
5.1.4. Synthesis of Calixarene-starPCL$_{20}$PHEA$_m$ using SET-LRP, **18-20** 193
5.2. Results and discussion 195
5.2.1. Ring opening polymerisation of ε-caprolactone using A_4B_4 heterofunctional initiator, **16** 195
5.2.2. Amphiphilic A4B4 Miktoarm Satr Polymers, **18-20**……205
5.3. Conclusion 219
5.4. References 220

Chapter 6 221
Self-assembly of Amphiphilic A_2B_2 and A_4B_4 Miktoarm Star Polymers 221
6.0. Introduction 222
6.1. Experimental 223
6.1.1. Materials 223
6.1.2. Instrumentation 224
6.1.3. TEM 224
6.1.4. CMC spectroscopic measurements 224
6.2. Results and Discussion 225
6.2.1. Calixarene-A2B2starPCL100PHEAm, **8-10** 225
6.2.1.1. TEM Studies 225
6.2.1.2. CMC determination 227
6.2.3. Calixarene-A4B4starPCL20PHEAm, **18-20** 231
6.2.3.1. TEM Studies 231
6.2.3.2. CMC determination 233
6.3. Conclusion 235
6.4. References 236

Chapter 7 237
Summary, Conclusions and Future Work 237
7.0. Summary and Conclusions 238
7.1. Future work 242
7.2. References 243

Abbreviations

APCL	Atmospheric Chemical Ionisation
ASAP	Atmospheric Solids Analysis Probe
ATRP	Atom Transfer Radical Polymerisation
CMC	Cryticla Micelle Concetration
COSY	Corelation Spectroscopy
CRP	Controlled Radical Polymerisation
Đ	Dispersity
DMF	Dimethylformamide
DMSO	Dimethyl Sulfoxide
DP	Degree of Polymerisation
DPMK	Diphenylmethyl Potassium
DSC	Differential Scanning Calorimetry
DTC	Dimethyltrimethylene Carbonate
EBIB	Ethyl-2-bromo-2-methylpropionoate
FT-IR	Fourier Transform Infrared Spectroscopy
HEA	2-hydroxylethyl Acrylate
HMBC	Heteronuclear Multiple-bond Correlation
HMW	High Molecular Weight
HSQC	Heteronuclear Single Quantum Coherence
IB	Isobutylene
IR	Infrared
ISET	Inner Spere Electron Transfer
MA	Methyl Acrylate
MeCN	Acetonitrile
Me_6TREN	Tris[2-(dimethylamino)ethyl]amine
MMA	Methyl Methacrylate
MS	Mass Spectroscopy
NMP	Nitroxide-mediated Polymerisation
NMR	Nuclear Magnetic Resonance
NOESY	Nuclear Overhauser Spectroscopy
OEOBP	Oligo(ethylene oxide)-2-bromopropanoate

OSET	Outer-spehere Electron Transfer
PCL	Poly(ε-caprolactone)
PEG	Poly ethylene glycol
PHEA	Poly(2-hydroxylethyl-acrylate)
PO	Propylene Oxide
PNPMI	Poly(N-phenylmaleimides)
PRE	Persistent Radical Effect
PVCl	Poly Vinyl Chloride
RAFT	Reversible Addition–fragmentation Radical Polymerisation
ROP	Ring Opening Polymerisation
SARA-ATRP	Supplemental Activator and Reducing Agent ATRP
SEC	Size Exclusion Chromatography
SET-DTLRP	Single Electron Transfer and Degenerative Transfer Living Radical Polymerisation
SET-LRP	Single Electron Transfer Living Radical Polymerisation
TEA	Triethyl amine
TEM	Transmission Electron Microscope
TGA	Thermogravimetric Analysis
THF	Tetrahydrofuran
TREN	Tris[2-aminoethyl]amine
VCl	Vinyl Chloride

Chapter 1

Introduction

1.1. Calixarenes

Calixarenes are phenolic containing macrocycles that typically have high melting points and low solubility in common organic solvents. Calixarenes are derived from the condensation of aldehydes and phenols under various conditions. In Greek the word *calix* means vase; calixarene was derived from this word due to its resemblance to the Greek calix crater. Arene refers to the presence of aromatic groups.[1]

In 1872, Adolf von Baeyer reacted phenol and formaldehyde in the presence of an acid catalyst that resulted in a resinous material, which was the beginning of phenol-formaldehyde chemistry.[2] He was unable to elucidate the structures within the crude product due to its cement like properties and therefore abandoned this research to pursue work on synthetic dyes for which he won the 1905 Noble prize.

In 1944, Zinke *et al*. took the challenge of deciphering the structure of the Baeyers's resinous material. Due to phenols ability to react through the *ortho* or *para* position, the *para* position was blocked off to reduce the complexity of the reacting system. This allowed for less crosslinking and a compound that was easier to work with. Through this, the cyclic tetramer structure of calix[4]arene was proposed.[3] It was determined that there was no ether linkages present and found a molecular weight corresponding to a cyclic tetramer and concluded that *para* functionalised phenol condensation reactions only lead to a cyclic tetrameric structure.[4] However, they had ignored a high molecular weight compound as it was thought to be a complication resulting from a coupling of tetramers. In 1955, Conforth *et al*. repeated the synthesis and found that there were two compounds present with different melting points. It was concluded that the two compounds present were diastereoisomers that arose from hindered rotation resulting in different conformers.[5] In 1978, Gutche *et al*. were studying compounds that could potentially mimic enzymes. The work reported by Zinke *et al*. was studied and it was proved through more advanced analytical techniques that the material produced was actually a mixture of cyclic tetramer and octamers and they further coined the term calixarene.[6,7]

1.2. Synthesis of Calixarenes

There have been two fundamentally different syntheses for the production of calixarenes, with one being a lengthy multistep procedure, developed by Hayes and Hunter and the second being a one pot base catalysed condensation of *tert*-butyl phenol with formaldehyde.[8,3,5,9] The Hayes and Hunter synthesis consisted of 10-steps. The first step was protection of one of the *ortho* positions of *para*-cresol. The newly protected *para*-cresol was reacted with formaldehyde in the presence of sodium hydroxide leading to a hydroxymethylation product. The hydroxymethylated product was then further reacted with *para*-cresol in the presence of acid leading to the formation of a methylene bridge. These steps were further repeated to obtain a linear tetra aromatic product. The bromine was removed *via* catalytic hydrogenation. The product was treated under high dilution conditions to affect cyclization. The multiple steps represent a tedious synthesis for the formation of *p*-methylcalix[4]arene (Scheme 1.1).[8]

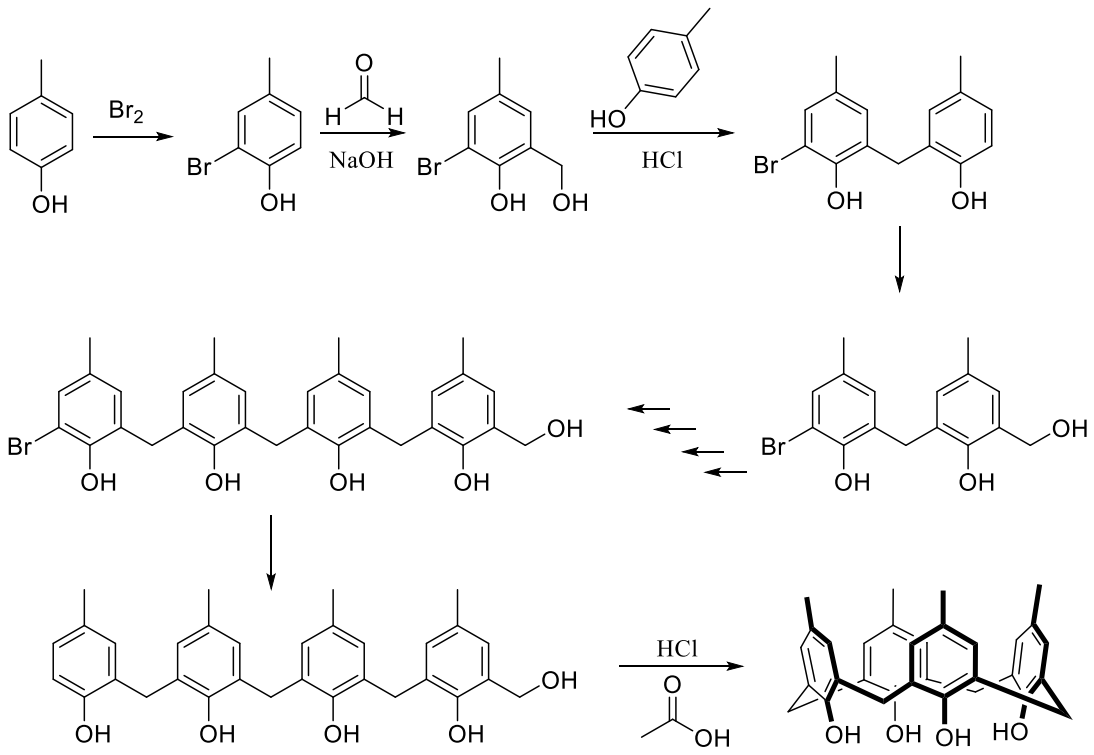

Scheme 1.1. Hayes and Hunter non-convergent stepwise synthesis

The capricious event of preparing calixarenes using phenol-formaldehyde chemistry remained for many years, with puzzling variability in yields, even when carried out under identical conditions. A breakthrough in calixarene chemistry was brought

about when Gutsche *et al.* carried out a careful investigation into a one pot synthesis first developed by Zinke and Cornforth.[3,5,9] The one pot synthesis consisted of the careful addition of sodium hydroxide, with the amount being dependent upon the size of calixarene desired, to a mixture of formaldehyde and *p-tert*-butylphenol and led to a robust procedure that consistently gave yields of ~50%.[9] The amount of sodium hydroxide relative to the phenol analogue had a profound effect on the cyclooligomerisation process, with the addition of 0.045 equiv. leading to the production of only the calix[4]arene, whilst the addition of 0.300 equiv. led to the sole production of calix[6]arene. The pathway of the base induced reaction has been subject to many years of investigation. The first step is the deprotonation of the phenol analogue leading to the formation of the phenoxide ion, which nucleophilically attacks the highly reactive formaldehyde carbonyl. The reaction can be terminated and characterised at this stage with the formation of hydroxymethyl phenols.[10] If the reaction is allowed to continue, the deprotonation followed by nucleophilic attack continues until a linear oligomer is obtained (Scheme 1.2.).

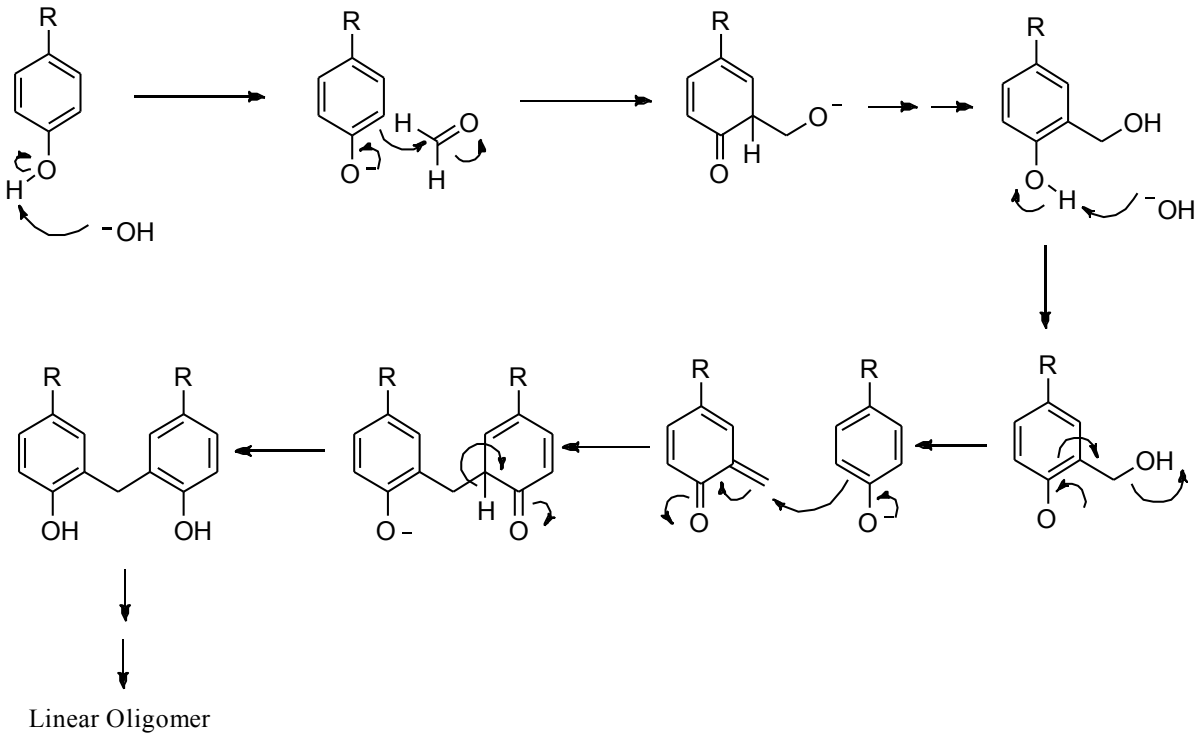

Scheme 1.2. Mechanistic pathway to linear oligomer.

To this day the manner in which the linear oligomers are converted into the cyclic analogue remains a mystery.

1.3. Conformations of calixarenes

Cornforth was first to recognise that calix[4]arenes were capable of assuming various conformations, where the aromatic groups are projecting downward or upward relative to a defined plane around the methylene bridges.[5] Gutsche later named the four distinct conformations as “cone”, “partial cone”, “1,3-alternate” and “1,2-alternare” (Fig. 1.1).[11]

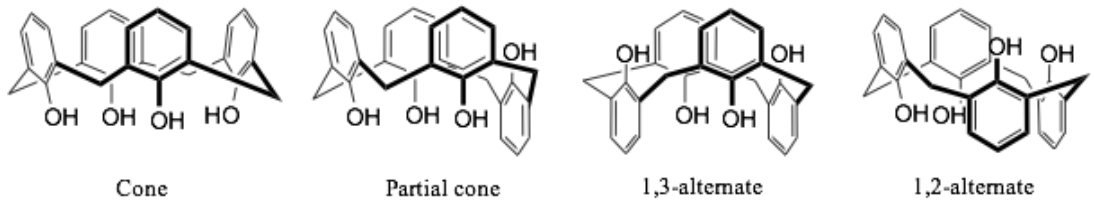

Figure 1.1. Four distinct conformations of a calix[4]arene molecule

For the series of calix[n]arenes, as n becomes larger the number of conformations in turn increases. Calix[6]arene exhibits eight conformations, whilst calix[8]arene exhibits 16 different conformations and so on. Additionally, as the macrocycles increase in size there can be a departure from the distinct “up” or “down” conformation, with the aryl groups laying in a planar fashion relative to the surrounding aryls.

In the solid state, calix[4]arenes containing four *endo*-hydroxyl units exist in the cone conformation. In 1979, Andreetti *et al*. reported the first X-Ray structure to show the cone conformation and since then many other examples have been reported.[12,13,14,15] When one or more of the *endo*-hydroxyl units is converted to a alkoxy moiety the conformation of calix[4]arene commonly remains in the cone conformation, as observed by the crystal structures of the mono-methyl, distal di-methyl , tri-ethyl and tetra-methyl ether analogues of *p-tert*-butylcalix[4]arene.[16,17] There are fewer reports of X-Ray structures of calix[4]arenes in the partial cone conformation. The majority of molecules that exhibit the conformation are tetra-alkyl ethers such as tetraethyl and tetrapyridymethyl ethers of *p-tert*-butylcalix[4]arene anologues.[18,19] The 1,3-alternate conformation is the second most encountered conformation. Among the first reported was an aluminium complex of *p-tert*-butylcalix[4]arene and 5-allyl-25-methoxy-26,27,28-

tribenzylcalix[4]arene.[20,21] The first reported example of 1,2-alternate conformation was a complex of $AlMe_3$ with a tetra-methyl ether analogue of *p-tert*-butylcalix[4]arene, but it is noted that the 1,2-alternative conformation is the least encountered.[20]

In solution at ambient temperature all n hydroxy-calix[n]arenes (Fig. 1.1) are conformationally mobile, with the degree of mobility dependent upon the individual calixarene macrocycle. Calix[4]arenes exhibit all four conformations as shown above (Fig. 1.1) *via* the aryl groups rotating around the axis of the carbon atom bound to the methylene carbon. The barrier to this rotation is highly dependent upon the macrocyclic system. NMR spectroscopy is the most valued tool in determining the conformations of calixarene compounds. It was shown by Gutsche *et al*. that for *p-tert*-butylcalix[4]arene the cone is the most stable conformation, but as the temperature of the system is raised, inter-conversion occurs on the NMR timescale. This is observed in the ^1H NMR spectrum *via* a change in splitting pattern of the methylene protons. At lower temperatures a set of doublets is observed due to the non-equivalence of the protons, with one pointing down to the oxy environment and one pointing up to the aromatic region, as the temperature is raised the doublets coalesce to form a singlet.[22] Jaime *et al.* reported a single rule that could be used to determine the conformation of calix[4]arenes utilising ^{13}C NMR spectroscopy. The chemical shift of the carbon of the bridging methylene group explicitly gave information as to the conformation. An inspection of 24 different calix[4]arene compounds revealed that when the phenolic rings next to each methylene carbon is in the *syn* position (cone) the signal would appear at 31 ppm, whereas when an *anti*-position was present (1,3-alternative) a signal was observed at 37 ppm (Fig. 1.2). The discrepancy in chemical shift is thought to be brought about by steric interactions.[23]

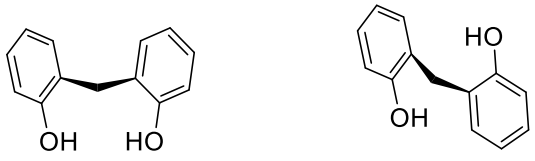

(a) *Syn* (b) *Anti*

Figure 1. 2. *Syn*- (a) and *anti*- (b) conformation of aromatics with respect to each other

The preference for *p-tert*-butylcalix[4]arene to exist in the cone formation is a consequence of the strong hydrogen bonding between the hydroxyl moiety. This strong hydrogen bonding is observed in the ^{1}H NMR spectroscopy by a sharp singlet at ~10.5 ppm and additionally in the infrared spectrum *via* an unusually low stretching frequency at ~3150 cm^{-1}.[22]

1.4. pKa Values for Calix[4]arenes

The acidity of Calix[4]arenes are considerably higher than that of their monomeric analogues, which has been calculated to be 10.9. The most conclusive analysis was reported by Shinkai *et. al*., who used a tetra *ipso* nitrated calix[4]arene (Scheme 1.5) for the investigation due to the nitro moiety allowing the macrocycle to be water soluble.[24] A potentiometric titration was carried out on the functionalised calix[4]arene. It was measured that calix[4]arenes have a super acidic proton, with pKa_1, pKa_2, pKa_3 and pKa_4 to be <1, ~10, ~12 and >14, respectively. The high acidity of pKa_1 is a consequence of strong hydrogen bonding between the phenolic moieties of the macrocycle as observed in the IR spectra and ^{1}H NMR spectra, an illustration of the hydrogen bonding is shown in Figure 1.3.

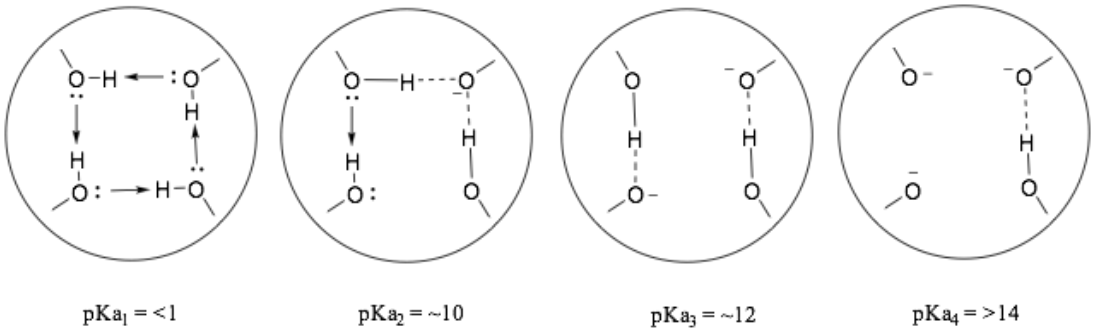

Figure 1.3. Schematic of the intramolecular hydrogen bonding within a calix[4]arene in a cone conformation.

pKa determination of mono- di, and tri-methylated calix[4]arenes was later carried out by Apaki *et. al*. whom calculated the values to be ~4, 12 and 12 respectively.[25] These results revealed that the mono-alkylation has a small effect on the pKa_1, thus indicates a minimal disruption to the hydrogen bonding of the system relative to the tetra hydroxyl parent compound (Fig. 1.4).

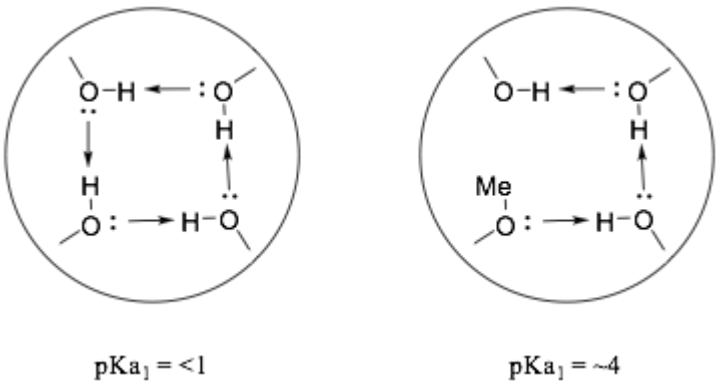

Figure 1.4. Hydrogen bonding in a mono-alkylated calix[4]arene.

The di- and tri-methylated compounds exhibit pKa's comparable to their monomeric counterpart indicating weak hydrogen bonding within the macrocycle. The findings were further quantified by IR and ^{1}H NMR spectroscopy, where the acidic proton of monoalkylated calix[4]arene (Fig. 1.4) exhibits a vibration at 3150 cm^{-1} and an NMR signal at 9.54 ppm, whereas the di- and tri-alkylated calix[4]arenes exhibited IR vibration at 3450 and 3470 cm^{-1} and NMR OH signals at 7.19 ppm and 6.20 ppm respectively.[25]

1.5. Reactions of Calix[4]arenes

There are various routes to the functionalisation of calix[4]arenes. Modifications can be made to the lower and upper rims, and as discussed previously, the distinct pKa's can allow for selective functionalisation (Fig. 1.5).

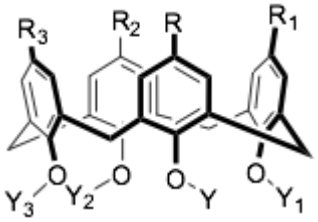

Figure 1.5. Potential functional areas of calix[4]arenes.

The earliest prepared derivatives of calix[4]arenes were esters. Most notably a study by Shu *et al*. into the esterification of calix[4]arene with benzoyl chloride showed that the Lewis acid used controlled the selective nature of the reaction and the residing conformation.[26] When calix[4]arene was in the presence of excess benzoyl

chloride in THF, using NaH as the base, a 1,3-alternate diametric diester was produced, whereas, when the solvent is changed to toluene a partial cone diametric diester was produced. When the reaction was run in pyridine a tribenzoate calixarene was produced, and when the reaction was run in chloroform in the presence of aluminium chloride a tetrabenzoate was formed in two different conformations: 1,3-alternate and partial cone.[26]

Alkylation reactions of the lower rim have been the most widely studied class of functionalisation of calixarenes. Strategies for the preparation of mono-, di- (various regiochemistries, 1-2 or 1-3), tri- or tetra-ethers have been developed. The synthesis of monoethers has been reported to be quite a challenge. Inhibiting polyalkylation is a major challenge due to the similar pKa's of the parent calixarene and the monoalkylated analogue.[27] Calix[4]arenes can be alkylated selectively in a distal or proximal fashion depending on the alkylating conditions used (Scheme 1.3).

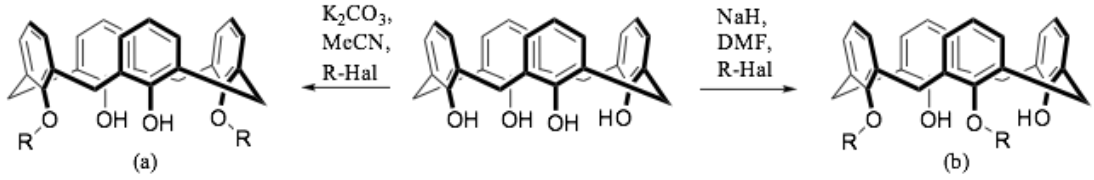

Scheme 1.3. Distal (a) and proximal (b) alkylation of calix[4]arene.

To induce a distil dialkylation a weak base, such as one equiv. of K_2CO_3, can be used in the presence of excess alkyl halide. Such reactions can often be achieved in very good yields.[28,29] Proximal di-alkylation can be achieved by treating calix[4]arene with a stoichiometric amount of strong base (e.g. NaH) and alkylating agent.[30] Two hypotheses have been used to rationalise the proximal selectivity. The first is a statistical argument, where there is a 2:1 chance of the proximal anions opposed to the distal anion. Secondly, the proximal anions are less stabilised due to the reduced hydrogen bonding, therefore have a more nucleophilic characteristic.[31]

Various strategies to functionalise the upper rim of calixarenes have been developed. Often it is paramount to remove any functionality in the *para* position i.e. *tert*-butyl moiety of *p-tert*-butylcalix[4]arene. A de-*tert*-butylation can be readily achieved *via*

treating calix[4]arene with aluminium chloride in toluene.[32] The reaction results from the aluminium complex coordinating to the hydroxyl moieties with the simultaneous formation of HCl. The Lewis acidic aluminium chloride will draw electron density away from the *tert*-butyl moiety facilitating the loss of the tertiary carbocation, which will react with the HCl, forming an alkyl chloride and the anionic aromatic ring will pick up the proton. The newly formed alkyl chloride reacts with a toluene solvent molecule *via* a reverse Friedel-Craft reaction. The proposed mechanism is shown, scheme 1.4.[33]

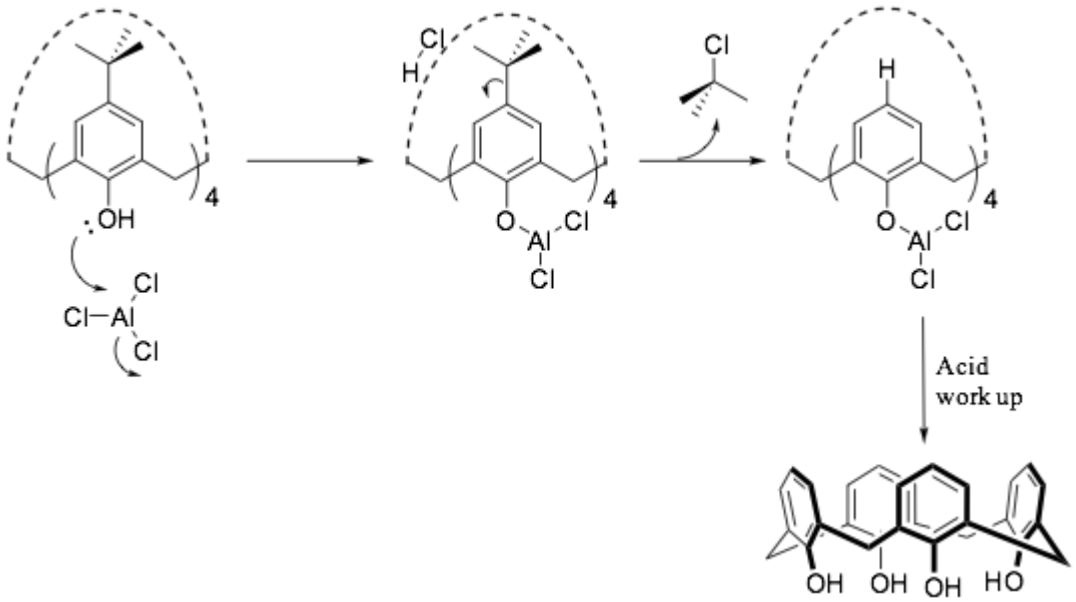

Scheme 1.4. Proposed mechanism for the de-*tert*-butylation of *p-tert*-butylcalix[4]arene.

With the *para* positon free several *para* functionalisation's can be explored, such as electrophilic substitution, *para*-Claisen rearrangement and the *para*-quinonethide route (Scheme 1.5).[1]

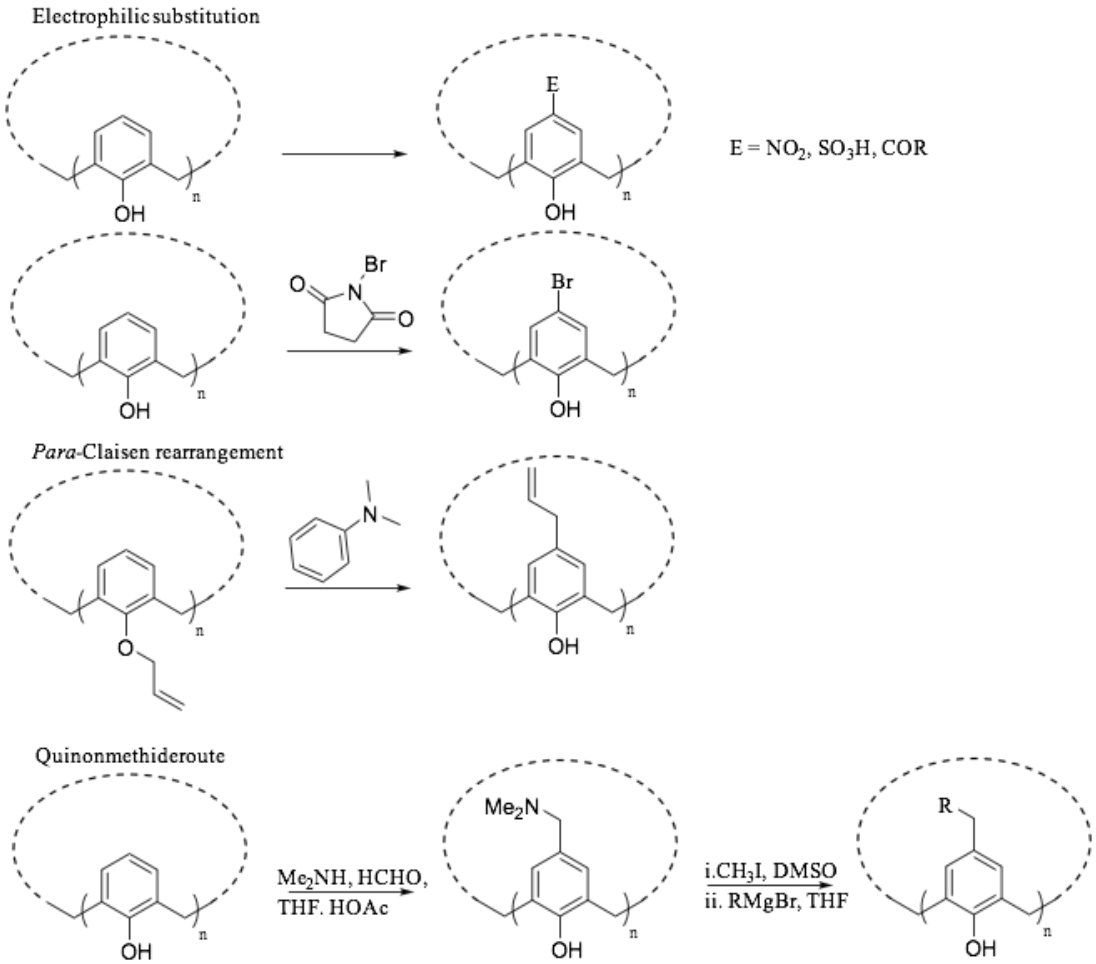

Scheme 1.5. Various routes to the para functionalisation of calixarenes.

An important form of electrophilic substitution is that of the bromination of the calixarene upper rim. First the lower rim must be alkylated, then the tetra-ethyl calixarene can be treated with N-bromosuccinimide leading to a *para* tetra brominated calixarene (Scheme. 1.5).[34,35]

1.6. Application of Calixarenes

Due to calixarenes unique three dimensional surface, availability and ease of functionalisation at both the upper and lower rim, they have become important building blocks as receptors, sensing and self-assembly, nanotechnology, ligands and drug discovery.[36] In polymer chemistry the three main applications are as ligands of metal complexes, which are used as catalysts for polymerisations, secondly as functionalised monomers, and thirdly as multifunctional cores for the synthesis of

star polymers.[37,38,39] For the relevance to this thesis the ability of calixarenes to act as cores for the synthesis of star polymers will be focused on.

1.7. Calixarene-core Initiators for the Synthesis of Star Polymers

In 1996, Jacob *et al*. reported the first well defined star polymer based on a calix[8]arene core with polyisobutylene (PIB) arms.[40] The living polymerisation of isobutylene (IB) was achieved *via* the octafunctional calix[8]arene in conjunction with $BCl_3/TiCl_4$. Molecular weights up to 3.1 x 10^4 g mol^{-1} and dispersities of 1.12 were observed. This study showed the potential of using calixarenes as cores for star polymers.[40]

In 1998, Sawamoto *et al*. reported on the construction of tetra-, hexa-, and octa-functional initiators with calix[n]arene cores (n = 4, 6 and 8), containing dichloroacetate.[41] The initiators facilitated the controlled atom transfer radical polymerisation (ATRP) of methyl methacrylate (MMA) in combination with a ruthenium or aluminium complex (Scheme 1.6).

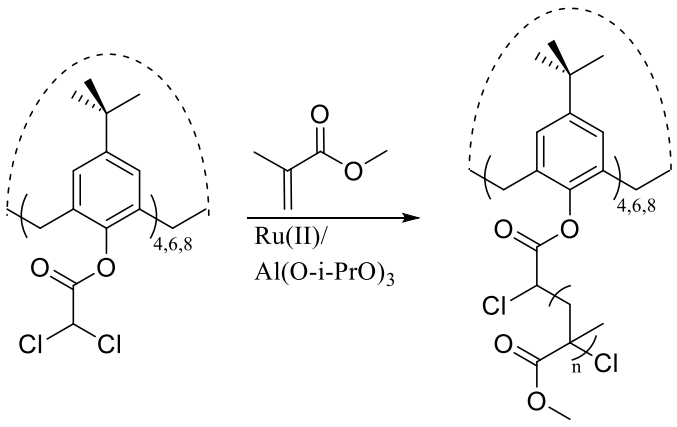

Scheme 1.6. Synthesis of star MMA centred around a calix[n]arene (n = 4, 6 or 8) core

It was reported that the attachment of the dichloroacetate moiety to the calix[6 and 8]arene was smooth, and was achieved under the relatively mild conditions of pyridine/DMF at ambient temperature in the presence of dichloroacetyl chloride. For calix[4]arene, the direct attachment of the acid chloride was not possible and the more aggressive conditions of *tert*-BuLi in toluene were required. The difficulty in

the attachment of the group was attributed to the strong hydrogen bonding between phenolic hydroxyl moieties. For the calix[4]arene the ^{1}H NMR data presented does not itself prove that the acetyl chloride was attached or if it was attached then to how many hydroxyls. Polymers with molecular weights of up to 1.0 x 10^{4} g mol^{-1} and with dispersities of ~1.2 were achieved.[41]

In 2000, Angot *et el*. reported on the synthesis of tetra-, hexa-, and octo-functional initiators with calix[n]arene cores (n = 4, 6 and 8), with 2-bromopropionyl units attached, to facilitate ATRP.[42] It was reported that the 2-bromopropionyl bromide moieties were directly attached to the hydroxyls of the calix[6 and 8]arene in THF with the addition of trimethylamine. It was also reported that *p-tert*-butylcalix[4]arene was insoluble in THF, therefore 2-bromopropionyl bromide could not directly be attached. The proposed attachment of 2-bromopropionyl bromide to the calix[4]arene was carried out in acetone in the presence of potassium carbonate. From the NMR data, it was reported that four 2-bromopropionyl moieties were attached, but it is likely that this is an incorrect characterisation. Two broad singlet resonances were observed in the region of 0.9 ppm to 1.5 ppm, corresponding to the *tert*-butyl moieties and two further multiplets were observed between 6.7 ppm and 7.2 ppm, corresponding to the aromatic protons. This would suggest that two 2-bromopropionyl moieties were attached in a diametric fashion, as it appears two sets of aromatic and *tert*-butyl species are present, i.e. phenolic and aryl ester. The initiators were used to carry out ATRP of styrene and MMA in bulk using CuBr/Cl 2,2'bipyridyl catalyst. It was noted that for larger molecular weight polymers, star-star coupling was observed due to bi-molecular termination.[42]

In 2003, Taton *et al*. reported on the polymerisation of ethylene oxide emanating from a calix[8]arene core.[43] A core-first strategy was employed. The secondary phenolic hydroxyls were converted to primary hydroxyls *via* treating the calix[8]arene with chloroethyl vinyl ether in the presence of Cs_2CO_3. The vinyl groups were removed *via* the presence of acid in an ether/dichloromethane mixture, leading to the desired primary hydroxyl. The polymerisation of ethylene oxide was carried out in THF at 40 ^{o}C in the presence of the initiator diphenylmethyl potassium

(DPMK) (Scheme 1.7). Molecular weights of up 1.7 x 10^5 g mol^{-1} were achieved with dispersities of ~1.2.[43]

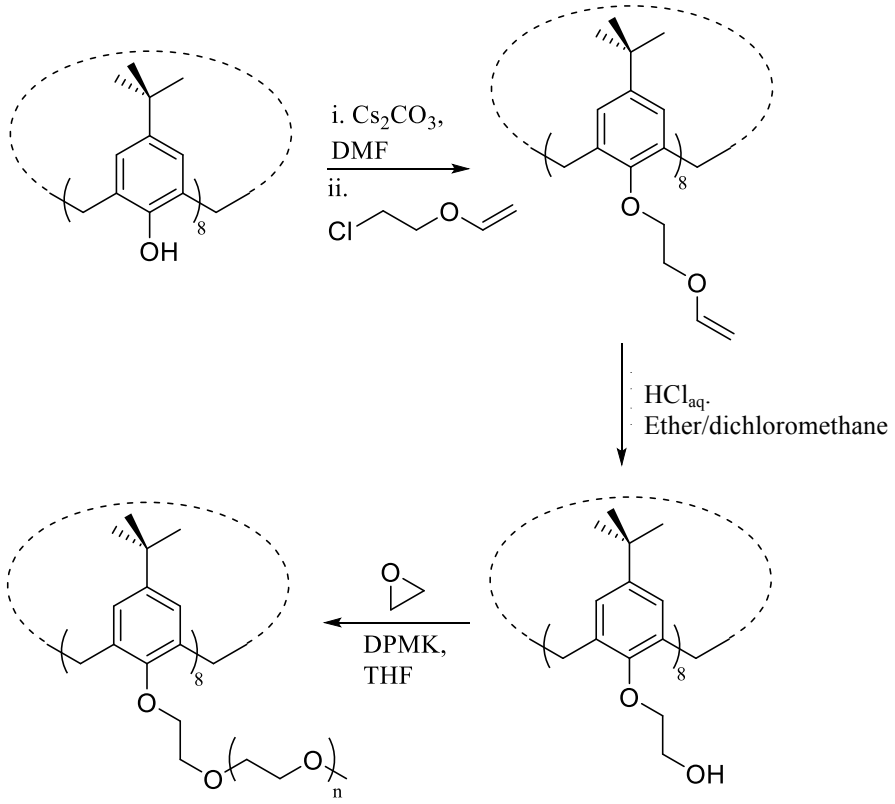

Scheme 1.7. Synthesis of eight arm star poly(ethylene oxide) centred around a calix[8]arene core.

In 2006, Zhu *et al*. reported the synthesis of a amphiphilic star shaped polymer centred around a calix[6]arene core. The amphiphilic nature came from the co-polymer grown from the secondary phenolic hydroxyls (Scheme 1.8). [44]

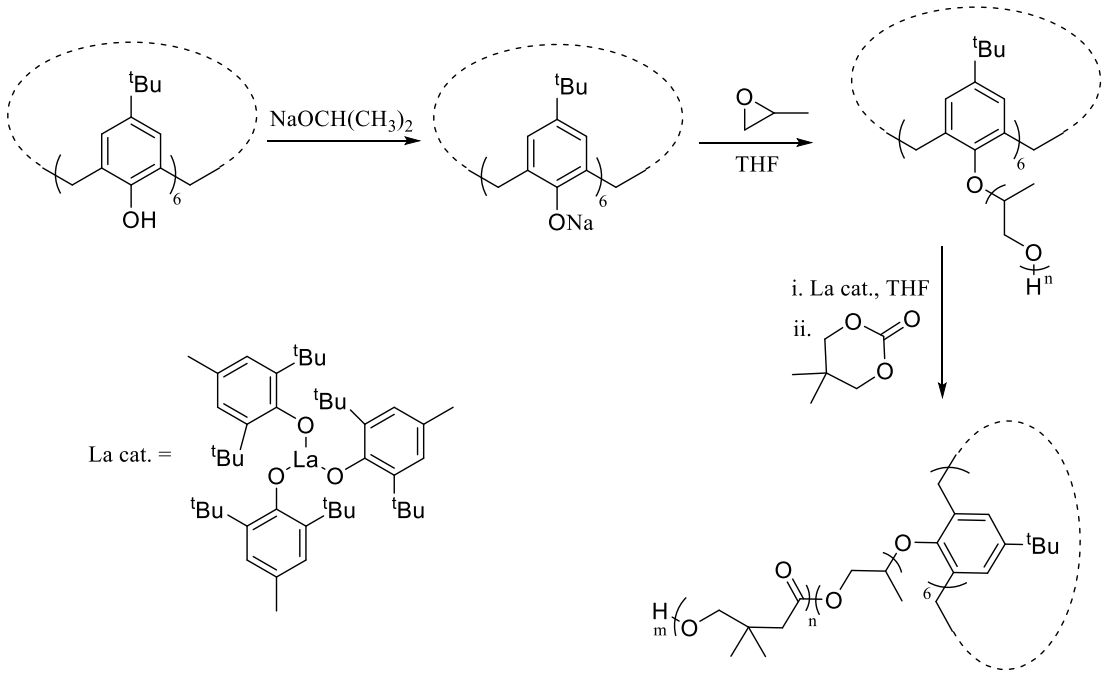

Scheme 1.8. Synthesis of six arm amphiphilic PPO-PDTC co-polymer centred around a calix[6]arene core.

The calixarene was treated with sodium isopropoxide and used as an initiator to ring open polymerise propylene oxide (PO). The hydroxyl chain end of PPO was then used to ROP dimethyltrimethylene carbonate (DTC) using a lanthanum catalyst, leading to a system with an amphiphilic nature. For the PPO, a molecular weight of 1.7 x 10^4 g mol^{-1} was achieved with a dispersity of 1.12. The addition of PDTC lead to a molecular weight of 5.2 x 10^4 g mol^{-1} and a dispersity of 1.63.[44]

In 2007, Lou *et al*. synthesised a star-shaped optically active poly(N-phenylmaleimides) (PNPMI) centred around a *p-tert*-butylcalix[5]arene core.[45] The material was designed to exhibit separation of small molecules based on chirality. The phenolic hydroxyls of the calixarene were first deprotonated using sodium hydride in THF. A solution of optically active N-phenylmeleimide derivatised compounds in toluene was introduced, leading to the polymerisation of the N-phenylmeleimide derivatives (Scheme. 1.9). Little control was maintained over the polymerisation, with dispersities up to 2.28 and molecular weights of 1.0 x 10^5 g mol^{-1}. Optical activity of up to +27.6 ($[\alpha]_D^{25}$) was measured. High temperature (100 ^oC) was required to facilitate more efficient polymerisations, but this lead to a decrease in stereo regularity, and hence the relatively low optical activity.[45]

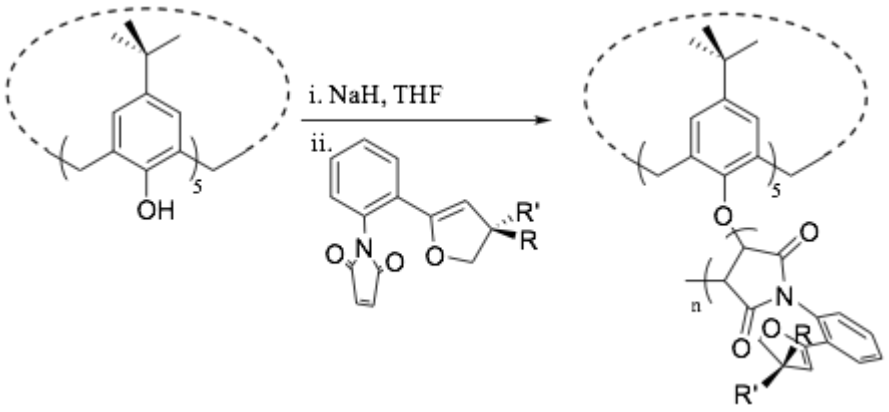

Scheme 1.9. Synthesis of star-shaped optically active poly(N-phenylmaleimides) (PNPMI) centred around a *p-tert*-butylcalix[5]arene core.

In 2008, Gou *et al*. reported the ring opening polymerisation (ROP) of ε-caprolactone using a functionalised *p-tert*-butylcalix[4 and 6]arene core as the initiator in the presence of a yttrium catalyst.[46] The lower rims of the calixarenes were converted to primary alcohols, *via* the addition of an alkyl ester moiety through a Williamson ether synthesis, the ester group was then reduced to give the desired primary alcohol. The introduction of an ethyl ether alcohol moiety substantially increased the solubility of the calixarene, and thus lead to a more efficient initiation of the ε-caprolactone (Scheme 1.10).[46]

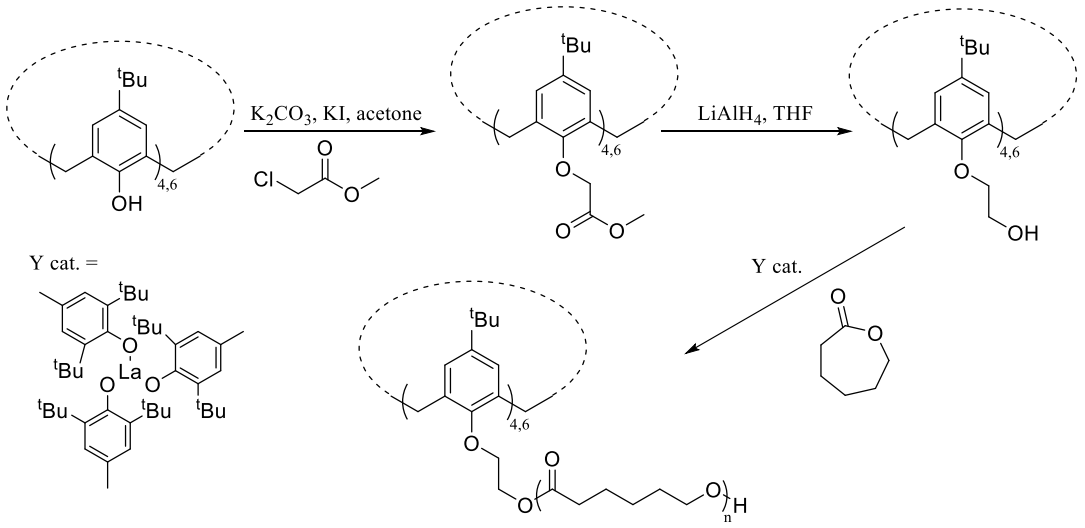

Scheme 1.10. Synthesis of star-shaped PCL emanating from a calix[4 and 6]arene core.

Molecular weights determined through ^{1}H NMR closely matched the theoretical values. Molecular weights of up to 3.0 x 10^{4} g mol^{-1} were calculated with dispersities in the range of 1.26 – 1.63 (SEC). The chromatograms of the SEC exhibited non-

uniformed distributions, as would be expected with the dispersity values. The distribution was attributed to unequal length of poly(ε-caprolactone) (PCL) arms emanating from the core.[46]

In 2010, Gou *et al*. reported the first miktoarm star polymer centred around a calix[4]arene core.[39] As discussed previously in the introduction (Section 1.5), calix[4]arenes can be alkylated in a selective manner. They synthesised an A_2B_2 heterofunctional initiator, which incorporated two alkyne moieties and two primary alcohols in diametric positions (Scheme 1.11). The alkyne moieties were introduced to facilitate the attachment of azide functionalised PEG *via* azide-alkyne "click" chemistry. The primary hydroxyls were introduced to facilitate the ROP of ε-caprolactone. The presence of the hydrophilic poly ethylene glycol (PEG) chains and hydrophobic PCL chains lead to an amphiphilic polymeric system.

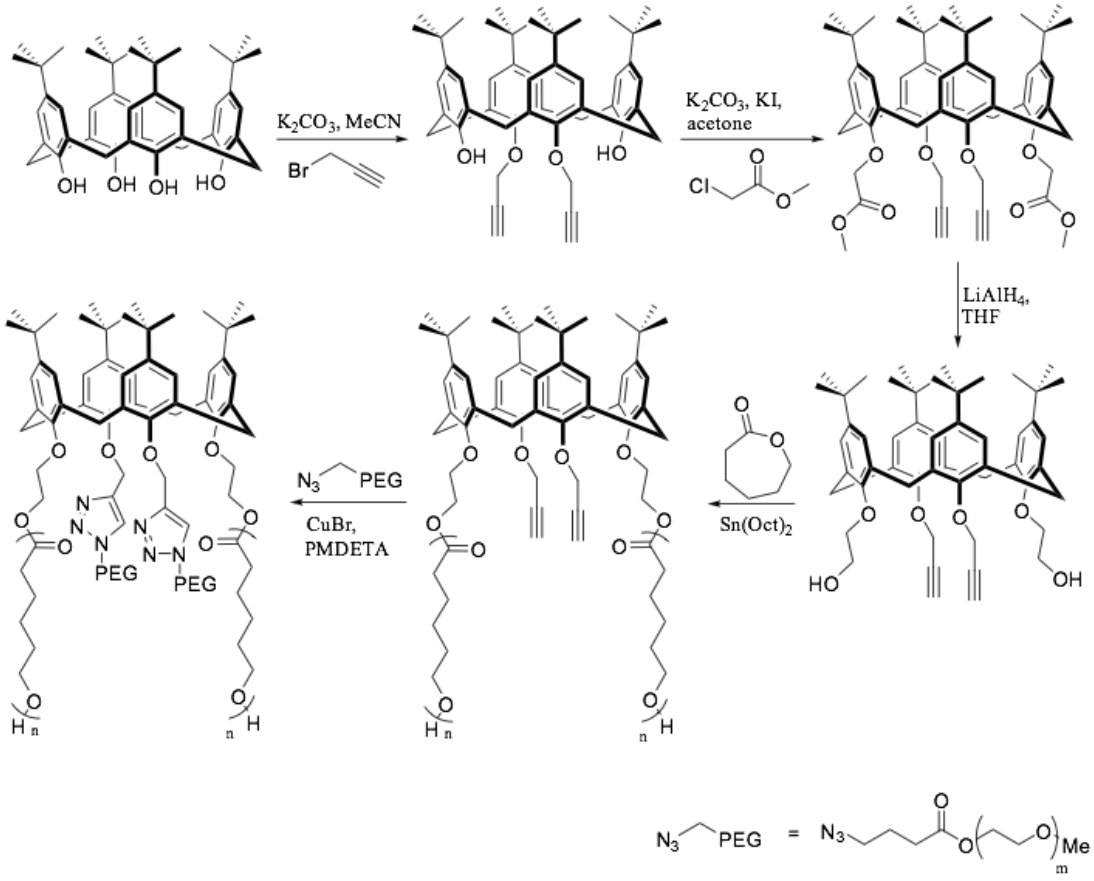

Scheme 1.11. Synthesis of miktoarm star polymer centred around a calix[4]arene core.

Molecular weights of up to 1.3 x 10^4 g mol^{-1} were calculated with dispersities of up to 1.29. However, the dispersities measured appear to be inaccurate, as the uniformed distribution covers an elution time of ~3 mL, which would suggest a wide range of chain length. The amphiphilic miktoarm star polymers exhibited self-assembly behaviour in water, forming micelles or wormlike aggregates depending on the length of PEG and PCL.[39]

1.8. Controlled Radical Polymerisation

Polymer synthesis, most profoundly for the polymerisation of vinyl monomers, has benefited greatly from the introduction and development of controlled radical polymerisations (CRP). When comparing CRP to other living techniques, such as living anionic polymerisation, similar control of polymeric structure is maintained but without the poor functional group tolerance and extremely demanding experimental conditions.[47] CRP has been readily applied to the synthesis of a wide range of vinyl monomers with well-defined structures, molecular weight and dispersities, which are unattainable by conventional free radical polymerisations.

A typical radical polymerisation includes three main processes: initiation, propagation and termination, with a further unwanted chain transfer step (Scheme 1.12).[48]

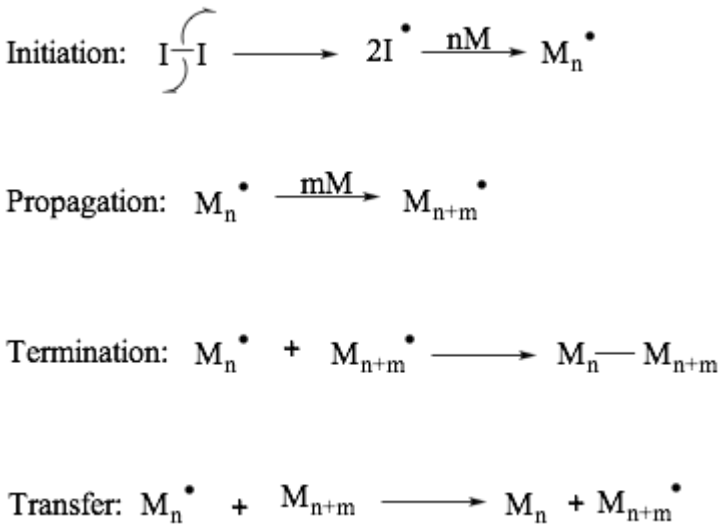

Scheme 1.12. Schematic representing the three main steps of radical polymerisation and the unwanted fourth step of chain transfer.

The first step corresponds to the generation of a reactive radical species that is capable of reacting with a monomer vinyl species. The second step corresponds to propagation, which is where the growth of the polymer is generated *via* monomer addition to the chain end radical. The third step is termination, which is a result of the coupling of two chain end radicals. A further reaction step is always present, known as a chain transfer reaction, which is a result of the active chain end radical transferring to the polymer chain *via* a reaction with a carbon hydrogen bond on the polymer backbone (Scheme 1.13). In a traditional free radical polymerization, the propagating radicals are very short lived and tend to terminate readily due to the rate constants of termination being much greater than that of propogation.[48]

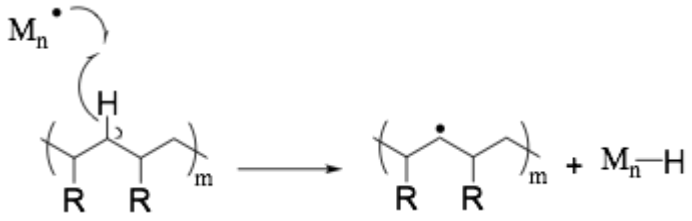

Scheme 1.13. Schematic depicting the chain transfer process.

In traditional free radical polymerisations, initiation is often slower than propagation, which leads to some chains growing significantly whilst others are just initiating, and in turn, with the presence of chain transfer between polymer chains, ill-defined polymers with uncontrolled molecular weights and large dispersity's are produced. CRP was developed to minimise chain transfer, minimise bimolecular termination

and prolong the life time of the chain end radical. In 1982, Otsu *et al*. introduced the concept of CRP *via* investigations into iniferters.[49,50] **Iniferters** refers to compounds that **ini**tiate, trans**fer** and **ter**minate a radical polymerisation.

To introduce control over a radical polymerisation, a very low concentration of reactive radical species must be maintained, which will greatly reduce termination. A low radical concentration is brought about *via* establishment of a dynamic equilibrium between dormant and active chain ends. Shifting the dynamic equilibrium to favour the dormant species will result in a low concentration of radical species. A key step in CRP is to allow the chain end to be reversibly deactivated, which will facilitate the dormant chain to be reactivated and propagate before deactivation back to the dormant state. A fast initiation is required in order to simultaneously initiate polymer chains that are rapidly trapped in the activation/deactivation process, which facilitates the slow propagation step of each chain to proceed at the same rate until the reaction is complete. In a truly living process the conclusion of the reaction is achieved upon complete consumption of monomer, but termination of polymer chains cannot be completely avoided for a radical polymerisation.[51]

The reversible deactivation equilibrium is achieved *via* one of two mechanisms. The first involves the trapping of the propagating chain in an activation-deactivation process, where the equilibrium constant is greatly shifted towards the dormant species (scheme 1.14).[52]

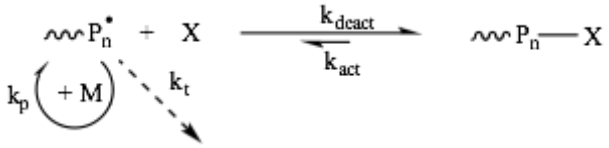

Scheme 1.14. Activation-deactivation process.

The second mechanism comprises a degenerative transfer process where the equilibrium reversibly moves a transfer agent between active centres, resulting in the

capping of one chain whilst simultaneously releasing another to propagate (scheme 1.15).[52]

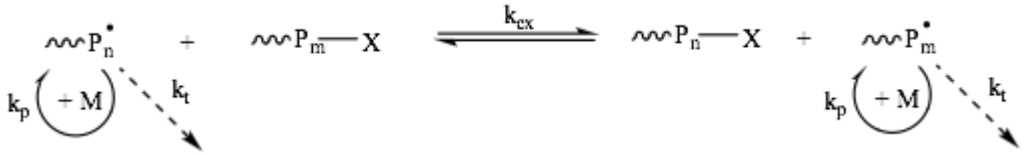

Scheme 1.15. Degenerative transfer process.

To date, the major techniques of CRP are nitroxide-mediated polymerisation (NMP),[53] reversible addition-fragmentation chain transfer radical polymerisation (RAFT),[54] atom transfer radical polymerisation (ATRP)[55,56] and single-electron transfer living radical polymerisation (SET-LRP).[57,58] For the aim of this thesis SET-LRP will be focused on

1.8.1. Single Electron Transfer-Living Radical Polymerisation (SET-LRP)

In 2002, Percec *et al*. utilised a Cu(0) catalyst for the controlled polymerisation of vinyl chloride (VCl).[59] The controlled polymerisation of VCl had proven unsuccessful using traditional ATRP (Cu(I)) catalysts due to insufficient activity towards reactivation of dormant chains. During a screening process for suitable catalysts for the polymerisation of VCl using a sulfonyl halide initiator, Cu(0) demonstrated the required activity to reactivate the dormant (PVCl) chains.[60] The use of Cu(0) also showed very low levels of bimolecular termination during polymerisation even though chain transfer remained. It was postulated that at the early stages of polymerisation insufficient amounts of deactivating Cu(II) were present.[58] A distinct mechanism was proposed that revolved around an outer-sphere electron transfer (OSET) process between the activating Cu(0) and an alkyl halide. The initiation step proceeds *via* a radical anion intermediate prior to decomposing to an alkyl radical and a halide ion, which associates to a Cu(I) ion formed in situ. On formation of the Cu(I), instantaneous disproportionation occurs leading to the formation of nascent Cu(0) activator and Cu(II), which deactivates the growing polymer chains. The nascent Cu(0) is thought to be very active, thus contributes to the fast rate of SET-LRP (Scheme 1.16).

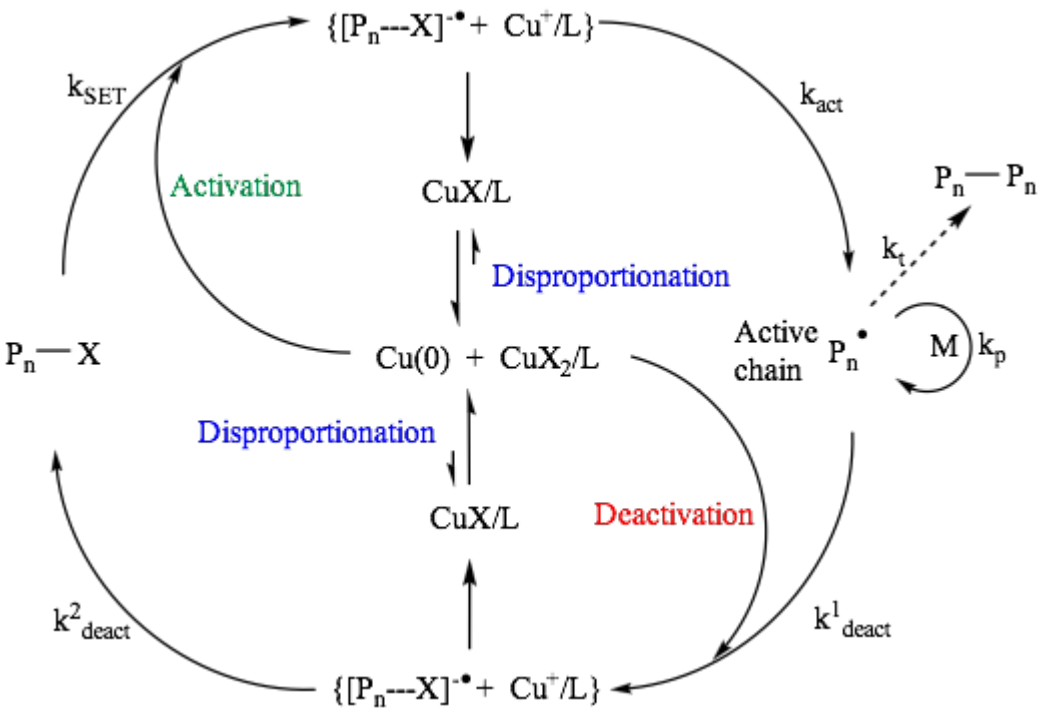

Scheme 1.16. Mechanism for SET-LRP.

During early VCl polymerisations, the mechanism proposed was based around competing SET and degenerative transfer processes (SET-DTLRP). It was considered that through modification of reaction conditions a purely SET-LRP process could be achieved.[61] The combination of active monomers, such as acrylates, to the SET-LRP system led to extremely fast polymerisation rates, even at ambient temperature, whilst still facilitating good control over the polymers molecular weight and dispersity with low levels of termination.

For SET-LRP reactions, components are chosen to maximise the OSET and disproportion processes. The components that have the greatest effect are solvent and ligand. In order to promote disproportionation and favour OSET, *via* solvation and stabilisation of the halide anion, polar solvents are required. To date, DMSO has proven the most successful solvent for fast and controlled polymerisation reactions. The success is attributed to its ability to stabilise nascent Cu(0) in a colloidal form, which increases the rate of polymerisation. Water, alcohols and other polar solvents (protic or aprotic) have been shown to be suitable solvents, although, alcohols suitability decreases with increased hydrophobicity.[62,63] Ionic liquids, DMF, acetone and ethylene glycol have additionally been employed in SET-LRP reactions.[64] Non-

polar solvents, such as toluene and acetonitrile, are unsuitable for SET-LRP as they do not promote disproportionation or stabilise Cu(0). However, with the addition of small amounts of polar additives, such as phenol, non-polar solvents can be effective, which further allows access to a wider range of non-polar monomers. The relative stabilities of Cu(I) and Cu(II) complexes are determined by the ligand selected. For SET-LRP, the most effective ligands are those which stabilise Cu(II), thus favour disproportionation. To date, the most effective ligands are those with an aliphatic nature such as TREN and Me_6TREN, as they inhibit the formation of a tetrahedral/distorted tetrahedral, which is the favoured conformation of Cu(I) (Fig. 1.6). TREN and Me_6TREN favour the trigonal bipyramidal Cu(II) complex.[65]

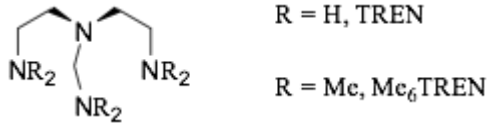

Figure 1.6. Structure of TREN and Me_6TREN.

The activation of alkyl halides is through a heterogeneous, surface activated process, which leads to an observed correlation between reaction rate and Cu(0) surface area. In the early reactions copper powder was used, but it was realised that any Cu(0) source could be suitable. Due to copper wire's uniformed surface area relative to copper powder, it has been shown to allow better control over the polymerisation.[61] Various copper salts exhibit activity (Cu_2Y, where Y = Se, Te, S and O). Importantly, Cu_2O exhibits activity, at a reduced level relative to copper wire, but does allow for some tolerance to oxygen within the SET-LRP process. All radical polymerisations have a sensitivity towards oxygen, however, with Cu(0) ability to scavenge oxygen to form Cu_2O, a polymerisation is able to continue, albeit with an observed lag period.[66,67]

SET-LRP makes use of several alkyl halides (Fig. 1.7). The OSET mechanism implies the alkyl halide bond is broken *via* a halide anion in a stepwise manner, resulting in the bond dissociation energy having a reduced effect over the process.[68]

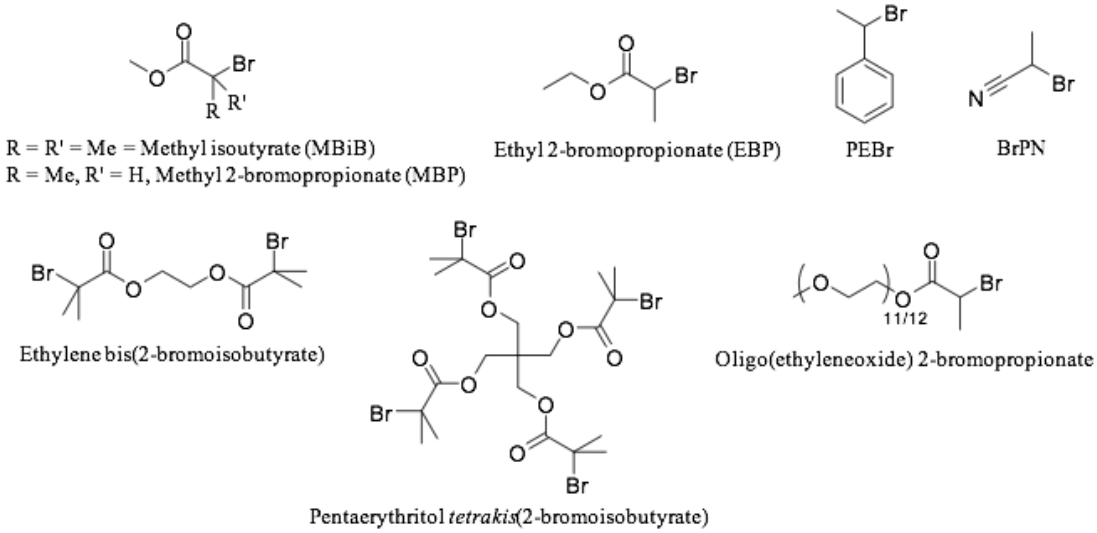

Figure 1.7. Common initiators used in SET-LRP.

Haddleton *et al*. showed SET-LRP exhibited remarkable tolerance to impurities, which allows for reaction components without extensive purification. Highly controlled polymerisations were carried out in a range of alcoholic drinks.[69] More importantly, the system has been shown to be tolerant to radical inhibitors, such as hydroquinone. It was shown that for the controlled polymerisation of methyl methacrylate with and without hydroquinone; both reactions proceeded with a high conversion with only a small difference in rates.[70]

1.8.2. SET-LRP vs SARA-ATRP

With respect to Cu(0) mediated polymerisations, there are two differing models; SET-LRP and supplemental activator and reducing agent (SARA) ATRP. The models differ in several key areas:

- Whether Cu(0) acts as the major activator or Cu(I) is the major activator and Cu(0) acts as a supplemental activator and reducing agent.
- Whether disproportionation or comproportionation (reduction of Cu(II) to Cu(I)) dominates.
- Whether the alkyl halide activation occurs *via* OSET or inner sphere electron transfer (ISET) process.

The two opposing models are illustrated in Figure 1.8.

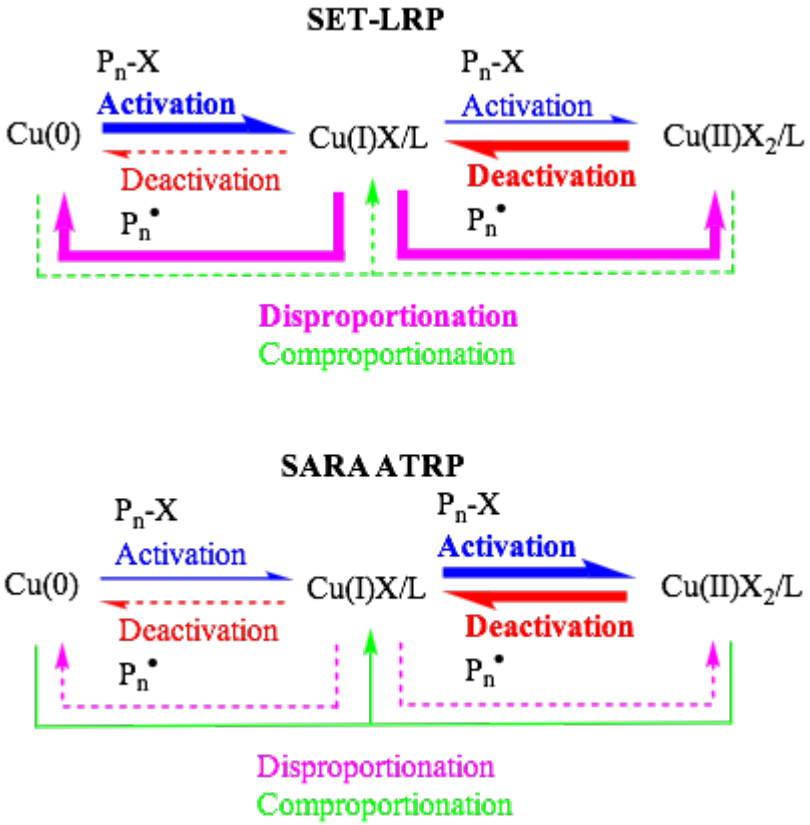

Figure 1.8. (Top) The mechanism of SET-LRP, (bottom) the mechanism of SARA-ATRP. Bold arrows indicate major reactions, solid arrows indicate supplemental or contributing reactions and dashed arrows indicate minor reactions that can be neglected from the mechanism.[71]

Figure 1.8 shows both the SET-LRP and SARA ATRP mechanism. The broad arrows show that the dominant reactions in SET-LRP are Cu(0) activation to Cu(I) and Cu(II) deactivation to Cu(I) with the Cu(I) disproportionation to Cu(0) and Cu(II). Whereas, for SARA-ATRP the dominant reactions are activation by Cu(I) to give Cu(II) and the deactivation of the reaction by Cu(II) to give Cu(I). Additionally, there is a more subtle comproportionation reaction between Cu(II) and Cu(0) to give more Cu(I).

1.8.1.1. Cu(0) or Cu(I) as the major activator

For controlled polymerisations fast activation is required to allow for simultaneous initiation and growth of all polymer chains.[52] Matyjaszewski *et al.* compared the relative activity of Cu(0) and Cu(I) as activators of alkyl halides. It was shown that the k_{act} of CuBr/Me_6TREN in pure DMSO and in the presence of monomer using methyl 2-bromopropioate (MBP) initiator and TEMPO (as a radical trap) was

extremely high.[72,73,74] Through UV-Vis spectroscopy the activation rates were measured as a function of $CuBr_2$ concentration in pure solvent and solvent monomer mix with the k_{act} determined to be 3.2 x 10^4 mol^{-1} s^{-1} and 2.0 x 10^4 mol^{-1} s^{-1}, respectively. Under aqueous conditions, electrochemical techniques were required due to the rate of production of $CuBr_2$ being so high.[75]

The rate of activation by Cu(0) in DMSO, using a range of ligand concentrations (1-20 mmol), was much lower, with an average k_{act} of 1.8 x 10^{-4} mol^{-1} s^{-1}. In the presence of methyl acrylate (MA) the rate was even slower with a k_{act} of 1.0 x 10^{-4} mol^{-1} s^{-1}.[74] Unlike the reactions for determining the k_{act} of Cu(I), no radical trap was employed as the reactions were selected to maximise termination and consume alkyl halide radicals. In aqueous conditions the k_{act} for Cu(0) was much lower than that of Cu(I). Using Cu(0) in the presence of Me_6TREN and an oligo(ethylene oxide) 2-bromopropionate (OEOBP) initiator with a oligo(ethylene oxide) acrylate (OEOA) and water mix a k_{act} was calculated to be 1.0 x 10^{-5} mol^{-1} s^{-1}.[75] Harrison *et al*. further measured the activity of Cu(0) in a range of solvents in the presence of a TEMPO radical trap using ethyl-2-bromo-2-methylproppionate (EBiB) as an initiator.[76] The reaction rates measured were high (k_{act}(DMSO) = 6.3 x 10^6 mol^{-1} s^{-1}), although, an induction period was observed. The induction period was thought to be a result of the time required to accumulate nascent Cu(0), but could also suggest that the reaction was activated by Cu(I), which was gradually generated in-situ.[76] Percec *et al*. proposed that Cu(0) must be very active in order to re-activate dormant PVCl chains where Cu(I) catalysts could not, which contradict these observations.[58] To prove activation was through a surface mediated process two experiments were carried out in which the Cu(0) was removed. In the first reaction, the polymerisation mixture was decanted between connected Schlenks, with one containing Cu(0) powder. The polymerisation proceeded on contact with catalyst, however, the reaction was interrupted reversibly when decanted into the catalyst free Schlenk.[77] For the second experiment, copper wire was used as the Cu(0) source. During the polymerisation the copper wire was removed; the reaction continued but at a vastly reduced rate. The continued reaction was attributed to activation *via* nascent Cu(0) produced in-situ. It was possible to completely stop the reaction if the solution was carefully decanted to remove the nascent Cu(0).[78] From these two experiments it was

concluded that the soluble Cu(I) was not important in the activation of the alkyl halide bond. However, Matyjaszewski *et al*. argued that the interruption was expected due to the low concentration of Cu(I) in solution, which is eliminated by the persistent radical effect (PRE) without a copper source.[71]

Percec additionally proposed that the nascent Cu(0) formed through disproportionation of Cu(I) is extremely active and contributes to the high rates of the SET-LRP reaction. To monitor the activity of nascent Cu(0) a source of alkyl halide was added to a mixture of pre-disproportionated CuBr/Me_6TREN in DMSO.[79] Full disproportionation was observed through formation of $CuBr_2$ (blue colour) and collection of nascent Cu(0) at the bottom of the flask. On addition of the alkyl halide source, all nascent Cu(0) disappeared within five minutes. The above procedure was further repeated using solvents that do not stabilise colloidal Cu(0) (e.g. methanol); a slower disappearance was observed. For systems where Cu(0) forms larger agglomerations with a smaller surface, slower rates are expected.[80] Haddleton *et al*. carried out a pre-disproportionation polymerisation in order to prove activation *via* Cu(0).[81] Immediate disproportionation was observed *via* the presence of $CuBr_2$ and colloidal Cu(0) on the mixing of CuBr/Me_6TREN in water. Addition of initiator and monomer lead to a polymerisation, with the nascent Cu(0) consumed in the process. Due to the fact that complete disproportionation was observed before the reaction, it was concluded that activation must be only due to nascent Cu(0). Matyjaszewski argued that under conditions of complete disproportionation only comproportionation can occur within the reaction mixture, which would generate the necessary Cu(I) concentration required to activate the reaction, and therefore the SARA ATRP model is correct.[71]

1.8.1.2. Disproportionation or comproportionation

In the SARA ATRP model the role of Cu(0) is to supplement Cu(I) activation and reduce Cu(II) to Cu(I) in a comproportionation process (Scheme 1.18).

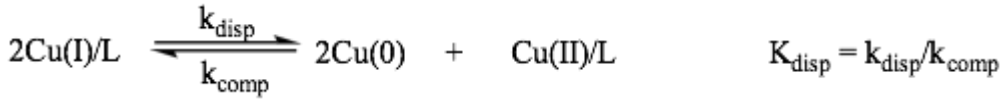

Scheme 1.18. Disproportionation/comproportionation equilibrium.

The equilibrium constant for the disproportionation in water is very large ($K_{disp} \sim 10^7$ M^{-1}), but in the popular solvent for SET-LRP, DMSO, disproportionation is slightly disfavoured. With the addition of a suitable ligand, such as Me_6TREN disproportionation becomes favoured.[80] Percec *et al*. demonstrated the disproportionation of Cu(I) in a variety of solvents *via* following the rate of $CuBr_2$ production, using UV-Vis spectroscopy, after the addition of CuBr/Me_6TREN. Within an hour disproportionation had reached equilibrium and nascent Cu(0) was observed in the reaction vessel within ten min.[80] For each of the solvents tested, K_{disp} favoured disproportionation, even with the addition of various monomers, including acrylates and methacrylates.[80,82] These results contradict a similar study by Matyjaszewski *et al*.,[83] who further studied the comproportionation *via* measuring the reduction in concentration of $CuBr_2$ in MeCN, DMF and DMSO. The study revealed that both disproportionation and comproportionation were slow relative to the rate of activation by Cu(I). In both model reactions, instantaneous disproportionation was not observed, and the equilibrium took ~2500 min to be reached. It was stated that, while disproportionation was favoured thermodynamically due to the relative stability of Cu(II) over Cu(I), kinetically, comproportionation will be favoured due to the low concentration of Cu(I) in the reaction mixture.[83] Additionally, disproportionation leads to the release of free ligand, which should shift the equilibrium even further to the comproportionation reaction. Nicolas *et al*. studied the comproportionation rate constant (k_{comp}) in a range of solvents and concluded that comproportionation was dominant in Cu(0) mediated polymerisations.[76] It was also noted that using the PMDETA ligand opposed to Me_6TREN was likely to decrease the effect of comproportionation.[76]

In addition to the above mentioned model studies, Percec and Haddleton both measured the $CuBr_2$ concentration during polymerisation reactions.[84,85] A constant increase in concentration of $CuBr_2$ was observed, thus concluding that $CuBr_2$ was not reduced by Cu(0) when the competing activation reaction was accessible.

Alternatively, the steady increase in $CuBr_2$ concentration could be generated through the PRE. The $CuBr_2$ concentration was monitored during a polymerisation reaction that demonstrated high-chain end retention (analysed as 99.9% *via* NMR spectroscopy and MALDI-MS), proving a linear increase in $CuBr_2$ concentration was possible in the absence of termination reactions. It was further observed that the addition of $CuBr_2$ at the beginning of the reaction had no effect on the rate at which $CuBr_2$ was produced or the final concentration of $CuBr_2$. If the PRE was influencing the reaction a difference in the values may be expected.[85]

The rate of copper mediated polymerisations has been shown to increase when using polar solvents, and with the addition of water. In the SET-LRP model, the increased rate has been attributed to the promotion of disproportionation, which provides active Cu(0) in solution. For the SARA ATRP model, the increased rate was brought about by the decreased stability of Cu(II) deactivator, which shifts the K_{ATRP}.[58] A key difference with SET-LRP relative to SARA ATRP is that an increase in disproportionation should simultaneously increase the concentration of both deactivator and activator, thus maintaining control over the polymerisation. Evidence for the SET-LRP model was demonstrated through a reaction that exhibited control over a polymerisation reaction despite increasing the rate of propagation through the addition of polar additives, such as phenol.[61]

1.8.1.3. OSET or ISET

A distinguishing feature between SET-LRP and SARA ATRP is the electron transfer (ET) process during initiation or activation. It is believed that SET-LRP occurs *via* a OSET mechanism with no bridging ligand and a weak interaction between the donor and acceptor.[86] In contrast, SARA ATRP is thought to proceed *via* an ISET process, which involves bridging of the halide followed by the atom transfer of the halide to the metal centre in a concerted process (Scheme 1.19).[87] For SET-LRP, the proposed OSET process has caused much debate centring on the validity of the radical-anion formation and OSET and ISET process relative rates.

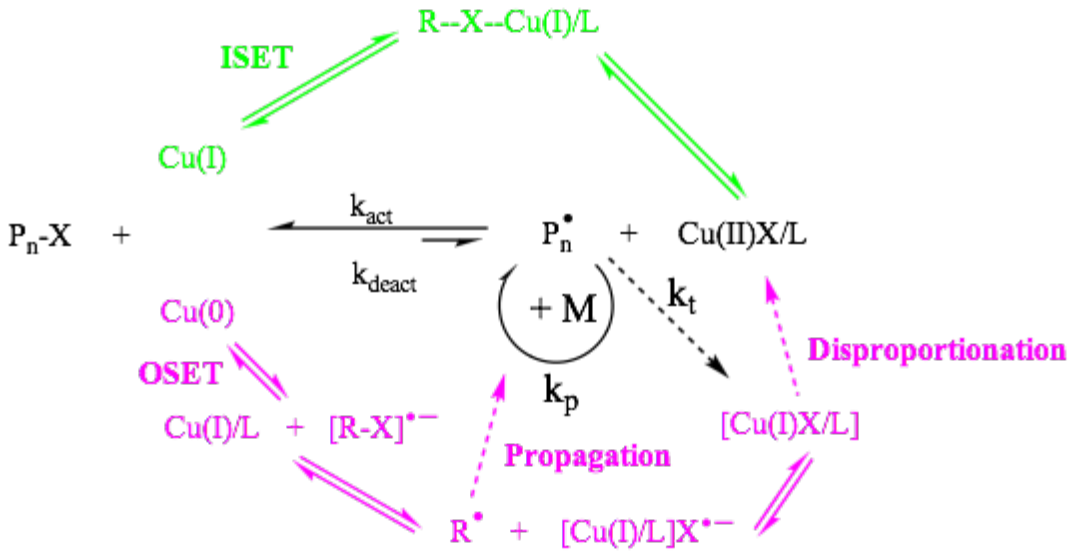

Scheme 1.19. Comparison of OSET (pink) and ISET (green) mechanisms in copper mediated polymerisations.

Radical anions are well known for aromatic compounds, such as naphthalene, where the radical-anion is used to initiate living anionic radical polymerisations.[47] Percec *et al*. have suggested that the formation of the radical anion is possible for activated alkyl halide initiators due to the presence of electron withdrawing moieties adjacent to the halogen. The radical that forms carries a slight positive charge, therefore is capable of interacting electrostatically with the released halide anion. This process is known as the stepwise model.[86] It was further proposed that the OSET mechanism is the reason for the propagating PVCl chains re-activation at ambient temperatures when using a Cu(0) catalyst, whilst this is not possible even at higher temperatures when using the most powerful of Cu(I) ATRP catalysts.[88] Through a computational study, it was demonstrated that the homolytic bond dissociation energy of an alkyl halide was greater than its heterolytic bond dissociation, which is attributed to the relative insensitivity of SET-LRP to the alkyl halide bond dissociation.[68] Through a study of the polymerisation of styrene in DMSO using a CuBr catalyst and a NH_2Capten ligand it was proposed that the ligand orientation would prevent halide bridging and therefore ISET (Fig.1.9).[89] If the bridging halide was inhibited then activation can only occur through a OSET process. Additionally, the ability of non-transition metal OSET donors, such as $Na_2S_2O_4$ to catalyse controlled polymerisations is further evidence for the OSET process.[90]

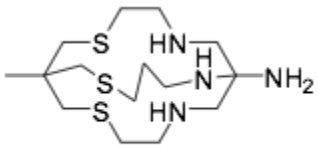

NH_2Capten

Figure 1.9. Structure of NH_2Capten.

Matyjaszewski *et al*. compared the reaction kinetics of a Cu(I)/TPMA catalysed system and a polymerisation activated *via* aromatic anions (OSET donor), and it was concluded that the rate of OSET is much slower than that of ISET.[91,92] They additionally proposed that OSET was a side reaction that may occur in the presence of a very active CuBr/Me_6TREN catalyst system when in a large concentration.[52] Isse *et al*. claimed that the dissociative ET process proceeded *via* a concerted process not step-wise. Additionally, it was suggested that the radical anion would not form as an intermediate species because the introduction of a single electron into an alkyl halide bond would only give a weakly associated radical anion complex.[93] It was proposed that for a reasonable rate of reaction a OSET donor would require a greatly negative potential, which is not the case for copper catalysts.

The experiments used to clarify the correct model for SET-LRP or SARA ATRP are somewhat convoluted, which relays the complexity of the system. Gao *et al*. carried out a study and suggested that both SET-LRP and SARA ATRP coexisted in Cu(0)/Me_6TREN catalysed polymerisations.[94]

1.9. Ring Opening Polymerisation of ε-caprolactone

Polycaprolactone (PCL) is a type of poly aliphatic ester, which is composed of repeating units of hexanoate. The polymer is semi-crystalline and can have a crystallinity of up to 69%.[95] The mechanical, thermal and physical properties of PCL depend on its degree of crystallinity and molecular weight. At ambient temperature, PCL is highly soluble in a range of non-polar and polar solvents such as dichloromethane, chloroform, toluene and dimethylformamide (DMF). Additionally, the polymer itself is miscible with a variety of other polymers, such as poly(vinyl

chloride) and nitrocellulose.[96] PCL has been reported to degrade within several months to years, depending on the crystallinity, molecular weight and the method of degradation.[97] PCL has been applied to a variety of fields, such as packaging,[98] adhesives,[99] microelectronics,[100] tissue engineering[101] and drug delivery systems.[102]

For the synthesis of PCL there are two methods: the condensation polymerisation of 6-hydroxycaproic acid and the ring opening polymerisation (ROP) of ε-caprolactone (Scheme 1.20).

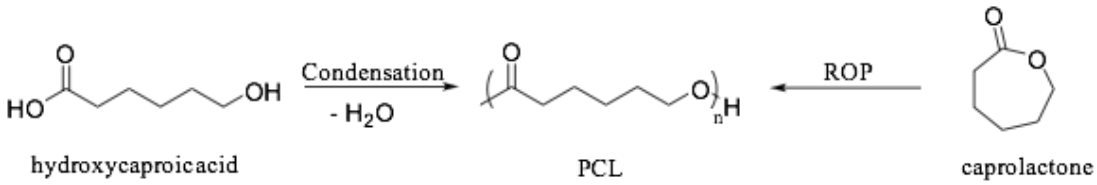

Scheme 1.20. Synthesis of PCL *via* condensation polymerisation of hydroxycaproic acid and ROP of ε-caprolactone.

1.9.1. Polycondensation

Braud *et al*. performed a condensation reaction using 6-hydroxycaproic acid leading to the formation of PCL oligomers. The reaction was run at 150 ^{o}C and under vacuum to remove the water produced, and thus shifted the equilibrium towards the formation of polymer, with the reaction running.[103] The condensation reaction leads to low molecular weight polymers, therefore is rarely used.[103]

1.9.2. Ring Opening Polymerisation

ROP is the method of choice when synthesising PCL, as high molecular weights, and in a more controlled fashion, can be achieved. There are four mechanisms for the ROP of lactones, which all require catalysts for activation: anionic, cationic, monomer activated and coordination-insertion ROP.

1.9.2.1. Anionic ROP

In anionic ROP, an anionic species is required (organometallic species, such as butyl lithium or aluminium alkoxide) to attack the carbonyl of ε-caprolactone and cleave the ester bond. The metal will stabilise the anionic charge on the oxygen and allow for further nucleophilic attack on ε-caprolactone and thus propagation of polymer chain will occur through the alkoxide species (Scheme. 1.21).[104]

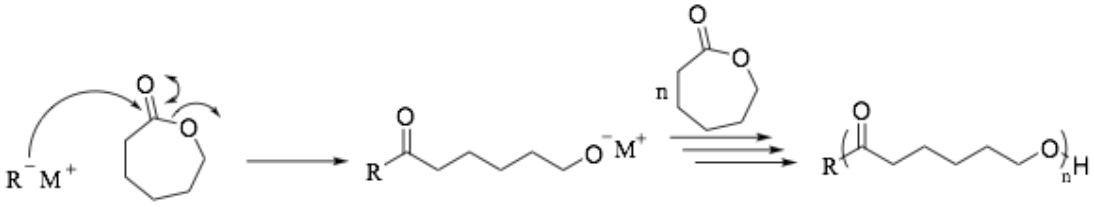

Scheme. 1.21. Synthesis of PCL *via* anionic ROP.

A major drawback of anionic ROP is the significant presence of intramolecular transesterification, also known as back biting, in the later stages of the reaction. This leads to cyclic polymers or relatively low molecular weight polymers if the reaction is quenched before significant back-biting occurs.[104]

1.9.2.2. Cationic ROP

In cationic ROP, a cationic species coordinates to the oxygen of the carbonyl species, thus pulling electron density away from the carbonyl carbon making it susceptible to attack from the carbonyl oxygen of ε-caprolactone *via* a bimolecular nucleophilic substitution reaction (Scheme. 1.22).[104]

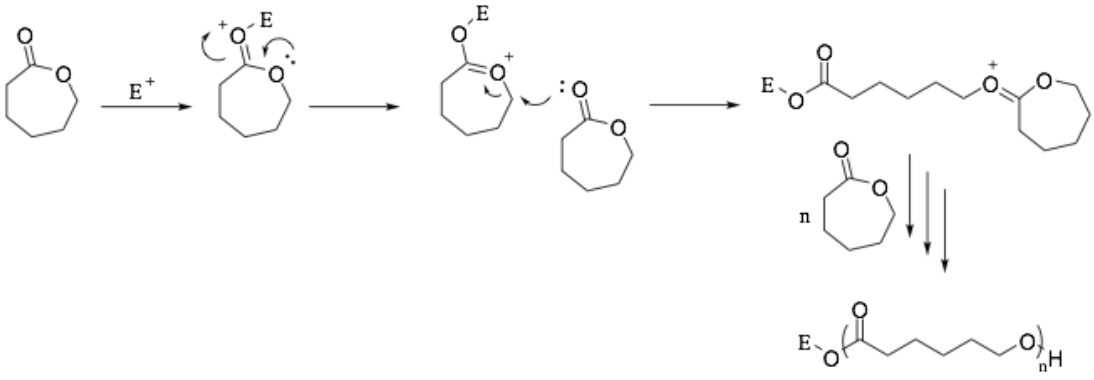

Scheme. 1.22. Synthesis of PCL *via* cationic ROP.

Dittrich *et al*. and Kricheldorf *et al*. demonstrated that trifluoromethanesulfonic acid and trifluoromethanesulfonate were some of the few initiators that were capable of initiating cationic polymerisations, although poor control was observed.[105,106] The poor control and lack of initiators makes cationic polymerisation one of the least favoured techniques.

1.9.2.3. Monomer Activated ROP

Monomer activated ROP is similar to that of cationic ROP. A electrophile is introduced into the system that activates the monomer molecule (such as a Bronsted acid), which makes the carbonyl carbon more susceptible to nucleophilic attack form a nucleophile, such as an alcohol (Scheme. 1.23).[107] Little control is maintained over the polymerisation.

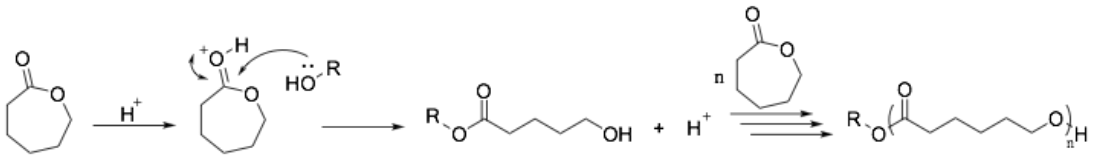

Scheme 1.23. Synthesis of PCL *via* monomer activated ROP.

1.9.2.4. Coordination-insertion ROP

Coordination insertion is by far the most common form of ROP. It is a pseudo-anionic polymerisation, by which the propagation is postulated to proceed *via* monomer coordination to the metallic centre followed by monomer insertion into the metal chain end through cleavage of the acyl-oxygen bond (Scheme. 1.24).[108] Insertion of a new lactone monomer propagates the growing chain.

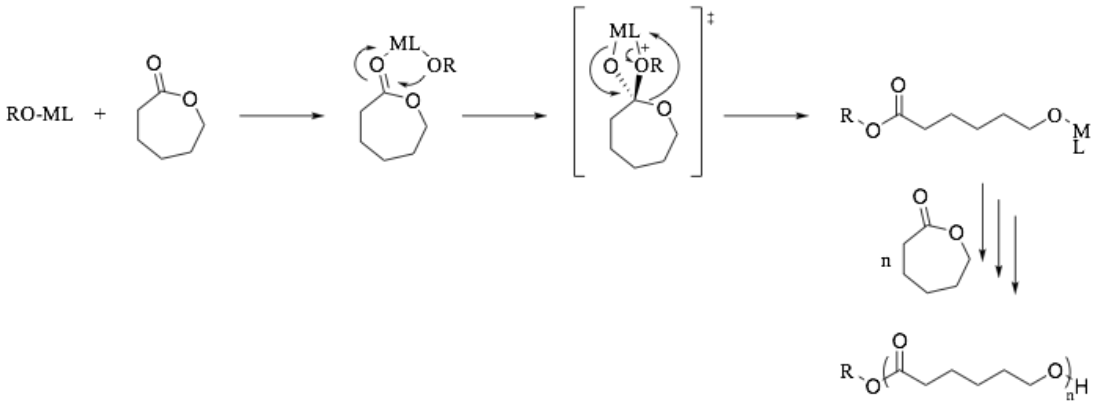

Scheme. 1.24. Synthesis of PCL *via* coordination-insertion mechanism.

There are many variants on the design of the metal based catalysts, which have an effect on the mechanism operating. Many studies have been carried out into the identity of the metal and the ligand design, which greatly influence the rate and control over the polymerisation.[96,109] As with all ROP, the transesterification reaction is a problematic side reaction.

By far, the most widely used catalyst is tin(II) *bis*(2-ethylhexanoate) ($SnOct_2$), due to its commercial availability, ease of handling and solubility in common organic solvents and melt (Fig. 1.10). Moreover, it is approved by the Federal Drug agency (FDA) of the USA.

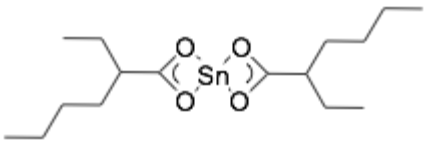

Figure 1.10. Structure of tin(II) bis(2-ethylhexanoate) ($SnOct_2$).

$SnOct_2$ must be used in combination with a nucleophilic source (alcohol) to initiate the reaction, which also facilitates relative control over the polymerisation. One issue with using $SnOct_2$ is that high temperatures are required, which encourages intramolecular and intermolecular transesterification reaction, which in turn broadens the dispersity.[110]

1.10. Aims

This project involves the development of several novel heterofunctional initiators with a calix[4]arene centre that can facilitate a "core" first method for the synthesis of miktoarm star polymers. *p-tert*-butylcalix[4]arene will be selected as a base compound due to its low toxicity, relatively low cost and its ability to facilitate selective functionalisation on both the upper and lower rims of the macrocycle. The first initiator to be developed is to consist of two types of functionality in an A_2B_2 fashion diametrically opposed on the lower rim. The diametric functionalisation should be obtained due to calix[4]arenes ability to direct alkylation on the lower rim. The second initiator to be developed is to also consist of two types of heterofunctionality but in an A_4B_4 fashion, with one type of functionality occupying the lower rim and the second occupying the upper rim. To introduce the two different types of functionality on both initiators, classic organic chemistry as well as more cutting edge techniques are to be used. The A_nB_n heterofunctionality will be to allow for the synthesis of two different types of polymer from a single core. One type of functionality to be introduced is a primary hydroxyl, which will facilitate the ring opening polymerisation of ε-caprolactone that will give a hydrophobic polymer chain. The second functionality will be an alkyl halide, which can facilitate the Cu(0) mediated controlled radical polymerisation of 2-hydroxylethylacrylate that leads to a hydrophilic polymer. The combination of hydrophobic and hydrophilic polymer chains attached to a single core should lead to interesting self-assembly properties. The self-assembly properties are to be characterised by TEM and CMC determination, and the effects of length of hydrophilic chain are to be quantified.

1.11. References.

(1) Gutsche, C. D. *Calixarene: An Introduction*; 2nd ed.; The Royal Society of Chemistry: Cambridge, 2008.
(2) Baeyer, A. *Chem. Ber.* **1872**, *5*, 25.
(3) Zinke, A.; Ziegler, E. *Ber. D. Deut. Chem. Ges.,* **1944**, *77*, 264.
(4) Zinke, A.; Zigeuner, G.; Hossinger, K.; Hoffmann, G. *Mon. F. Chem.,* **1948**, *79*, 438.
(5) Cornforth, J. W.; Hart, P. D.; Nicholls, G. A.; Rees, R. J. W.; Stock, J. A. *Briti. J. Pharm. Chem.,* **1955**, *10*, 73.
(6) Gutsche, C. D.; Muthukrishnan, R. *J. Org. Chem.* **1978**, *43*, 4905.
(7) Gutsche, C. D.; Gutsche, A. E.; Karaulov, A. I. *J. Incl. Phen.* **1985**, *3*, 447.
(8) Hayes, B. T.; Hunter, R. F. *J. App. Chem.,***1958**, *8*, 743.
(9) Gutsche, C. D.; Iqbal, M.; Stewart, D. *J. Org. Chem.* **1986**, *51*, 742.
(10) Ullman, F. *Ber. D. Deut. Chem. Ges.,* **1909**, *42*, 2539.
(11) Gutsche, C. D.; Dhawan, B.; Levine, J. A.; No, K. H.; Bauer, L. J. *Tetrahedron* **1983**, *39*, 409.
(12) Andreetti, G. D.; Ungaro, R.; Pochini, A. *J. Chem. Soc.-Chem. Commun.* **1979**, 1005.
(13) Andreetti, G. D.; Pochini, A.; Ungaro, R. *J. Chem. Soc.-Perkin Trans. 2* **1983**, 1773.
(14) Ohtsuchi, M.; Suzuki, K.; Armah, A. E.; Yamagata, Y.; Fujii, S.; Tomita, K.; Asfari, Z.; Vicens, J. *Acta Crystallogr. Sect. C-Cryst. Struct. Commun.* **1993**, *49*, 639.
(15) Juneja, R. K.; Robinson, K. D.; Johnson, C. P.; Atwood, J. L. *J. Am. Chem. Soc.* **1993**, *115*, 3818.
(16) Alfieri, C.; Dradi, E.; Pochini, A.; Ungaro, R. *Gazz. Chim. Ital.* **1989**, *119*, 335.
(17) Grootenhuis, P. D. J.; Kollman, P. A.; Groenen, L. C.; Reinhoudt, D. N.; Vanhummel, G. J.; Ugozzoli, F.; Andreetti, G. D. *J. Am. Chem. Soc.* **1990**, *112*, 4165.
(18) Iwamoto, K.; Araki, K.; Shinkai, S. *J. Org. Chem.* **1991**, *56*, 4955.
(19) Ferguson, G.; Gallagher, J. F.; Pappalardo, S. *Acta Crystallogr. Sect. C-Cryst. Struct. Commun.* **1993**, *49*, 1537.
(20) Bott, S. G.; Coleman, A. W.; Atwood, J. L. *J. Incl. Phen.,* **1987**, *5*, 747.
(21) Vrielink, A.; Codding, P. W.; Gutsche, C. D.; Lin, L. G. *J. Incl. Phen.,* **1986**, *4*, 199.
(22) Gutsche, C. D.; Bauer, L. J. *J. Am. Chem. Soc.* **1985**, *107*, 6052.
(23) Jaime, C.; Demendoza, J.; Prados, P.; Nieto, P. M.; Sanchez, C. *J. Org. Chem.* **1991**, *56*, 3372.
(24) Shinkai, S.; Araki, K.; Koreishi, H.; Tsubaki, T.; Manabe, O. *Chem. Lett.* **1986**, 1351.
(25) Araki, K.; Iwamoto, K.; Shinkai, S.; Matsuda, T. *Bull. Chem. Soc. Jpn.* **1990**, *63*, 3480.
(26) Shu, C.-M.; Liu, W.-C.; Ku, M.-C.; Tang, F.-S.; Yeh, M.-L.; Lin, L.-G. *The J. Org.Chem.,* **1994**, *59*, 3730.
(27) Groenen, L. C.; Ruel, B. H. M.; Casnati, A.; Verboom, W.; Pochini, A.; Ungaro, R.; Reinhoudt, D. N. *Tetrahedron* **1991**, *47*, 8379.

(28) Dijkstra, P. J.; Brunink, J. A. J.; Bugge, K. E.; Reinhoudt, D. N.; Harkema, S.; Ungaro, R.; Ugozzoli, F.; Ghidini, E. *J. Am. Chem. Soc.* **1989**, *111*, 7567.
(29) Van Loon, J. D.; Arduini, A.; Coppi, L.; Verboom, W.; Pochini, A.; Ungaro, R.; Harkema, S.; Reinhoudt, D. N. *The J. Org. Chem.,***1990**, *55*, 5639.
(30) Brunink, J. A. J.; Verboom, W.; Engbersen, J. F. J.; Harkema, S.; Reinhoudt, D. N. *Re. De. Trav. Chim. De. Pays-Bas-J. Ro. Neth. Chem. Soc.,* **1992**, *111*, 511.
(31) Araki, K.; Iwamoto, K.; Shigematsu, S.; Shinkai, S. *Chem. Lett.* **1992**, 1095.
(32) Gutsche, C. D.; Levine, J. A.; Sujeeth, P. K. *J. Org. Chem.* **1985**, *50*, 5802.
(33) Tashiro, M.; Yamato, T. *J. Org. Chem.* **1979**, *44*, 3037.
(34) Gutsche, C. D.; Pagoria, P. F. *The J.Org. Chem.,* **1985**, *50*, 5795.
(35) Sliwa, W.; Deska, M. *Arkivoc* **2011**, 496.
(36) Nimse, S. B.; Kim, T. *Chem. Soc. Rev.,* **2013**, *42*, 366.
(37) Frediani, M.; Sémeril, D.; Mariotti, A.; Rosi, L.; Frediani, P.; Rosi, L.; Matt, D.; Toupet, L. *Macro. Rap. Comm.,* **2008**, *29*, 1554.
(38) Mighani, H.; Tashakkorian, H.; Mighani, M. *Chi. J. Pol. Sci.,* **2014**, *32*, 551.
(39) Gou, P. F.; Zhu, W. P.; Shen, Z. Q. *J. Polym. Sci. Pol. Chem.* **2010**, *48*, 5643.
(40) Jacob, S.; Majoros, I.; Kennedy, J. P. *Macromolecules* **1996**, *29*, 8631.
(41) Ueda, J.; Kamigaito, M.; Sawamoto, M. *Macromolecules* **1998**, *31*, 6762.
(42) Angot, S.; Murthy, K. S.; Taton, D.; Gnanou, Y. *Macromolecules* **2000**, *33*, 7261.
(43) Taton, D.; Saule, M.; Logan, J.; Duran, R.; Hou, S.; Chaikof, E. L.; Gnanou, Y. *J. Polym. Sci. Pol. Chem.* **2003**, *41*, 1669.
(44) Zhu, W. P.; Ling, J.; Shen, Z. Q. *Macromol. Chem. Phys.* **2006**, *207*, 844.
(45) Lou, L. P.; Jiang, L. M.; Liu, J. Z.; Sun, W. L.; Shen, Z. Q. *Polymer International* **2007**, *56*, 796.
(46) Gou, P.; Zhu, W.; Shen, Z. *Front. Chem. China* **2008**, *3*, 330.
(47) Szwarc, M. *Nature* **1956**, *178*, 1168.
(48) Colombani, D. *Prog. Poly. Sci.,* **1997**, *22*, 1649.
(49) Otsu, T.; Yoshida, M. *Makro. Chemie-Rap. Comm.,* **1982**, *3*, 127.
(50) Otsu, T.; Yoshida, M.; Tazaki, T. *Makro. Chemie-Rap. Comm.,* **1982**, *3*, 133.
(51) Cowie, J. M. G. *Polymers: chemistry and physics of modern materials*; 3rd ed.; Taylor & Francis: Boca Raton, 2008.
(52) Braunecker, W. A.; Matyjaszewski, K. *Prog. Poly. Sci.,* **2007**, *32*, 93.
(53) Hawker, C. J.; Bosman, A. W.; Harth, E. *Chem. Rev.* **2001**, *101*, 3661.
(54) Chiefari, J.; Chong, Y. K.; Ercole, F.; Krstina, J.; Jeffery, J.; Le, T. P. T.; Mayadunne, R. T. A.; Meijs, G. F.; Moad, C. L.; Moad, G.; Rizzardo, E.; Thang, S. H. *Macromolecules* **1998**, *31*, 5559.
(55) Kato, M.; Kamigaito, M.; Sawamoto, M.; Higashimura, T. *Macromolecules* **1995**, *28*, 1721.
(56) Wang, J. S.; Matyjaszewski, K. *J. Am. Chem. Soc.* **1995**, *117*, 5614.
(57) Percec, V.; Barboiu, B. *Macromolecules* **1995**, *28*, 7970.
(58) Rosen, B. M.; Percec, V. *Chem. Rev.* **2009**, *109*, 5069.
(59) Percec, V.; Popov, A. V.; Ramirez-Castillo, E.; Monteiro, M.; Barboiu, B.; Weichold, O.; Asandei, A. D.; Mitchell, C. M. *J. Am. Chem. Soc.* **2002**, *124*, 4940.
(60) Asandei, A. D.; Percec, V. *J. Polym. Sci. Pol. Chem.* **2001**, *39*, 3392.
(61) Percec, V.; Guliashvili, T.; Ladislaw, J. S.; Wistrand, A.; Stjerndahl, A.; Sienkowska, M. J.; Monteiro, M. J.; Sahoo, S. *J. Am. Chem. Soc.* **2006**, *128*, 14156.

(62) Nguyen, N. H.; Rosen, B. M.; Percec, V. *J. Polym. Sci. Pol. Chem.* **2010**, *48*, 1752.
(63) Lligadas, G.; Percec, V. *J. Polym. Sci. Pol. Chem.* **2008**, *46*, 2745.
(64) Nguyen, N. H.; Rosen, B. M.; Jiang, X.; Fleischmann, S.; Percec, V. *J. Polym. Sci. Pol. Chem.* **2009**, *47*, 5577.
(65) Rosen, B. M.; Percec, V. *J. Polym. Sci. Pol. Chem.* **2007**, *45*, 4950.
(66) Nguyen, N. H.; Percec, V. *J. Polym. Sci. Pol. Chem.* **2011**, *49*, 4756.
(67) Jiang, X. A.; Rosen, B. M.; Percec, V. *J. Polym. Sci. Pol. Chem.* **2010**, *48*, 2716.
(68) Guliashvili, T.; Percec, V. *J. Polym. Sci. Pol. Chem.* **2007**, *45*, 1607.
(69) Waldron, C.; Zhang, Q.; Li, Z. D.; Nikolaou, V.; Nurumbetov, G.; Godfrey, J.; McHale, R.; Yilmaz, G.; Randev, R. K.; Girault, M.; McEwan, K.; Haddleton, D. M.; Droesbeke, M.; Haddleton, A. J.; Wilson, P.; Simula, A.; Collins, J.; Lloyd, D. J.; Burns, J. A.; Summers, C.; Houben, C.; Anastasaki, A.; Li, M. X.; Becer, C. R.; Kiviaho, J. K.; Risangud, N. *Polymer Chemistry* **2014**, *5*, 57.
(70) Lligadas, G.; Percec, V. *J. Polym. Sci. Pol. Chem.* **2008**, *46*, 3174.
(71) Konkolewicz, D.; Wang, Y.; Krys, P.; Zhong, M. J.; Isse, A. A.; Gennaro, A.; Matyjaszewski, K. *Poly. Chem.,* **2014**, *5*, 4396.
(72) Matyjaszewski, K.; Paik, H. J.; Zhou, P.; Diamanti, S. J. *Macromolecules* **2001**, *34*, 5125.
(73) Pintauer, T.; Braunecker, W.; Collange, E.; Poli, R.; Matyjaszewski, K. *Macromolecules* **2004**, *37*, 2679.
(74) Peng, C. H.; Zhong, M. J.; Wang, Y.; Kwak, Y.; Zhang, Y. Z.; Zhu, W. P.; Tonge, M.; Buback, J.; Park, S.; Krys, P.; Konkolewicz, D.; Gennaro, A.; Matyjaszewski, K. *Macromolecules* **2013**, *46*, 3803.
(75) Konkolewicz, D.; Krys, P.; Gois, J. R.; Mendonca, P. V.; Zhong, M. J.; Wang, Y.; Gennaro, A.; Isse, A. A.; Fantin, M.; Matyjaszewski, K. *Macromolecules* **2014**, *47*, 560.
(76) Harrisson, S.; Couvreur, P.; Nicolas, J. *Macromolecules* **2012**, *45*, 7388.
(77) Lligadas, G.; Rosen, B. M.; Bell, C. A.; Monteiro, M. J.; Percec, V. *Macromolecules* **2008**, *41*, 8365.
(78) Levere, M. E.; Nguyen, N. H.; Sun, H. J.; Percec, V. *Polymer Chemistry* **2013**, *4*, 686.
(79) Jiang, X.; Rosen, B. M.; Percec, V. *J. Polym. Sci. Pol. Chem.* **2010**, *48*, 403.
(80) Levere, M. E.; Nguyen, N. H.; Leng, X. F.; Percec, V. *Polymer Chemistry* **2013**, *4*, 1635.
(81) Zhang, Q.; Wilson, P.; Li, Z. D.; McHale, R.; Godfrey, J.; Anastasaki, A.; Waldron, C.; Haddleton, D. M. *J. Am. Chem. Soc.* **2013**, *135*, 7355.
(82) Rosen, B. M.; Jiang, X.; Wilson, C. J.; Nguyen, N. H.; Monteiro, M. J.; Percec, V. *J. Polym. Sci. Pol. Chem.* **2009**, *47*, 5606.
(83) Wang, Y.; Zhong, M. J.; Zhu, W. P.; Peng, C. H.; Zhang, Y. Z.; Konkolewicz, D.; Bortolamei, N.; Isse, A. A.; Gennaro, A.; Matyjaszewski, K. *Macromolecules* **2013**, *46*, 3793.
(84) Levere, M. E.; Willoughby, I.; O'Donohue, S.; Wright, P. M.; Grice, A. J.; Fidge, C.; Becer, C. R.; Haddleton, D. M. *J. Polym. Sci. Pol. Chem.* **2011**, *49*, 1753.
(85) Levere, M. E.; Nguyen, N. H.; Percec, V. *Macromolecules* **2012**, *45*, 8267.
(86) Zhang, N.; Samanta, S. R.; Rosen, B. M.; Percec, V. *Chem. Rev.* **2014**, *114*, 5848.

(87) Konkolewicz, D.; Wang, Y.; Zhong, M. J.; Krys, P.; Isse, A. A.; Gennaro, A.; Matyjaszewski, K. *Macromolecules* **2013**, *46*, 8749.
(88) Queffelec, J.; Gaynor, S. G.; Matyjaszewski, K. *Macromolecules* **2000**, *33*, 8629.
(89) Bell, C. A.; Whittaker, M. R.; Gahan, L. R.; Monteiro, M. J. *J. Polym. Sci. Pol. Chem.* **2008**, *46*, 146.
(90) Percec, V.; Popov, A. V.; Ramirez-Castillo, E.; Coelho, J. F. J.; Hinojosa-Falcon, L. A. *J. Polym. Sci. Pol. Chem.* **2004**, *42*, 6267.
(91) Lin, C. Y.; Coote, M. L.; Gennaro, A.; Matyjaszewski, K. *J. Am. Chem. Soc.* **2008**, *130*, 12762.
(92) Isse, A. A.; Bortolamei, N.; De Paoli, P.; Gennaro, A. *Electrochimica Acta* **2013**, *110*, 655.
(93) Isse, A. A.; Gennaro, A.; Lin, C. Y.; Hodgson, J. L.; Coote, M. L.; Guliashvili, T. *J. Am. Chem. Soc.* **2011**, *133*, 6254.
(94) Gao, Y. S.; Zhao, T. Y.; Zhou, D. Z.; Greiser, U.; Wang, W. X. *Chem. Commun.* **2015**, *51*, 14435.
(95) Iroh, J. O. *Polymer Data Handbook*; Oxford University Press: New York, 1999.
(96) Labet, M.; Thielemans, W. *Chem. Soc. Rev.,* **2009**, *38*, 3484.
(97) Gross, R. A.; Kalra, B. *Science* **2002**, *297*, 803.
(98) Ikada, Y.; Tsuji, H. *Macro. Rap. Comm.,* **2000**, *21*, 117.
(99) Joshi, P.; Madras, G. *Polymer Degradation and Stability* **2008**, *93*, 1901.
(100) von Ahnen, I.; Piret, G.; Prinz, C. N. *Microele. Eng.,* **2015**, *135*, 52.
(101) Wong, H. M.; Chu, P. K.; Leung, F. K. L.; Cheung, K. M. C.; Luk, K. D. K.; Yeung, K. W. K. *Prog. Nat.Science-Mat. Int.,* **2014**, *24*, 561.
(102) Schlesinger, E.; Ciaccio, N.; Desai, T. A. *Mat. Sci. & Eng. C-Mat. Bio. App.,* **2015**, *57*, 232.
(103) Braud, C.; Devarieux, R.; Atlan, A.; Ducos, C.; Vert, M. *J. Chrom.B* **1998**, *706*, 73.
(104) Stridsberg, K. M.; Ryner, M.; Albertsson, A. C. In *Degradable Aliphatic Polyesters*; Albertsson, A. C., Ed.; Springer-Verlag Berlin: Berlin, 2002; Vol. 157.
(105) Dittrich, W.; Schulz, R. C. *Ange. Makro. Chem.,* **1971**, *15*, 109.
(106) Kricheldorf, H. R.; Dunsing, R. *Makro. Chemie-Macro. Chem. Phy.,* **1986**, *187*, 1611.
(107) P. Dubois, O. C., J.-Marie. Raquez *Handbook of RING-Opening Polymerisation*; WILEY-VCH Verlag GmbH & Co. KGaA: Weinheim, 2009.
(108) Ling, J.; Shen, J. G.; Hogen-Esch, T. E. *Polymer* **2009**, *50*, 3575.
(109) Dechy-Cabaret, O.; Martin-Vaca, B.; Bourissou, D. *Chem. Rev.* **2004**, *104*, 6147.
(110) Moller, M.; Kange, R.; Hedrick, J. L. *J. Polym. Sci. Pol. Chem.* **2000**, *38*, 2067.

Chapter 2

A_2B_2 Heterofunctional Initiator With Calix[4]arene Core

2.0. Introduction

Heterofunctional initiator systems are of much interest for their use in the synthesis of Miktoarm star polymeric systems. Macrocyclic compounds, such as calix[n]arenes, provide a suitable scaffold for such initiator systems due to their propensity for selective functionalisation of the lower and upper rims, allowing for versatile and intricate heterofunctional initiating systems.

In 2010, Gou *et al*. described the first calix[4]arene based A_2B_2 heterofunctional initiator, which employed initiating sites for both ring opening polymerisation (ROP) and azide-alkyne "click" chemistry (Fig. 2.1).[1]

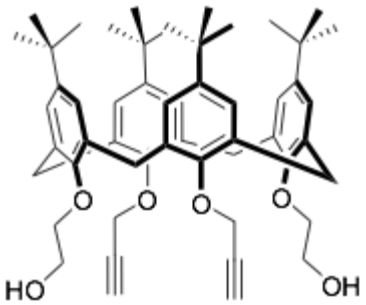

Figure 2.1. Heterofunctional initiator.

The overview of this chapter is to illustrate the synthesis of several novel derivatised calix[4]arene compounds that led to the synthesis of a novel A_2B_2 heterofunctional initiator. The ability of calix[4]arenes to be selectively alkylated on the lower rim was utilised. Traditional and cutting edge organic manipulations were used in the modification of compounds. The final A_2B_2 heterofunctional initiator incorporated primary hydroxyl moieties to allow for ROP of ε-caprolactone and alkyl-halogen moieties to facilitate single electron transfer living radical polymerisation (SET-LRP).

In the design of the synthetic strategy for an A_2B_2 heterofunctional initiator it was proposed to selectively allylate the lower rim of calix[4]arene diametrically, which would allow for two phenolic hydroxyls to be esterified with the acyl bromide moiety required for SET-LRP, but the esterification process could not be achieved, even under very basic conditions (Scheme. 2.1).

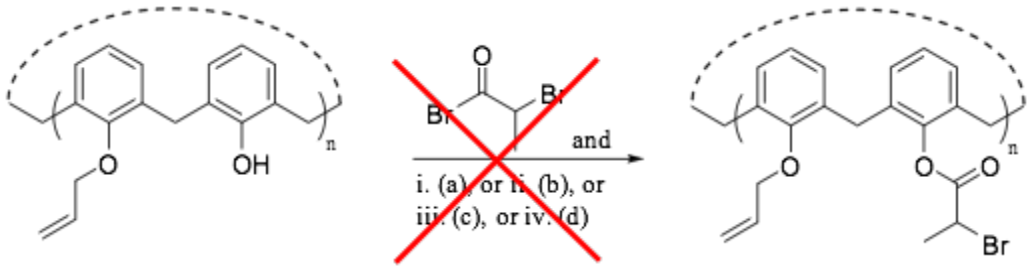

Scheme 2.1. Attempted Synthesis. (a) K_2CO_3, MeCN, reflux, (b) n-BuLi, toluene, -78 ^oC, (c) NaH, DMF/THF. (d) NEt_3, DICHLOROMETHANE.

An alternative strategy was implemented to introduce the alkyl halide moiety. The final synthetic strategy employed is shown in Scheme 2.2.

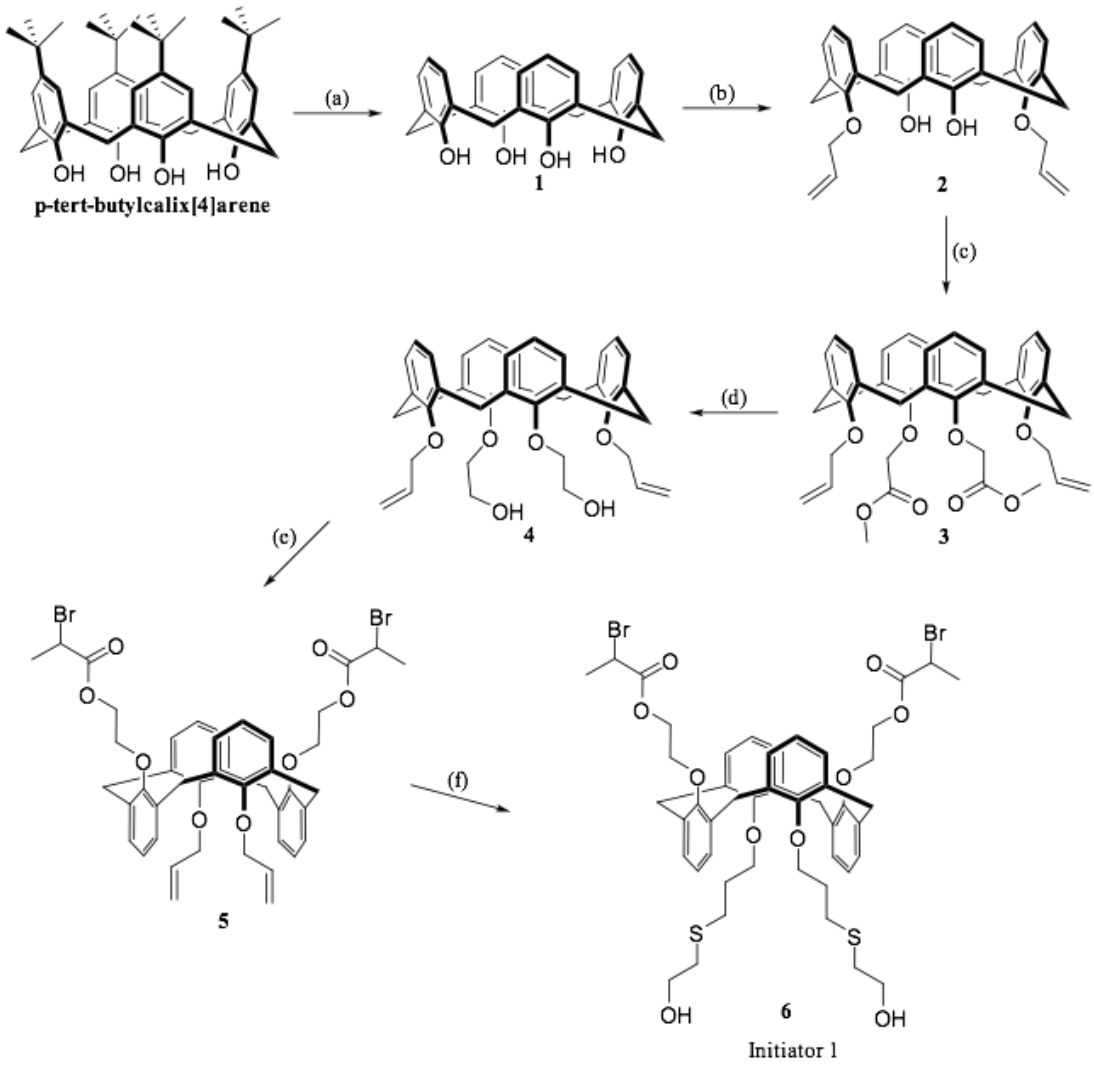

Scheme 2.2. Synthetic strategy employed for the synthesis of initiator 1. (a) $AlCl_3$, phenol, toluene. (b) allyl iodide, K_2CO_3, MeCN, (c) Methyl chloroacetate, K_2CO_3, KI, MeCN. (d) $LiAlH_4$, THF. (e) 2-bromopropionyl bromide, TEA, dichloromethane. (f) 2-mercaptoethanol, dichloromethane, UV.

The first step was a de-*tert*-butylation of the *p-tert*-butylcalix[4]arene, **1**. The second step was to selectively alkylate the lower rim of calix[4]arene with allyl moieties, **2**. The third step was introduction of an ester moiety *via* a Williamson ether synthesis of methyl chloroacetate to the remaining free phenolic hydroxyls on lower rim, **3**. The alkyl ester moiety was selected as is could be reduced to a primary hydroxyl that could facilitate the esterification of 2-bromopropionyl bromide. The fourth step was the reduction of the ester moiety, with $LiAlH_4$ selected as the reducing agent, **4**. The fifth step was the esterification of the primary hydroxyl with the acyl bromide of 2-bromopropionyl bromide, **5**. The sixth step was a photo initiated thiol-ene "click" reaction between the alkene of the allyl moiety of **5** and 2-mercaptoethanol, **6**, which was selected as it would introduce a primary hydroxyl to facilitate ROP. The reaction conditions and an in depth analysis of all compounds synthesised is described herein.

2.1. Experimental

2.1.1. Materials

p-tert-butylcalix[4]arene, allyl iodide (98%), anhydrous potassium carbonate (>99%), anhydrous potassium iodide (>99%), methyl chloroacetate (99%), lithium aluminium hydride pellets (95%), trimethylamine (>99.5%), 2-bromopropionyl bromide (97%), 2-mercaptoethanol (>99%) and magnesium sulfate were purchased from Sigma Aldrich and used without further purification. Chloroform, dichloromethane, hexane, ethyl acetate, methanol analytical grade solvents and hydrochloric acid (c.HCl, 37%) were purchased from Fisher Scientific and used without further purification. Dry acetonitrile (MeCN), Tetrahydrofuran (THF) and dichloromethane were obtained from the Durham University Chemistry Department Solvent Purification Service (SPS). Deuterated chloroform ($CDCl_3$) for NMR analysis was purchased from Apollo Scientific.

2.1.2. Instrumentation

^1H and ^{13}C NMR spectra were recorded using a Varian VNMRS 700 spectrometer operating at 700 MHz and 176 MHz respectively, with *J* values given in Hz. $CDCl_3$ was used as deuterated solvent for ^1H and ^{13}C NMR analysis and the spectra were

referenced to the solvent traces at 7.26 ppm and 77.0 ppm respectively. The following abbreviations are used in describing NMR spectra: s = singlet, d = doublet, t = triplet, q = quartet, quin = quintet, m = multiplet, b = broad, o = overlapped, dd = doublet of doublets, dq = doublet of quartets. Pure shift ^{1}H NMR spectroscopy was used when simplification and increased resolution of spectra was required, which is brought about from ^{1}H-^{1}H decoupling. 2D NMR experiments were also used to fully assign the proton and carbon environments in the products. ^{1}H-^{1}H Correlation Spectroscopy (COSY) demonstrated proton-proton correlations over two or three bonds. ^{1}H-^{13}C Heteronuclear Shift Correlation Spectroscopy (HSQC) demonstrated correlation between directly bonded proton and carbons atoms. ^{1}H-^{13}C Heteronuclear Multiple-Bond Correlation (HMBC) demonstrated the correlation between proton and carbon environments through several bonds.

Atmospheric Solids Analysis Probe Mass **S**pectrometry (ASAP MS) was carried out using a *LCT Premier XE* mass spectrometer and an Acquity UPLC (Waters Ltd, UK). A melting point tube was dipped into the sample solution (1 mg mL^{-1}). Samples were run isothermally at 350 °C. The sample was vaporised from the melting point tube enabling atmospheric pressure chemical ionisation (APCI) to occur.

Fourier transform-infra-red (FT-IR) spectroscopy was conducted using a Perkin Elmer 1600 series spectrometer.

Elemental analyses of small molecules were obtained using an Exeter CE-440 elemental analyser at the University of Durham.

Thiol-ene reactions were conducted using a *Fusion UV LC6B Benchtop Conveyor*. The samples were placed in glass vials and dissolved in chloroform. The samples were passed under the UV source on a conveyer belt, with a UV exposure time of 15 seconds. The UV lamp was operating at 200 watt cm^{-2}.

2.1.3. Synthesis of calix[4]arene, 1

The synthesis of compound **1** was carried out following a known procedure.[2] To a 500 mL 3-necked round bottomed flask fitted with a septum, stopper and nitrogen inlet, *p-tert*-butylcalix[4]arene (40.001 g, 94.34 mmol) was added. The system was heated to 100 ^{o}C and placed under reduced pressure for 3 h. The system was allowed to cool and then flushed with dry nitrogen. Dry toluene (200 mL) was cannulated into the flask leading to an opaque cream solution, which was stirred vigorously. Phenol (5.64 mL, 64.14 mmol) was injected into the reaction mixture, which was followed by the addition of aluminium(III) chloride (40.000 g, 303.28 mmol). The solution turned yellow with simultaneous formation of a red residue that stuck onto the sides of the flask. The reaction was stirred for 3 h with the solution turning opaque yellow to orange as the red residue dissolved. The reaction mixture was poured over ice (600 g) turning white. The reaction mixture was transferred to a separating funnel with the addition of dichloromethane (800 mL). The pale yellow organic layer was collected and washed with HCl 10% (3 x 150 mL) and brine (400 mL) then dried over $MgSO_4$ and filtered. The translucent pale yellow solution was reduced *in vacuo* leading to a viscous cream coloured solution. Diethyl ether (50 mL) was added leading to the formation of a pale yellow solution and white solid, the mixture was allowed to stand for 2 h at -24 ^{o}C. The white solid was collected and washed with diethyl ether. Mass = 21.43 g, yield = 84%. ν_{max} (Perkin Elmer FT-IR, Diamond, cm^{-1}). 3152 (m, OH). ^{1}H NMR (700 MHz, $CDCl_3$) δ: 3.55 (s, 4 H_a), 4.25 (s, 4H_b), 6.73 (t, 4H_c, J = 7.6), 7.06 (d, 4H_d, J = 7.6), 10.20 (s, 2H_e). ^{13}C NMR (176 MHz, $CDCl_3$) δ: 31.8 (**a'**), 122.4 (**b'**), 128.4 (**c'**), 129.1 (**d'**), 148.9 (**e'**). Mass spectrum (ASAP MS); m/z = 425.2, (100%) $[M + H]^+$.

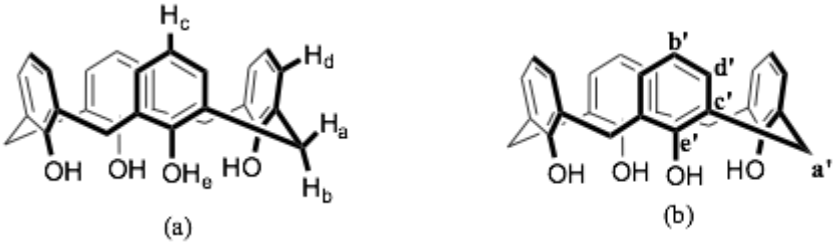

Figure 2.2. Labelling of the chemical environments in compound **1** (a) proton (b) carbon

2.1.4. Synthesis of 25,27-*bis*(prop-2-en-1-yloxy)calix[4]arene, 2

The synthesis of compound **2** was performed using a modified known procedure.[2] To a 150 mL 2-necked round bottomed flask fitted with a septum, reflux condenser and stopper, **1** (3.253 g, 7.67 mmol) and potassium carbonate (1.063 g, 7.69 mmol) were added. The flask was evacuated (0.5 h) then purged with dry nitrogen. Under nitrogen dry MeCN (60 mL) was transferred in *via* cannula. Allyl iodide (1.40 mL, 15.30 mmol) was syringed into the reaction mixture leading to a cream/yellow coloured solution. The reaction mixture was refluxed for 48 h. A blue/green coloured solution resulted. The MeCN was reduced *in vacuo* resulting in a blue/green coloured residue. The residue was taken up in HCl 10% (50 mL) and dichloromethane (150 mL) and added to a separating funnel. The translucent pale red/orange organic phase was collected and further washed with brine (2 x 50 mL), then dried over magnesium sulphate and filtered. The volume of dichloromethane was reduced *in vacuo* to ~5 mL. Methanol (30 mL) was added and the remaining dichloromethane was removed *in vacuo* leading to the precipitation of a pale red solid. The pale red solid was collected under reduced pressure. The product was purified *via* column chromatography using hexane:ethyl acetate in a 20:1 on silica. Mass = 2.784 g, yield = 72%. M.p. = 255-56 ºC.[1] ν_{max} (Perkin Elmer FT-IR, Diamond, cm^{-1}). 3290 (m, OH), 1638 (m, C=C). ^{1}H NMR (700 MHz, $CDCl_3$) δ: 3.39 (d, 4 H_a, J = 13.2), 4.33 (d, 4H_b, J = 13.2), 4.55 (d, 4H_c, J = 4.8 Hz), 5.42 (dd. 4H_d, J_1 =10.8 Hz, J_2 = 1.6 Hz) 5.78 (dd, 2H_e, J1 = 16.8 Hz, J2 = 1.6 Hz) 6.27 (m, 2H_f), 6.66 (t, 2H_g, J = 7.2 Hz), 6.75 (t, 2H_h, J = 7.2 Hz), 6.91 (d, 4H_i, J = 7.2 Hz), 7.06 (d, 4H_j, J = 7.02 Hz), 7.97 (s, 2H_k) . ^{13}C NMR (176 MHz, $CDCl_3$) δ: 31.6 (**a'**), 76.8 (**b'**), 118.1 (**c'**), 119.2 (**d'**), 125.6 (**e'**), 128.3 (**f'**), 128.6 (**g'**), 129.1 (**h'**), 132.9 (**i'**), 133.5 (**j'**), 151.9 (**k'**), 153.4 (**l'**). Mass spectrum (ASAP MS); *m/z* = 505.230, (100%) $[M][H]^+$. CHN expected = %C = 80.93, %H = 6.39, %N 0.00; measured %C = 81.01, %H = 6.45, %N 0.00.

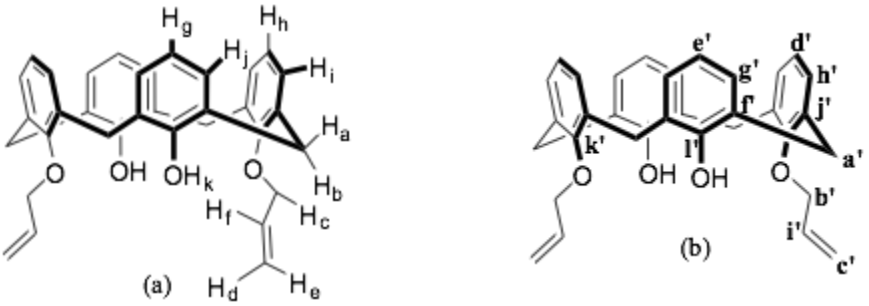

Figure 2.3. Labelling of the chemical environments in compound **2** (a) proton (b) carbon

2.1.5. Synthesis of 25,27-bis(prop-2-en-1-yloxy)-26,28-bis(ethyleneacetate)-calix[4]arene, 3

To a 150 mL 2-necked round bottomed flask fitted with a septum, reflux condenser and stopper, **2** (1.650 g, 3.27 mmol), potassium carbonate (1.112 g, 8.05 mmol) and potassium iodide (0.201 g, 1.21 mmol) were added. The flask was evacuated (0.5 h) then purged with dry nitrogen. Under nitrogen dry MeCN (40 mL) was transferred in *via* cannula. Methyl chloroacetate (0.70 mL, 7.99 mmol) was syringed into the reaction mixture leading to a cream/yellow opaque solution. The reaction mixture was refluxed for 48 h. A cream coloured opaque solution resulted. The MeCN was reduced *in vacuo* resulting in a cream coloured residue. The residue was taken up in HCl 10% (40 mL) and dichloromethane (100 mL) and added to a separating funnel. The translucent pale yellow organic phase was collected and further washed with brine (2 x 40 mL), then dried over magnesium sulphate and filtered. The volume of dichloromethane was reduced *in vacuo* leading to a brown sticky residue. The residue was purified *via* column chromatography using hexane:ethyl acetate in a 20:1 on silica, a white tacky residue was obtained. Mass = 1.102 g, yield = 52%. ν_{max} (Perkin Elmer FT-IR, Diamond, cm^{-1}). 1760. ^1H NMR (700 MHz, $CDCl_3$) δ: 3.16 (d, 1.1H_{a1}, J = 14.0 Hz), 3.20 (d, 4H_{a1}, J = 13.6 Hz), 3.60 (s, 1.5H_{b2}), 3.69 (d, 1.1H_{c2}, J = 13.3 Hz), 3.80 (s, 6H_{b1}), 3.81 (om, 1H_{d2}), 3.84 (s, 1.5H_{e2}), 4.00 (s, 1H_{f2}), 4.23 (dd, 1.1H_{g2}, J_1 = 12.7 Hz, j_2 = 5.0 Hz), 4.31 (dd, 1.1H_{h2}, J_1 = 12.7 Hz, J_2 = 5.0 Hz), 4.55 (d, 4H_{c1}, J = 13.6 Hz), 4.57 (s, 4H_{d1}), 4.61 (d, 4H_{e1}, J = 6.5 Hz), 5.16 (d, 2H_{f1}, J = 9.5 Hz), 5.21 (d, 2H_{g1}, J = 17.2 Hz), 5.27 (d, 1H_{k2}, J = 10.7 Hz), 5.42 (d, 1H_{l2}, J = 16.9 Hz), 6.13 (m, 1.1H_{m2}), 6.31 (d, 1H_{n2}, J = 7.6 Hz), 6.42 (m, H_{h1}), 6.51 (m, 6H_{i1}), 6.52 (om, 2H_{o2}), 6.71 (t, 2H_{j1}, J = 7.5 Hz), 6.79 (d, 4H_{k1}, J = 7.5 Hz), 6.89 (t, 0.6H_{p2},

J = 7.5 Hz), 6.97 (t, 0.6H_{q2}, *J* = 7.5 Hz), 7.07 (d, 1H_{r2}, *J* = 7.5 Hz), 7.09 (d, 1H_{s2}, *J* = 7.4 Hz), 7.30 (d, 1H_{t2}, *J* = 7.5 Hz). ^{13}C NMR (176 MHz, $CDCl_3$) δ:31.5 (**a$_1$'**), 31.8 (**a$_2$'**), 35.4 (**b$_2$'**), 51.2 (**c$_2$'**), 51.8 (**b$_1$'**), 52.0 (**d$_2$'**), 67.3 (**e$_2$'**), 70.2 (**f$_2$'**), 71.4 (**c$_1$'**), 75.1 (**g$_2$'**), 76.0 (**d$_1$'**), 116.5 (**h$_2$'**), 117.1 (**e$_1$'**), 122.4 (**i$_2$'**), 122.5 (**j$_2$'**), 122.6 (**f$_1$'**), 122.7 (**k$_2$'**), 122.9 (**g$_1$'**), 128.4 (**h$_1$'**), 128.6 (**i$_1$'**), 128.7 (**l$_2$'**), 129.1 (**m$_2$'**), 129.4 (**n$_2$'**), 131.1 (**o$_2$'**), 132.2 (**p$_2$'**), 133.6 (**q$_2$'**), 133.9 (**r$_2$'**), 134.2 (**j$_1$'**), 134.7 (**s$_2$'**), 135.9 (**k$_1$'**), 136.4 (**t$_2$'**), 155.1 (**u$_2$'**), 155.3 (**v$_2$'**), 155.5 (**l$_1$'**), 156.3 (**m$_1$'**), 156.7 (**w$_2$'**), 170.0 (**x$_2$'**), 170.2 (**n$_1$'**), 171.1 (**y$_2$'**). Mass spectrum (ASAP MS); *m/z* = 649.272, (100%) $[M+H]^+$. CHN expected = %C = 74.06, %H = 6.22, %N 0.00; measured %C = 74.45, %H = 6.48, %N 0.00.

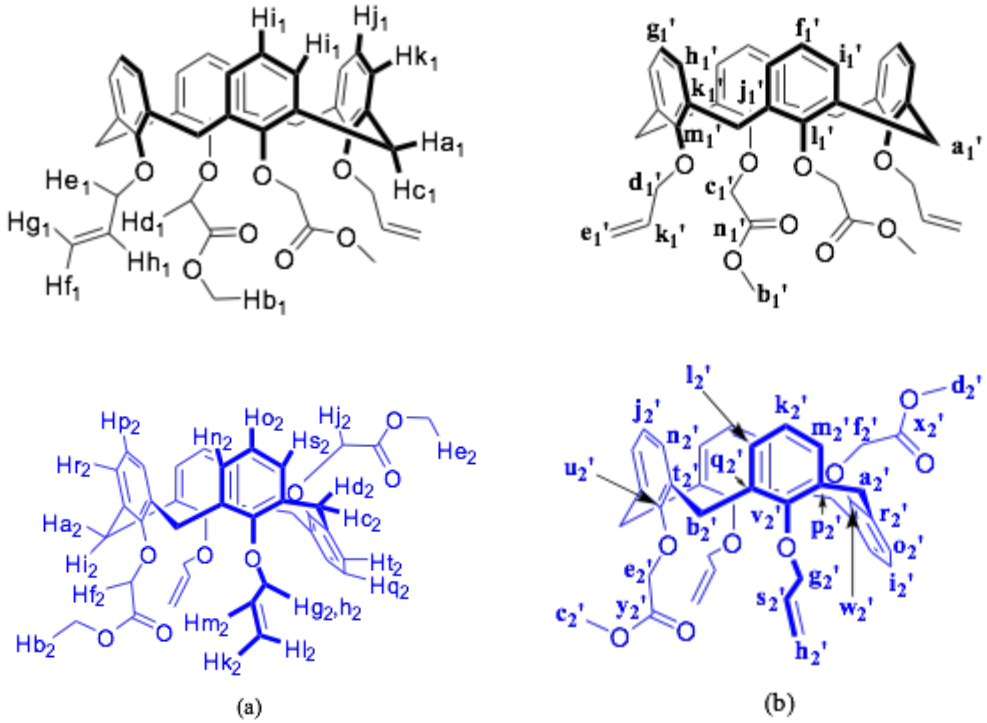

Figure 2.4. Labelling of the chemical environments in compound **3** (a) proton (b) carbon

2.1.6. Synthesis of 25,27-*bis*(prop-2-en-1-yloxy)-26,28-*bis*(ethanolxy)calix[4]arene, 4

To a 50 mL 2-necked round bottomed flask fitted with a septum and reflux condenser, **3** (0.855 g, 1.01 mmol), was added. The flask was evacuated (0.5 h) then purged with dry nitrogen. Under nitrogen, dry THF (20 mL) was transferred in *via* cannula forming a translucent colourless solution. $LiAlH_4$ (1M in diethyl ether, 3.96

mL, 3.96 mmol) was injected in drop wise. The solution first turned opaque then translucent and was left to stir at 23 ^{o}C for 0.5 h and then a further 1.5 h at 50 ^{o}C. The reaction mixture was carefully quenched by the drop wise addition of water. The solvent was removed under reduced pressure leading to a white residue, which was collected in dichloromethane (50 mL) and HCl 10% (30 mL) and added to a separating funnel. The translucent pale yellow organic phase was collected and further washed with brine (2 x 25 mL), then dried over magnesium sulphate and filtered. The volume of dichloromethane was reduced *in vacuo* leading to a white amorphous solid. The residue was purified *via* column chromatography using dichloromethane on silica; a white amorphous solid was obtained. Mass = 0.695 g, yield = 89%. ν_{max} (Perkin Elmer FT-IR, Diamond, cm^{-1}). 3380. ^{1}H NMR (700 MHz, $CDCl_3$) δ: 3.21 (d, 4H$_a$, *J* = 13.5 Hz), 3.88 (m, 4H$_b$), 4.17 (m, 4H$_c$), 4.34 (d, 4H$_d$, *J* = 6.4 Hz), 4.38 (d, 4H$_e$, J = 13.5 Hz), 4.79 (t, 2H$_f$, *J* = 6.2 Hz), 5.28 (m, 2H$_g$), 5.29 (dm, 2H$_h$, *J* = 19.1), 6.17 (d, 4H$_i$, *J* = 7.6 Hz), 6.20 (m, 2H$_j$), 6.28 (t, 2H$_k$, *J* = 7.6 Hz), 6.99 (t, 2H$_l$, *J* = 7.4 Hz), 7.17 (d, 4H$_m$, *J* = 7.5 Hz). ^{13}C NMR (176 MHz, $CDCl_3$) δ: 31.0 (**a'**), 61.7 (**b'**), 77.3 (**c'**), 77.4 (**d'**), 119.3 (**e'**), 123.1 (**f'**), 123.1 (**g'**), 128.0 (**h'**), 129.3 (**i'**), 133.1 (**j'**), 135.5 (**k'**),136.9 (**l'**), 153.1 (**m'**), 157.3 (**n'**). Mass spectrum (ASAP MS); *m/z* = 593.290, (100%) $[M+H]^+$. CHN expected = %C = 77.00, %H = 6.80, %N 0.00; measured %C = 77.23, %H = 6.94, %N 0.00.

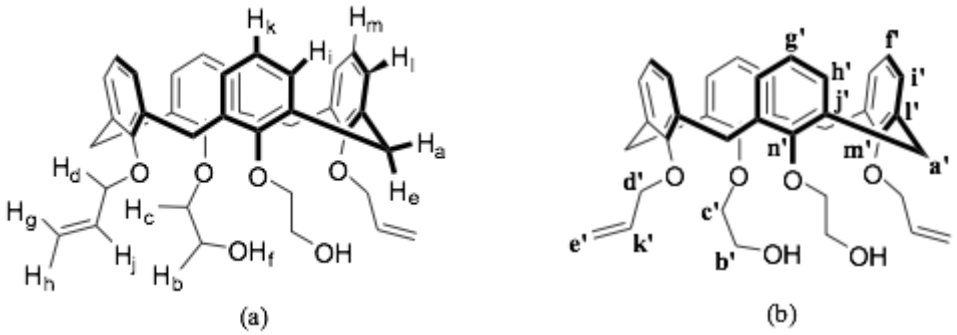

Figure 2.5. Labelling of the chemical environments in compound **4** (a) proton (b) carbon

2.1.7. Synthesis of 25,27-*bis*(prop-2-en-1-yloxy)-26,28-*bis*(ethoxyester-2-bromo-acetate)calix[4]arene, 5

To a 50 mL 2-necked round bottomed flask fitted with a septum and reflux condenser, **4** (0.345 g, 0.63 mmol) was added. The flask was evacuated (0.5 h) then purged with dry nitrogen. Under nitrogen, dry chloroform (15 mL) was transferred in

via cannula forming a translucent colourless solution. NEt_3 (0.300 mL, 2.16 mmol) was injected in followed by the drop wise addition of 2-bromopropionyl bromide (0.264 mL, 2.52 mmol). The solution turned translucent brown and was left to stir at 23 ^oC for 2 h, and turned yellow over this period. The reaction mixture was carefully quenched by the drop wise addition of water. The reaction mixture was collected in additional chloroform (20 mL) and washed with HCl 10% (30 mL) and with brine (2 x 25 mL), then dried over magnesium sulphate and filtered. The volume of dichloromethane was reduced *in vacuo* leading to a brown sticky residue. The residue was purified *via* column chromatography using hexane:ethyl acetate in a ratio of 9:1 on silica. A colourless sticky residue was obtained. Mass = 0.421 g, yield = 78%. ν_{max} (Perkin Elmer FT-IR, Diamond, cm^{-1}). 2850-3100 (m, CH), 1739 (s, C=O), 1638 (m, C=C). ^1H NMR (700 MHz, $CDCl_3$) δ: 1.87 (d, $6H_a$, J = 6.8 Hz), 3.60-3.72 (m, $4H_b$) 3.68 (s, $6H_c$), 4.15 (m, $4H_d$), 4.16 (m, $4H_e$), 4.45 (q, $2H_f$, J = 6.8 Hz), 5.08 (dd, $2H_g$, J_1 = 17.2 Hz, J_2 = 2 Hz), 5.14 (dd, $2H_h$, J_1 = 10.8 Hz, J_2 = 1.6 Hz), 5.84 (m, $2H_i$), 6.69 (t, $2H_j$, J = 7.6 Hz), 6.80 (t, $2H_k$, J = 7.6 Hz), 6.99 (d, $4H_l$, J = 7.6Hz), 7.09 (d, $4H_m$, J = 7.6 Hz). ^{13}C NMR (176 MHz, $CDCl_3$) δ:.21.8 (**a'**), 36.9 (**b'**), 40.0 (**c'**), 65.1 (**d'**), 68.6 (**e'**), 71.8 (**f'**), 116.2 (**g'**), 122.5 (**h'**), 130.0 (**i'**), 131.0 (**j'**), 133.4 (**k'**), 133.9 (**l'**), 134.3 (**m'**), 155.4 (**n'**), 156.2 (**o'**), 170.4 (**p'**). Mass spectrum (ASAP MS); *m/z* = 862.162, (100%) $[M+H]^+$. CHN Expected = %C = 62.26, %H = 5.38, %N = 0.00; Measured %C = 62.11, %H = 5.36, %N = 0.00.

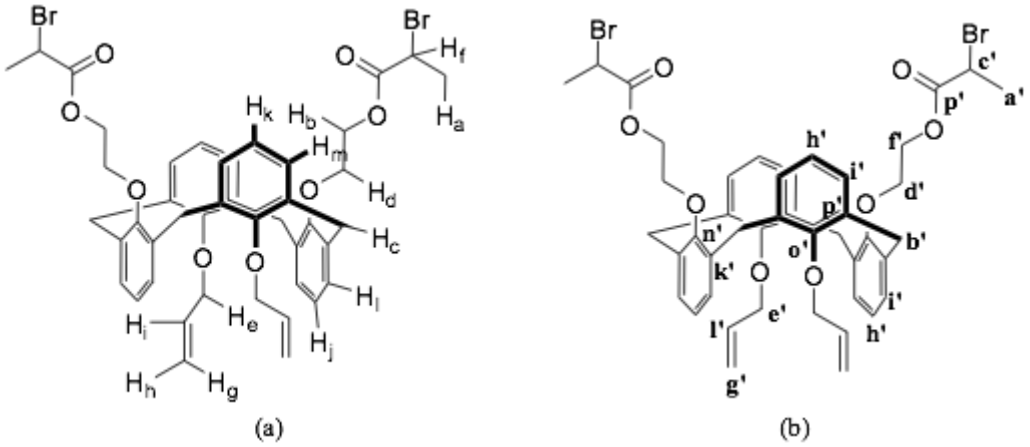

Figure 2.6. Labelling of the chemical environments in compound **5** (a) proton (b) carbon

2.1.8. Synthesis of 25,27-*bis*(3-(hydroxyethyl)thioether-propan-1-yloxy)-26,28-*bis*(ethoxyester-2-bromo-acetate)calix[4]arene, 6

To a 10 mL glass vial, 25,27-*bis*(prop-2-en-1-yloxy)-26,28-*bis*(ethoxyester-2-bromo-acetate)calix[4]arene, **5** (0.300 g, 0.35 mmol), was added and dissolved in chloroform (3 mL). To the vial, 2-mercaptoethanol (0.098 mL, 1.39) was added. The sample was irradiated with a broad wavelength UV lamp for 30 seconds, a colourless solution remained. The chloroform was removed *in vacuo* leaving a viscous colourless liquid. The residue was purified *via* column chromatography using hexane:ethyl acetate on silica, starting at a ratio of 10:1 slowly moving to pure ethyl acetate resulting in a tacky colourless residue. Mass = 0.326 g, yield = 92%. ν_{max} (Perkin Elmer FT-IR, Diamond, cm^{-1}). 3306 (s, OH), 2923 (s, CH), 1732 (s, C=O). ^{1}H NMR (700 MHz, $CDCl_3$) δ: 1.62 (quin, $4H_a$, J = 8.1 Hz) 1.85 (d, $6H_b$, J = 8.0 Hz), 2.36 (t, $4H_c$, J = 8.4 Hz), 2.74 (t, $4H_d$, J = 7.0 Hz), 3.55 (t, $4H_e$, J = 6.5 Hz), 3.60 (t, $4H_f$, J = 7.8 Hz), 3.75 (t, $4H_g$, J = 7.0 Hz), 3.79 (s, $8H_h$), 3.83 (m, $4H_i$), 4.38 (q, $2H_k$, J = 8.1 Hz), 6.84 (m, $8H_l$), 7.05 (d, $4H_l$, J = 8.9 Hz), 7.10 (m, $4H_i$).^{13}C NMR (176 MHz, $CDCl_3$) δ: 21.7 (**a'**), 28.1 (**b'**), 30.0 (**c'**), 35.2 (**d'**), 37.5 (**e'**), 39.9 (**f'**), 60.5 (**g'**), 64.4 (**h'**), 67.6 (**i'**), 69.4 (**j'**), 122.8 (**k'**), 129.7 (**l'**), 133.9 (**m'**), 155.6 (**n'**), 156.9 (**o'**), 170.2 (**p'**). Mass spectrum (ASAP MS); *m/z* = 1019.182, (7.61%) $[M+H]^+$. CHN Expected = %C = 57.38, %H = 4.41, %N = 0.00; Measured %C = 57.48, %H = 4.56, %N = 0.00.

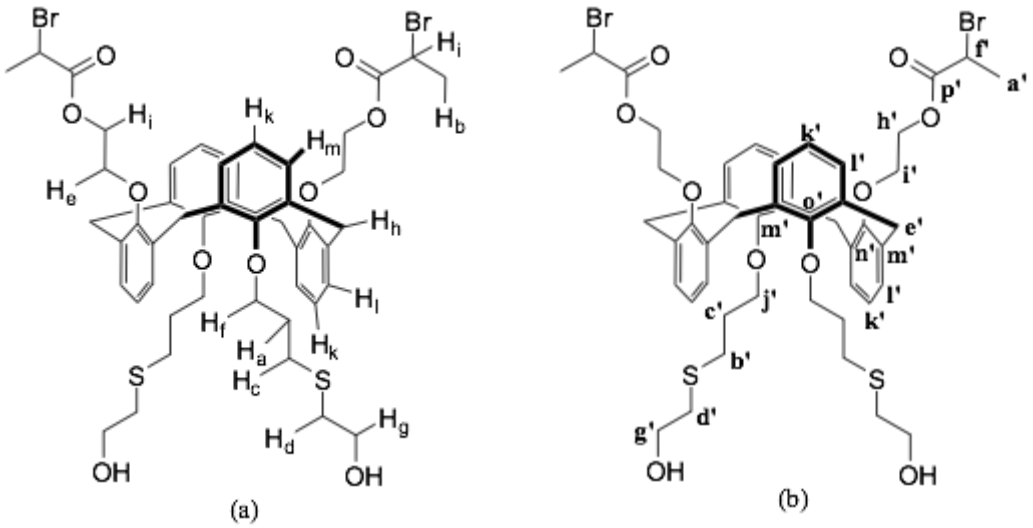

Figure 2.7. Labelling of the chemical environments in compound **6** (a) proton (b) carbon

2.2. Results and Discussion

2.2.1. Calix[4]arene, 1

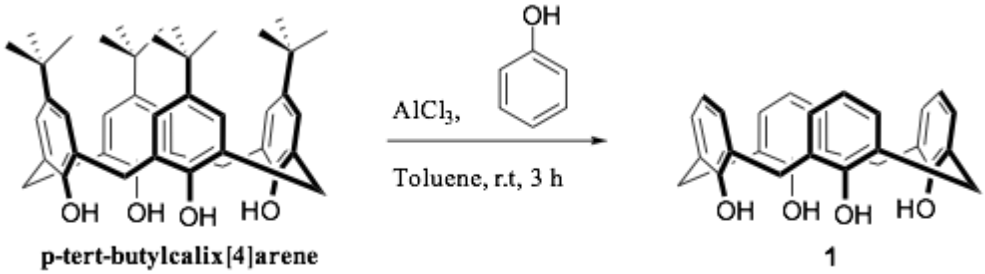

Scheme 2.3. Synthesis of **1**

The synthesis of **1** was carried out according to the classic procedure using aluminium(III) chloride in the presence of phenol in toluene (Scheme. 2.3).[2,3] The *tert*-butyl moiety of **1** are removed *via* an aluminium(III) chloride catalysed transalkylation.[4,5] The aluminium(III) chloride initially reacts with phenol forming an alkoxide complex in the toluene solvent. ***p-tert*-butylcalix[4]arene** is added to the mixture at once. The aluminium complex coordinates to the hydroxyl moieties as a Lewis acid with the simultaneous formation of HCl. The Lewis acidic aluminium chloride draws electron density away from the *tert*-butyl moiety facilitating the loss of the tertiary carbocation. This will react with the HCl formed in-situ, forming an alkyl chloride and the anionic aromatic ring will pick up the proton. The newly formed alkyl chloride reacts with a toluene solvent molecule *via* a reverse Friedel-Craft reaction. The proposed mechanism is shown, Scheme 1.4 (Chapter 1).[4] A complete thorough analysis of **1** discussed is herein to further the previous characterisation.[2,3]

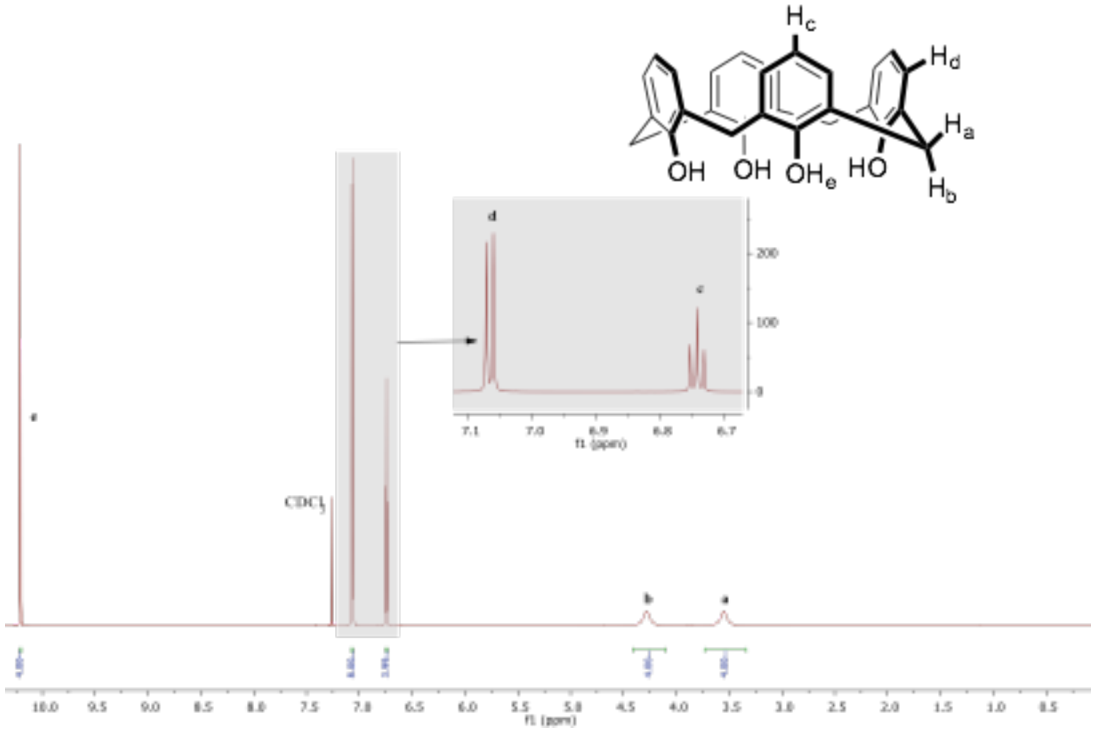

Figure 2.8. ^{1}H NMR spectrum of **2** in $CDCl_3$.

The ^{1}H NMR spectrum (Fig. 2.8) showed that the desired calix[4]arene, **1**, had been synthesised. The *tert*-butyl moiety singlet resonance of the starting material is no longer observed at 1.21 ppm. Two singlet resonances with integrals of four are observed at 3.55 and 4.25 ppm, **a** and **b**, which correspond to the methylene protons H_a and H_b, respectively. The two broad singlet resonances indicate that at room temperature the molecule is in the cone conformation.[6] A triplet resonance is observed at 6.73 ppm, **c**, corresponding to the hydrogen atoms *para* to the hydroxyl moiety of the aromatic ring, H_c. The triplet multiplicity is brought about by coupling to hydrogen atoms either side of H_c, H_d (Fig. 2.8). A doublet resonance is observed at 7.06 ppm, **d**, corresponding to the *meta* hydrogen atoms with respect to the hydroxyl of the phenolic ring, H_d. The doublet multiplicity is brought about by coupling to the single *para* hydrogen atom with respect to the hydroxyl of the phenolic ring, H_c. The coupling between H_c and H_d is confirmed by COSY NMR spectroscopy (Fig. 2.9).

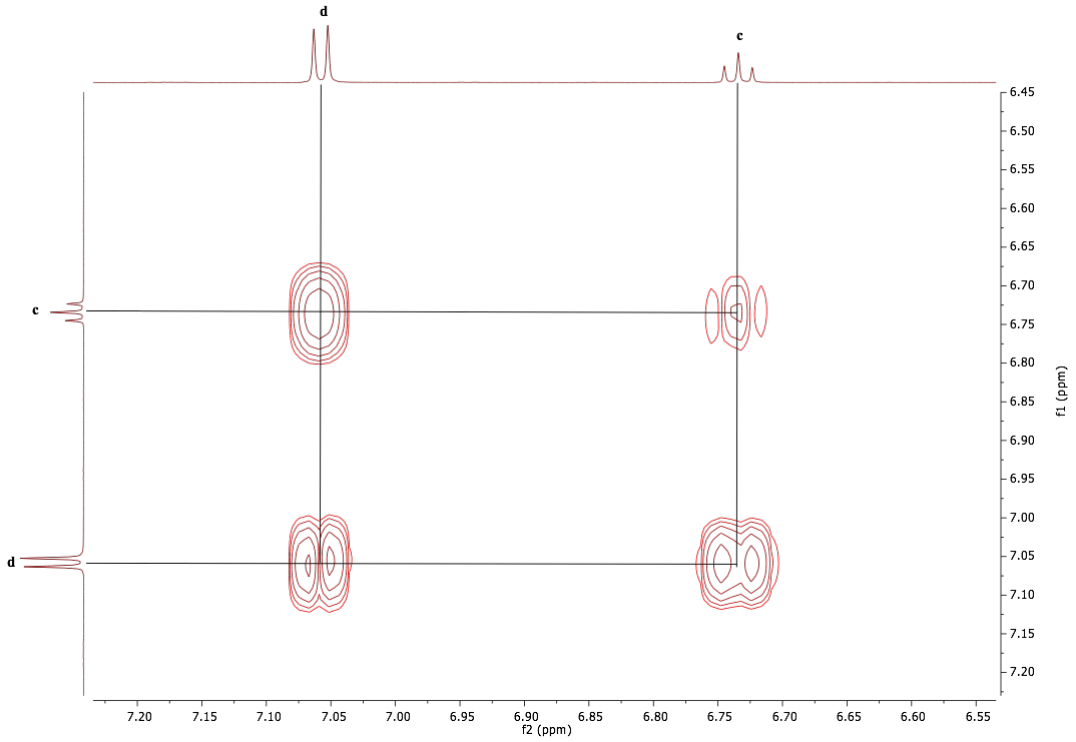

Figure 2.9. COSY spectrum of **1**, showing the coupling between NMR resonances **c** and **d** in $CDCl_3$.

A sharp ^{1}H NMR resonance is observed at 10.20 ppm (Fig. 2.8) corresponding to the proton of the hydroxyl moiety, H_e. The sharp peak resonating at a downfield position is a result of strong hydrogen bonding between the four hydroxyl moieties of the calix[4]arene, leading to the protons being highly deshielded. Infrared spectroscopy was carried out and a broad absorption was observed at 3120 cm^{-1}, indicating the presence of hydroxyl moieties with strong hydrogen bonding. To assign the ^{13}C NMR spectrum, HSQC NMR and HMBC NMR spectroscopy were carried out. Using HSQC NMR spectroscopy the carbon atoms directly attached to hydrogen atoms could be easily assigned.

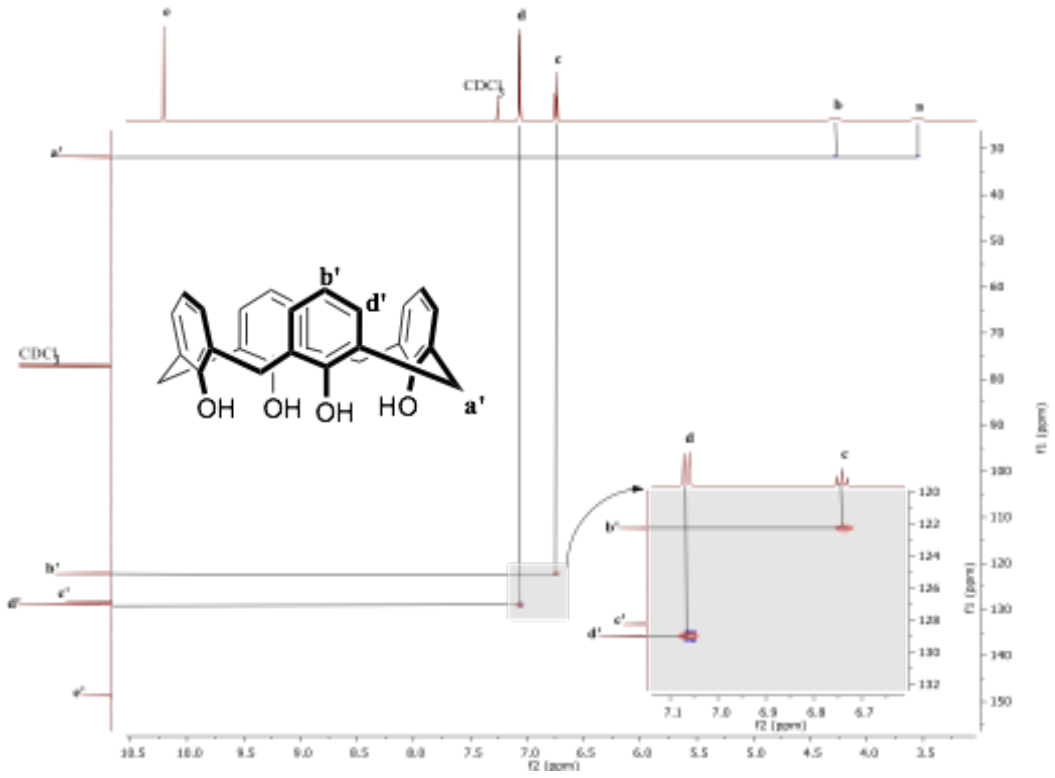

Figure 2.10. HSQC NMR spectrum of **1**, showing the coupling between hydrogen and carbon atoms, in $CDCl_3$.

From the HSQC spectrum (Fig. 2.10) it is observed that the methylene proton resonances, **a** and **b**, couple to a ^{13}C NMR resonance at 31.8 ppm, **a'**, thus **a'** must correspond to the bridging methylene carbon atom between aromatics. The fact that the methylene carbon atom exhibits a resonance at 31.8 ppm is further evidence that the calix[4]arene exists in the cone conformation.[7] The HSQC NMR spectrum (Fig. 2.10) shows **c** coupling to a ^{13}C NMR resonance at 122.4 ppm, **b'**, thus corresponds the carbon atom of the aromatic ring in the *para* position relative to the phenolic hydroxyl moiety. **d** couples to a ^{13}C NMR resonance at 129.1 ppm, **d'**, thus corresponds the carbon atom of the aromatic ring in the *meta* position relative to the phenolic hydroxyl moiety. Using HMBC NMR spectroscopy the remaining ^{13}C NMR resonances could be assigned accurately.

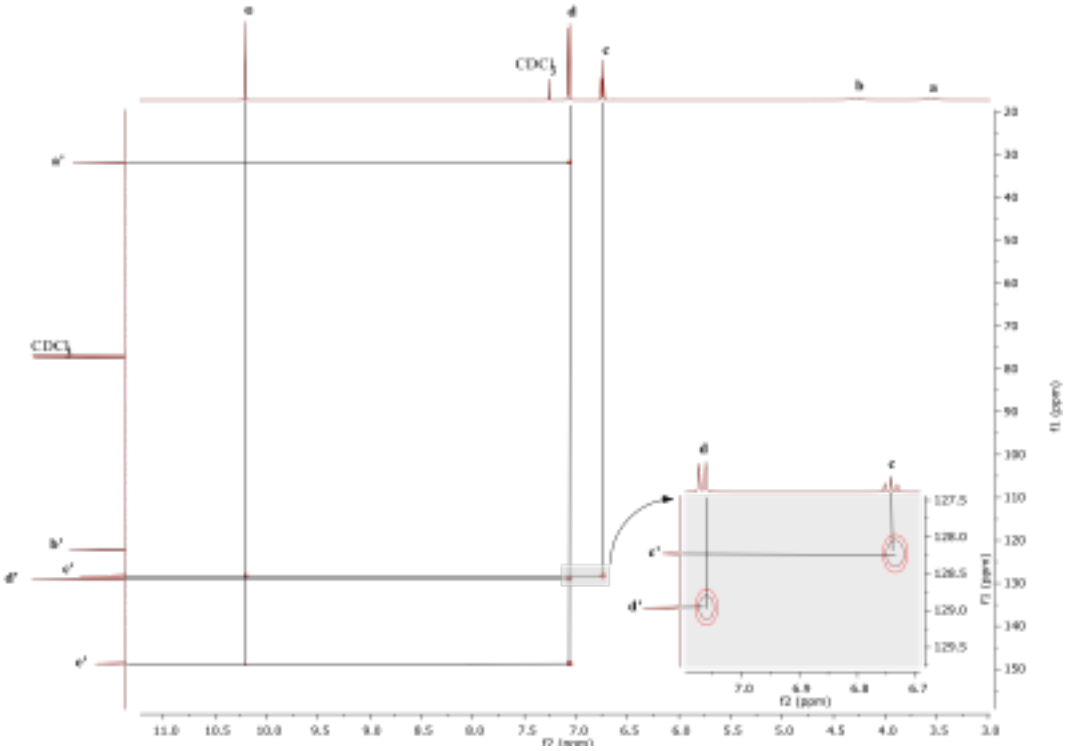

Figure 2.11. HMBC NMR spectrum of **1**, showing the coupling between hydrogen and carbon atoms in $CDCl_3$.

The HMBC NMR spectrum (Fig. 2.11) shows **c** coupling to a ^{13}C NMR resonance at 128.4 ppm, **c'**. Additionally, **c'** couples to the ^{1}H NMR resonance **e** corresponding to the hydroxyl hydrogen atom. Due to fact that in HMBC NMR spectroscopy of aromatic systems, two bond coupling is often not observed or is very weak, **c'** must correspond to the carbon atom in the *ortho* position with respect to the hydroxyl moiety of the phenolic ring (Fig. 2.12). The HMBC NMR spectrum (Fig. 2.11) shows **d** coupling to three ^{13}C NMR resonances, **a'**, **d'** and **e'**. In theory, single bond coupling is not expected, so a coupling between **d** and **d'** would not be expected but as shown can be observed. Due to the fact that the ^{13}C NMR resonance at 148.9 ppm, **e'**, exhibits a strong coupling to **d** through three bonds, no coupling to **c**, which would be a five bound coupling, and a weak coupling to **e**, **e'** must correspond to the *ipso* carbon atom of the phenolic ring with respect to the hydroxyl moiety (Fig. 2.12). The *ipso* carbon atom would be expected to be the most downfield carbon atom as it resides next to an oxygen. The complete assignment of the ^{13}C NMR spectrum is shown in Figure 2.12.

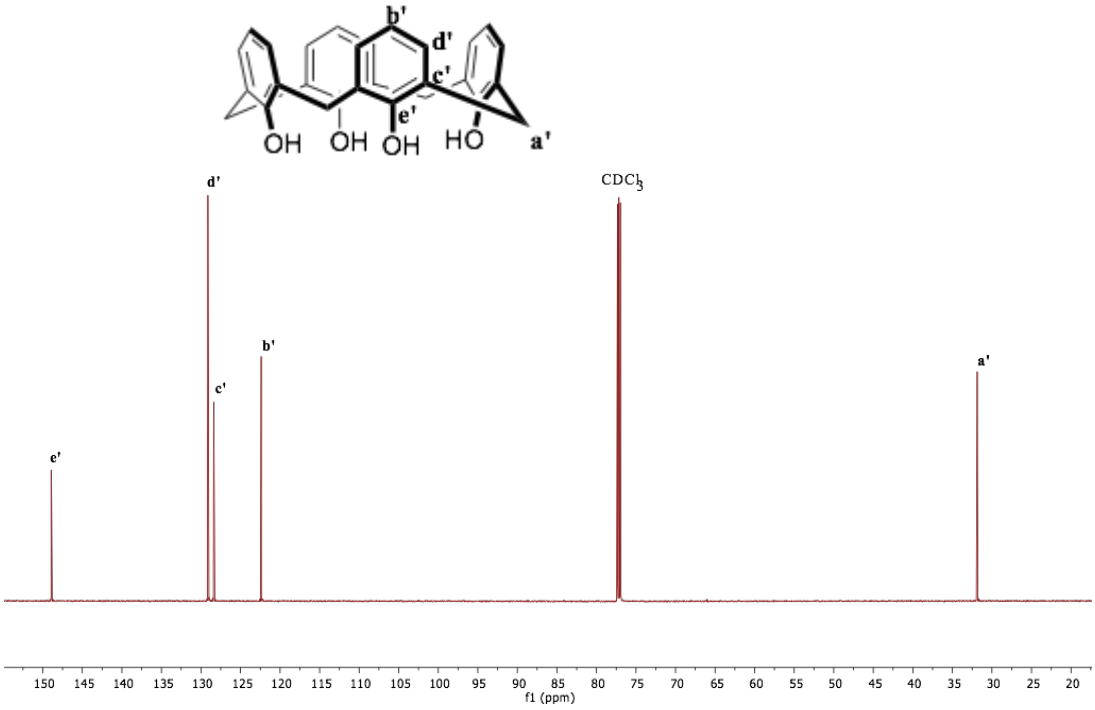

Figure 2.12. ^{13}C NMR spectrum of **1** in $CDCl_3$.

ASAP mass spectrometry was carried out and the molecular ion was seen at 425.161 Da (100%, Fig. 2.13), which corresponds to the empirical formula $C_{28}H_{24}O_4^+$.

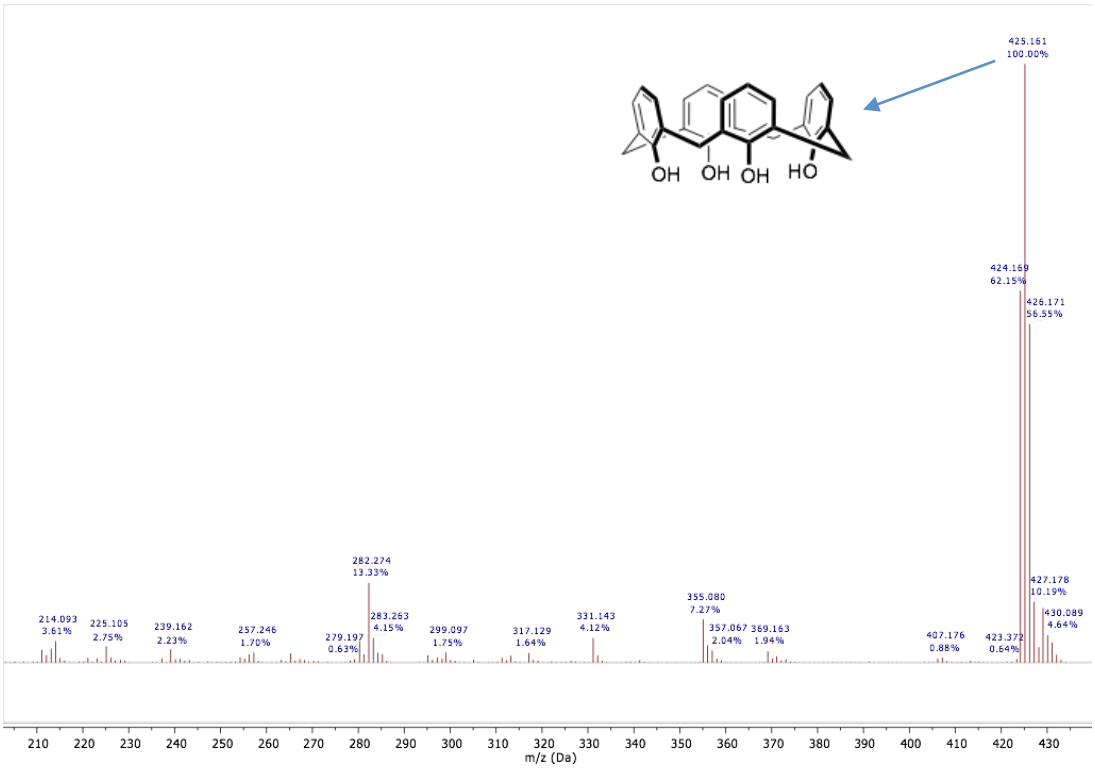

Figure 2.13. ASAP MS spectrum of **1**.

2.2.2. 25,27-*bis*(prop-2-en-1-yloxy)calix[4]arene, 2

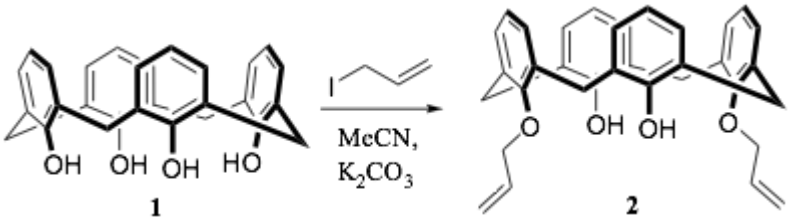

Scheme 2.5. Synthesis of **2**

Compound **2** is a known compound and was successfully synthesised according to the literature with the modification of replacing methyl iodide with allyl iodide (Scheme 2.5).[2] Previously discussed in the section 1.4 (Fig. 1.3), the lower rim can be alkylated diametrically due to the way in which the hydroxyl moieties are deprotonated in a step by step fashion resulting from their distinct pKa values. The distinct pKa values result from stabilising effects from the adjacent hydroxyl moiety, which increase as alkylation proceeds.[8] After the first deprotonation, alkylation occurs leading to a neutral molecule, which results in the diametric proton becoming acidic with a pKa of ~4 due to the stabilisation from two adjacent hydroxyl moieties, a mechanistic route is shown (Scheme 2.6).[9]

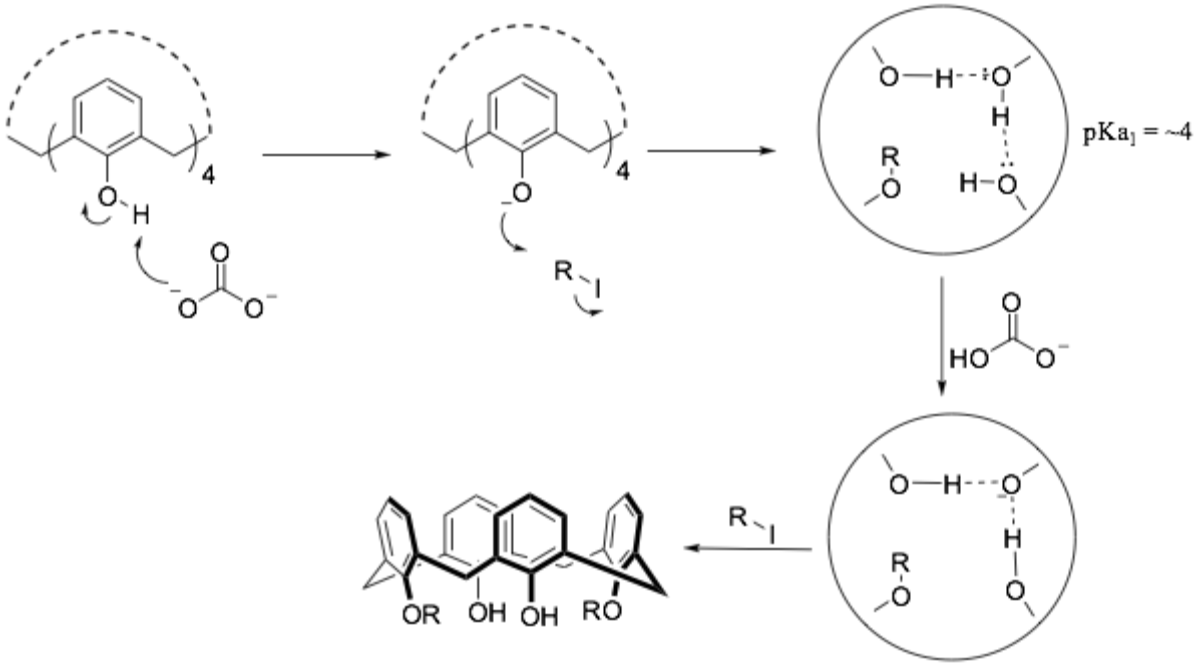

Scheme 2.6. Proposed reaction mechanism for the selective alkylation of **2**.

In dry MeCN, calix[4]arene, **1**, was treated with 1 eq. of weak base followed by the addition of 2 eq. of allyl iodide and refluxed over 48 h.

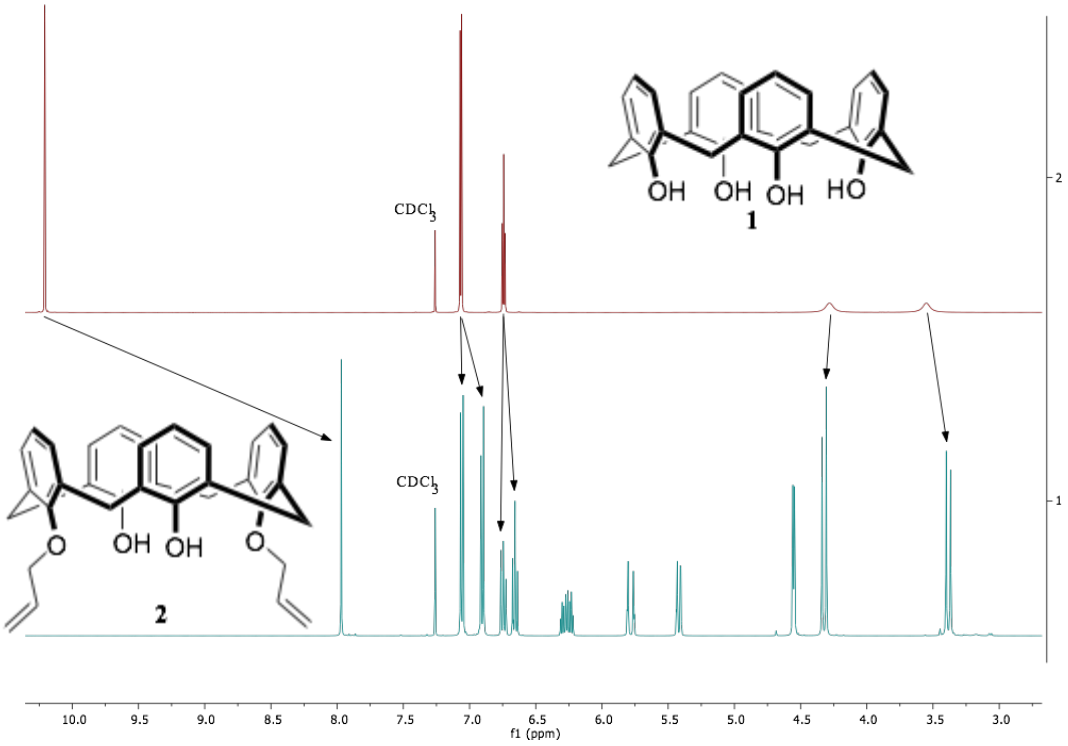

Figure 2.14. ^{1}H NMR of starting material, **1**, and product, **2** in $CDCl_3$.

The stacked ^{1}H NMR spectra (Fig. 2.14) shows the comparative resonance signals observed for the precursor, **1**, and the product of the selective dialkylation reaction, **2**.

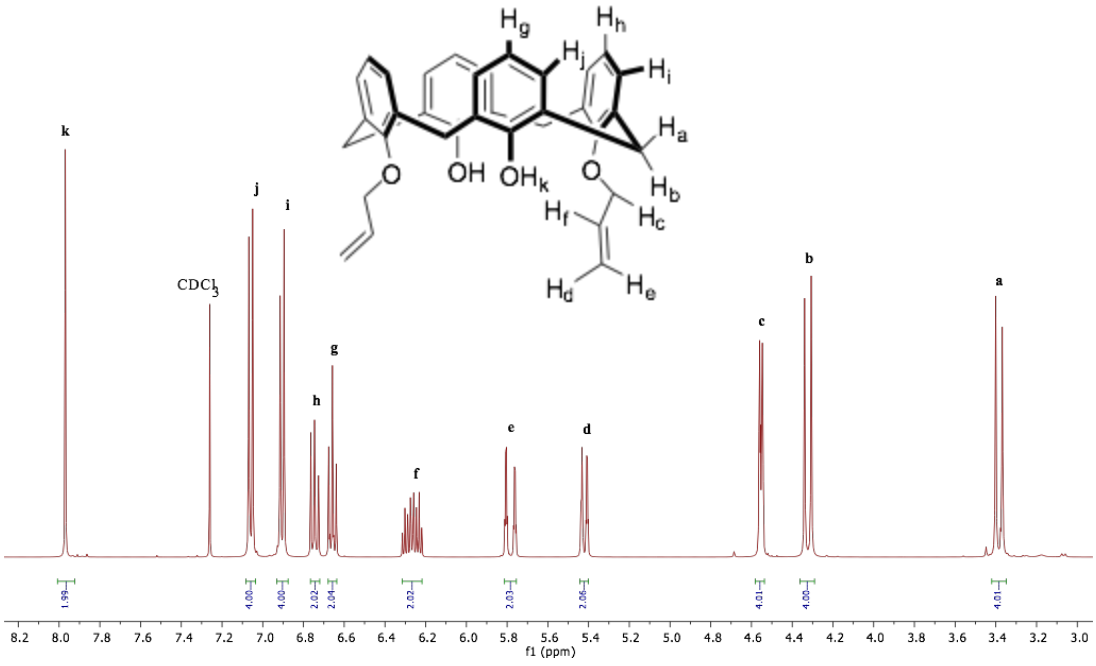

Figure 2.15. ^{1}H NMR spectrum of compound **2** in $CDCl_3$.

The ^{1}H NMR spectrum (Fig. 2.15) shows the presence of two sets of doublet resonance signals at 3.39 ppm and 4.33 ppm corresponding to protons H_a and H_b, respectively, with integral values of four per doublet. The presence of two sets of doublets indicates that **2** exists in the cone conformation.[6] Due to the cone formation of the calix[4]arene with its C_{2v} symmetry, one proton (H_b) of the methylene points down towards the oxo environment with the second methylene proton (H_a) pointing up and away from the oxo environment corresponding to H_b and H_a, respectively.[6] The oxo environment deshields the proton, thus the doublet resonance is downfield at 4.33 ppm, **b**, relative to the less deshielded proton with the doublet resonance at 3.39 ppm, **a**. The presence of the set of doublet resonances indicates that the calix[4]arene has been alkylated selectively in a diametric fashion as three sets of doublets would be expected if the calix[4]arene had been functionalised in a 1,2 manner opposed to the diametric 1,3. ^{1}H NMR resonances **c**, **d**, **e** and **f** correspond to the presence of the allyl ether functionality. The aliphatic linking ether methylene of the allyl ether moiety is observed as a doublet resonance with an integral of four at 4.55 ppm, **c**, corresponding to H_c. The doublet multiplicity is brought about *via* coupling to the non-terminal alkene proton of the allyl moiety. A multiplet resonance with an integral value of two is observed at 6.27 ppm, **f**, corresponding to the non-terminal alkene proton of the allyl moiety, H_f. The multiplet resonance results from the proton, H_f, coupling to three non-degenerate protons, H_c, H_d and H_e. The proton of H_f is the most deshielded of the allyl ether moiety due to it residing in an alkene environment and additionally coupling to a proton attached to a carbon ether environment, H_c. Two sets of double doublet resonances are observed at 5.42 ppm and 5.78 ppm, **d** and **e**, with integral values of two, corresponding to the terminal alkene protons of the allyl moiety, H_d and H_e, respectively. Two sets of double doublet resonances are observed due to H_d and H_e being non-degenerate, which results from their *cis* and *trans* orientation with respect to H_f. H_d has a J_1 coupling value of 10.8 Hz, whereas H_e has a J_1 coupling value of 16.8 Hz. The larger coupling constant of H_e indicates a longer range coupling with respect to H_f, thus must correspond to the *trans* proton and H_d must correspond to the proton in the *cis* position. H_d and H_e both exhibit a second J_2 coupling constant of 1.6 Hz due to coupling to one another. Two sets of triplet resonances with integrals of two are

observed at 6.66 ppm and 6.75 ppm, **g** and **h** respectively, resulting from the protons in the *para* position with respect to oxygen attached to the aromatic rings. Two sets of *para* aromatic protons are present due to the two types of aromatic present within the macrocycle, i.e. two phenolic and two aryl ether units. Additionally, two sets of doublet resonances with integrals of four are observed at 6.91 ppm and 7.06 ppm, **i** and **j**, resulting from the hydrogen atoms in the *meta* position with respect to oxygen attached to the aromatic rings. The COSY NMR spectrum (2.16) shows resonances **g** and **j,** and **h** and **i,** coupling, indicating resonances **g** and **j** belong to one of the two types of aromatics and **h** and **i** belonging to the second. To ascertain which protons belong to which type of aromatic unit the HMBC NMR spectrum must be referred to, and is discussed later. The ^{1}H NMR spectrum (Fig. 2.15) shows a singlet resonance with an integral of two at 7.97 ppm, **k**, which corresponds to the hydroxyl moiety of the phenolic rings, H_k. The sharp resonance corresponding to H_k is due to relatively strong hydrogen bonding within the lower rim of the calixarene. The strong hydrogen bonding is further confirmed by IR spectroscopy where a relatively sharp absorption is observed at 3290 cm^{-1}, corresponding to the hydroxyl moiety.

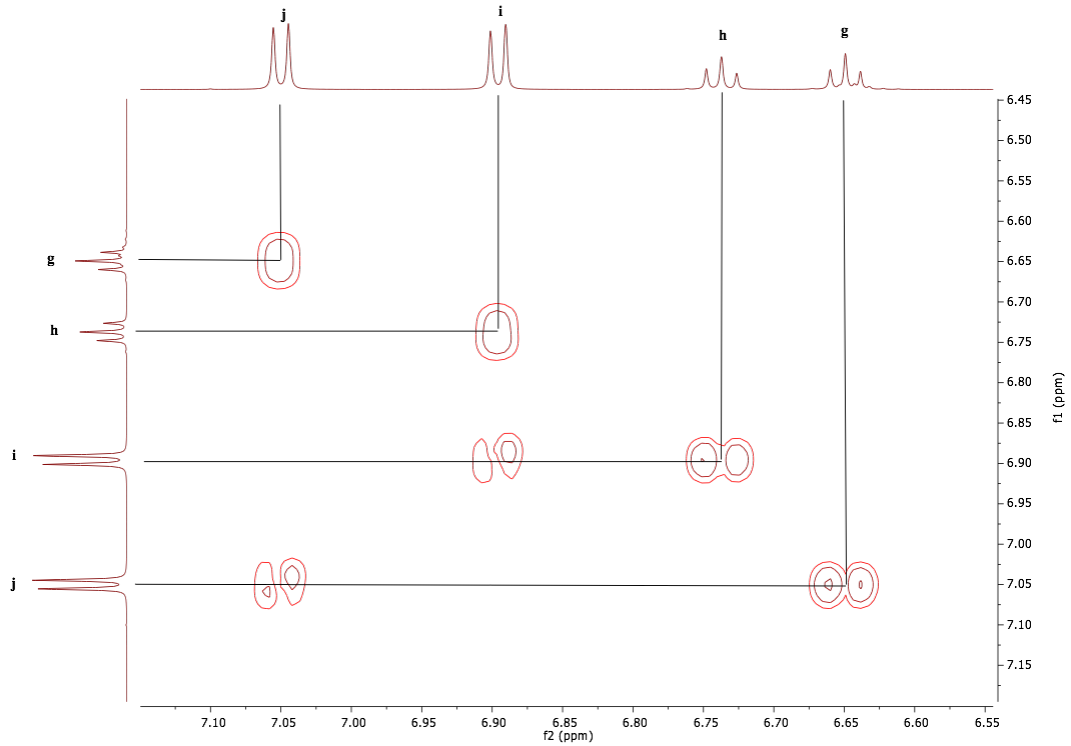

Figure 2.16. ^{1}H COSY NMR spectrum of **2**, showing the coupling between the aromatic protons in $CDCl_3$.

Using HSQC NMR spectroscopy the carbon atoms directly attached to hydrogen atoms could be easily assigned.

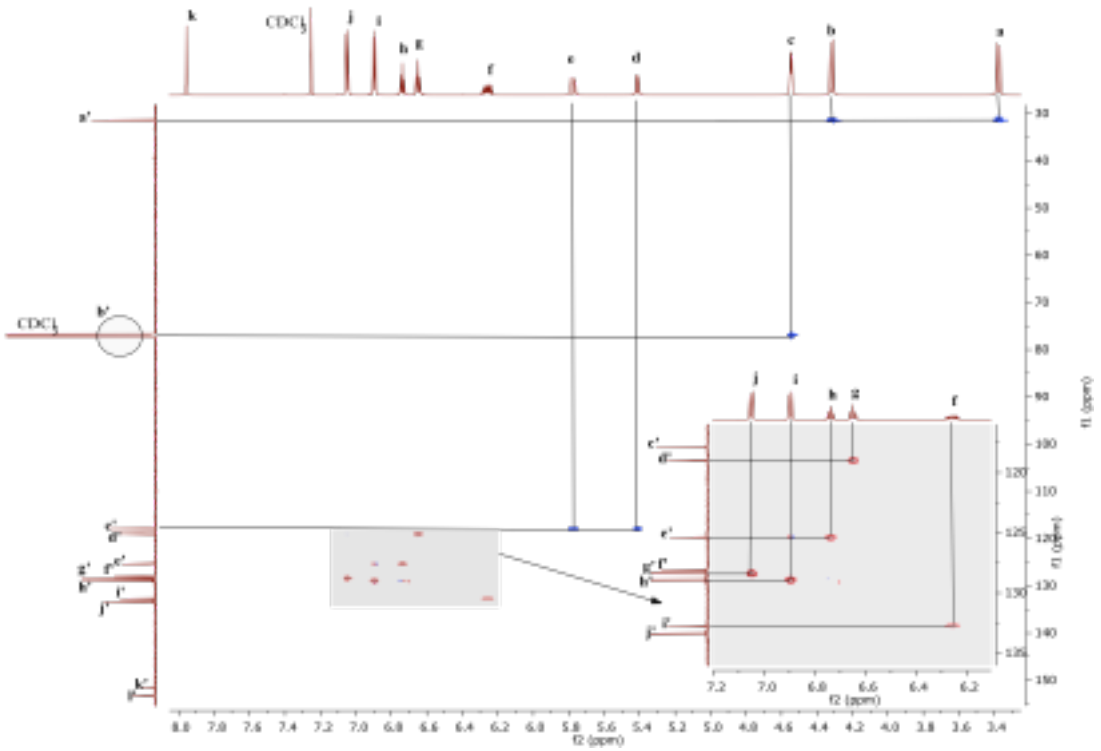

Figure 2.17. HSQC NMR spectrum of compound **2**, showing coupling between various hydrogen and carbon atoms in $CDCl_3$.

The HSQC NMR spectrum (Fig. 2.17) shows resonances **a** and **b** coupling to a ^{13}C NMR resonance at 31.6 ppm, **a'**, which corresponds to the bridging methylene carbon atom between aromatic rings. The fact that the resonance for the methylene carbon atom is observed at 31.6 ppm is further indication that the calixarene exists in the cone conformation.[7] Resonance **c** couples to a ^{13}C NMR resonance at 76.8 ppm, **b'**, which corresponds to the ether linking methylene carbon atom of the allyl moiety. ^{1}H NMR resonances **d** and **e**, couple to a ^{13}C NMR resonance at 118.1 ppm, **c'**, which corresponds to the terminal alkene carbon atom of the allyl moiety. Resonance **f** couples to a ^{13}C NMR resonance at 132.9 ppm, **i'**, which corresponds to the non-terminal alkene carbon atom of the allyl moiety. Resonances **g**, **h**, **i** and **j** exhibit couplings to ^{13}C NMR resonances at: 119.2, **d'**; 125.6, **e'**; 128.6, **g'**; and 129.1 ppm, **h'**, respectively. Using HMBC the hydrogen and carbon atoms of the phenolic and aryl ether rings and quaternary carbon atoms can be assigned accurately.

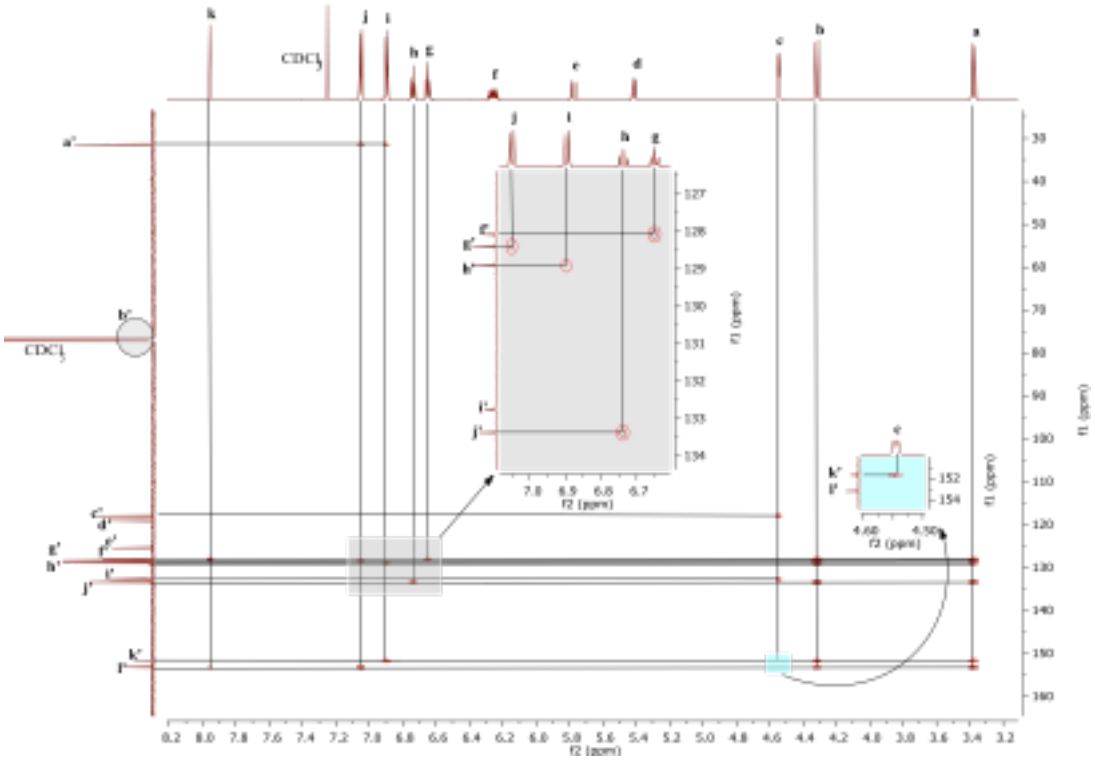

Figure 2.18. HMBC NMR spectrum of compound **2** in $CDCl_3$, showing coupling between multiple bonds of various hydrogens.

The HMBC spectrum (Fig. 2.18) shows resonance **k** coupling to two ^{13}C NMR resonances at 128.3 ppm and 153.4 ppm, **f'** and **l'**, respectively, indicating the carbon resonances are part of the phenolic aromatic system and not the aryl ether system. **l'** exhibits a coupling to ^{1}H NMR resonance **j**, corresponding to H_j, therefore ^{1}H NMR resonances **j** and **g** correspond to the aromatic protons of the phenolic units, H_j and H_g respectively (Fig. 2.15). Due to fact that in HMBC spectroscopy of aromatic systems two bond coupling is often not observed or is very weak, resonances **f'** and **l'** can be accurately assigned to the calixarene structure. The HMBC spectrum shows resonance **f'** exhibiting coupling to **g** and **k** but not **j**, therefore must correspond to the *ortho* carbon atom of the phenolic ring with respect to the hydroxyl moiety and orthogonal to the bridging methylene carbon atoms. **l'** exhibits coupling to **j** and the methylene hydrogen atoms, **a** and **b**, and very weakly to the hydroxyl moiety protons, therefore corresponds to the carbon atom of the phenolic ring in the *ipso* position relative to the hydroxyl moiety. The HMBC spectrum (Fig. 2.18) shows resonance **c** coupling to a ^{13}C NMR resonance at 153.4 ppm, **k'**, which corresponds to the *ipso* carbon atom of the aryl ether unit with respect to oxygen and additionally confirms the chemical attachment of the allyl moiety to the aromatic ring through an

ether linkage. Resonance **k'** exhibits coupling to ^{1}H NMR resonance **i**, corresponding to H_i, therefore ^{1}H NMR resonances **i** and **h** correspond to the aromatic protons of the phenolic units, H_i and H_h, respectively (Fig. 2.15). The HMBC spectrum (Fig. 2.18) shows resonance **j'** exhibiting coupling to ^{1}H NMR resonances **a**, **b** and **h**, therefore corresponds to the *ortho* carbon atom of the aryl ether unit with respect to oxygen. The complete assignment of the ^{13}C NMR spectrum is shown in Figure 2.19.

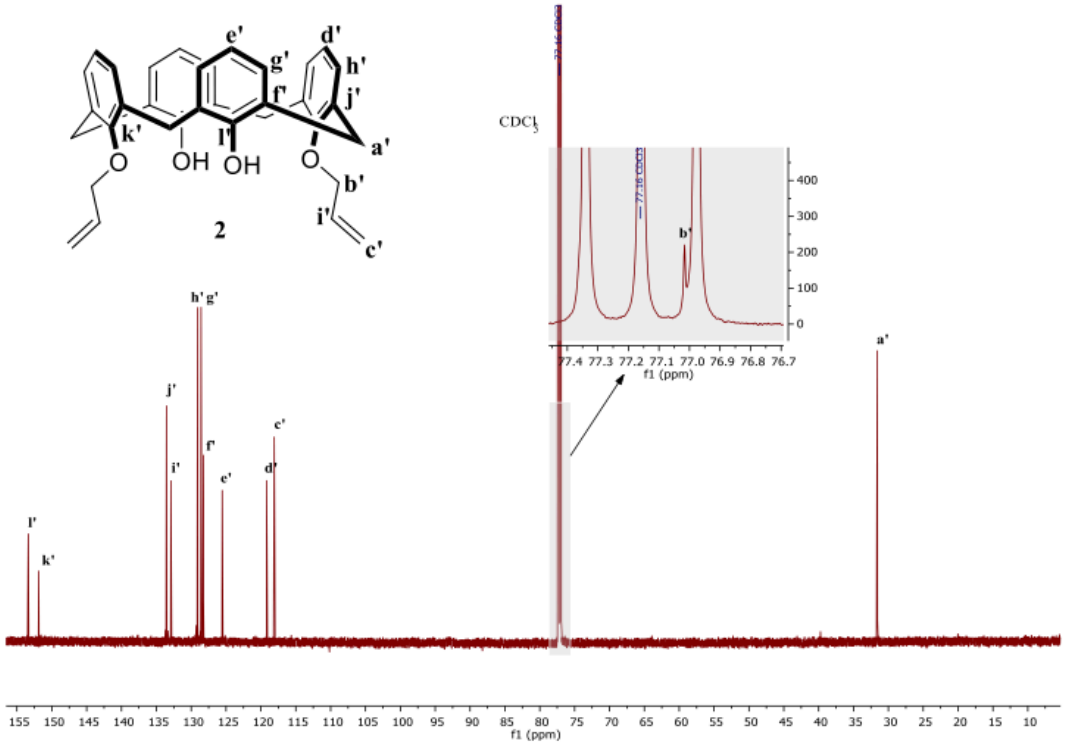

Figure 2.19. ^{13}C NMR spectrum of compound **3** in $CDCl_3$.

ASAP mass spectrometry was carried out and the molecular ion was seen at 505.230 Da (100%, Fig. 2.20), which corresponds to the empirical formula $C_{34}H_{33}O_4^+$.

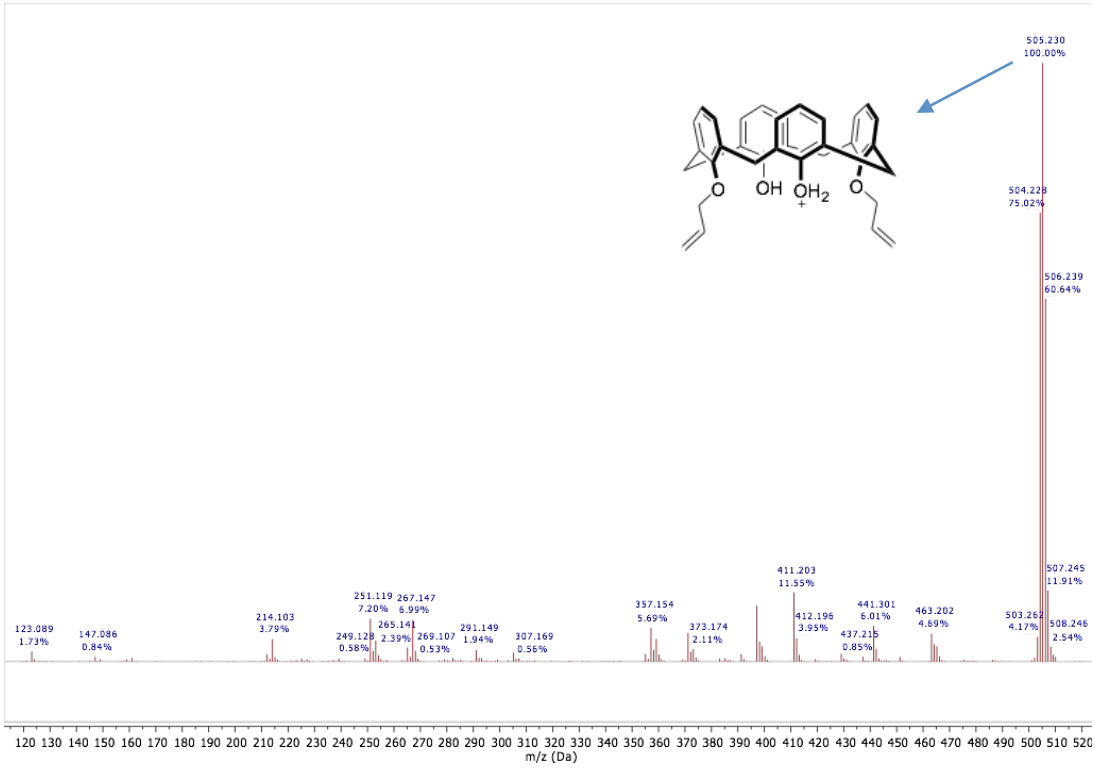

Figure 2.20. ASAP MS spectrum of **2**.

2.2.3. 25,27-*bis*(prop-2-en-1-yloxy)-26,28-*bis*(ethyleneacetate)-calix[4]arene, 3

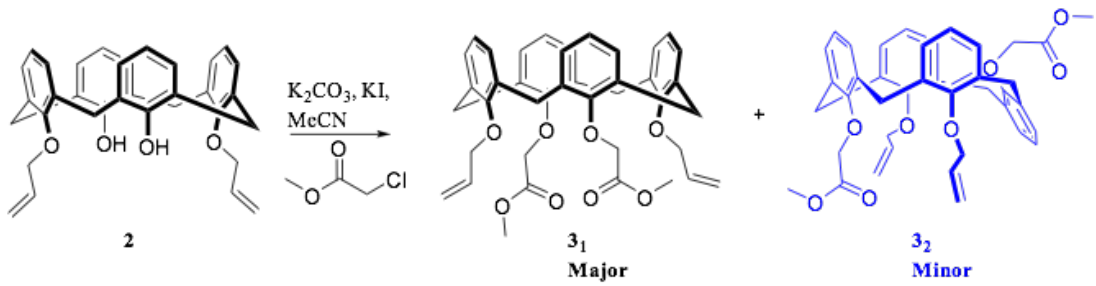

Scheme 2.7. Synthesis of **3**.

The novel compound **3**, was successfully synthesised using an excess of potassium carbonate and methyl chloroacetate in the presence of a catalytic amount of potassium iodide (Scheme 2.7). The addition of potassium iodide leads to an exchange equilibrium between the halogen ions of Cl^- and I^-, known as the Finkelstein reaction (scheme 2.8).[10] Iodide is a much better nucleofuge than that of chloride, therefore will lead to an increase in yield.

Scheme 2.8. Finkelstein reaction.

Compound **3** was obtained in a yield of 52%. An attempt at increasing the yield using the stronger base NaH in DMF/THF was unsuccessful, partly due to the fact that a partial and full reduction of the ester moiety was observed. In the synthesis of **3**, two distinct conformations were observed, cone and partial flattened cone corresponding to $\mathbf{3_1}$ and $\mathbf{3_2}$, respectively (Scheme 2.7). $\mathbf{3_1}$ is the major conformer and $\mathbf{3_2}$ is the minor conformer and contribute to ~66% and ~34% of the reaction product respectively, as determined *via* the ratio of integral values for the non-terminus alkene protons of the allyl moiety from the ^{1}H NMR spectrum (Fig. 2.21). The cone conformation has a C_{2v} symmetry, which leads to relatively simple NMR spectra, in contrast the partial flattened cone has much reduced symmetry resulting in much more complex spectra. A full characterisation is described below, first looking at the major product in the cone conformation, $\mathbf{3_1}$.

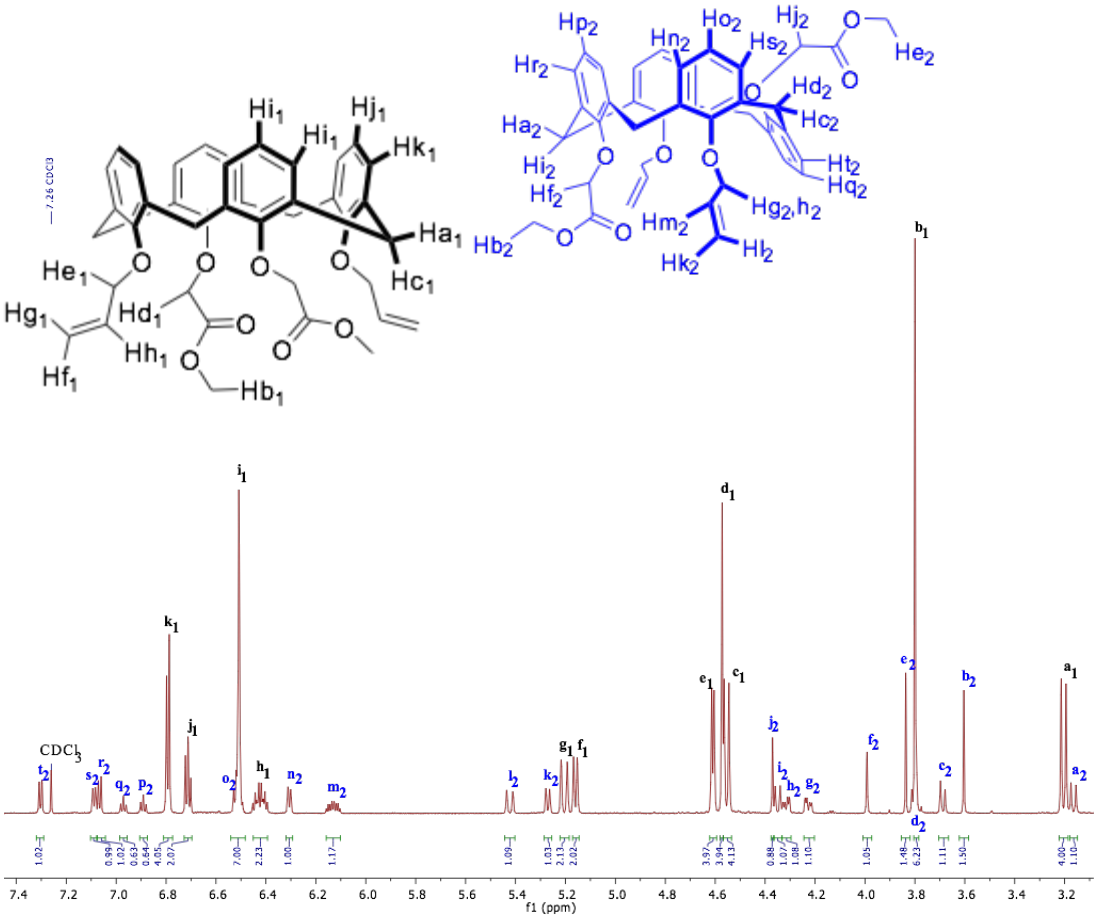

Figure 2.21. ^{1}H NMR spectrum of **3** in $CDCl_3$.

The ^{1}H NMR spectrum (Fig. 2.21) exhibits a doublet resonance with its integral set to four at 3.20 ppm, $\mathbf{a_1}$, and has a *J* coupling constant of 13.6 Hz. The COSY NMR spectrum (Fig. 2.22) shows $\mathbf{a_1}$ coupling to a second doublet with an integral of four at 4.55 ppm, $\mathbf{c_1}$, and has a *J* coupling constant of 13.6 Hz. $\mathbf{a_1}$ and $\mathbf{c_1}$ correspond to the bridging methylene protons between aromatics, with resonance $\mathbf{a_1}$ corresponding to the proton pointing up to the aromatic region and $\mathbf{c_1}$ corresponds to the proton pointing down to the oxo region, H_{a1} and H_{c1}, respectively. The fact that two doublets are observed indicated that the compound is in the cone conformation.[6] The ^{1}H NMR spectrum (Fig. 2.21) exhibits a singlet resonance with an integral of six at 3.60 ppm, $\mathbf{b_1}$. $\mathbf{b_1}$ corresponds to the methyl functionality of the methyl ether acetate moiety, H_{b1}. A second singlet with an integral of four is observed at 4.57 ppm, $\mathbf{d_1}$, corresponding to the ether linking methylene group of the methyl ether acetate moiety. A doublet resonance with an integral of four is observed at 4.57 ppm, $\mathbf{e_1}$.

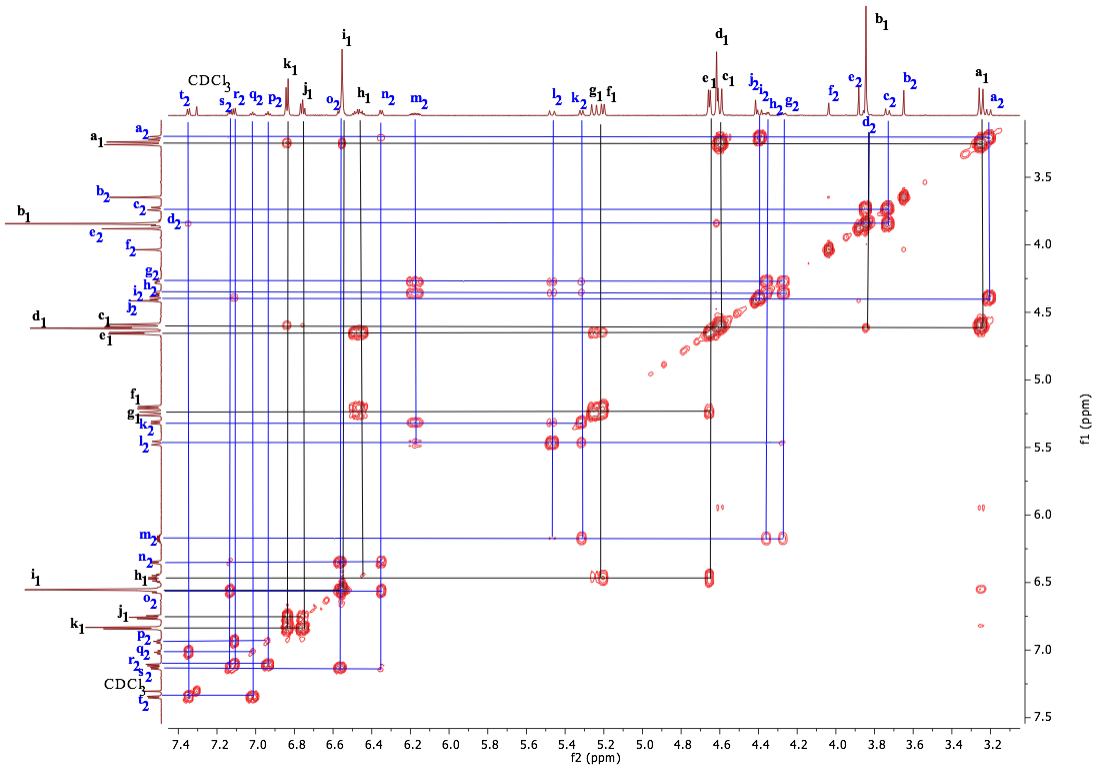

Figure 2.22. COSY NMR spectrum of **3** in $CDCl_3$.

The COSY NMR spectrum (Fig. 2.2.3.2) shows $\mathbf{e_1}$ exhibiting coupling to resonances $\mathbf{f_1}$, $\mathbf{g_1}$ and $\mathbf{h_1}$, which all correspond to the protons of the allyl moiety. $\mathbf{e_1}$ corresponds to the aliphatic methylene ether linking protons of the allyl moiety, H_{e1}. $\mathbf{f_1}$ and $\mathbf{g_1}$ correspond to the *cis* and *trans* terminal alkene protons of the allyl moiety, respectively, H_{f1} and H_{g1}, relative to the non-terminal alkene proton H_{h1}, corresponding to ^{1}H NMR resonance $\mathbf{h_1}$. The ^{1}H NMR spectrum (Fig. 2.21) exhibits an overlapped multiplet resonance with an integral of six at 6.51 ppm, $\mathbf{i_1}$. The overlapping of resonances is proved *via* a HSQC experiment and is discussed later. $\mathbf{i_1}$ corresponds to the one set of aromatic protons in the *meta* and *para* positions with respect to the oxygen of one of the aryl ether units. To confirm which aryl ether unit the $\mathbf{i_1}$ resonance corresponds to the HMBC spectrum must be referred to as is discussed later. The ^{1}H NMR spectrum (Fig. 2.21) exhibits a triplet resonance with an integral of two at 6.71 ppm, $\mathbf{j_1}$. The COSY NMR spectrum (Fig. 2.22) shows $\mathbf{j_1}$ exhibiting coupling to a doublet resonance with an integral of four at 6.79 ppm, $\mathbf{k_1}$. Resonance $\mathbf{j_1}$ and $\mathbf{k_1}$ correspond to *para* and *meta* protons, respectively, of one of the two types of aryl ether units, i.e. either the allyl moiety attached or the methyl acetate moiety. As expressed above, the HMBC experiment will be referred to for

the determination of which aryl ether unit. Using an HSQC NMR experiment the carbon atoms directly bonded to hydrogen atoms can easily be assigned.

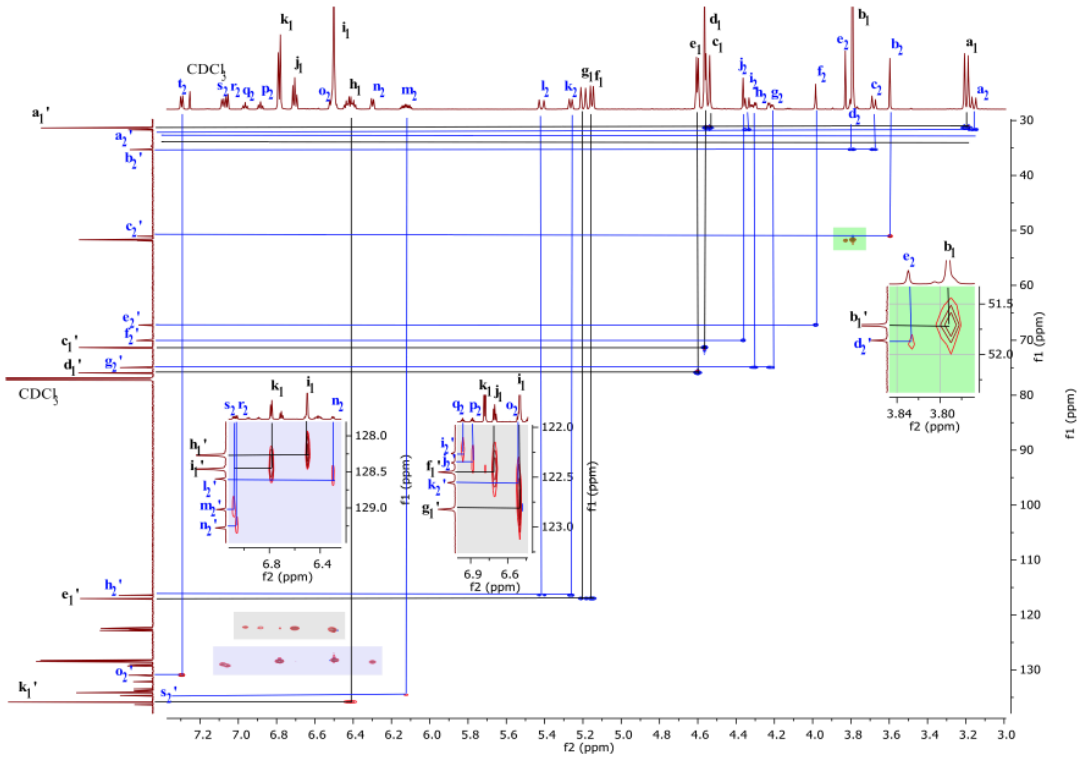

Figure 2.23. HSQC NMR spectrum of **3** in $CDCl_3$.

The HSQC spectrum (Fig. 2.23) shows resonances $\mathbf{a_1}$ and $\mathbf{c_1}$ coupling to a ^{13}C NMR resonance at 31.5 ppm, $\mathbf{a_1}$**'**, which corresponds to the methylene bridging carbon atom between aromatics. The fact that the $\mathbf{a_1}$**'** resides in the ~31 ppm region indicates the calixarene exists in the cone conformation.[7] The HSQC spectrum (Fig. 2.23) shows resonances $\mathbf{b_1}$ coupling to a ^{13}C NMR resonance at 51.8 ppm, $\mathbf{b_1}$**'**, which corresponds to the methyl carbon atom of the methyl ether acetate moiety. Resonance $\mathbf{d_1}$ couples to a ^{13}C NMR resonance at 71.4 ppm, $\mathbf{c_1}$**'**, which corresponds to the ether linking methylene carbon atom of the methyl ether acetate moiety. Resonance $\mathbf{e_1}$ couples to a ^{13}C NMR resonance at 76.0 ppm, $\mathbf{d_1}$**'**, which corresponds to the aliphatic methylene ether linking carbon atom of the allyl moiety. Resonances $\mathbf{f_1}$ and $\mathbf{g_1}$ couple to a ^{13}C NMR resonance at 117.1 ppm, $\mathbf{e_1}$**'**, which corresponds to the terminal alkene carbon atom of the allyl moiety. Resonance $\mathbf{h_1}$ couples to a ^{13}C NMR resonance at 135.9 ppm, $\mathbf{k_1}$**'**, which corresponds to the non-terminal alkene carbon atom of the allyl moiety. Resonance $\mathbf{i_1}$ couples to two ^{13}C NMR resonance at 122.9 ppm and 128.4 ppm, $\mathbf{g_1}$**'** and $\mathbf{h_1}$**'**, which correspond to the *para* and *meta* carbon

atoms, respectively, of one of the aryl ether unit pairs. Resonances **j_1** and **k_1** couple to ^{13}C NMR resonances at 122.6 ppm and 128.6 ppm, **f_1'** and **i_1'**, which correspond to the *para* and *meta* carbon atoms, respectively, of one of the aryl ether unit pairs. To determine which aromatic resonances belong to which of the two types of aryl ether the HMBC NMR experiment is referred to.

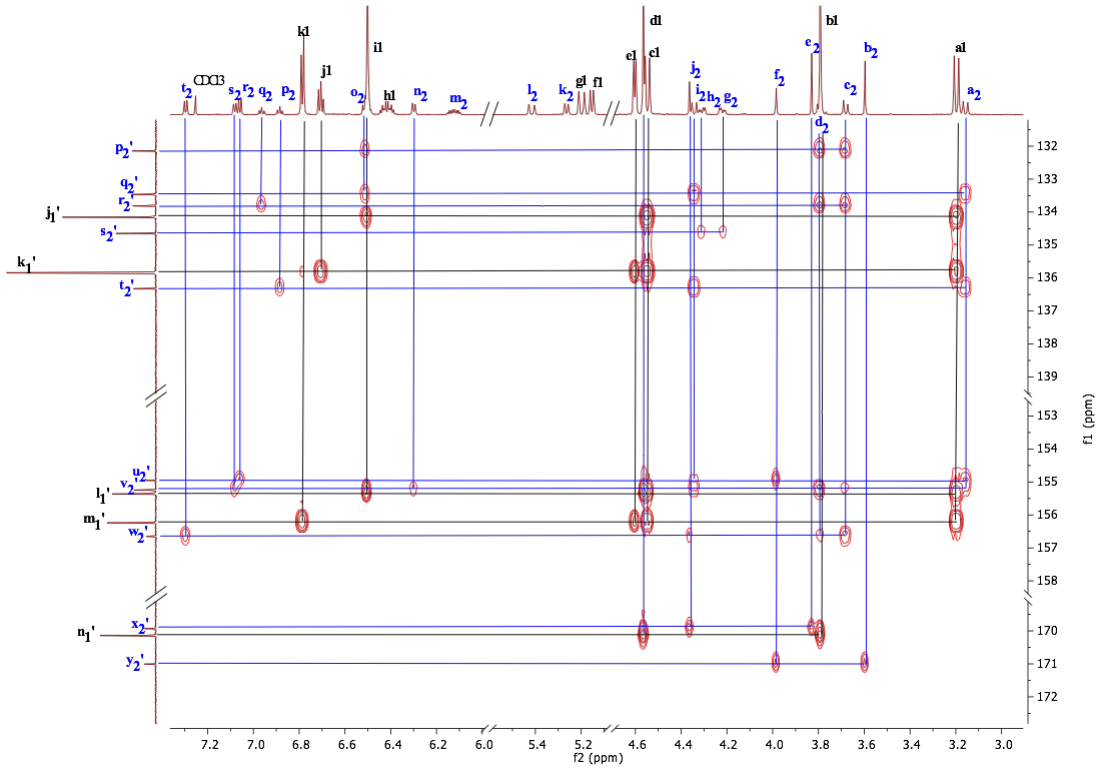

Figure 2.24. HMBC NMR spectrum of **3** in $CDCl_3$.

The HMBC NMR spectrum (Fig. 2.24) shows, most significantly, resonance **d_1** coupling to ^{13}C NMR resonances at 155.5 ppm, **l_1'**, which corresponds to the *ipso* carbon atom of the aryl ether unit with methyl acetate ether moiety attached. **l_1'** exhibits coupling to ^{1}H NMR resonance **i_1**, therefore the protons corresponding to the **i_1** resonance belong to the aryl ether units with the methyl acetate ether moiety attached, H_{i1}. ^{1}H NMR resonance **e_1** couples to a ^{13}C NMR resonance at 156.3 ppm, **m_1'**, which corresponds to the *ipso* carbon atom of the aryl ether unit with the allyl moiety attached. Additionally, **m_1'** exhibits coupling to resonance **k_1**, therefore resonance **k_1** correspond to the *para* and *meta* protons of the aryl ether units with the allyl moiety attached, H_{k1}. The HMBC NMR spectrum (Fig. 2.24) shows resonance **i_1** exhibiting coupling to ^{13}C NMR resonance at 134.2 ppm, **j_1'**, which corresponds to the *ortho* carbon atom of the aryl ether unit with the methyl acetate ether moiety

attached. Resonance **j$_1$** exhibits coupling to ^{13}C NMR resonance at 135.9 ppm, **k$_1$'**, which corresponds to the *ortho* carbon of the aryl ether unit with the allyl ether moiety attached. ^{13}C NMR resonance **k$_1$'** is two overlapped resonances. The final carbon atom to assign in the ^{13}C NMR spectrum corresponding to the cone conformation calixarene is at 170.2 ppm, **n$_1$'**, which corresponds to the carbonyl carbon of the ester moiety (Fig. 2.25).

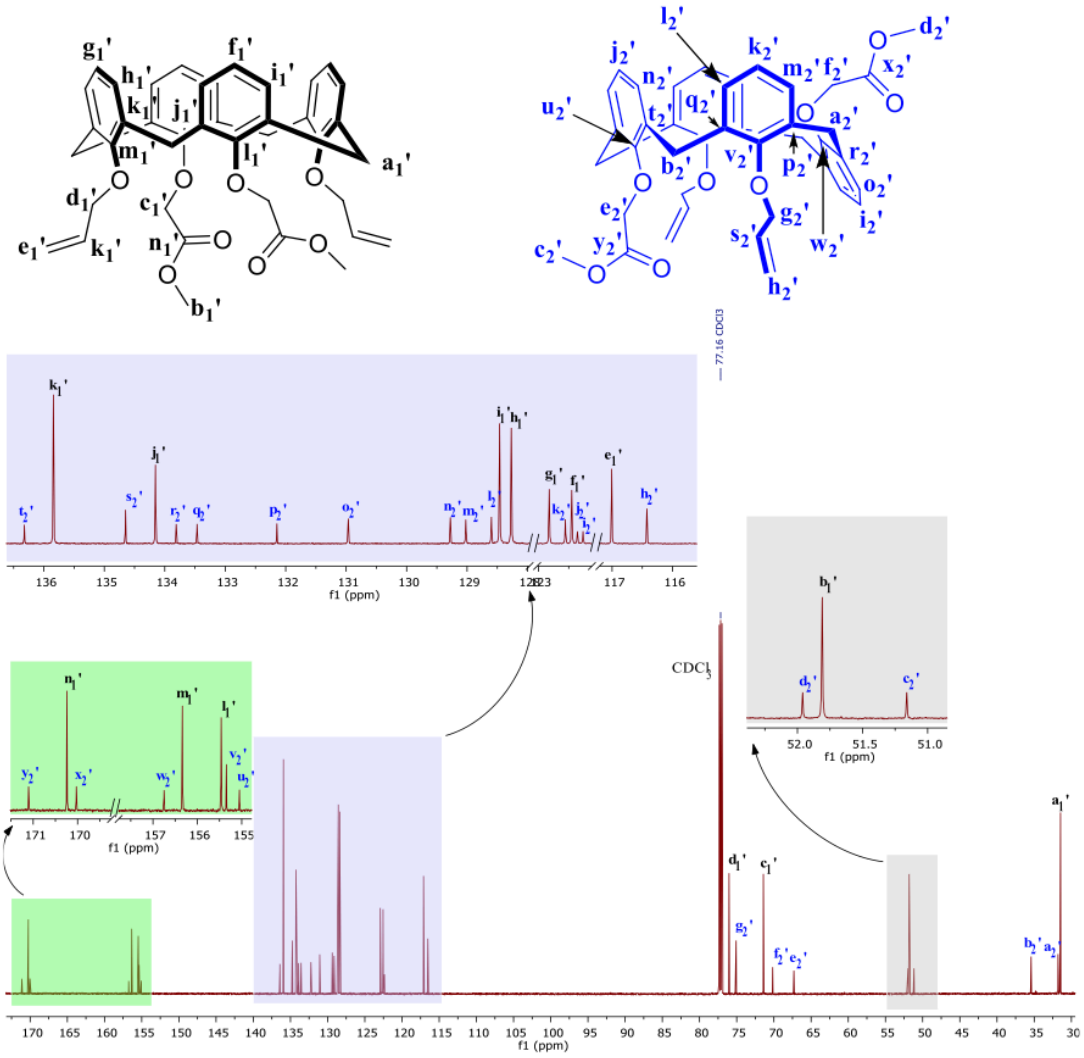

Figure 2.25. ^{13}C NMR spectrum of **3** in $CDCl_3$.

For the determination of the conformation of the minor product, **3$_2$**, the same protocol was applied as described previously with the addition of using a NOESY NMR experiment. One of the key steps to assigning **3$_2$** with the flattened partial cone conformation was observing two ^{13}C NMR resonances (Fig. 2.25) at 31.8 ppm and 35.4 ppm, **a$_2$'** and **b$_2$'**, respectively, with equal intensity. The HSQC NMR spectrum (Fig. 2.23) showed **a$_2$'** coupling to two sets of ^{1}H NMR doublets at 3.16 ppm and

4.35 ppm, **a_2** and **i_2** respectively and **b_2'** coupling to two sets of ^{1}H NMR doublets at 3.69 ppm and 3.81 ppm, **c_2** and **d_2**, respectively, which all correspond to bridging methylene protons, H_{a2}, H_{i2}, H_{c2}, and H_{d2}. The integrations of **a_2**, **c_2**, **d_2** and **i_2** are all equal, thus suggesting they correspond to one molecule. The fact that the **a_2'** ^{13}C NMR resonance resides in the 31 ppm region indicates the aromatic either side are in the *syn* conformation, i.e. cone, whereas for the **b_2'** resonance, which resides at ~35 ppm, suggests the aromatics either side are closer to the *anti*-position, i.e. at 180^o to each other; it is noted that if the aromatic either side of the methylene carbon atom existed at a complete 180^o to each other a ^{13}C NMR resonance would be expected to be observed at ~ 38 ppm, and would couple to a singlet proton resonance in the ^{1}H NMR spectrum. Thus for the carbon atom corresponding to **b_2'** resonances the aromatics either side are likely to exist at angles between 90^o and 180^o to each other (Fig. 2.26).[7]

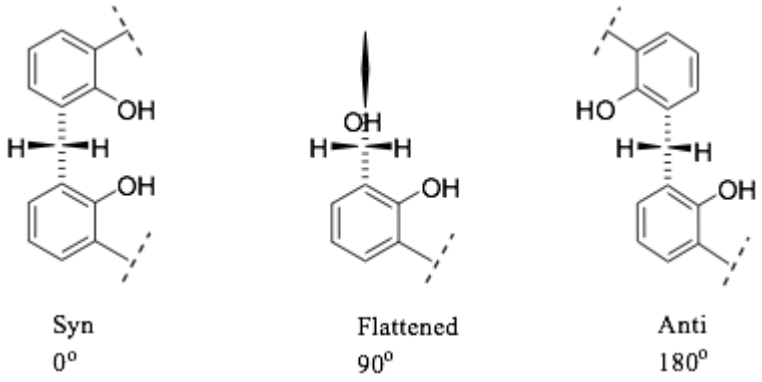

Figure 2.26. Depiction of the aromatics orientation relative to the bridging methylene carbon/protons.

Further confirmation that there was in fact just one secondary compound came from the ^{1}H NMR resonances corresponding to the allyl moiety (**g_2**, **h_2**, **k_2** and **i_2**, Fig 2.21), where only one type of ally moiety resonance was observed, indicating that there was a line of symmetry through the calixarene as depicted (Fig. 2.27).

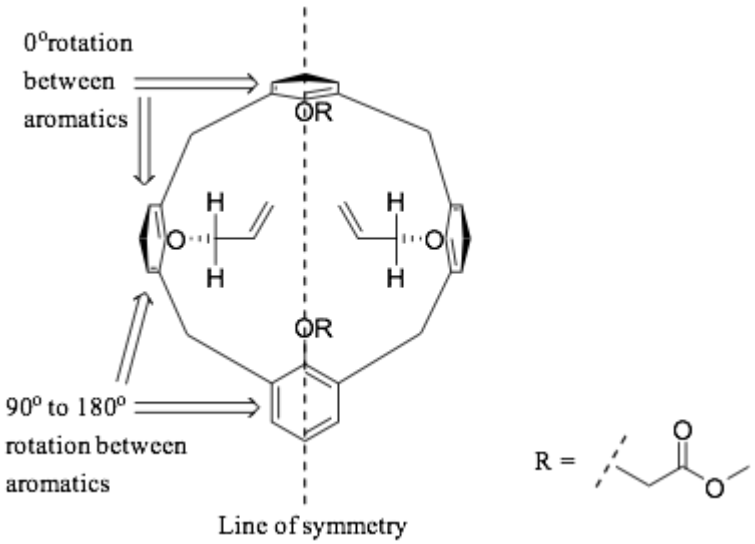

Figure 2.27. Depiction of calixarene macrocycle in a flattened partial cone conformation with a line of symmetry through the centre.

Two types of methyl acetate ether moiety were present as indicated *via* the ^{1}H NMR spectrum (Fig. 2.23) with two methyl ester singlets at 3.60 ppm and 3.84 ppm, **b_2** and **e_2**, respectively, and two methylene ether linking groups at 4.00 ppm and 4.37 ppm, **f_2** and **j_2** respectively. The HMBC NMR spectrum (Fig. 2.24) showed **b_2** and **f_2** coupled to the same ^{13}C NMR carbonyl resonance at, 170.0 ppm, **x_2'**, and **e_2** and **j_2** coupled to the same ^{13}C NMR carbonyl resonance at 171.1 ppm, **y_2'**. Using the HSQC and HMBC NMR analysis as described previously for **3_1**, the aromatic protons were assigned. The NOESY NMR spectrum (Fig. 2.28) shows a resonance at 6.31 ppm, **n_2**, corresponding to H_{n2} (Fig. 2.23), interacting through space with the methylene ether linking protons of the methyl acetate ether unit, H_{j2}. The NOESY NMR spectrum (Fig. 2.28) also shows a resonance at 7.09 ppm, **s_2**, corresponding to H_{s2} (Fig. 2.23), interacting through space with the H_{r2} protons, confirming the flattened partial cone conformation. The full assignment of both the ^{1}H and ^{13}C NMR spectrums are shown in Figures 2.23 and 2.25, respectively.

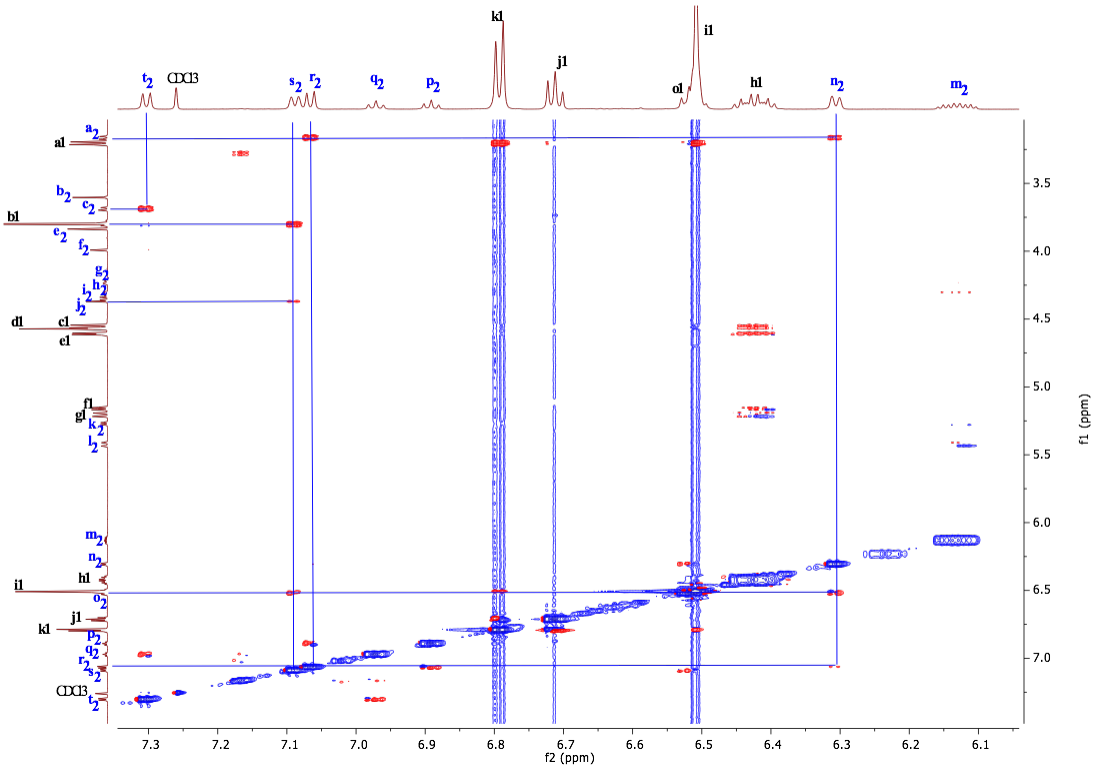

Figure 2.28. NOESY NMR spectrum of **3** in $CDCl_3$.

ASAP MS was carried out and the molecular ion was observed at 649.275 Da (100%), which is consistent with the empirical formula $C_{40}H_{41}O_8^+$ (Fig. 2.29).

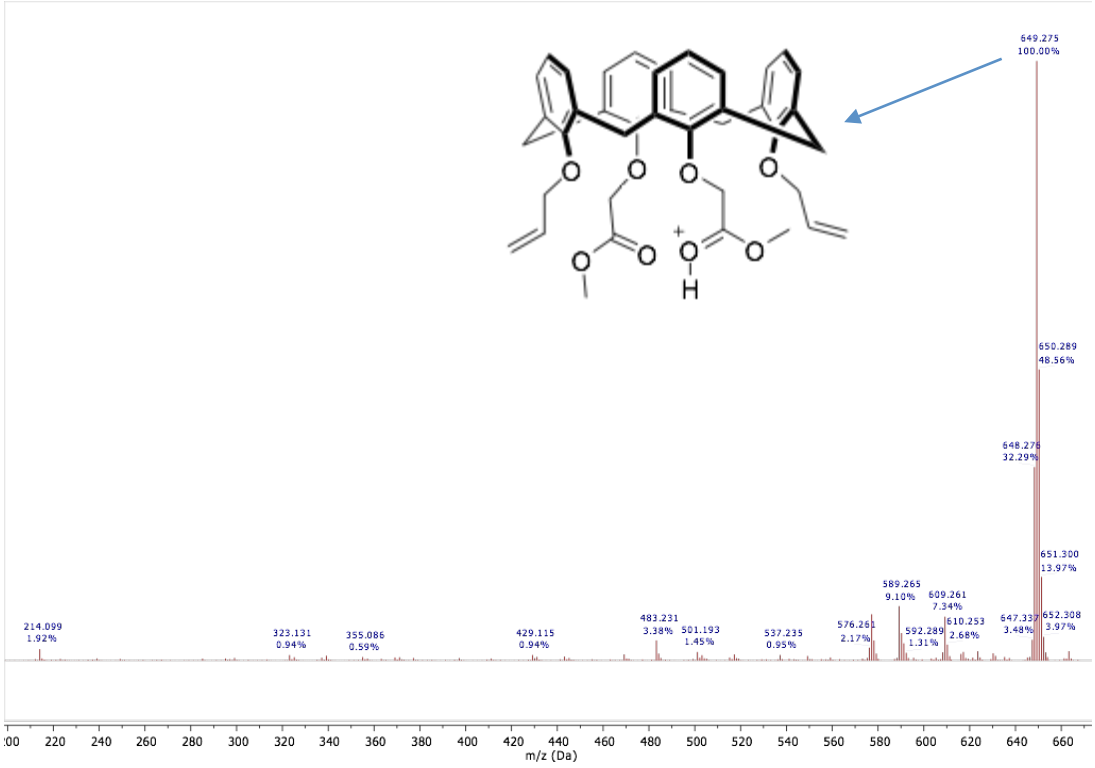

Figure 2.29. ASAP MS spectrum of **3**.

Further confirmation that **3** has been synthesised was observed through FT-IR spectroscopy where there was loss of a OH absorption at 3292 cm^{-1} and the presence of a new carbonyl absorption at 1760 cm^{-1}. Additionally, CHN analysis was carried out with the results closely matching the predicted values; CHN expected = %C = 74.06, %H = 6.22, %N 0.00; measured %C = 74.45, %H = 6.48, %N 0.00.

2.2.4. 25,27-*bis*(prop-2-en-1-yloxy)-26,28-*bis*(ethanoloxy)-calix[4]arene, 4

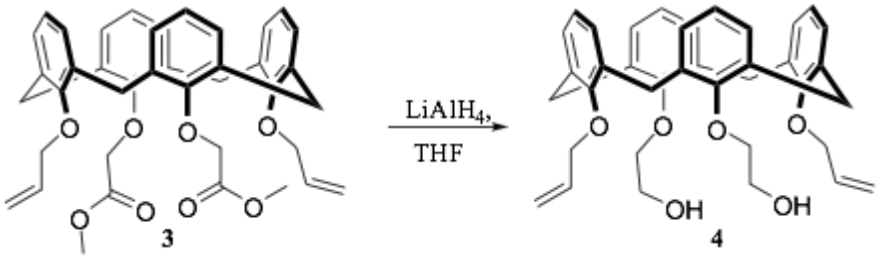

Scheme 2.9. Synthesis of **4**.

Compound **4** was successfully synthesised, *via* the reduction of the ester moieties of **3** (Scheme 2.9). **3** was added to a suspension of $LiAlH_4$ in THF, leading to the complete reduction of ester functionality in a yield of 89%. A full characterisation is described below.

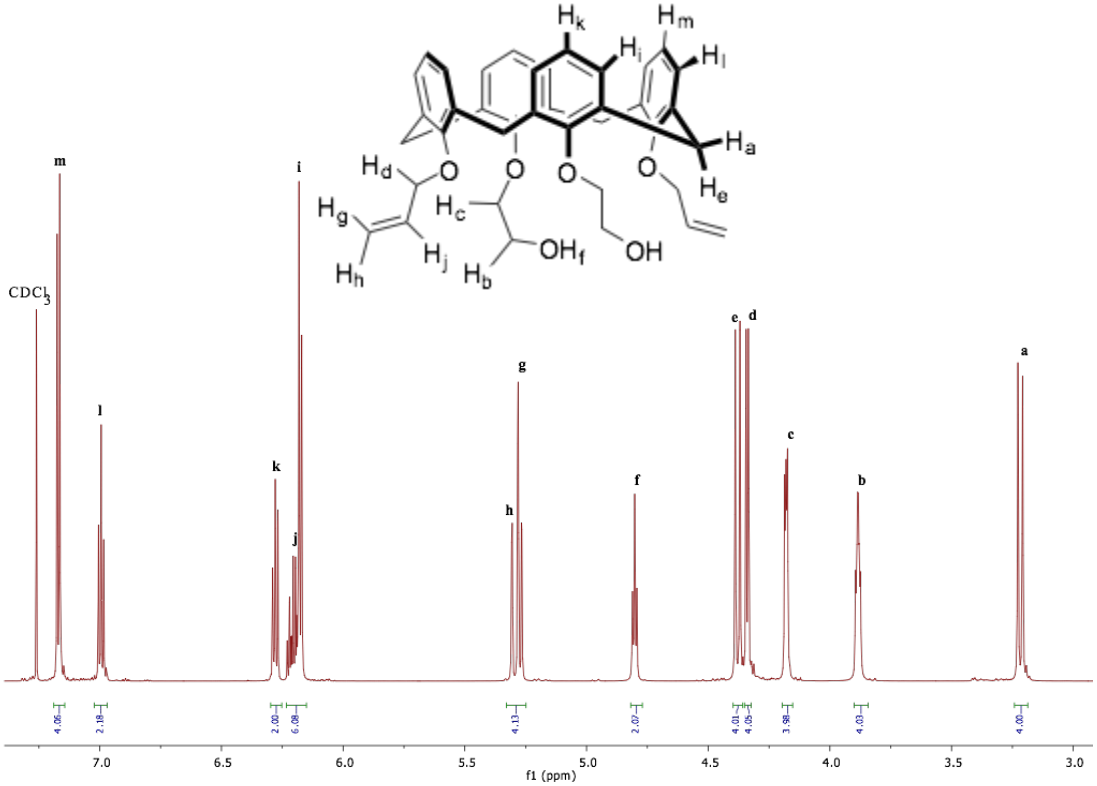

Figure 2.30. ^{1}H NMR spectrum of **4** in $CDCl_3$.

The ^{1}H NMR spectrum (Fig. 2.30) exhibits a doublet resonance with an integral set to four at 3.21 ppm, **a**, which has a *J* coupling of 13.5 Hz. The COSY NMR spectrum (Fig. 2.31) shows **a** exhibiting coupling to a doublet resonance at 4.38 ppm, **e**. **e** has an integral of four and a *J* coupling of 13.5 Hz. Resonances **a** and **e** correspond to the methylene protons that bridge the aromatics, with **a** corresponding to the protons pointing up to the aromatic region and **e** corresponding to the protons pointing down to the oxy environment, H_a and H_e, respectively. The presence of two sets of doublets indicates that the calixarene exists in the cone conformation.[6] The ^{1}H NMR spectrum (Fig. 2.30) exhibits a multiplet resonance with an integral of four at 3.88 ppm, **b**. The COSY NMR spectrum (Fig. 2.31) shows **b** exhibiting coupling to a multiplet resonance at 4.17 ppm, **c**, and a triplet resonance at 4.79 ppm, **f**, which have integrals of four and two, respectively. Additionally, the COSY spectrum shows that resonances **c** and **f** do not couple. Therefore, resonances **b**, **c** and **f** correspond to the ethanol ether moiety. **f** exhibits no HSQC NMR (Fig. 2.32) coupling and has an integral of two, therefore corresponds to the proton of the hydroxyl moiety, H_f, which was further confirmed *via* a D_2O shake. The fact that resonance **f** couples to **b** and not **c** indicates that **b** corresponds to the ethylene

protons next to the hydroxyl oxygen, H_b and **c** must therefore correspond to the ethylene protons next to the linking aryl ether oxygen, H_c. The ^{1}H NMR spectrum (Fig. 2.30) exhibits a doublet resonance with an integral of four at 4.34 ppm, **d**.

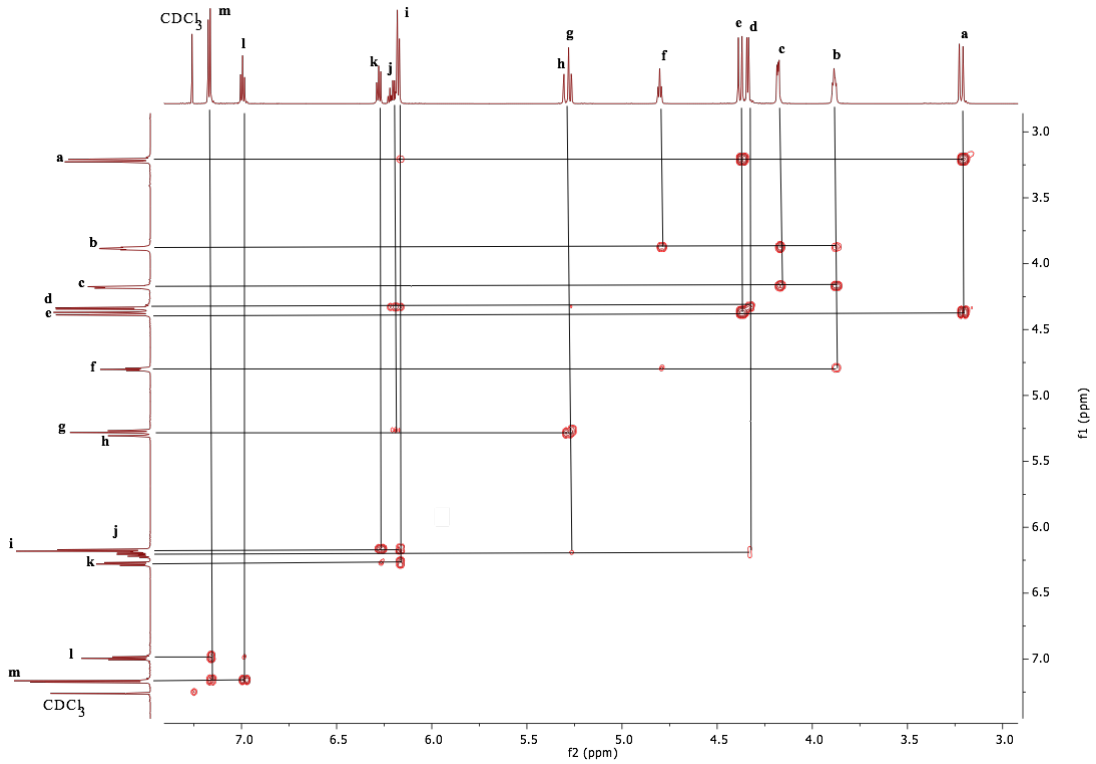

Figure 2.31. COSY NMR spectrum of **4** in $CDCl_3$.

The COSY NMR spectrum (Fig. 2.31) shows **d** exhibiting coupling to multiplet resonances at 5.28 ppm, 5.29 ppm and 6.20 ppm, **g, h** and **j**, respectively. Resonances **d**, **g, h** and **i** correspond to protons of the allyl moiety. Resonance **d** corresponds to the aryl ether linking aliphatic protons of the allyl moiety, H_b. Resonances **g** and **h** correspond to the terminal alkene protons in the *cis* and *trans* positions, H_g and H_h respectively, with respect to the non-terminal alkene proton. Resonance **j** corresponds to the non-terminal alkene protons of the allyl moiety, H_j. The ^{1}H NMR spectrum (Fig. 2.30) exhibits a doublet resonance with an integral of four at 6.17 ppm, **i**, which has a *J* coupling of 7.6 Hz. The COSY NMR spectrum (Fig. 2.31) shows **i** exhibiting coupling to a triplet resonance at 6.28 ppm, **k**. **k** has an integral of two and a *J* coupling of 7.6 Hz. Resonances **i** and **k** correspond to the hydrogen atoms attached to one of the two types of aryl ether in the *meta* and *para* position, respectively with respect to the aryl ether oxygen. To ascertain if resonances **i** and **k** correspond to the aryl ether unit with the allyl moiety or the

ethanol moiety the HMBC NMR spectrum must be referred to and discussed later. The ^{1}H NMR spectrum (Fig. 2.30) exhibits a triplet resonance with an integral of two at 6.99 ppm, **l**, which has a *J* coupling of 7.5 Hz. The COSY NMR spectrum (Fig. 2.31) shows **l** exhibiting coupling to a doublet resonance at 7.17 ppm, **m**. **m** has an integral of four and a *J* coupling of 7.5 Hz. Resonances **l** and **m** corresponds to the hydrogen atoms attached to one of the two types of aryl ether in the *para* and *meta* position, respectively with respect to the aryl ether oxygen. To ascertain if resonances **l** and **m** correspond to the aryl ether unit with the allyl moiety or the ethanol moiety the HMBC NMR spectrum must be referred to and discussed later. To ascertain which aromatic proton resonances belong to which aryl ether unit and assign the ^{13}C NMR spectrum HSQC and HMBC NMR spectroscopy were carried out. The carbon atoms directly attached to hydrogen atoms could be easily assigned using a HSQC NMR experiment and are discussed below.

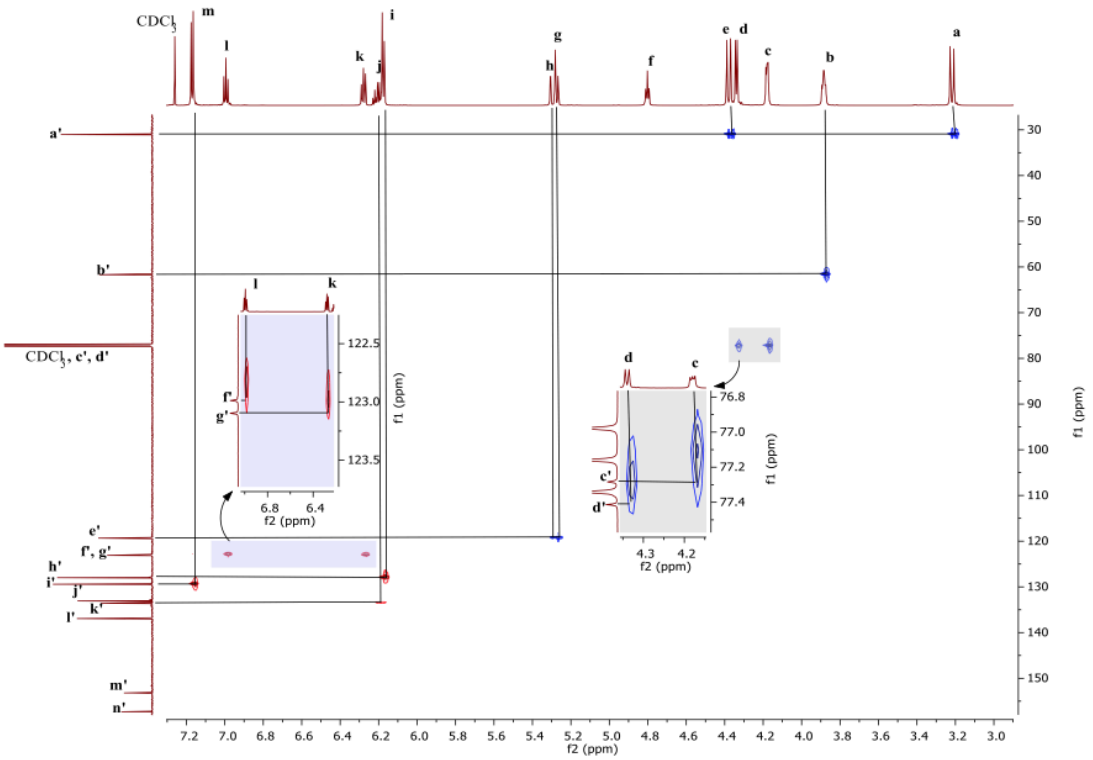

Figure 2.32. HSQC NMR spectrum of **4** in $CDCl_3$.

The HSQC spectrum (Fig. 2.32) shows resonances **a** and **e** coupling to a ^{13}C NMR resonance at 30.9 ppm, **a'**, corresponding to the bridging methylene carbon atom between the aromatics. The fact that the bridging methylene carbon atom resonance resides in the 31.0 ppm region indicates that the calixarene exists in a cone

conformation.[11] Resonance **b** couples to a ^{13}C NMR resonance at 61.7 ppm, **b'**, corresponding to the carbon atom next to the hydroxyl functionality of the ethanol ether moiety. Resonance **c** couples to a ^{13}C NMR resonance at 77.3 ppm, **c'**, corresponding to the carbon atom next to the aryl ether oxygen of the ethanol ether moiety. Resonance **d** couples to a ^{13}C NMR resonance at 77.4 ppm, **d'**, corresponding to the aliphatic methylene carbon atom of the allyl moiety. Resonance **f** exhibits no coupling to a ^{13}C NMR resonance, therefore further confirming that **f** corresponds to the hydroxyl proton. Resonance **g** and **h** both couple to a ^{13}C NMR resonance at 119.3 ppm, **e'**, corresponding to the terminal alkene carbon atom of the allyl moiety. Resonance **i** couples to a ^{13}C NMR resonance at 128.0 ppm, **h'**, which corresponds to one of the *meta* carbon atoms of the aryl ether units. Resonance **j** couples to a ^{13}C NMR resonance at 133.5 ppm, **k'**, corresponding to the non-terminal alkene carbon atom of the allyl moiety. Resonance **k** couples to a ^{13}C NMR resonance at 123.1 ppm, **g'**, which corresponds to one of the *para* carbon atoms of the aryl ether units. Resonance **l** couples to a ^{13}C NMR resonance at 123.1 ppm, **f'**, which corresponds to one of the *para* carbon atoms of the aryl ethers. Resonance **m** couples to a ^{13}C NMR resonance at 129.3 ppm, **i'**, which corresponds to one of the *meta* carbon atoms of the aryl ethers. To ascertain which aromatic protons belong to which of the aryl ether units the HMBC NMR spectrum must be referred to, additionally, the HMBC NMR spectrum allows for identification of quaternary carbons.

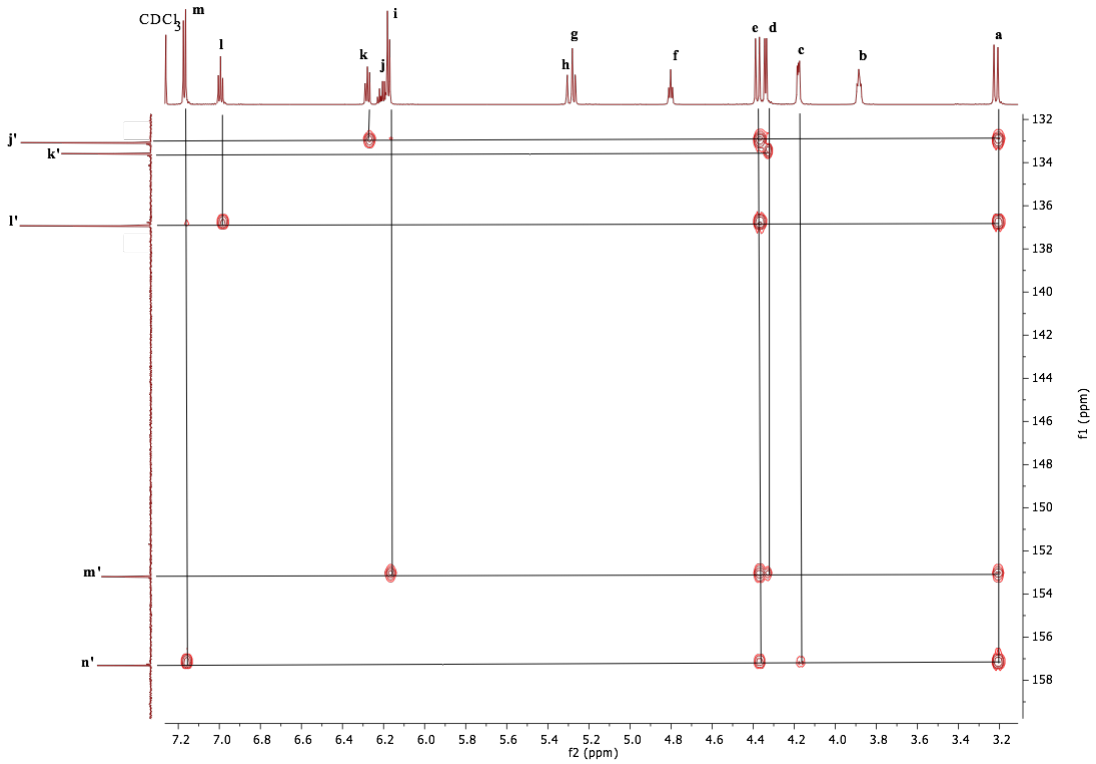

Figure 2.33. HMBC NMR spectrum of **4** in $CDCl_3$.

The HMBC NMR spectrum (Fig. 2.33) shows a ^{13}C NMR resonance at 153.1 ppm, **m'**, coupling to ^{1}H NMR resonances **a**, **d**, **e** and **i**. The fact that a coupling is observed between **m'** and **d**, which corresponds to the aliphatic methylene protons of the allyl moiety indicates **m'** corresponds to the *ipso* carbon of the aryl ether moiety with the allyl moiety attached. Additionally, the coupling between **m'** and **i** indicates that **i** corresponds to the *para* protons of the aryl ether unit with the allyl moiety attached, H_i (Fig. 2.30), and therefore ^{1}H NMR resonance **k** corresponds to the *meta* protons of the aryl ether unit with the allyl moiety attached, H_k (Fig. 2.30). The HMBC NMR spectrum (Fig. 2.33) shows a ^{13}C NMR resonance at 157.3 ppm, **n'**, coupling to ^{1}H NMR resonances **a**, **c**, **e** and **m**. The fact that a coupling is observed between **n'** and **c**, which corresponds to the ether linking protons of the ethanol ether moiety, indicates **n'** corresponds to the *ipso* carbon atom of the aryl ether moiety with the ethanol ether moiety attached. Additionally, the coupling between **n'** and **m** indicates that **m** corresponds to the *para* protons of the aryl ether unit with the ethanol ether moiety attached, H_m (Fig. 2.30), and therefore ^{1}H NMR resonance **l** corresponds to the *meta* protons of the aryl ether unit with the ethanol ether moiety attached, H_l (Fig. 2.30). The HMBC NMR spectrum (Fig. 2.33) shows a ^{13}C NMR resonance at 133.1 ppm, **j'**, coupling to ^{1}H NMR resonances **a**, **e** and **k**, therefore

corresponds to the *ortho* carbon atom of the aryl ether unit with the ethanol ether moiety attached. The HMBC NMR spectrum (Fig. 2.33) shows a ^{13}C NMR resonance at 136.9 ppm, **l'**, coupling to ^{1}H NMR resonances **a**, **e** and **l**, therefore corresponds to the *ortho* carbon atom of the aryl ether unit with the allyl moiety attached. The complete assignment of the ^{13}C NMR spectrum is shown in Figure 2.34.

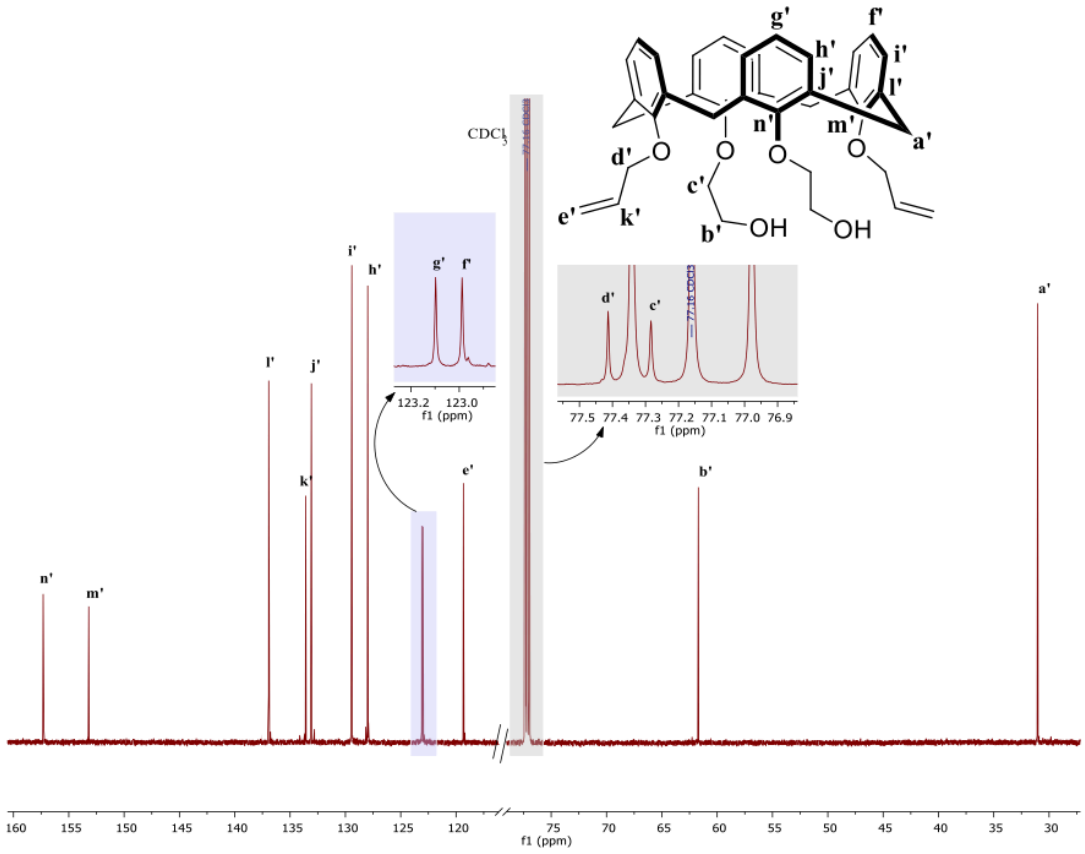

Figure 2.34. ^{13}C NMR spectrum of **4** in $CDCl_3$.

ASAP MS was carried out and the molecular ion was observed at 593.290 Da (100%, which is consistent with the empirical formula $C_{38}H_{41}O_6^+$ (Fig. 2.35). Two further major fragments were observed at 549.274 Da (23.51%) and 505.243 Da (48.84%) corresponding to the empirical formulas $C_{36}H_7O_5^+$ and $C_{32}H_{35}O_4^+$, respectively (Fig. 2.35).

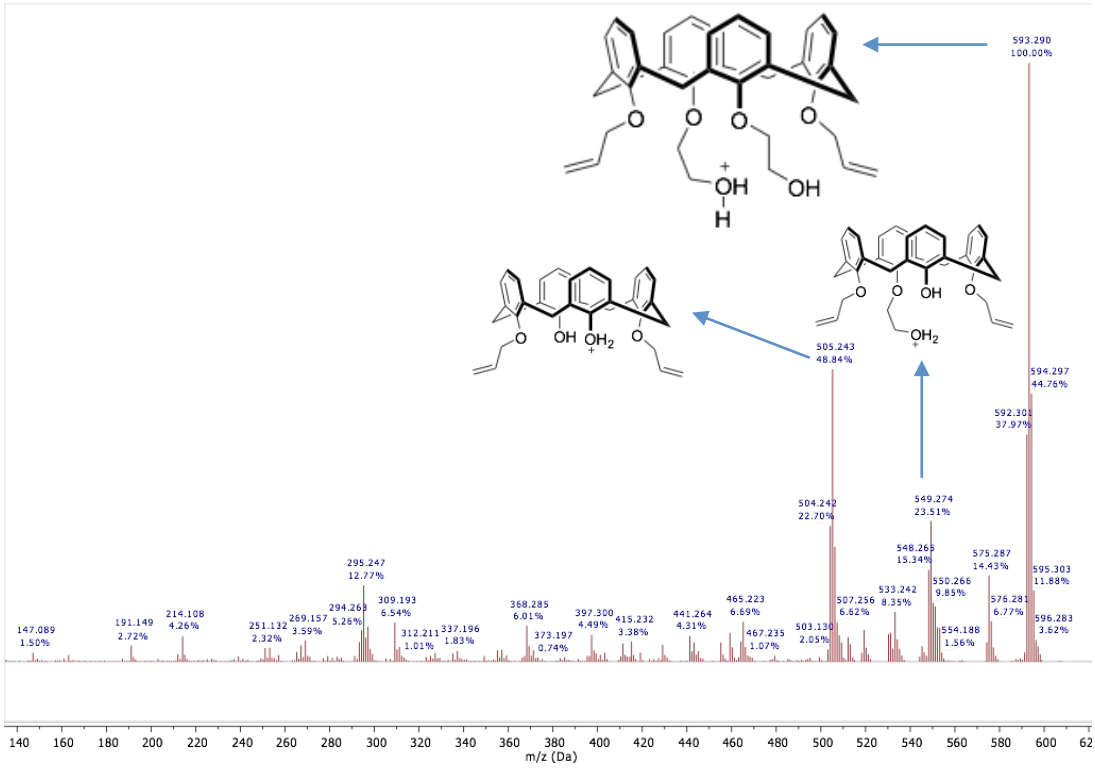

Figure 2.35. ASAP MS spectrum of **4**

CHN analysis was carried out on **4**, with the result closely matching the predicted values; CHN expected = %C = 77.00, %H = 6.80, %N 0.00; measured %C = 77.23, %H = 6.94, %N 0.00.

2.2.5 25,27-*bis*(prop-2-en-1-yloxy)-26,28-*bis*(ethoxyester-2-bromo-acetate)calix[4]arene, 5

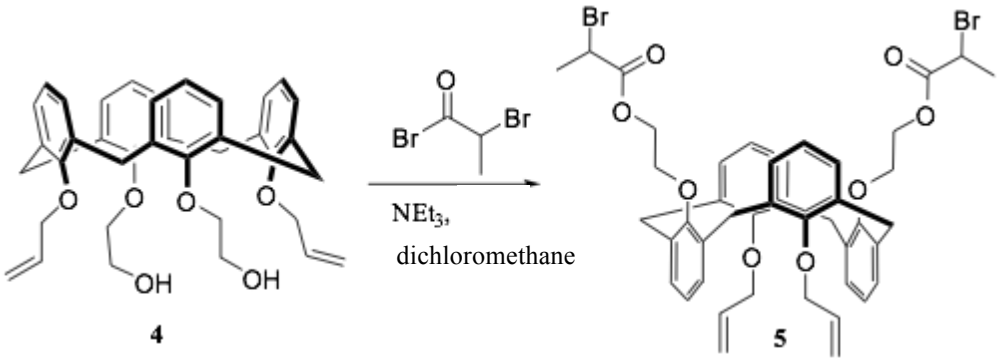

Scheme 2.10. Synthesis of **5**

The novel compound **5**, was successfully synthesised *via* performing an esterification of **4** with the acyl bromide, 2-bromopropionyl bromide, in the presence

of TEA, used as a scavenger for the HBr side product (Scheme 2.10). The reaction was completed within two hours obtaining a 78% yield after column chromatography purification.

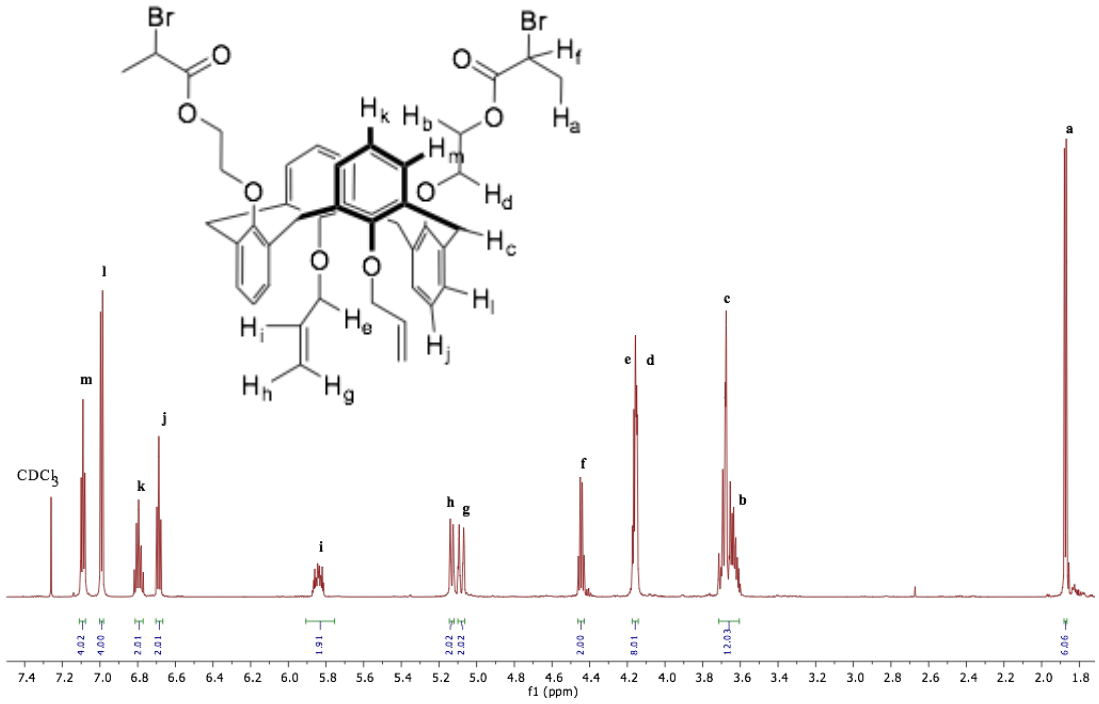

Figure 2.36. ^{1}H NMR spectrum of compound **5** in $CDCl_3$.

The ^{1}H NMR spectrum (Fig. 2.36) exhibits a doublet resonance at 1.87 ppm, **a**, with the integral set to six and a *J* coupling of 6.8 Hz, which corresponds to H_a. The COSY NMR spectrum (Fig 2.37) shows that **a** couples with a quartet resonance at 4.45 ppm, **f**. **f** has an integral of two and has a *J* coupling value of 6.8 Hz, therefore must correspond to H_f (Fig. 2.36). With H_a and H_f exhibiting integrals of six and two, respectively, suggests that the desired addition of two acyl bromide groups was achieved. A singlet resonance is observed at 3.68 ppm, **c** (Fig. 2.36), which is overlapped by a multiplet resonance from 3.60-3.72 ppm, **b**. The presence of a singlet resonance, **c**, corresponding to the methylene protons, H_c, indicates that the calixarene is in a 1,3-alternate conformation opposed to the cone conformation as observed in the previous systems. To assign the resonance signal **b** accurately the COSY NMR spectrum must be consulted. **b** exhibits coupling to itself and **e** only, therefore must correspond to H_b or H_e. To distinguish between H_b and H_e, the HSQC and HMBC NMR spectrum must be analysed and is discussed later. The ^{1}H NMR

spectrum (Fig. 2.36) exhibits two overlapped multiplet resonances at 4.15 ppm and 4.16 ppm, **d** and **e**, respectively, and has an overall integral of eight. It can be observed from the COSY NMR spectrum (Fig 2.37), as discussed above, **e** couples to **b** and corresponds to H_b and H_e. The resonance signal **d** couples to **g** and **i**. In the ^{1}H NMR spectrum (Fig. 2.37) the resonances at 5.08 ppm, 5.14 ppm and 5.84 ppm, corresponding to **g**, **h** and **I**, respectively are produced from the alkene of the allyl moiety. **i** exhibits a multiplet resonance and corresponds to the hydrogen atom H_i (Fig 2.36), therefore couples to three non-degenerate hydrogen atoms, H_e, H_g and H_h and has an integral of two. **g** exists as a double doublet resonance and has a J_1 coupling of 17.2 Hz. **h** also exists as a double doublet resonance but has a J_1 coupling of 10.8 Hz. Both **g** and **h** correspond to the terminal hydrogen atoms of the allyl moiety, with **g** in the *trans* position, H_g, and **h** in the *cis* position, H_h, relative to the stereo chemical position of H_i. As stated above in the COSY NMR spectrum (Fig 2.37) resonance **d** couples to **g** and **i**, H_g and H_i, respectively, therefore **d** must correspond to the hydrogen atom of the ether linkage of the allyl moiety, H_d (Fig 2.36). The ^{1}H NMR spectrum (Fig 2.36) exhibits a triplet resonance at 6.69 ppm, **j**; a multiplet resonance at 6.80 ppm, **k**; a doublet resonance at 6.99 ppm, **l**; and what appears to be a triplet resonance at 7.09 ppm, **m**, which all correspond to the aromatic hydrogen atoms. To ascertain which aromatic hydrogen atoms couple and therefore belong to the same aromatic system the COSY NMR spectrum was consulted (Fig. 2.37).

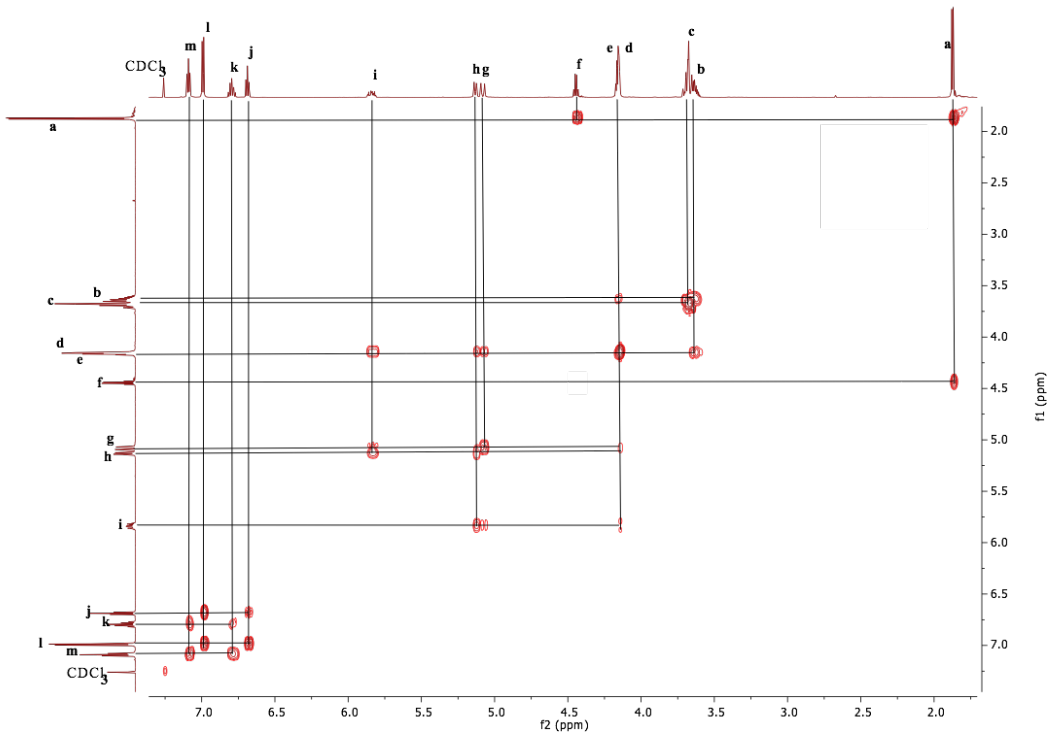

Figure 2.37. ^{1}H COSY NMR spectrum of **5** in $CDCl_3$, showing the coupling between protons.

The ^{1}H COSY NMR spectrum (Fig. 2.37) shows that **j** couples with **l,** and **k** couples with **m**. **j** has an integral of two and **l** has an integral of four (Fig 2.36), therefore it can be deduced that **j** corresponds to the hydrogen atoms *para* to oxygen of two of the aryl ether units corresponding to H_j, and **l** corresponds to the hydrogen atoms in the *meta* position of the same aryl ether system, H_l. **k** has an integral of two and **m** has an integral of four (Fig 2.36), therefore it can be deduced that **k** corresponds to the hydrogen atoms *para* to oxygen of two of the aryl ether units corresponding to H_k, and **m** corresponds to the hydrogen atoms in the *meta* position of the same aryl ether system, H_m. To ascertain which aromatic hydrogen atoms, H_j and H_k, and H_l and H_m, belong to which of the two types of aromatic rings, ^{13}C NMR, HSQC NMR and HMBC NMR spectroscopy was carried out and were fully analysed. Firstly the HSQC NMR spectrum was analysed, as the majority of ^{13}C NMR resonances could be assigned (Fig. 2.38).

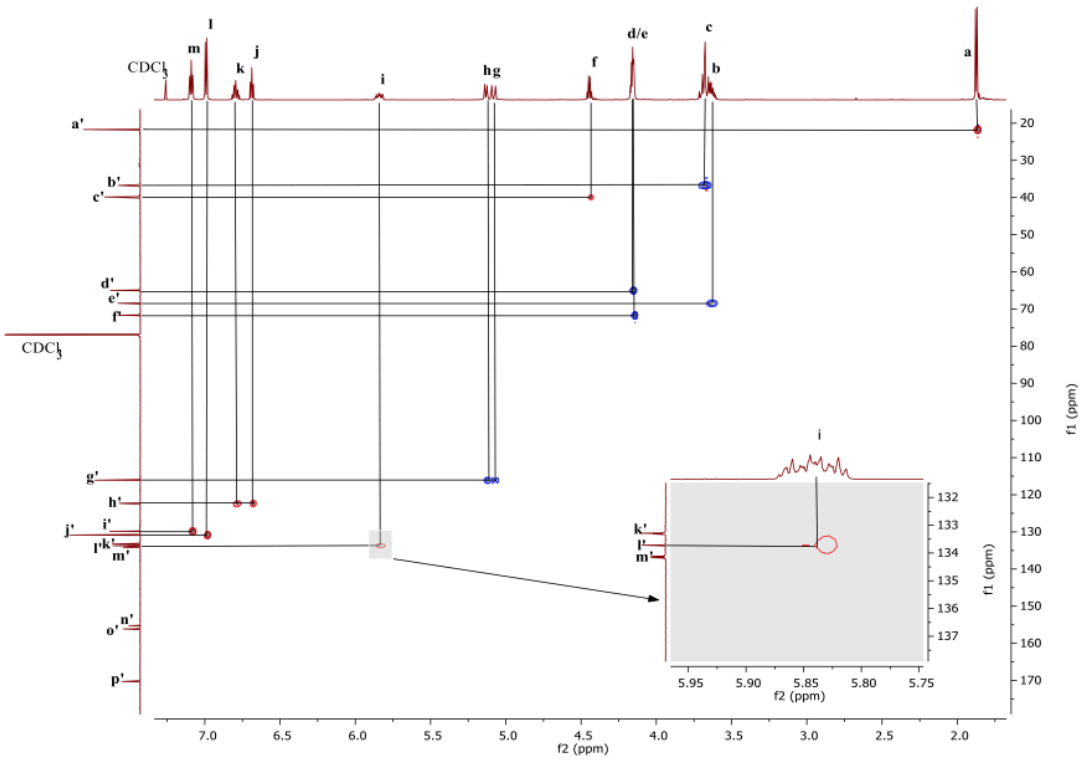

Figure 2.38. HSQC NMR spectrum of compound **5** in $CDCl_3$, showing coupling between various hydrogen and carbon atoms.

The HSQC NMR spectrum (Fig. 2.38) shows resonance **a**, couples to a ^{13}C NMR resonance at 21.8 ppm, **a'**, corresponding to the methyl carbon atom next to the alkyl bromide moiety. Additionally, the fact that the resonance phasing of the coupling between **a'** and **a** is blue indicates it is either a methyl or methine carbon environment that further indicates the methyl carbon assignment. Resonance **b** couples to a ^{13}C NMR resonance at 68.8 ppm, **e'**, with a blue phasing, corresponds to the carbon atom bonded to the hydrogen atoms of either H_b or H_d. The HMBC NMR spectrum is required to distinguish between H_b or H_d and is discussed later. The HSQC NMR spectrum (Fig. 2.38) shows resonance **c** couples to a ^{13}C NMR resonance at 36.9 ppm, **b'**, corresponding to the bridging methylene carbon atom, which is further confirmed by the fact the coupling resonance phasing between **c** to **b'** is blue, indicating it is a methylene environment. Confirmation of the 1,3-alternate conformation is brought about by the chemical shift of **b'** at 36.9 ppm, as it is well documented that a bridging methylene of a calix[4]arene with a chemical shift around 37 to 38 ppm corresponds to a anti conformation between aromatics either side of the bridge.[7] **d** couples to a ^{13}C NMR resonance at 71.8 ppm, **f'**, corresponding to the ether linking ethylene carbon atom of ether ethylene ester. The resonance

signals of **g** and **h** couple to a single ^{13}C NMR resonance at 116.2 ppm, **g'**, corresponding to the terminal alkene carbon atom of the allyl moiety. Resonance **i** couples to a ^{13}C NMR resonance at 133.9 ppm, **l'**, which corresponds to the carbon atom at the non-terminal end of the allyl moiety. Resonances **j** and **k** couple to a single ^{13}C NMR resonance at 122.5 ppm, **h'**, which corresponds to the *para* carbon atoms of the aryl ethers units. Resonance **l** couples to a ^{13}C NMR resonance signal at 131.0 ppm, **j'**, which corresponds to one of the *meta* carbon atoms of one of the aryl ether units. Resonance **m** couples to a ^{13}C NMR resonance at 130.0 ppm, **i'** which corresponds to one of the *meta* carbon atoms of one of the aryl ether units. Using HMBC NMR spectroscopy the hydrogen and carbon atoms of the different aryl ether rings could be assigned accurately and the quaternary carbon atoms could additionally be assigned accurately with respect to position within the aromatic rings and which aryl ether system they belong too.

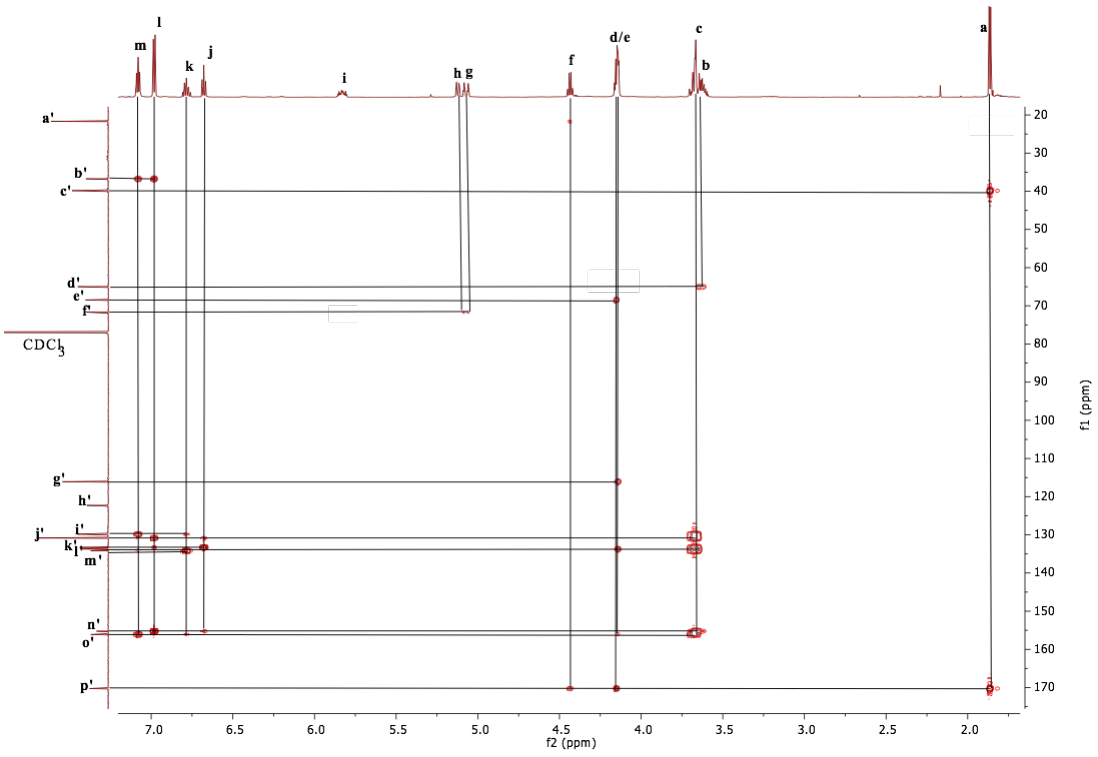

Figure 2.39. HMBC NMR spectrum of compound **5** in $CDCl_3$, showing coupling between multiple bonds of various hydrogen and carbon atoms.

The HMBC NMR spectrum (Fig. 2.39) shows **b** couples to **d'**, and **e** couples to **e'** and **p'**. The ^{13}C NMR resonance at 170.4 ppm, **p'**, corresponds to the carbon of the carbonyl moiety (Fig. 2.40). Therefore, resonance **e** corresponds to H_e (Fig. 2.36) and resonance **b** corresponds to H_b (Fig. 2.36). As confirmed by HSQC NMR

spectroscopy (Fig. 2.38), **b** couples to **e'** and **e** couples to **d'**, therefore the ^{13}C NMR resonance **d'** corresponds to the ethylene carbon atom next to the ester moiety and **e'** corresponds to the ethylene carbon atom linking the ethylene ester moiety to the aromatic ring. The HMBC spectrum (Fig. 2.39) shows **d** couples a resonance at 156.2 ppm, **o'**, therefore **o'** corresponds to the *ipso* carbon atom of the aryl ether allyl moiety. The correct assignment of **o'** is further confirmed by the fact that a coupling is observed to **k** and **m**, which correspond to H_k and H_m, respectively (Fig. 2.36). **m'** exhibits no coupling in the HSQC spectrum (Fig 2.38) but exhibits strong coupling in the HMBC spectrum (Fig. 2.39) to **k, m**, and **c**, corresponding to H_k, H_m and H_c, respectively, therefore must correspond to the *ortho* carbon atom of the aryl ether allyl moiety. The final two unassigned ^{13}C NMR resonances at 133.4 ppm and 155.4 ppm, which correspond to **k'** and **n'** respectively must be the *ipso* and *ortho* carbon atoms of the aryl ether ethylene ester moiety. The HMBC spectrum (Fig 2.39) shows **k'** coupling to **c** and **j**, therefore corresponds to the *ortho* carbon atom of the aryl ether ethylene ester moiety. **n'** exhibits no coupling in the HSQC spectrum but exhibits coupling in the HMBC spectrum (Fig. 2.39) to **l**, **j** and **c**, therefore must correspond to the *ipso* carbon atom of the ethylene ester aryl ether moiety. The complete ^{13}C NMR assignment is shown in Figure 2.40.

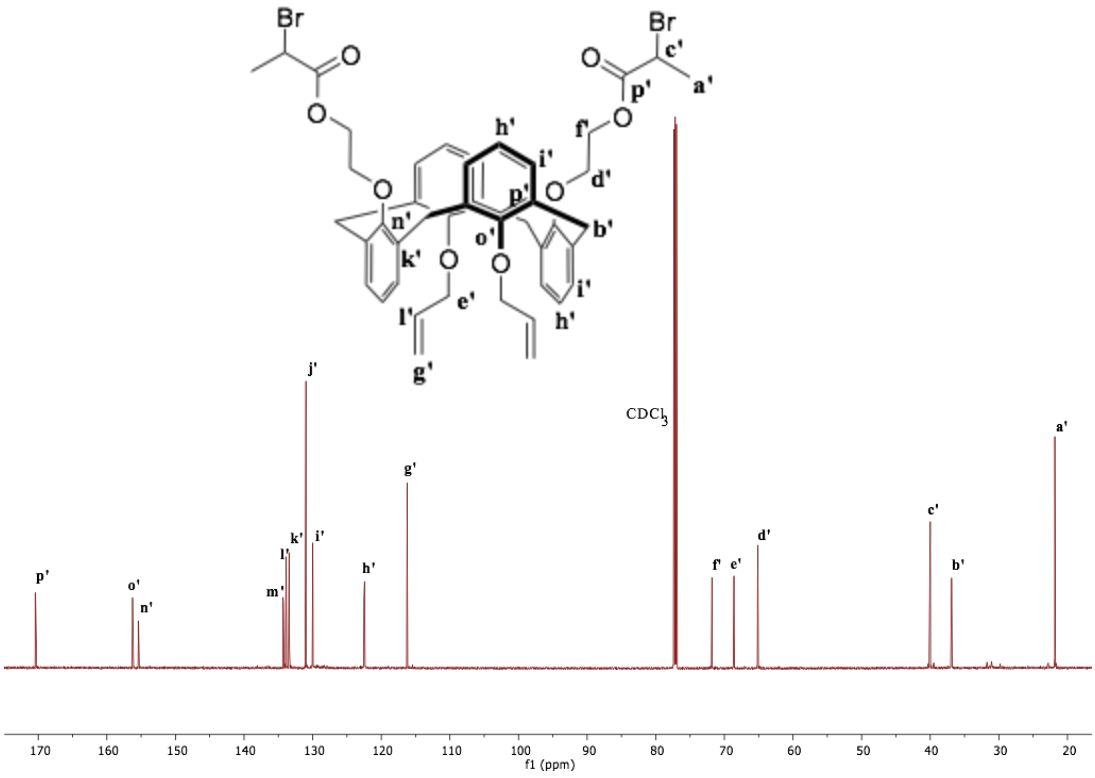

Figure 2.40. ^{13}C NMR spectrum of compound **5** in $CDCl_3$.

ASAP MS was carried out and the molecular ion was observed at 862.162 Da (100%, $[M]^+$), which is consistent with the empirical formula $C_{44}H_{47}Br_2O_8^+$ (Fig. 2.41). Several other fragments were observed and are illustrated in Figure 2.41.

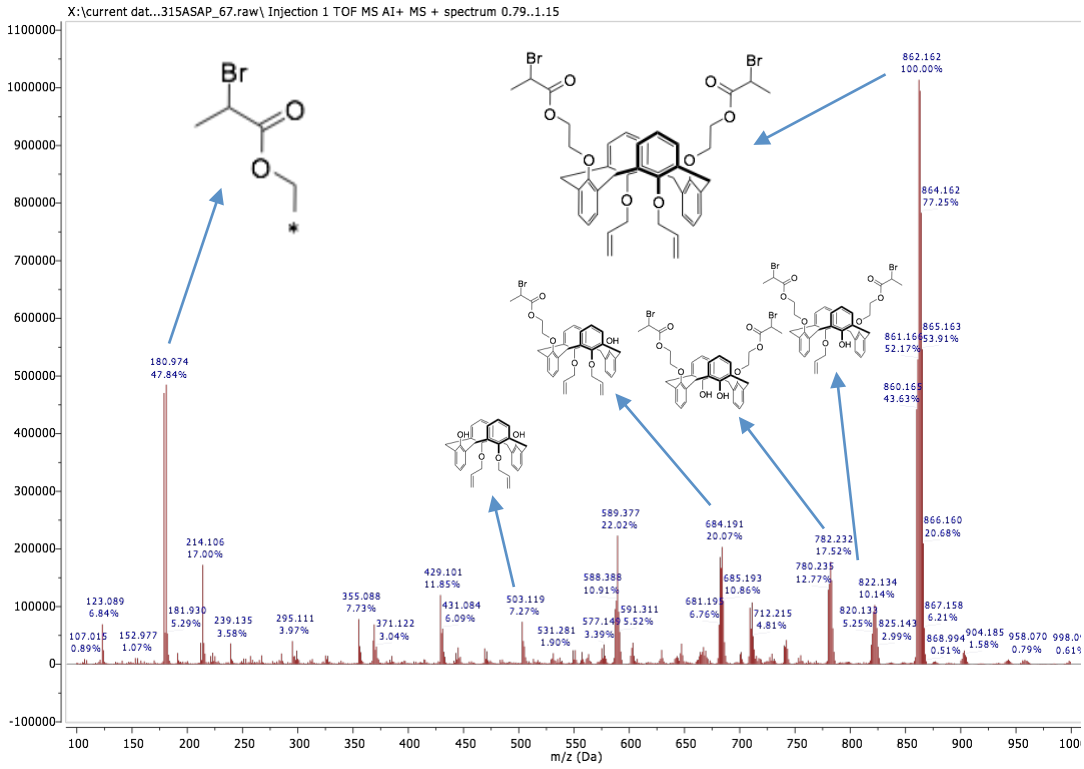

Figure 2.41. ASAP MS sprectrum of compound **5**.

CHN analysis was carried out with the results closely matching the predicted values. CHN Expected = %C = 62.26, %H = 5.38, %N = 0.00; Measured %C = 62.11, %H = 5.36, %N = 0.00.

2.2.6. 25,27-*bis*(3-(hydroxyethyl)thioether-propan-1-yloxy)-26,28-*bis*(ethoxyester-2-bromo-acetate)calix[4]arene, 6

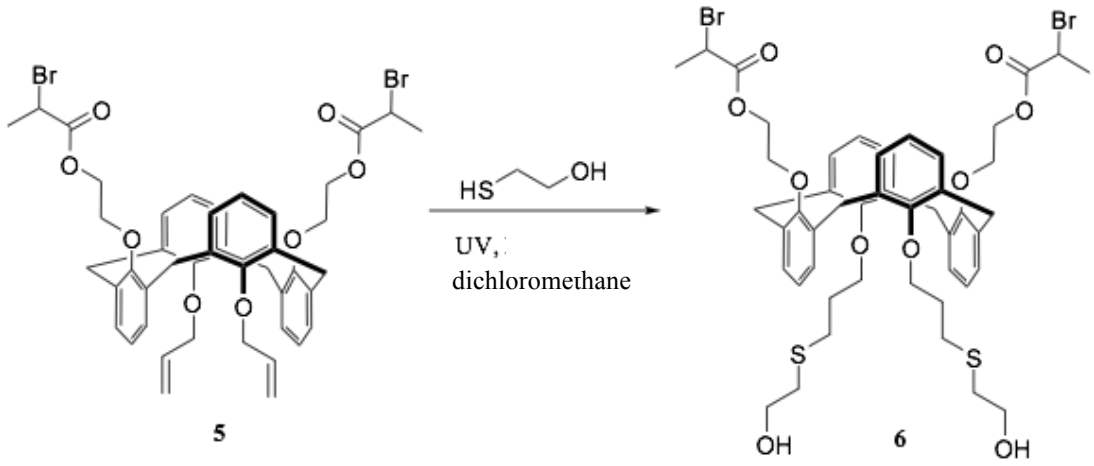

Scheme 2.11. Synthesis of **6**.

The novel compound **6**, was successfully synthesised *via* performing photo initiated thiol-ene "click" chemistry on the double bonds of the allyl moiety (Scheme 2.11). The hydrothiolation of C=C bonds (thiol-ene reaction) has been known since 1905.[12] Thiol-ene reactions are most commonly conducted under radical conditions, which can be initiated thermally but more often photochemically. In 2007, Schlaad *et al*. recognised thiol-ene as a "click" reaction.[13] Their identification was recognition of the simple, robust and highly efficient nature of the reaction. The radical reaction proceeds *via* a step growth process. The proposed mechanism involves the formation of a thiyl radical, which is produced on exposure to a UV source. The thiyl radical adds across the double bond in an anti-Markovnikov fashion, leaving a carbon centred radical, which then undergoes a chain transfer reaction in which a hydrogen radical is abstracted from a thiol moiety, thus generating a new thiyl radical (Scheme 2.12). Termination occurs *via* radical coupling mechanisms.[14]

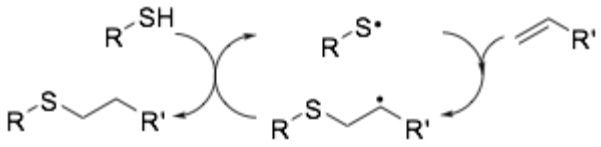

Scheme 2.12. The radical-mediated thiol-ene reaction mechanism.

Compound **5** was exposed to 30 seconds of a wide emission UV spectrum at an intensity of 200 W cm^{-2} in the presence of an excess of 2-mercaptoethanol. A yield of 92% was achieved, after carrying out flash column chromatography.

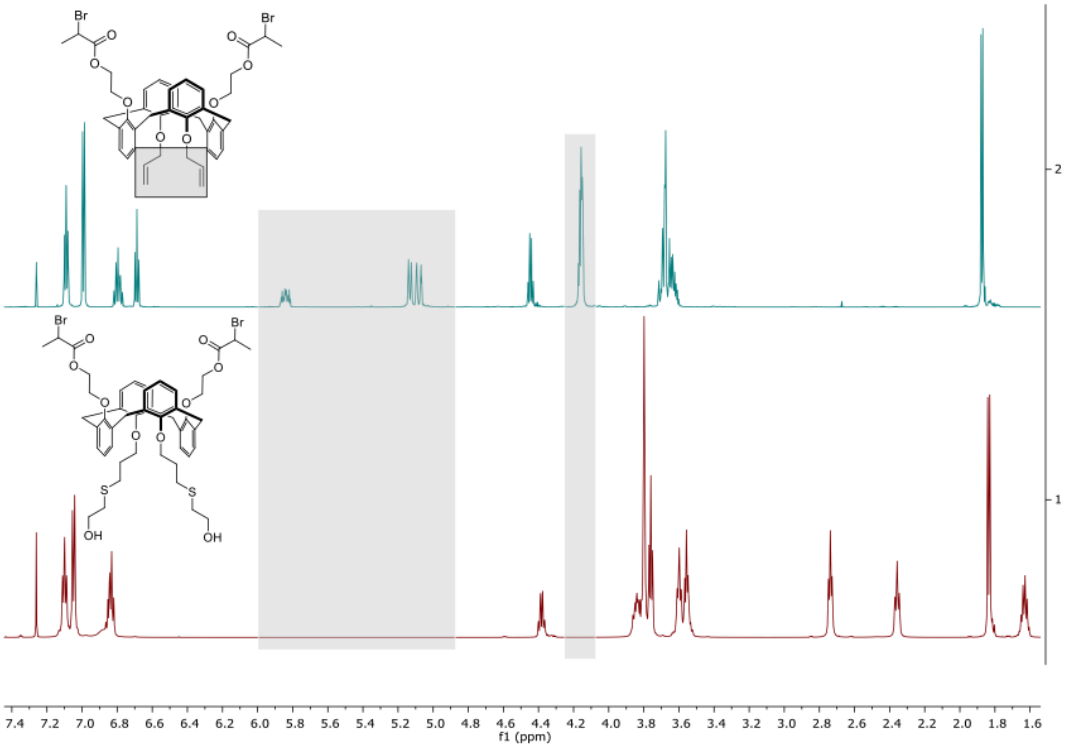

Figure 2.42. ^{1}H NMR spectrum of compound **6** in $CDCl_3$.

The stacked ^{1}H NMR spectra (Fig. 2.42) showed that the resonance for the allyl moiety of **5** had disappeared. A full analysis of **6** is discussed below.

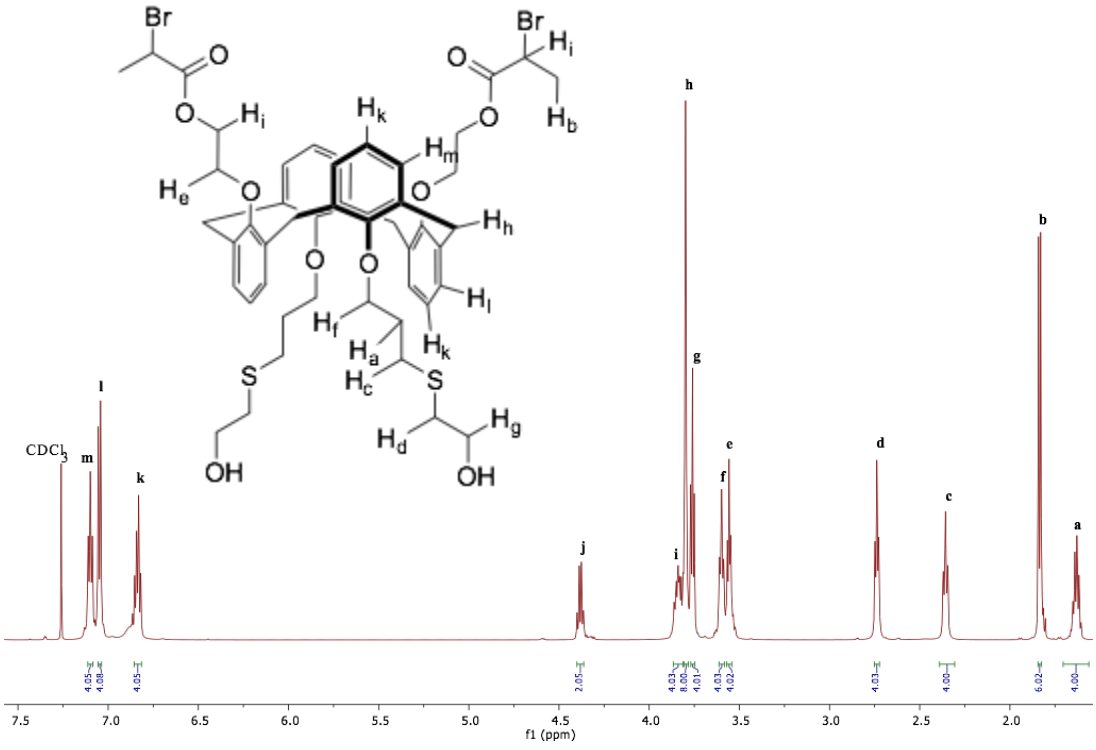

Figure 2.43. ^{13}C NMR spectrum of compound **6** in $CDCl_3$.

The ^1H NMR spectrum (Fig. 2.43) was fully assigned in combination with a COSY NMR experiment (Fig. 2.44). The ^1H NMR spectrum (Fig. 2.43) exhibits a multiplet resonance at 1.63 ppm, **a**. From the COSY NMR spectrum (Fig. 2.44), **a** exhibits coupling to resonance signals **c** and **f**, thus **a** must correspond to the hydrogen atoms on the second carbon atom along of the propylene ether and thio linker, H_a, due to the fact that H_a is the only hydrogen atom that should exhibit COSY coupling to two different hydrogen atoms. Additionally, it is the most up-field resonance due to it being the least de-shielded hydrogen atom of the system, which would be expected for a aliphatic hydrogen atom coupled to two other aliphatic hydrogen atoms. ^1H NMR resonances **c** and **f** must therefore correspond to the other two aliphatic protons of the propylene ether thio linking chain. Sulfur is less electron withdrawing than oxygen, thus the adjacent methylene protons to the sulfur would be expected to exhibit a resonance at a higher chemical shift relative to the methylene protons next to oxygen. The ^1H NMR triplet resonance at 2.36 ppm, **c**, with an integral of four must correspond to the propylene hydrogen atoms next to the linking thio moiety, H_c, and the triplet resonance **f**, at 3.60 ppm with an integral of four, must therefore correspond to the propylene hydrogen atoms of the ether linkage, H_f. The position of H_f is further confirmed by HMBC NMR spectroscopy and is discussed in detail later. The ^1H NMR spectrum (Fig. 2.43) exhibits a doublet resonance at 1.83 ppm, **b**, which has an integral of six and a J_1 coupling of 8.0 Hz. The COSY NMR spectrum (Fig. 2.44) shows that **b** exhibits a coupling to a resonance signal at 4.38 ppm, **j**, which has an integral of two and a J_1 coupling constant of 8.1 Hz. **b** and **j** exhibit no other COSY NMR coupling, therefore correspond to the methine and methyl hydrogen atoms of the ester functionality, with **b** and **j** corresponding to H_b and H_j respectively (Fig. 2.43). The ^1H NMR spectrum (Fig. 2.43) exhibits a triplet resonance at 2.74 ppm, **d**, which has an integral of four and a J_1 coupling of 7.0 Hz. The COSY NMR spectrum (Fig. 2.44) exhibits a coupling between resonances **d** and **g**. **g** corresponds to a triplet ^1H NMR resonance at 3.76 ppm and has a J_1 coupling constant of 7.0 Hz. **d** and **g** must correspond to the ethylene hydrogen atoms of the hydroxyl ethylene thioether moiety. As discussed above, sulfur is less electron withdrawing than oxygen, therefore **d** must correspond to the hydrogen atoms next

to the sulfur group, H_d, and **g** must correspond to the hydrogen atoms next to the hydroxyl moiety, H_g.

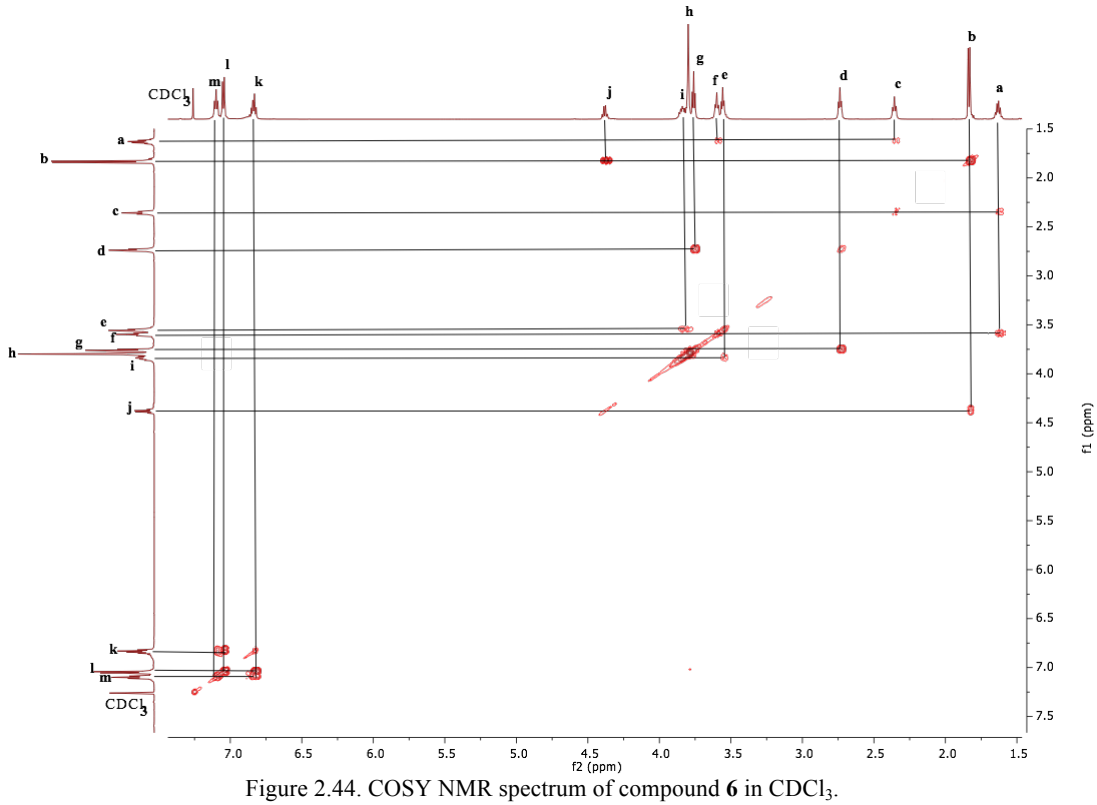

Figure 2.44. COSY NMR spectrum of compound **6** in $CDCl_3$.

The ^{1}H NMR spectrum (Fig. 2.43) exhibits a triplet resonance at 3.56 ppm, **e**, and has an integral of four. The COSY NMR spectrum (Fig. 2.44) shows that **e** exhibits a coupling to a multiplet resonance at 3.84 ppm, **i**, which has an integral of four. The ^{1}H NMR resonances of **e** and **i** must correspond to the ethylene ether ester linkage hydrogen atoms, H_e and H_i, respectively. To determine the exact position of the hydrogen atoms, i.e. next to the ester moiety or the ether linkage the HMBC NMR spectrum must be consulted and is discussed later. The ^{1}H NMR spectrum (Fig. 2.43) exhibits a multiplet resonance at 6.84 ppm, **k**, which has an integral of four. The COSY NMR spectrum (Fig. 2.44) shows that **k** couples to a doublet resonance at 7.05 ppm, **l**, and a multiplet resonance at 7.10 ppm, **m**. Resonances **l** and **m** have integrals of four respectively. The fact that **k** is a multiplet resonance, has an integral of four and couples to **l** and **m** indicates this is an overlapping signal corresponding to the *para* hydrogen atoms of the two different types of aryl ether system, H_k. The fact that the resonance signal of **k** corresponds to two different types of hydrogen atom is further confirmed by HSQC NMR spectroscopy and is discussed later. Resonances **l** and **m** must therefore correspond to the *meta* hydrogen atoms of the

two different aryl ether systems, H_m and H_l. To determine which hydrogen atoms belong to which of the aryl ether system the HSQC and HMBC NMR spectrums must be referred to.

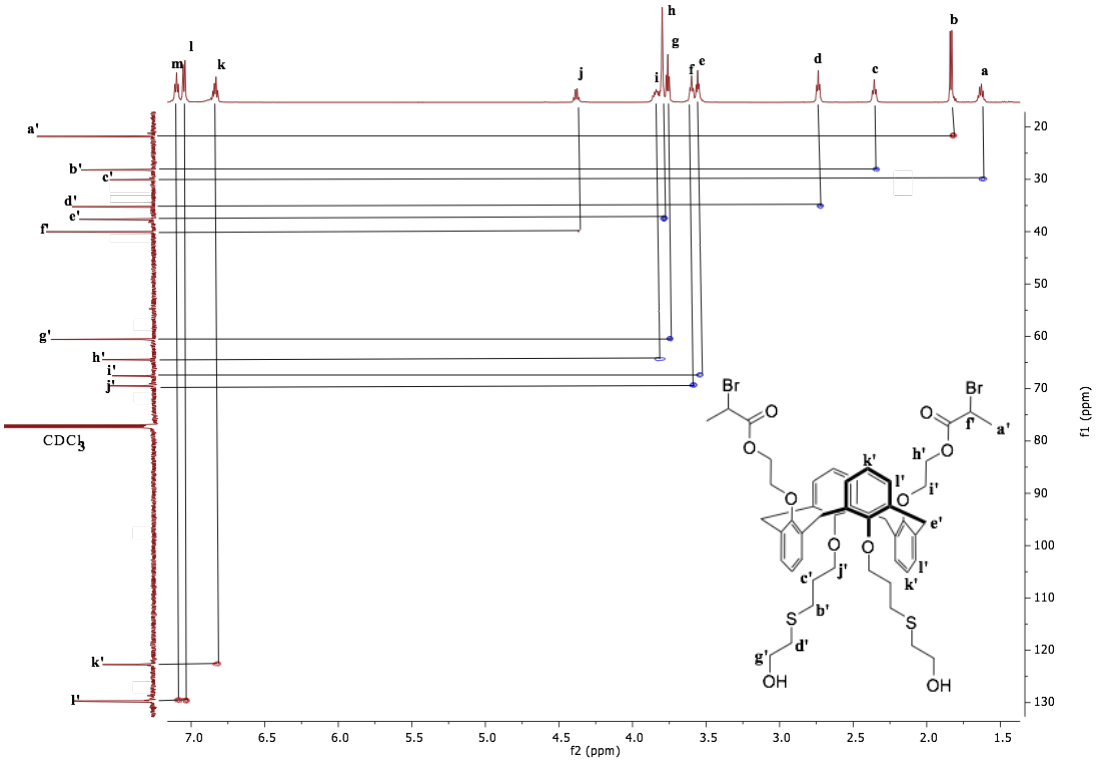

Figure 2.45. HSQC NMR spectrum of compound **6** in $CDCl_3$.

Using HSQC NMR spectroscopy the majority of ^{13}C NMR resonances were assigned. The HSQC NMR spectrum (Fig. 2.45) shows that **a** couples to a resonance at 30.1 ppm, **c'**, which corresponds to the second carbon atom along of the propylene ether and thio linker unit. Resonance **b** couples to a ^{13}C NMR resonance at 21.8 ppm, **a'**, and corresponds to the methyl of the ester moiety. Resonance **c** couples to a ^{13}C NMR resonance at 28.2 ppm, **b'**, and corresponds to the third methylene carbon atom along of the propylene ether and thio linker unit next to the sulfur. Resonance **d** couples to a ^{13}C NMR resonance at 35.2 ppm, **d'**, and corresponds to the methylene carbon atom of the ethylene ether and thio linker unit next to the sulfur. Resonance **e** exhibits a coupling with a ^{13}C NMR resonance at 67.5 ppm, **i'**, which corresponds to one of the carbon atoms of the ethylene ether ester linkage with the exact position being assigned through HMBC NMR spectroscopy and is discussed later. **f** exhibits a coupling to a ^{13}C NMR resonance at 69.5 ppm, **j'**, which corresponds to the carbon atom next to the phenolic oxygen of the propylene ether and thio linking chain. **g**

couples to a ^{13}C NMR resonance at 60.6 ppm, **g'**, which corresponds to the carbon atom next to the hydroxyl moiety of the hydroxyl ethylene thioether group. **h** couples to a ^{13}C NMR resonance at 37.6 ppm, **e'**, which corresponds to the methylene carbon atom that bridges the aromatics. The fact that the ^{13}C resonance for **e'** resides at 37.6 ppm further indicates the calixarene molecule is in a 1,3-alternate conformation.[7] **i** couples to a ^{13}C NMR resonance 64.5 ppm, **h'**, which corresponds to one of the carbon atoms of the ethylene ether ester linkage with the exact position being assigned through HMBC NMR spectroscopy and is discussed later. **j** couples to a ^{13}C NMR resonance at 40.0 ppm, **f'**, which corresponds to the methine carbon atom of the ester moiety. **k** couples to a ^{13}C NMR resonance at 122.7 ppm, **k'**, which corresponds to the *para* carbon atom with respect to the phenolic oxygen of the aryl ether systems. **l** and **m** both couple to a ^{13}C NMR resonance at 129.7 ppm, **l'**, and correspond to the *meta* carbon atoms with respect to the phenolic oxygen of the aryl ether systems. To complete the assignment of the ^{13}C NMR spectra and accurately assign the ethylene hydrogen atoms of the ethylene ether ester the HMBC NMR spectrum was analysed.

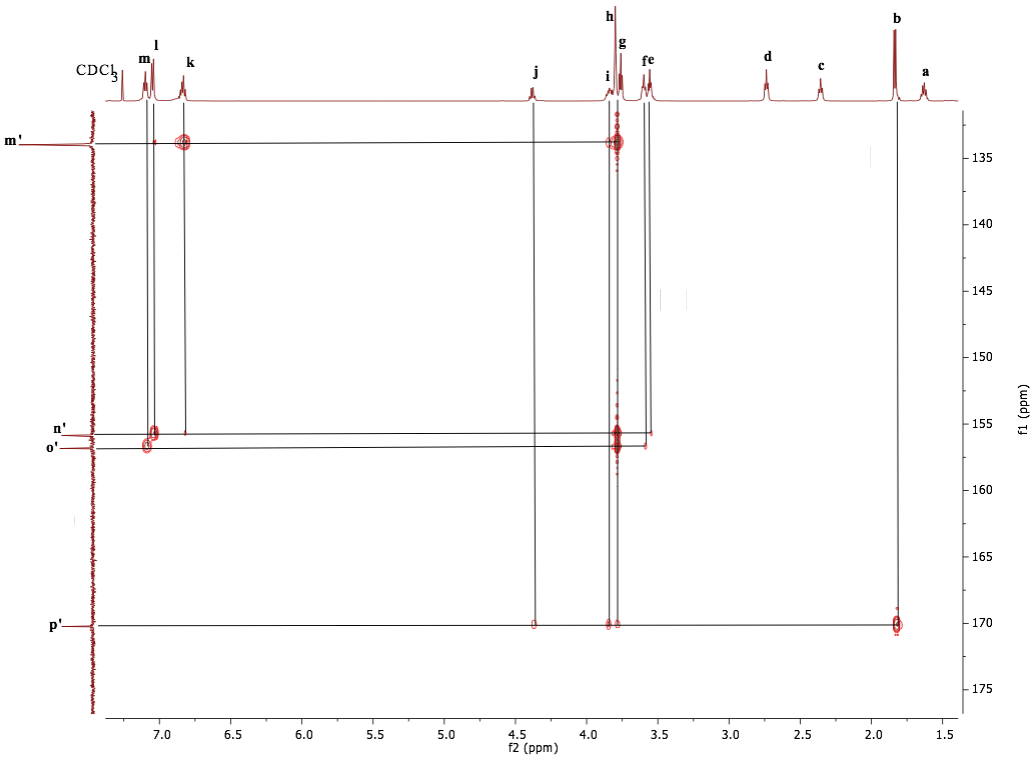

Figure 2.46. HMBC NMR spectrum of compound **6** in $CDCl_3$.

The HMBC NMR spectrum (Fig. 2.46) shows that **e** couples to a ^{13}C NMR resonance at 155.9 ppm, **n'**. **n'** additionally exhibits a coupling to **l** and **k**, corresponding to H_l and H_k respectively (Fig. 2.43), therefore **n**' must correspond to the *ipso* carbon atom of the aryl ether system with the ethylene ester moiety adjoined, (Fig. 2.47). With **n'** being assigned it was concluded that **e** must correspond to the hydrogen atoms of the ether linkage of the ethylene ester moiety, H_e (Fig. 2.43). The HMBC NMR spectrum (Fig. 2.46) shows that **f** couples to a ^{13}C NMR resonance at 156.8 ppm, **o'**. **o'** additionally exhibits coupling to resonances **m** and **k**, corresponding to H_m and H_k respectively (Fig. 2.43), therefore **o**' must correspond to the *ipso* carbon atom of the aryl ether system with the propylene ether and thio linking chain adjoined (Fig. 2.47). The final ^{13}C NMR resonance to be assigned is that of **m'**, which exhibits a resonance at 134.0 ppm. The HMBC NMR spectrum (Fig. 2.46) shows that **m'** couples to resonances **h** and **k**, thus correspond to the *ortho* carbon atoms of both types of aryl ether systems, (Fig. 2.47).

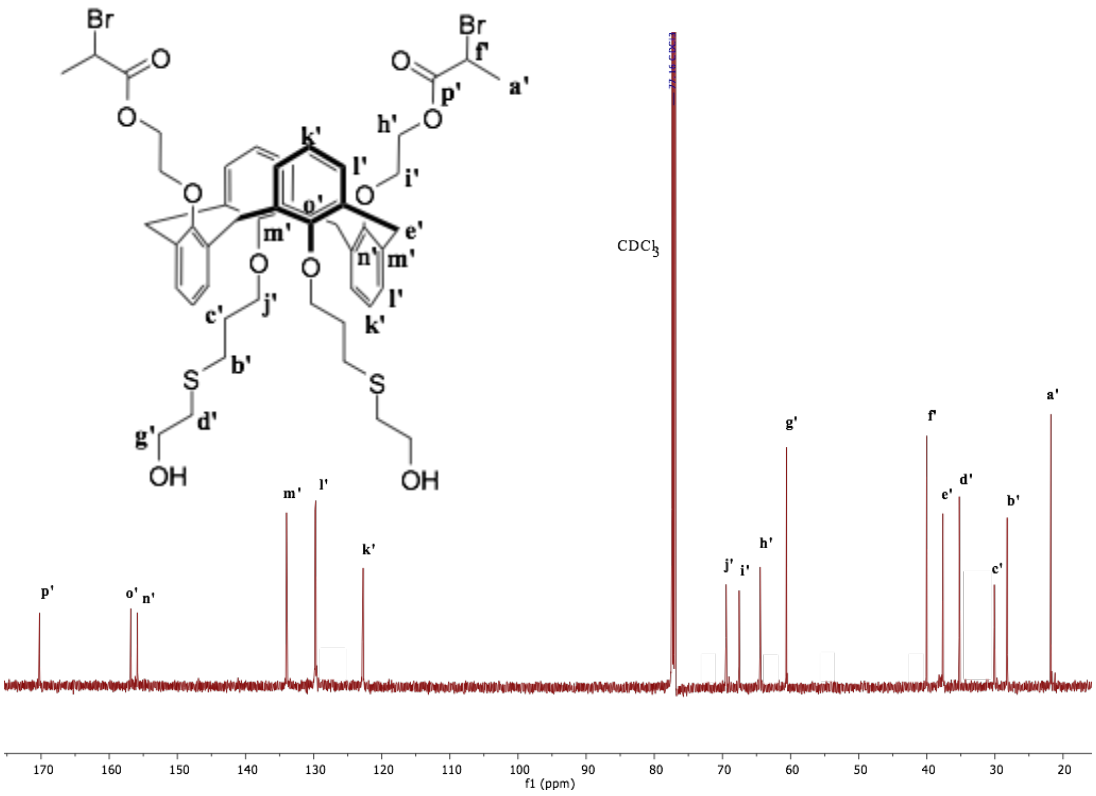

Figure 2.47. ^{13}C NMR spectrum of compound **6** in $CDCl_3$.

ASAP MS was carried out and the molecular ion was observed at 1019.182 Da (7.61%), which is consistent with the empirical formula $C_{48}H_{59}Br_2O_{10}S_2^+$ (Fig. 2.48). The ASAP MS spectrum (Fig. 2.48) additionally shows major peaks corresponding to fragments of **6** at 941.180 Da (51.72%) and 180.074 Da (100%), which are consistent with the empirical formulae $C_{46}H_{53}Br_2O_9S_1^+$ and $C_5H_8BrO_2^+$, respectively.

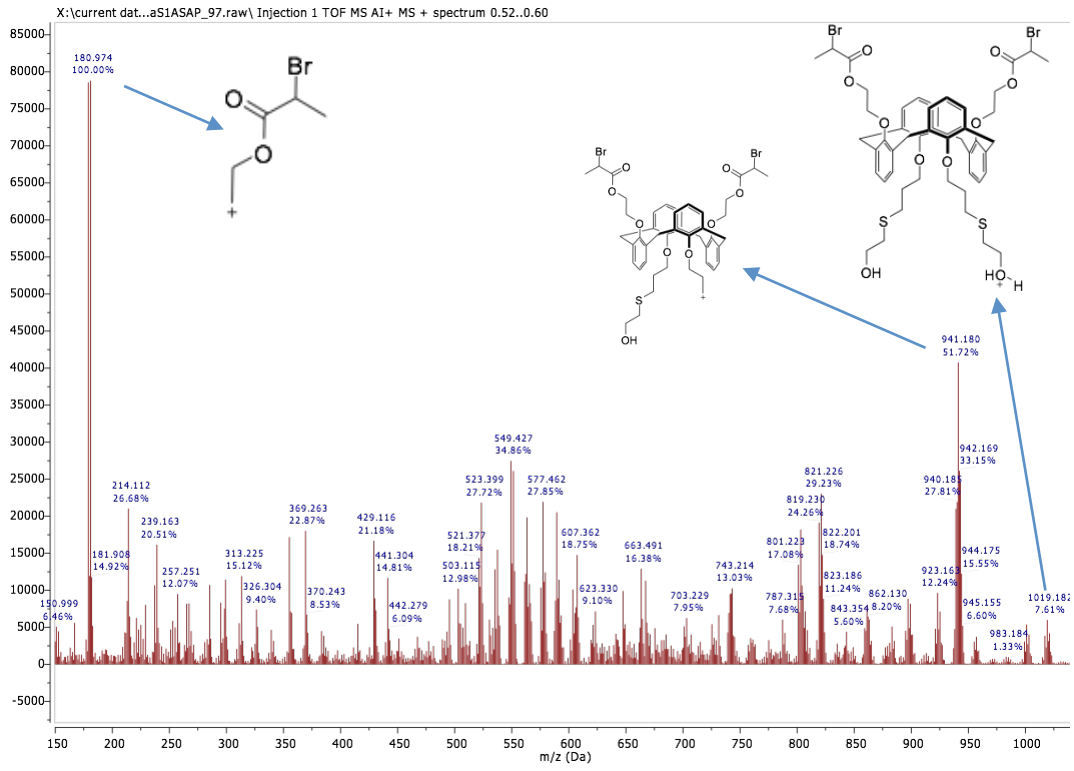

Figure 2.48. ASAP MS spectrum of compound **6**.

CHN analysis was carried out and the results obtained closely matched the predicted values. CHN Expected = %C = 57.38, %H = 4.41, %N = 0.00; Measured %C = 57.48, %H = 4.56, %N = 0.00.

2.3. Conclusion

This chapter described the synthetic strategy employed for the synthesis of a novel A_2B_2 heterofunctional initiator that incorporated an alkyl halogen moiety required for SET-LRP and a primary hydroxyl moiety required for ROP. Calix[4]arene, **1**, and 25,27-*bis*(prop-2-en-1-yloxy)calix[4]arene, **2**, are known compounds and were synthesised according to the literature.[2,3] A full characterisation was performed on

both **1** and **2** to further the characterisation that had been carried out previously. The novel compound 25,27-*bis*(prop-2-en-1-yloxy)-26,28-*bis*(ethyleneacetate)-calix[4]arene, **3**, was successfully synthesised *via* a Williamson ether synthesis between **2** and methyl chloroacetate and was fully characterised. **3** was taken forward and used as the precursor for the novel compound 25,27-*bis*(prop-2-en-1-yloxy)-26,28-*bis*(ethanolxy)calix[4]arene, **4**, which was synthesised *via* an ester reduction of **3**. The novel compound 25,27-*bis*(prop-2-en-1-yloxy)-26,28-*bis*(ethoxyester-2-bromo-acetate)calix[4]arene, **5**, was successfully synthesised *via* an esterification reaction with 2-bromopropionyl bromide; a full characterisation was carried out. The final step was to incorporate a primary hydroxyl moiety, which was achieved *via* a photo initiated thiol-ene click reaction with the allyl moieties of **5** and 2-mercaptoethanol, resulting in the successful synthesis of the novel compound 25,27-*bis*(3-(hydroxyethyl)thioether-propan-1-yloxy)-26,28-*bis*(ethoxyester-2-bromo-acetate)calix[4]arene, **6**; a full characterisation of **6** was carried out.

2.4. References

(1) Gou, P. F.; Zhu, W. P.; Shen, Z. Q. *J. Polym. Sci. Pol. Chem.* **2010**, *48*, 5643.
(2) Parker, D. *Macrocycle Synthesis: A Practical Approach*; Oxford University Press: United States, 1996.
(3) Gutsche, C. D.; Levine, J. A.; Sujeeth, P. K. *J. Org. Chem.* **1985**, *50*, 5802.
(4) Tashiro, M.; Yamato, T. *J. Org. Chem.* **1979**, *44*, 3037.
(5) Rha, S. G.; Chang, S. K. *J. Org. Chem.* **1998**, *63*, 2357.
(6) Gou, P. F.; Zu, W. P.; Shen, Z. Q. *Acta Polym. Sin.* **2007**, 967.
(7) Jaime, C.; Demendoza, J.; Prados, P.; Nieto, P. M.; Sanchez, C. *J. Org. Chem.* **1991**, *56*, 3372.
(8) Shinkai, S.; Araki, K.; Koreishi, H.; Tsubaki, T.; Manabe, O. *Chem. Lett.* **1986**, 1351.
(9) Araki, K.; Iwamoto, K.; Shinkai, S.; Matsuda, T. *Bull. Chem. Soc. Jpn.* **1990**, *63*, 3480.
(10) Streitwieser, A. *Chem. Rev.* **1956**, *56*, 571.
(11) Gutsche, C. D.; Bauer, L. J. *J. Am. Chem. Soc.* **1985**, *107*, 6052.
(12) Posner, T. *Ber. De. Deut. Chem. Ges.,***1905**, *38*, 646.
(13) Gress, A.; Volkel, A.; Schlaad, H. *Macromolecules* **2007**, *40*, 7928.
(14) Hoyle, C. E.; Lowe, A. B.; Bowman, C. N. *Chem. Soc. Rev.* **2010**, *39*, 1355.

Chapter 3

Amphiphilic A_2B_2 Miktoarm Star Polymer with Calix[4]arene Core

3.0. Introduction

Star polymers comprise of three or more linear polymer chains attached to a central core. Star polymers have attracted much attention due to their smaller hydrodynamic volumes and their lower melt, and solution viscosities relative to their linear counterparts with the same molecular weight.[1,2] Based on the chemical composition of the polymer arm, star shaped polymers can be classified into two categories; homoarm (regular) and heteroarm (miktoarm) star shaped polymers. Regular star shaped polymers comprise of arms with identical chemical composition with similar molecular weights (M_n) originating from a central junction point. Conversely, miktoarm star shaped polymers contain two or more arms with different chemical compositions (Fig. 3.1).[3,4]

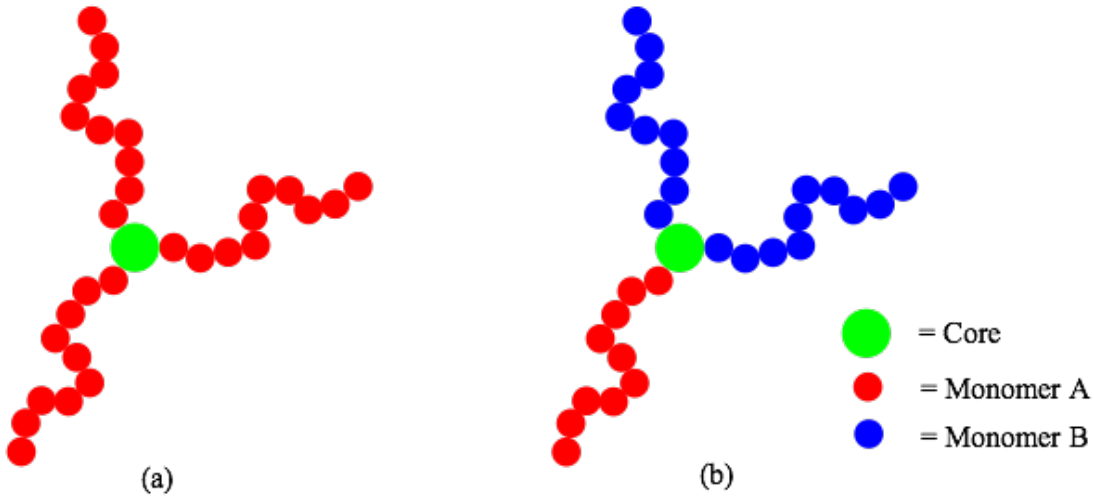

Figure 3.1. Diagram depicting (a) regular star and (b) miktoarm star polymer.

The synthesis of star polymers can be accomplished *via* one of the two strategies; "core first" and "coupling onto".[5,6] The "core first" strategy employs a multifunctional initiating core from which polymer arms are grown. The "core first" strategy allows for a precise number of arms *via* controlling the number of initiating sites on the core. The "coupling-onto" strategy employs coupling between a multifunctional core and a pre-formed polymer arm. Efficient coupling reactions, such as azide-alkyne "click" chemistry, allow the "coupling onto" strategy to synthesise high yielding and well-defined polymeric structures.

This chapter describes the synthesis of a novel amphiphilic A_2B_2 miktoarm star polymer, which employs the "core first" strategy. The multifunctional core encompasses two primary hydroxyls, which facilitate ring opening polymerisation (ROP) that will lead to the formation of a linear polymer bridged by a calixarene core. Two alkyl bromo moieties remain within the calixarene core, which facilitate single electron transfer living radical polymerisation (SET-LRP). The monomer selected for ROP was ε-caprolactone due to its biocompatibility and hydrophobic nature in its polymer form (poly(ε-caprolactone), PCL). To introduce an amphiphilic nature to the polymer system the monomer selected for SET-LRP was 2-hydroxylethyl acrylate (HEA) that forms poly(2-hydroxylethyl-acrylate) (PHEA), which is a hydrophilic polymer. The combination of hydrophilic and hydrophobic arms attached to a central core will lead to interesting properties, such as self-assembly in certain solvents.

3.1 Experimental

3.1.1. Materials

25,27-*bis*(3-(hydroxyethyl)thioether-propan-1-yloxy)-26,28-(ethoxyester-2-bromo-acetate)calix[4]arene, **6**, was synthesised according to Chapter 2.2.6. Tin(II) 2-ethylhexanoate (92.5 – 100%) and tris[2-(dimethylamino)ethyl]amine (Me_6TREN) was purchased from Sigma Aldrich and used without further purification. ε-caprolactone (97%) was purchased from Sigma Aldrich and distilled before use. HEA (96%) was purchased from Sigma Aldrich and purified as follows: HEA was added to water (20% v/v) and washed with hexane ten times to remove the unwanted ethylene glycol diacrylate. The HEA monomer was collected *via* extraction with diethyl ether (five times), which was dried over magnesium sulfate and filtered. Hydroquinone (0.05%) was further added.[7] Bare copper wire (24 standard wire gauge, diameter = 0.559 mm) was purchased from Fisher Scientific and was activated prior to use *via* dipping in concentrated nitric acid and then washing with water and drying. Chloroform, methanol, anhydrous dimethylformamide (DMF) and diethyl ether analytical grade solvents and concentrated nitric acid (~37%) were purchased from Fisher Scientific and used without further purification. Dry toluene was obtained from the Durham University Chemistry Department Solvent Purification Service (SPS). Deuterated chloroform ($CDCl_3$) and deuterated DMF (DMF-d_7) for NMR analysis was purchased from Apollo Scientific.

3.1.2. Instrumentation

^{1}H and ^{13}C NMR spectra were recorded using a Varian VNMRS 700 spectrometer operating at 700 MHz and 176 MHz respectively, with *J* values given in Hz. $CDCl_3$ or DMF-d_7 was used as deuterated solvent for ^{1}H and ^{13}C NMR analysis and the spectra were referenced to the solvent traces at 7.26 ppm, 77.0 ppm and 8.03 ppm, 163.15 ppm respectively. The following abbreviations are used in describing NMR spectra: s = singlet, d = doublet, t = triplet, q = quartet, quin = quintet, s = sextet, m = multiplet, b = broad, o = overlapped, dd = doublet of doublets, dq = doublet of quartets. 2D NMR experiments were also used to fully assign the proton and carbon environments in the products. ^{1}H-^{1}H Correlation Spectroscopy (COSY) demonstrated proton-proton correlations over two or three bonds. ^{1}H-^{13}C

Heteronuclear Shift Correlation Spectroscopy (HSQC) demonstrated correlation between directly bonded proton and carbons atoms. ^{1}H-^{13}C Heteronuclear Multiple-Bond Correlation (HMBC) demonstrated the correlation between proton and carbon environments through several bonds.

Fourier transform-infra-red (FT-IR) spectroscopy was conducted using a Perkin Elmer 1600 series spectrometer.

Measurements of molecular weight (M_n and M_w, corresponding to the number average and weight average molecular weight, respectively), and dispersity (Đ) of polymers synthesised were carried out *via* Size Exclusion Chromatography (SEC) on a Viscotek TDA 302 with triple detectors: refractive index, light scattering and viscosity. The columns used were PLgel 2 x 300 mm 5 μm mixed C, that have a linear range of molecular weight from 2.0 x 10^2 – 2.0 x 10^6 g mol^{-1}. The solvent used was THF or DMF at flow rates and temperatures at 1.0 mL min^{-1}, 35 ^oC and 1.0 mL min^{-1}, 70 ^oC respectively. The detectors were calibrated using narrow molecular weight distribution linear polystyrene or polyethylene glycol standards.

Differential scanning calorimetry (DSC) was carried out using a *TA Instrument Q1000 DSC*, ran in N_2 gas, with a flow rate of 30 mL min^{-1} and a heating rate of 10 ^oC min^{-1}.

Thermogravimetric analysis (TGA) was carried out using a *Perkin Elmer Pyris 1 TGA* connected to a *HIDEM HPR20 MS*, ran in N_2 gas with a heating rate of 10 ^oC min^{-1}.

3.1.3. Synthesis of Calixarene-PCL_{100} macro-initiator, 7

To a Schlenk vessel charged with a magnetic stirrer, 25,27-*bis*(3-(hydroxyethyl)thioehterl-propan-1-yloxy)-26,28-*bis*(ethoxyester-2-bromo-acetate)calix[4]arene, **6** (0.100 g, 0.01 mmol) was added. The system was sealed, evacuated and then purged with argon (Ar), which was repeated three times. Under Ar, freshly dried and distilled ε-caprolactone (2.18 mL, 1.965 mmol) was added *via* cannula. To the colourless solution, $Sn(Oct)_2$ (0.23 M, 0.022 mL) in dried toluene

was injected in; the reaction mixture was heated to 120 ^{o}C and stirred continuously for 24 h, forming a very viscous white/pale brown residue. The residue was dissolved in minimal chloroform and then precipitated into methanol; the precipitation process was repeated three times. The precipitated polymer was filtered and collected, resulting in a white fluffy material. Mass = 2.228 g, yield = 95%. ν_{max} (Perkin Elmer FT-IR, Diamond, cm^{-1}). 3441 (w, OH), 2850-2990 (s, CH), 1721 (s, C=O). ^{1}H NMR (700 MHz, $CDCl_3$) δ: .35 (quin, 391H_a, *J* = 7.9 Hz), 1.61 (sex, 772H_b, *J* = 7.8 Hz), 1.79 (d, 6H_c, *J* = 7.0 Hz), 2.27 (t, 388H_d, *J* = 7.6 Hz), 2.71 (m, 4H_e), 3.61 (t, 5H_f, *J* = 6.6 Hz), 4.03 (t, 380H_g, *J* = 6.7 Hz), 4.18 (m, 4H_h), 4.33 (q, 2H_i, *J* = 7.0 Hz) 6.68 – 6.84 (m, 4H_j), 6.95 – 7.07 (m, 8H_k). ^{13}C NMR (176 MHz, $CDCl_3$) δ: 21.6 (**a'**), 24.6 (**b'**), 25.6 (**c'**), 28.1 (**d'**), 28.4 (**e'**), 30.2 (**f'**), 34.2 (**g'**), 40.2 (**h'**), 62.5 (**i'**), 63.1 (**j'**), 64.2 (**k'**), 129.6 (**l'**), 170.3 (**m'**), 173.4 (**n'**). SEC (THF) M_n = 2.2 x10^4 g mol^{-1}, M_w = 3.7 x 10^4, Đ = 1.7. DSC , T_m = 51.53 ^{o}C, T_c = 32.67 ^{o}C, %crystallinity = 31.43%. TGA, Onset X_1 = 264.85 ^{o}C, Onset X_2 = 336.86 ^{o}C, ΔY_1 = 94.149%, ΔY_2 = 5.851%.

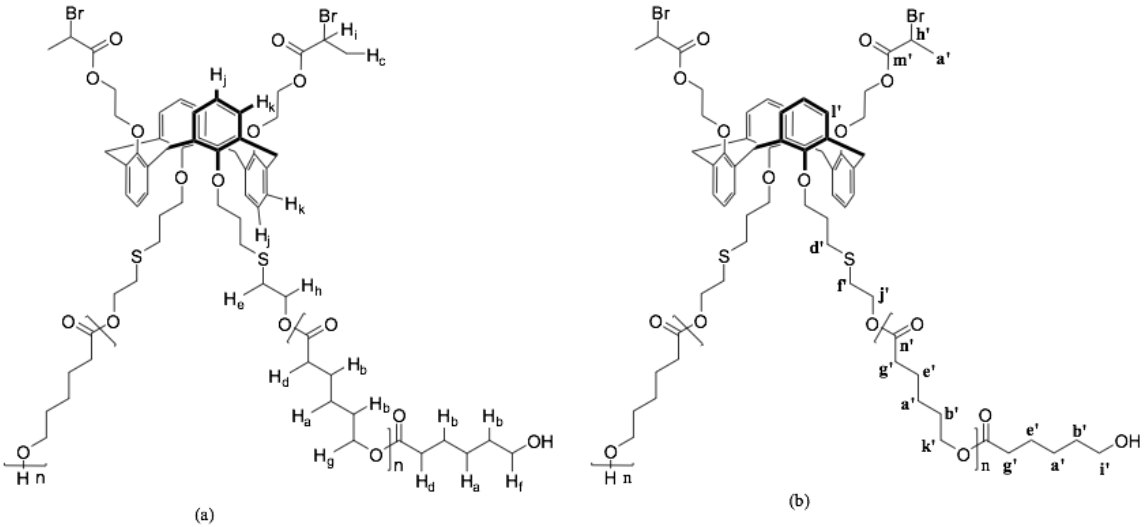

Figure 3.2. Labelling of the chemical environments in **7** (a) proton (b) carbon.

3.1.4. Synthesis of Calixarene-star$PCL_{100}PHEA_m$ Miktoarm Star Polymer, 8-10 - Typical Polymerisation Procedure

To a Schlenk vessel charged with a magnetic stirrer, **7** (0.100 g, 0.001 mmol), activated copper wire (2 cm, activated using nitric acid) and $CuBr_2$ (0.001 g, 0.005 mmol) were added. The system was evacuated and purged with Ar. Dry DMF (0.5 mL) was added *via* a syringe. HEA (appropriate amount for desired M_n) was further added under Ar. The pale white/colourless solution was deoxygenated with dry Ar for 0.5 h. To initiate the polymerisation a deoxygenated stock solution of Me_6TREN in DMF (0.03 mL, 0.02518 M) was injected in, the solution remained colourless. The reaction mixture was stirred at 25 ^oC for 16 h, leading to a very pale blue translucent viscous solution. Further DMF (appropriate amount) was added to the reaction vessel; the free flowing solution was precipitated into diethyl ether, the precipitation process was carried out a further two times. The white precipitate was collected and further washed with diethyl ether and chloroform resulting in a tacky white material. Yield = 63-75%. ν_{max} (Perkin Elmer FT-IR, Diamond, cm^{-1}). 3441 (w, OH), 2850-2990 (s, CH), 1721 (s, C=O). ^1H NMR (700 MHz, DMF-d_7) δ: 1.38 (quin, $400H_a$, J = 7.0 Hz), 1.62 (sex, $772H_b$, J = 8.2 Hz), 151-179 (m, $1100H_c$), 2.27 (t, $388H_d$, J = 7.2 Hz), 2.37-2.56 (m, $560H_e$), 3.72 (s, $1140H_f$), 4.03 (t, $380H_g$, J = 6.3 Hz), 4.14 (m, $1077H_h$), 4.85 (s, $543H_i$), 6.71-6.85 (m, $4H_j$), 7.08-7.22 (m, $8H_k$). ^{13}C NMR (176 MHz, DMF-d_7) δ: 24.7 (**a'**), 25.5 (**b'**), 28.5 (**c'**), 33.9 (**d'**), 35.9 (**e'**), 41.6 (**f'**), 59.9 (**g'**), 63.9 (**h'**), 66.3 (**i'**), 173.2 (**j'**), 174.8 (**k'**). M_{nNMR} = 4.0 – 8.2 x10^4 g mol^{-1}. SEC (DMF), M_n = 4.0 – 8.2 x10^4 g mol^{-1}, Đ = 1.8 – 2.4.

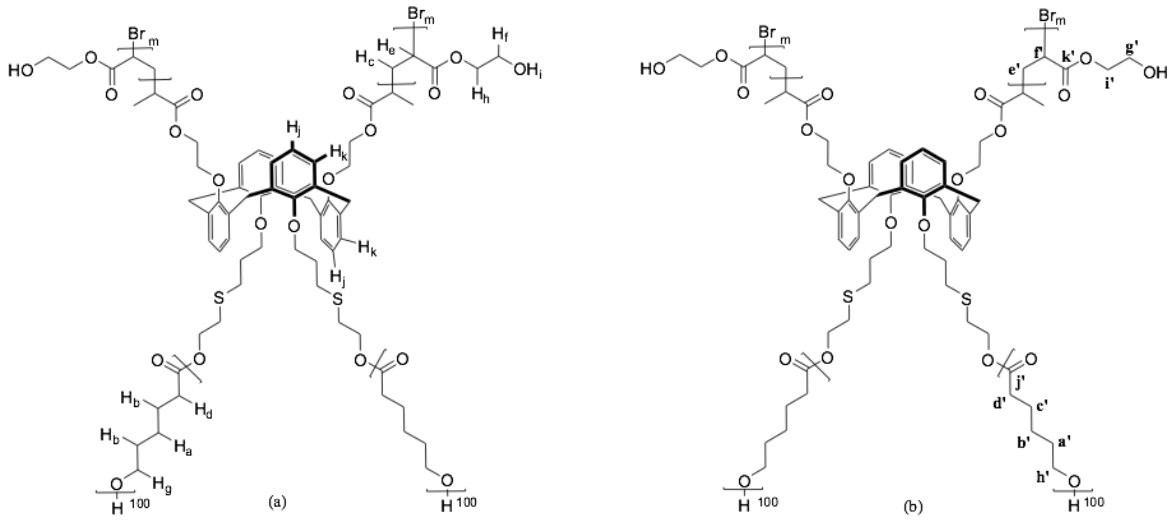

Figure 3.3. Labelling of the chemical environments in **8-10** (a) proton (b) carbon.

3.2. Results and discussion

3.2.1. Calixarene-PCL$_{100}$, 7

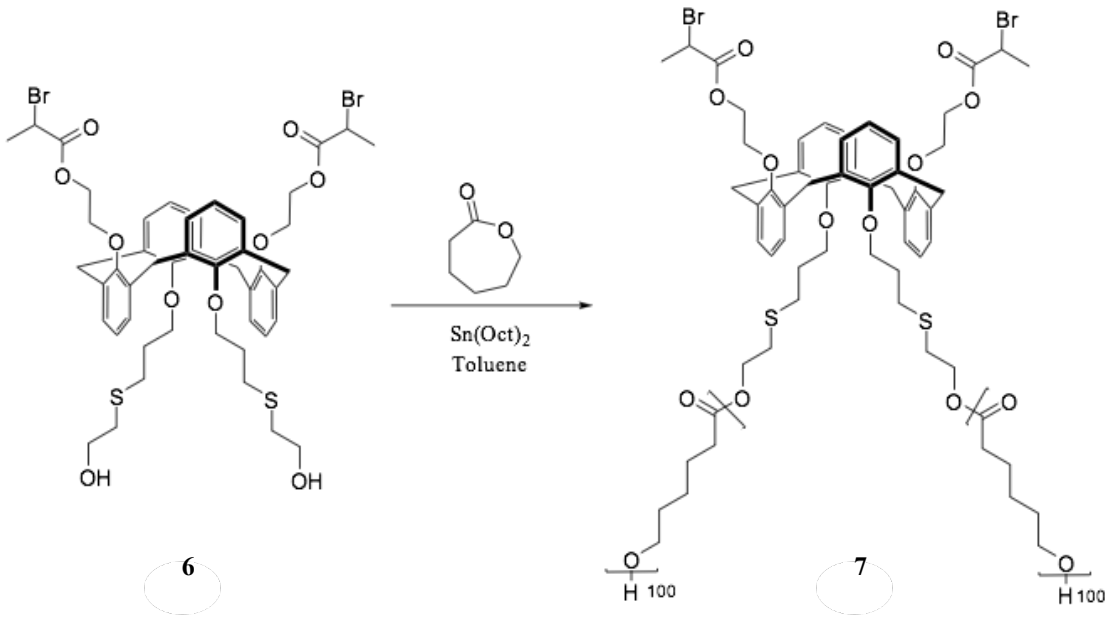

Scheme 3.1. ROP of ε-caprolactone using heterofunctional calix[4]arene based initiator.

The primary hydroxyls of **6** was used to ROP ε-caprolactone using $Sn(Oct)_2$ with the reaction run in bulk, leading to a linear PCL with bridging calix[4]arene core (Scheme 3.1). A monomer to initiator to catalyst ratio of 200:1:0.05 was used to target a molecular weight of 2.0 x 10^4 g mol^{-1}, therefore a degree of polymerisation (**DP**) of 100 per arm. The polymer has been fully analysed and the results are discussed below.

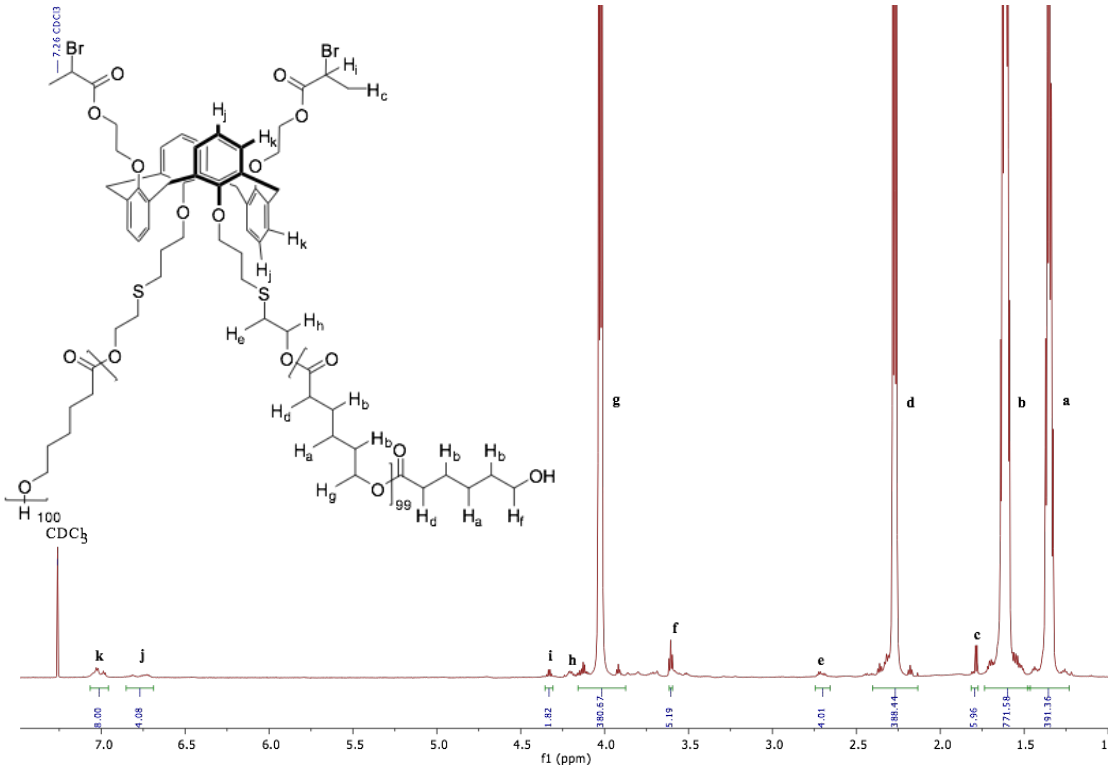

Figure 3.4. ^{1}H NMR spectrum of **7**, in $CDCl_3$.

The ^{1}H NMR spectrum (Fig. 3.4) shows the resonances of the calixarene initiator aromatic ring CH protons, with two multiplets observed at 6.68-6.84 and 6.95-7.07 ppm, **j** and **k**, corresponding to H_j and H_k, respectively. The mulitplets are observed due to the many different conformations of the calixarene core present. **j** and **k** had their integral values set to four and eight, respectively, with the **DP** of the PCL determined with respect to these values. The ^{1}H NMR spectrum (Fig. 3.4) shows the resonances for the PCL backbone protons **a**, **b**, **d**, **f** and **g**. A quintet resonance with an integral of 391 is observed at 1.35 ppm, **a**, corresponding to the hydrogen atoms of the PCL on the third carbon atom with respect to the carbonyl carbon atom, H_a. A sextet resonance with an integral of 772 is observed at 1.61 ppm, **b**, corresponding to the methylene hydrogen atoms of the PCL on the second and fourth carbon with respect to the carbonyl carbon, H_b. A triplet resonance with an integral of 388 is observed at 2.27 ppm, **d**, corresponding to the methylene hydrogen atoms of the PCL on the first carbon atom with respect to the carbonyl carbon atom, H_d. A triplet resonance with an integral of 380 is observed at 4.03 ppm, **g**, corresponding to the methylene hydrogen atoms of the PCL backbone on the fifth carbon atom with respect to the carbonyl carbon atom, H_g. A triplet resonance with an integral of five is observed at 3.61 ppm, **f**, corresponding to the PCL methylene protons conjoint

with the hydroxyl moiety on the fifth carbon of the end chain, H_f. H_f has an integral greater than four due to it overlapping a second resonance. Due to the low concentration of calixarene core with respect to PCL, and the broadness of the PCL resonances, not all of the calixarene core proton resonances could be observed clearly, therefore not all protons could be accounted for.

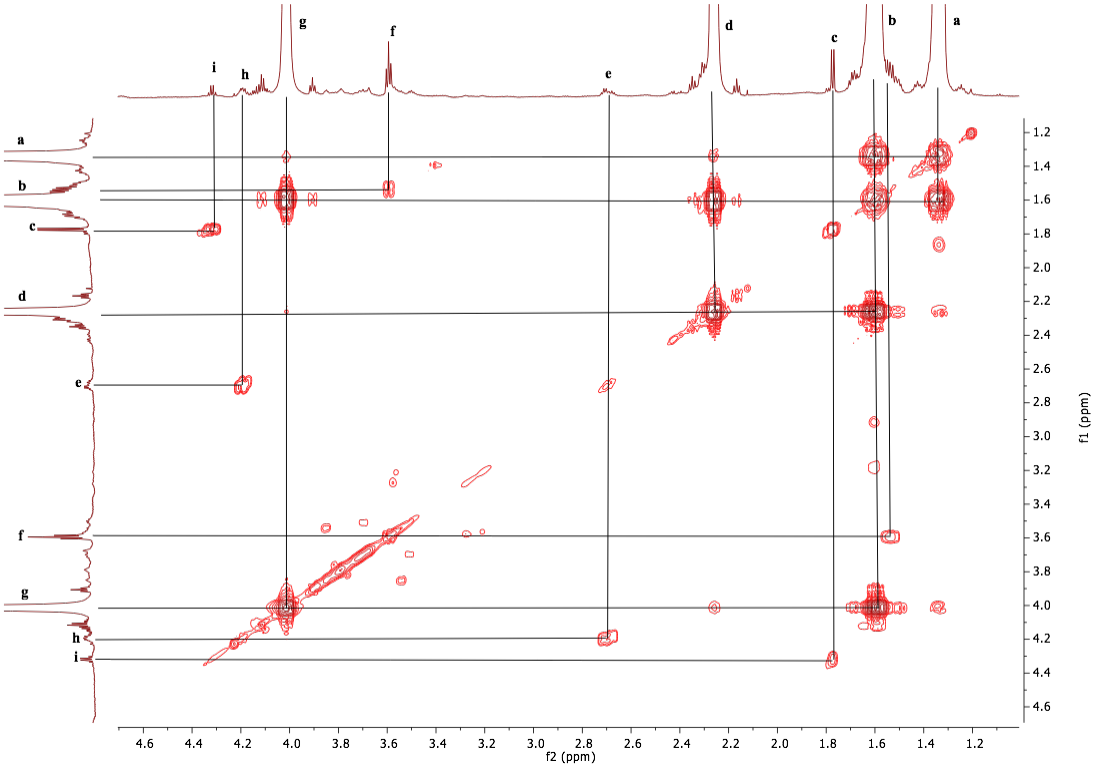

Figure 3.5. ^{1}H COSY NMR spectrum of **7** in $CDCl_3$.

The ^{1}H NMR spectrum (Fig. 3.4) shows a doublet resonance with an integral of six at 1.79 ppm, **c**, and a J_1 coupling constant of 7.0 Hz, which corresponds to the methyl protons of the bromopropanoate moiety, H_c. The COSY NMR spectrum (Fig. 3.5) shows resonance **c** exhibiting a coupling to a quartet multiplicity resonance at 4.33 ppm, **i**. The ^{1}H NMR spectrum (Fig. 3.4) shows that **i** has an integral of two and a J_1 coupling constant of 7.0 Hz, therefore corresponds to the methine protons of the bromopropanoate moiety, H_i. To further characterise the ^{1}H NMR spectrum, more in-depth analysis was required. The ^{13}C NMR spectrum (Fig. 3.8) exhibits a resonance at 173.6 ppm, **n'**, which corresponds to the ester carbonyl carbon atom of the PCL. The HMBC NMR spectrum (Fig. 3.6) shows that **n'** exhibits a coupling to a ^{1}H NMR resonance at 4.20 ppm, **h**. The ^{1}H NMR resonance **h** corresponds to the ethylene protons next to the ether oxygen linking the calixarene core to the PCL, H_h

(Fig. 3.4). The fact that a multiple bond coupling was observed between **m'** and **h** confirms that the hydroxyl of the calixarene core was the initiation site for the ROP of the ε-caprolactone, and there is a covalent bond between the calixarene core initiator and PCL, therefore it can be concluded that the calixarene core is chemically bound opposed to physically bound. The COSY NMR spectrum (Fig. 3.5) shows **h** exhibiting a coupling to a multiplet resonance at 2.71 ppm, **e**, which corresponds to the ethylene protons next to the thio ether sulfur linking the calixarene core to the PCL, H_e (Fig. 3.5).

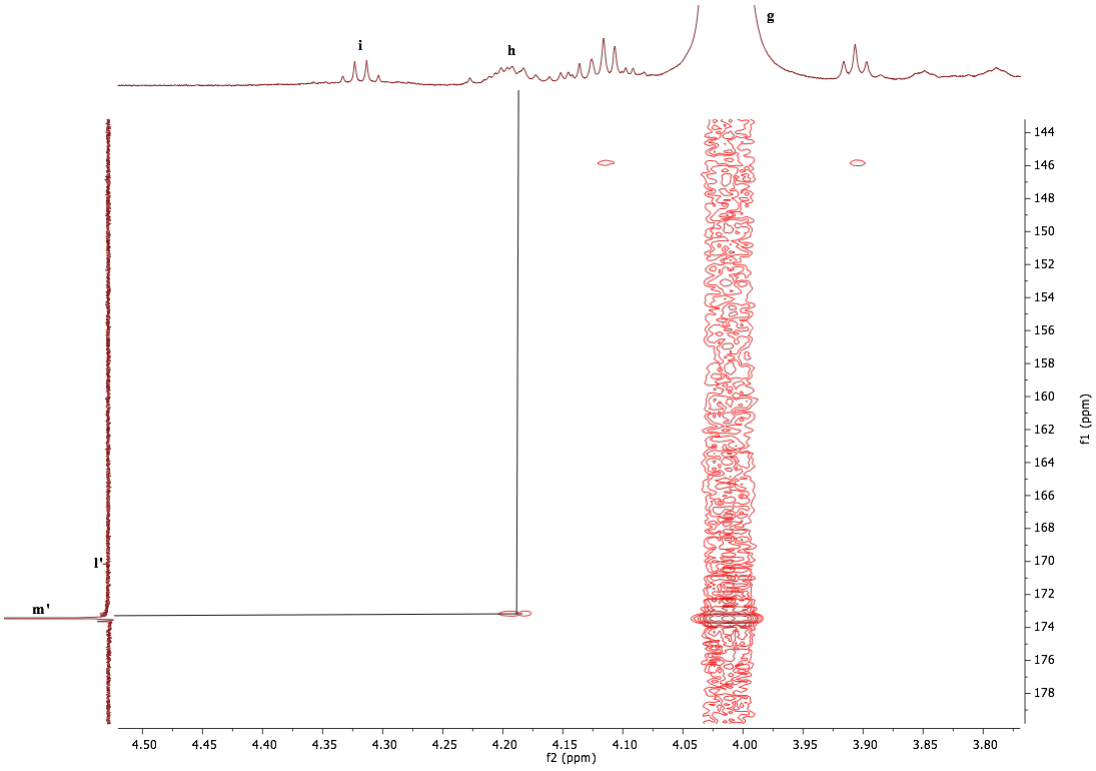

Figure 3.6. HMBC NMR spectrum of **7** in $CDCl_3$.

Using HSQC NMR spectroscopy the carbon atoms directly attached to hydrogen atoms could be easily assigned. The HSQC NMR spectrum (Fig. 3.7) shows **a** couples to a ^{13}C NMR resonance at 25.6 ppm, **c'**, corresponding to the third carbon atom along of the PCL with respect to the carbonyl carbon atom. Resonance **b** exhibits coupling to two ^{13}C NMR resonances, at 24.6 ppm, **b'**; and 28.4 ppm, **e'**; corresponding to the second and fourth carbon atoms along of the PCL with respect to the carbonyl carbon atom, respectively. Resonance **c** exhibits coupling to a ^{13}C NMR resonance at 21.7 ppm, **a'**, corresponding to the methyl carbon atom of the bromopropanoate moiety. Resonance **d** exhibits coupling to a ^{13}C NMR resonance at

34.2 ppm, **g'**, corresponding to the first carbon atom along of the PCL with respect to the carbonyl carbon atom. Resonance **e** exhibits coupling to a ^{13}C NMR resonance at 62.5 ppm, **f'**, corresponding to the ethylene carbon atom next to the thio ether sulfur linking the calixarene core to the PCL. Resonance **f** exhibits coupling to a ^{13}C NMR resonance at 30.5 ppm, **i'**, which corresponds to the methylene carbon atom next to the terminus PCL hydroxyl moiety. Resonance **g** exhibits coupling to a ^{13}C NMR resonances at 64.2 ppm, **k'**, which corresponds to the non-terminus fifth carbon atom along of the PCL with respect to the carbonyl carbon atom. Resonance **h** exhibits coupling to a ^{13}C NMR resonances at 63.2 ppm, **j'**, which corresponds to the ethylene carbon atom next to the ether oxygen linking the calixarene core to the PCL. Resonance **i** exhibits coupling to a ^{13}C NMR resonance at 39.9 ppm, **h'**, which corresponds to the methine carbon atom of the bromopropanoate moiety. Resonance **k** exhibits coupling to a ^{13}C NMR resonance at 129.7 ppm, **l'**, which corresponds to *meta* carbon atom of the of the calixarene core with respect to the aryl ether oxygen. Resonance **j** exhibits coupling in the HSQC spectrum but due to the low concentration of calixarene core a ^{13}C NMR resonance is not observed.

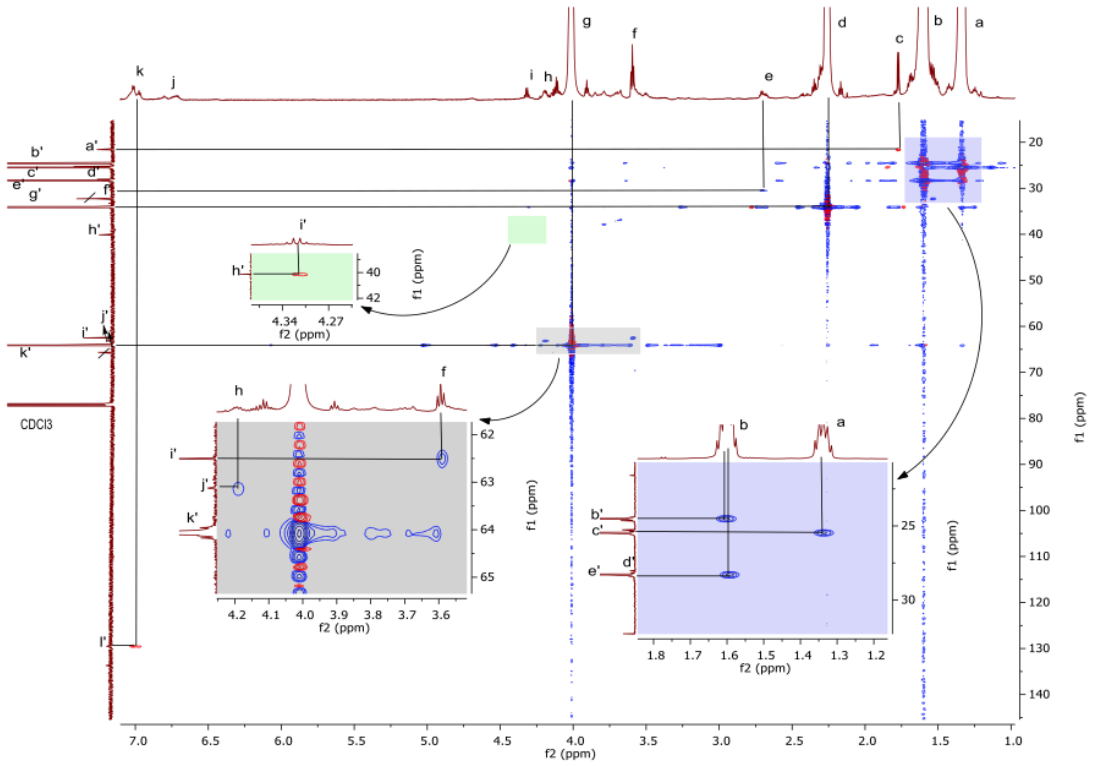

Figure 3.7. HSQC NMR spectrum of product of the ring opening polymerisation of ε-caprolactone using **6,** in $CDCl_3$.

By comparing the ^{13}C NMR spectrum of **6** and **7** the ^{13}C NMR resonances at 28.1 ppm and 170.3 ppm could be assigned, corresponding to the propylene carbon atom next to the sulfur of the thio ether of the calixarene core and the carbonyl of the bromopropanoate moiety respectively. As expressed previously due to the low concentration of calixarene core relative to PCL backbone not all ^{1}H and ^{13}C NMR resonances could be fully assigned, but what could be assigned in the ^{13}C NMR spectrum is shown in Figure 3.8.

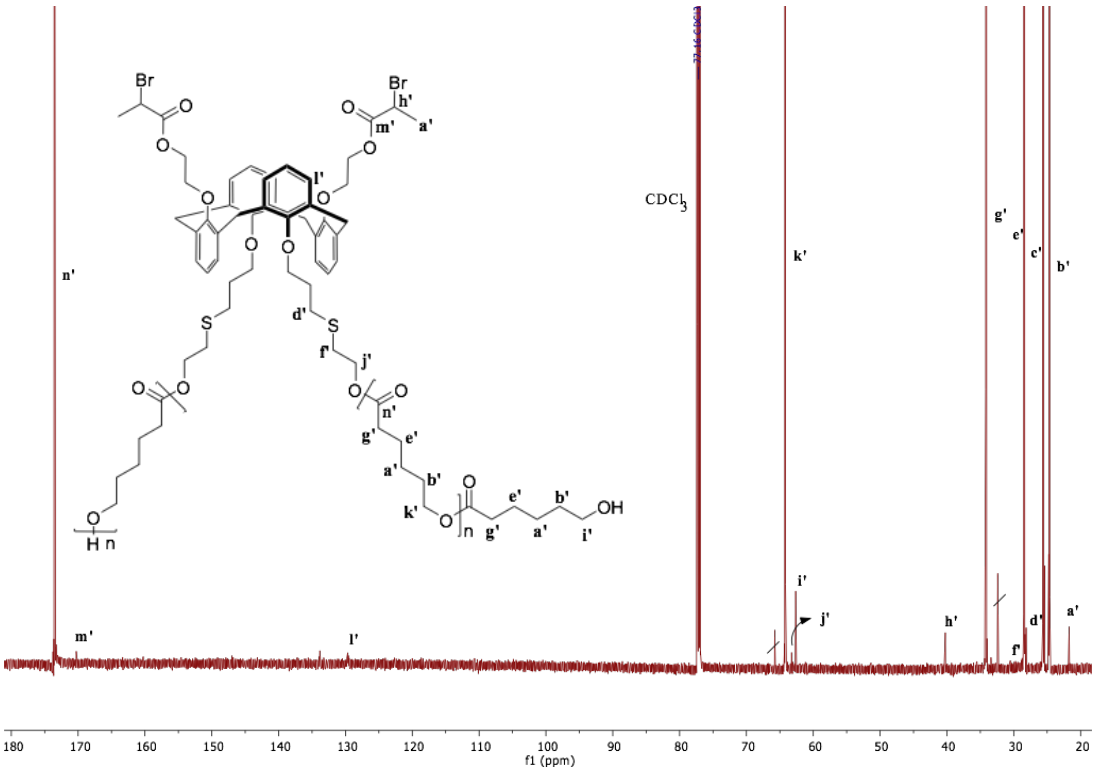

Figure 3.8. ^{13}C NMR spectrum of **7** in $CDCl_3$.

As expressed previously, ^{1}H NMR (Fig. 3.4) resonances **j** and **k** had their integral values set to four and eight respectively, with the **DP** of the PCL being determined with respect to these values. From the ^{1}H NMR, comparing resonances **j** and **k**, the molecular weight (M_n) was calculated to be 2.2 x 10^4 g mol^{-1}. Each ε-caprolactone unit has a molecular weight of 114.14, therefore the total number of units in the PCL is 193, thus if the length of each arm was the same, 193 corresponds to ~97 units per arm. To further characterise **7**, size exclusion chromatography (SEC) was carried out. The chromatogram is shown in Figure 3.9.

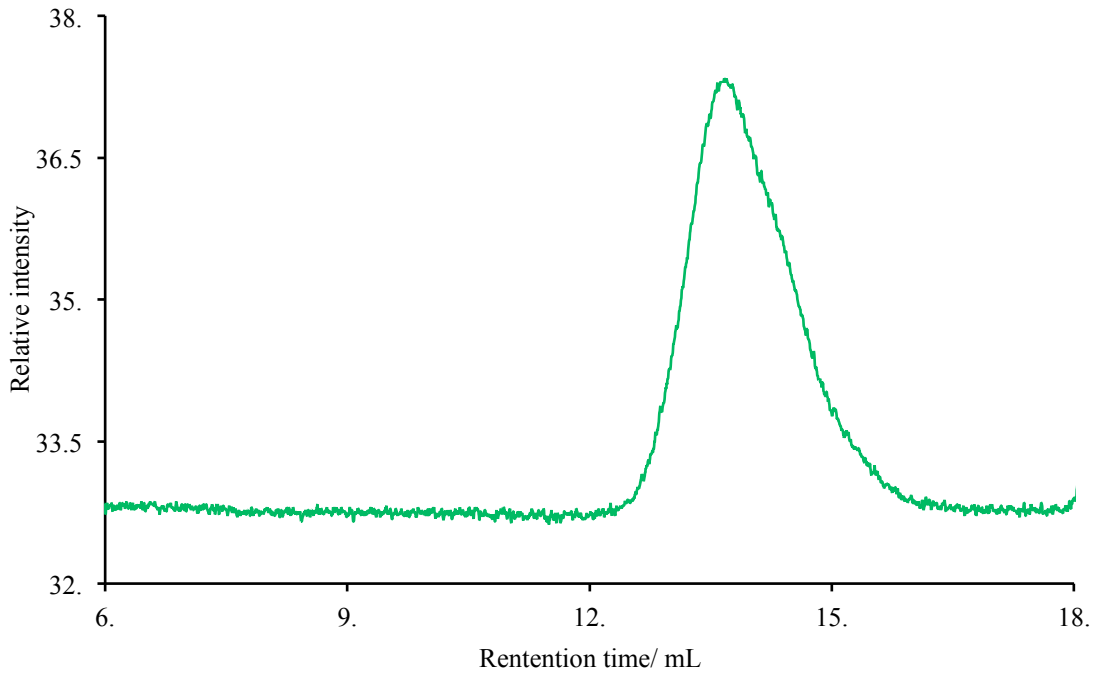

Figure 3.9. SEC chromatogram of **7**, using THF as the eluent at 1 mL min^{-1} and the molecular weights determined with respect to polystyrene standards.

The SEC chromatogram (Fig. 3.9) shows a slightly broad distribution at 13.8 mL, with a lower molecular weight shoulder being observed at 14.5 mL. Using a conventional calibration method (polystyrene standards), the number average molecular weight (M_n) and a weight average molecular weight (M_w) were calculated to be 2.2 x 10^4 g mol^{-1} and 3.7 x 10^4 g mol^{-1}, respectively. The dispersity, Đ (Đ = M_w/M_n) was calculated to be 1.68. The relatively high dispersity indicates that there was a lack of control over the polymerisation and that the **DP** of each arm is not likely to be equal, suggesting that the rate of initiation of the system is slower than the rate of propagation. The M_n calculated *via* SEC agrees with what was calculated through ^{1}H NMR spectroscopy. Table 3.1 illustrates the theoretical and measured molecular weights and dispersity measured.

Table 3.1. Characterisation of **2**.

Sample	M_n**(theo)** **g mol^{-1}**	M_n**(NMR)** **g mol^{-1}**	M_n**(SEC)** **g mol^{-1}**	**Đ**
7	2.0 x 10^4	2.2 x 10^4	2.2 x 10^4	1.68

7 was further characterised by differential scanning calorimetry (DSC) and thermogravimetric analysis (TGA). The DSC (Fig. 3.10) shows on the second scan that **2** had an endotherm (melting transition, T_m) and exotherm (crystallisation transition, T_c) at 51.53 ^oC and 32.67 ^oC, respectively. The degree of crystallinity (%X) was calculated according to equation 1.[8]

$$\%X = 100(\Delta H_c / \Delta H_{co}) \quad (1)$$

Where ΔH_c is the enthalpy of crystallinity and ΔH_{co} is the standard enthalpy of crystallinity for PCL, which is 139.5 J g^{-1}.[9] %X was calculated to be 31.43%. It is reported that neat linear PCL has a %X of 46.72%.[8] Thus, the architecture of **2** has reduced the crystallinity of PCL, which is likely to be a resultant of the packing fashion of the PCL, as not all the arms can line up in an orderly fashion due the presence of the calixarene cores.

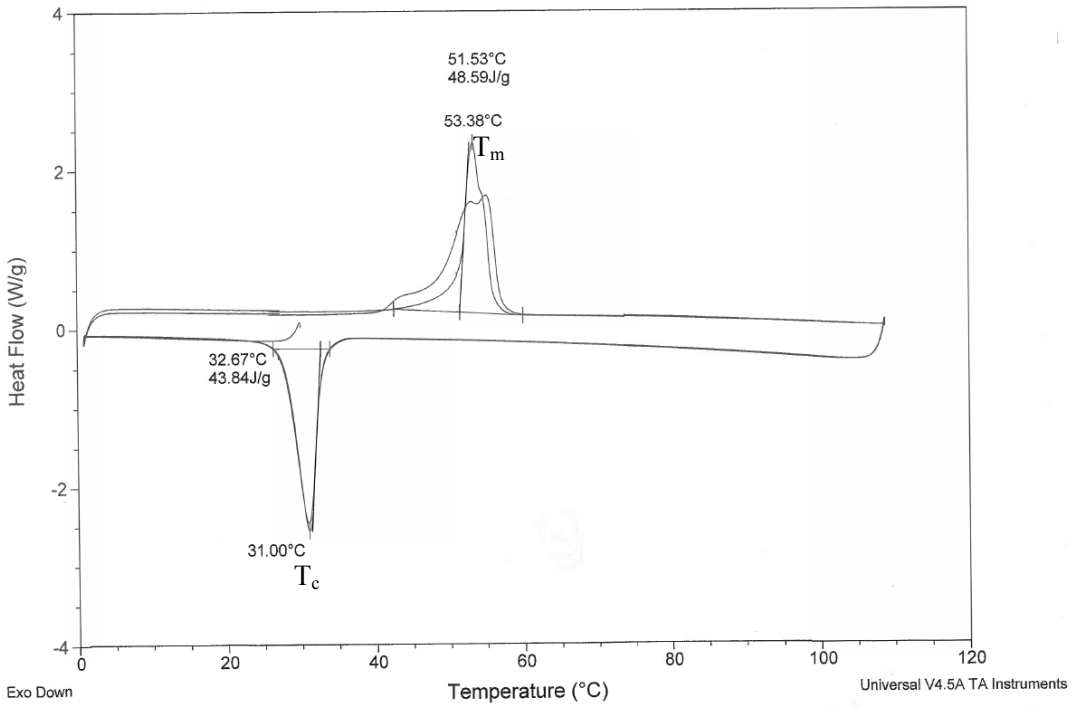

Figure 3.10. DSC of **7**, run in N_2 gas, with a flow rate of 30 mL min^{-1} and a heating rate of 10 ^oC min^{-1}.

The TGA thermogram (Fig. 3.11) shows **7** has two distinct thermal events corresponding to the decomposition of PCL. The first (X_1) and second (X_2) thermal events of the decomposition of PCL had onsets of 264.85 ^oC and 336.86 ^oC, respectively.

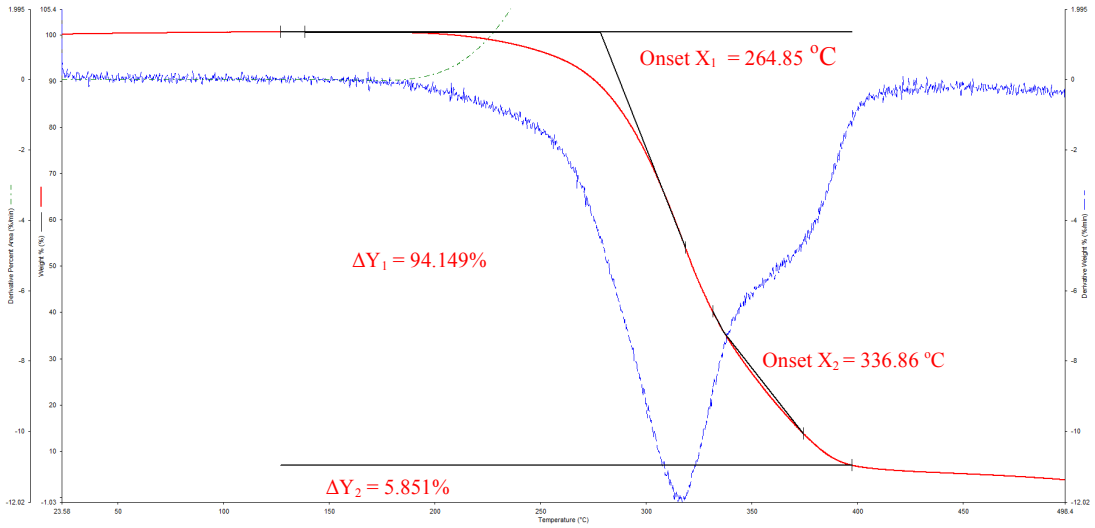

Figure 3.11. TGA of **7**, run in N_2 gas with a heating rate of 10 °C min^{-1}. Red line = TGA trace, blue dashed line = first derivative.

Two distinct thermal events are observed due to a thermal degradation that involves a double mechanism.[10] The first degradation process implies a statistical rupture of the PCL chains *via* ester pyrolysis reaction. The produced products of the ester pyrolysis are H_2O, CO_2 and 5-hexenoic acid (Scheme 3.2).

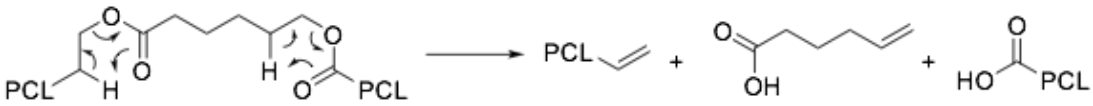

Scheme 3.2. First thermal degradation of PCL, *via* an ester pyrolysis reaction.

The second degradation process is an unzipping depolymerisation, which results in ε-caprolactone (cyclic monomer starting material) (Scheme 3.3).

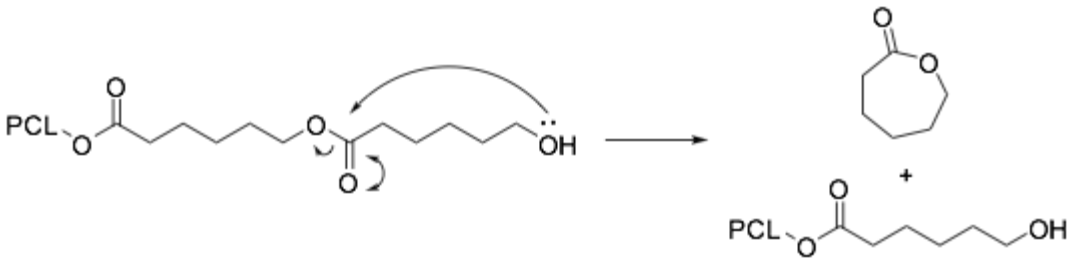

Scheme 3.3. Second degradation process *via* unzipping depolymerisation

A first derivative of the TGA thermogram was calculated (blue dashed line, Fig. 3.11), which indicates the point of the greatest rate of change; two inflection points were observed, clearly showing the two degradation processes for PCL. The percentage of PCL was calculated to be 94.149% (ΔY_1). A ΔY_2 was calculated to be

5.851%, starting from 398.10 ^{o}C, which corresponds to the percentage of calixarene. The ^{1}H NMR spectrum (Fig. 3.4) indicates that there are ~193 units to the PCL per calixarene core, therefore a M_n ratio of 22,000:1019, which corresponds to 95.57% PCL and 4.43% calixarene core. From TGA, looking at ΔY_1 and ΔY_2, the percentages of PCL and calixarene core were calculated to be 94% and 6%, respectively, which is close to the calculated value through ^{1}H NMR spectroscopy but is not an exact match.

3.2.2. Amphiphilic Miktoarm Star polymer, 8 - 10

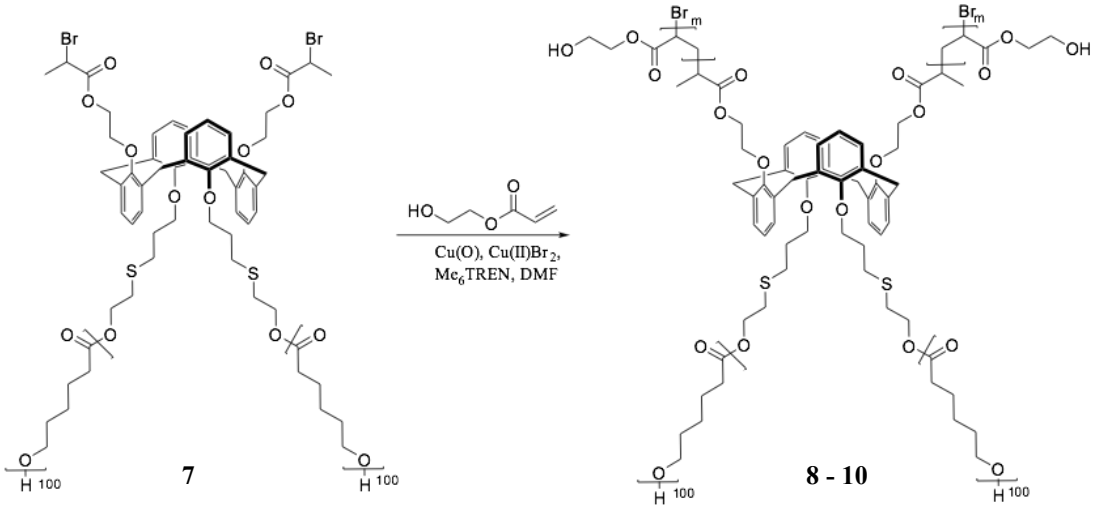

Scheme 3.04. SET-LRP of HEA using **7** macro-initiator leading to the formation of an A_2B_2 miktoarm star polymer, **calixarene-A_2B_2starPCL$_{100}$PHEA$_n$**, **8 - 10**.

The synthesis of an amphiphilic A_2B_2 Miktoarm star polymer was carried out *via* a copper(0) mediated radical polymerisation, SET-LRP, using **7**, as a macro-initiator (Scheme 3.04). The hydrophilic monomer utilised was 2-hydroxylethyl acrylate (HEA) (Scheme 3.04). The reaction used activated copper wire in the presence of the multidentate amine ligand, Me_6TREN, in the aprotic polar solvent DMF. $CuBr_2$ (5%) was added to the reaction system to give control at the early stages of the reaction due to Cu(II) ability to act as a deactivator as discussed in the introduction. A monomer to initiator to $CuBr_2$ to ligand ratio of X:1:0.05:0.18 was used to target various molecular weights of 1.0 x 10^4 g mol^{-1} to 4.0 x 10^4 g mol^{-1}, therefore **DP**'s of 50-200 per arm. The various polymers have been fully analysed and the results are discussed below.

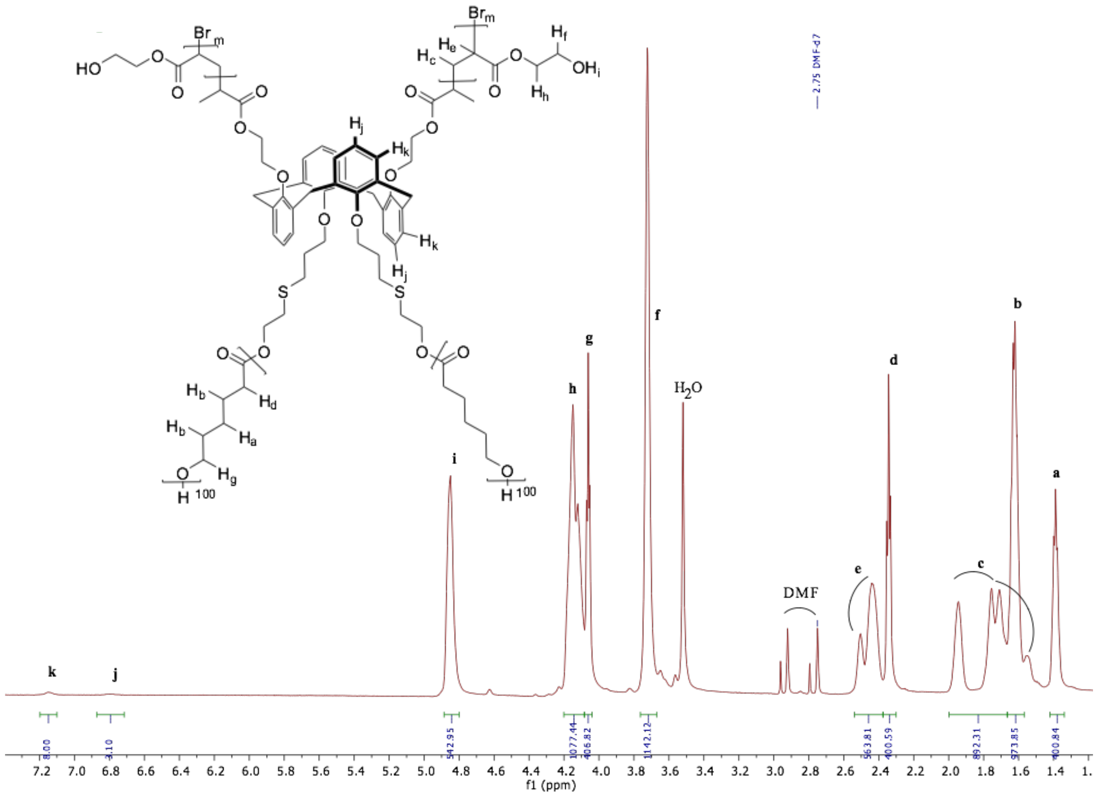

Figure 3.12. [1]H NMR spectrum of **10** in DMF-d7.

The [1]H NMR spectrum (Fig. 3.12) shows the resonances of the calixarene initiator aromatic protons, with two multiplets being observed at 6.71-6.85 and 7.08-7.22 ppm, **j** and **k**, corresponding to H_j and H_k, respectively. The multiplets are observed due to the many different conformations of the calixarene core present. [1]H NMR (Fig. 3.12) resonances **j** and **k** had their integral values set to four and eight respectively, with the **DP** of PHEA determined with respect to these values. Additionally, the **DP** of PHEA could be determined from comparing its integral with respect to **a**, corresponding to H_a of the PCL, as the chain length is known as discussed in Section 3.2.1. The [1]H NMR spectrum (Fig. 3.12) shows the resonances for the PCL backbone protons **a**, **b**, **d** and **g**. A quintet resonance with an integral of 400 is observed at 1.39 ppm, **a**, corresponding to the hydrogen atoms of the PCL on the third carbon atom with respect to the carbonyl carbon atom, H_a. A sextet resonance is observed at 1.62 ppm, **b**, corresponding to the methylene hydrogen atoms of the PCL on the second and fourth carbon with respect to the carbonyl carbon atom, H_b. A triplet resonance with an integral of 400 is observed at 2.34 ppm, **d**, corresponding to the methylene hydrogen atoms of the PCL on the first

carbon atom with respect to the carbonyl carbon atom, H_d. A triplet resonance with an integral of 406 is observed at 4.06 ppm, **g**, corresponding to the methylene hydrogen atoms of the PCL backbone on the fifth carbon atom with respect to the carbonyl carbon atom, H_g. The ^{1}H NMR spectrum (Fig. 3.12) shows a multiplet resonance between 1.52 – 1.80 ppm, **c**. The COSY NMR spectrum (Fig. 3.13) shows **c** exhibiting a coupling with a multiplet between 2.38 – 2.54 ppm, **e**. Resonances **c** and **e** correspond to the methine and methylene protons of the PHEA backbone. To ascertain which protons belong to which resonance the HSQC NMR spectrum must be referred too, and is discussed later.

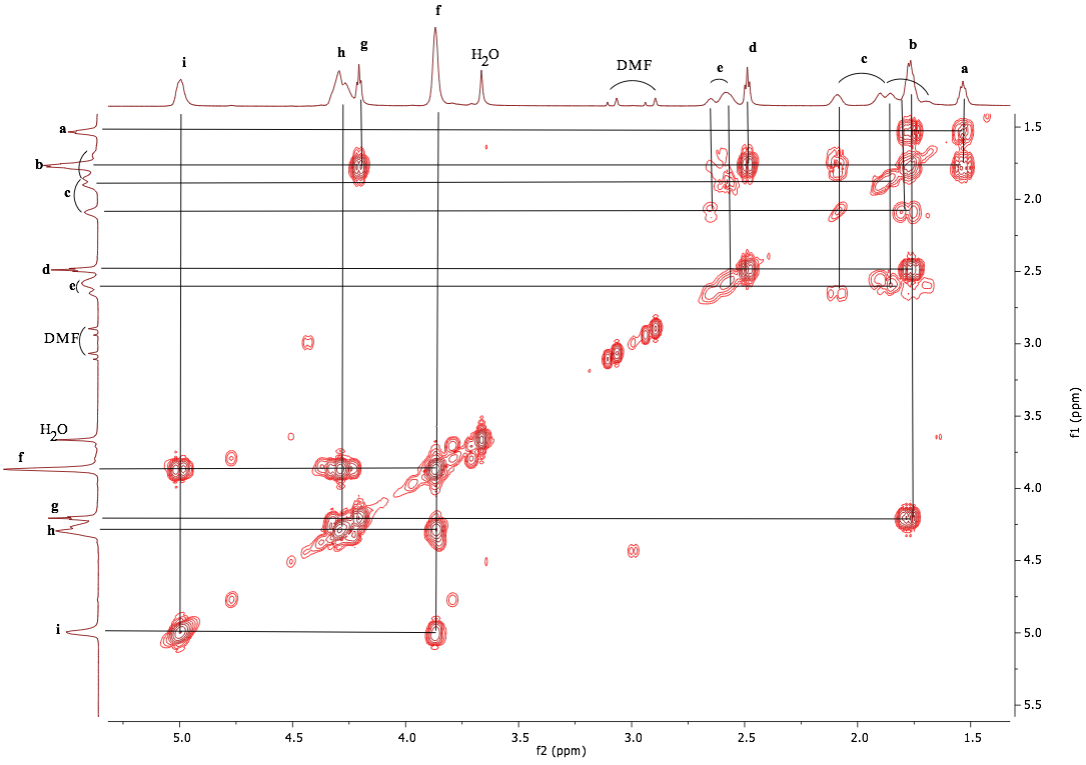

Figure 3.13. COSY NMR spectrum of the product of the SET-LRP of HEA on **7,** in DMF-d7.

The ^{1}H NMR spectrum (Fig. 3.12) shows a broad singlet resonance with an integral of 1142 at 3.72 ppm, **f**. The COSY NMR spectrum (Fig. 3.13) shows **f** exhibiting coupling with a multiplet resonance at 4.14 ppm, **h**, and a singlet at 4.85 ppm, **i**. Resonances **h** and **i** have integrals of 1077 and 543, respectively, therefore **i** corresponds to the proton of the hydroxyl moieties of PHEA and **f** and **h** correspond to the ethylene protons of the ethylene ether hydroxyl moiety of the PHEA. To determine the exact assignment of resonances **f** and **h** the HMBC spectrum must be referred to. The HMBC NMR spectrum (Fig. 3.14) shows **h** coupling to a ^{13}C NMR

resonance at 174.6 ppm, **k'**, where **k'** corresponds to the carbon atom of the carbonyl of the PHEA, therefore **h** corresponds to the ethylene protons of the 2-hydroxyl ethyl closest to the carbonyl, H_h (Fig. 3.12) and, **f** must therefore correspond to the ethylene protons closest to the hydroxyl moiety, H_f (Fig. 3.12). The HMBC NMR spectrum (Fig. 3.14) shows **k'** additionally exhibiting a coupling to **e**, therefore indicating **e** corresponds to the methine carbon atom of the PHEA backbone, H_e, which is further confirmed by the HSQC NMR spectrum. To assign the ^{13}C NMR spectrum the HSQC spectrum was first referred to.

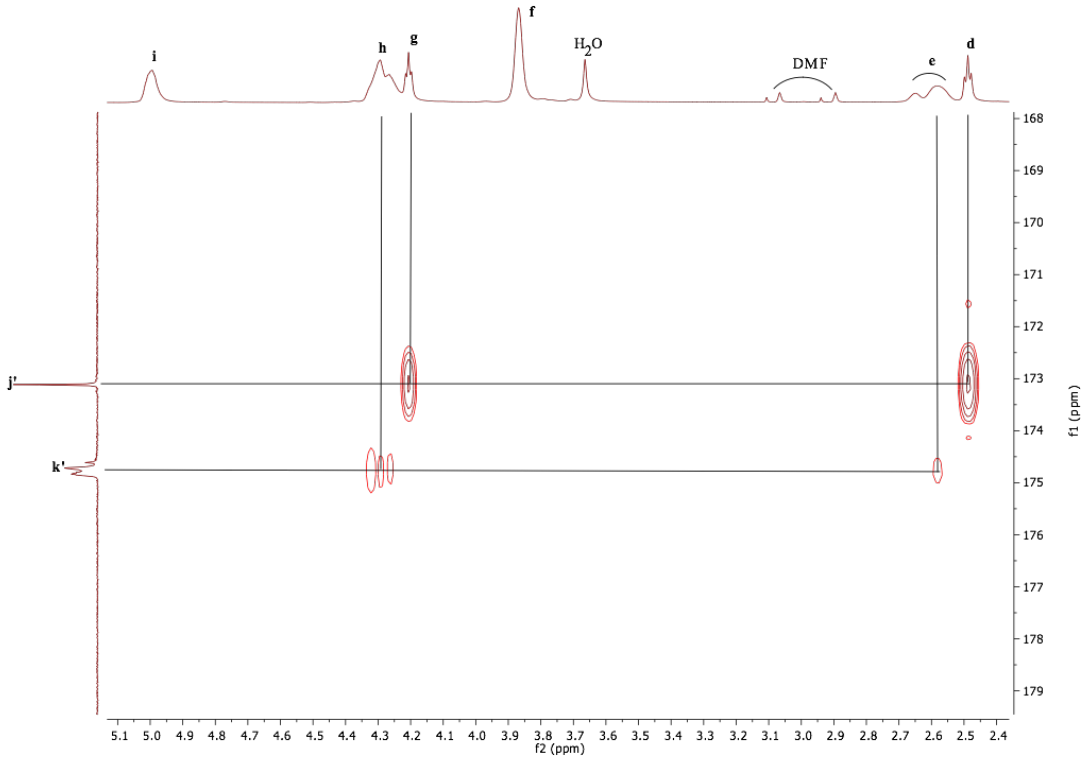

Figure 3.14. HMBC NMR spectrum of **10** in DMF-d7.

The HSQC NMR spectrum (Fig. 3.15) shows **a** couples to a ^{13}C NMR resonance at 25.5 ppm, **b'**, corresponding to the third carbon atom along of the PCL with respect to the carbonyl carbon atom. Resonance **b** exhibits coupling to two ^{13}C NMR resonances; at 24.7 ppm, **a'**; and 28.5 ppm, **c'**, corresponding to the second and fourth carbon atoms along of the PCL with respect to the carbonyl carbon atom, respectively. Resonance **c** exhibits coupling to a ^{13}C NMR resonance at 36.0 ppm, **e'**, corresponding to the methylene carbon atom of the PHEA backbone. The phasing of the **c-e'** coupling (blue) corresponds to a methylene environment, confirming that **c** corresponds to H_c (Fig. 3.12). The HSQC NMR spectrum (Fig. 3.15) shows that

resonance **d** exhibits coupling to a ^{13}C NMR resonance at 33.8 ppm, **d'**, corresponding to the first carbon atom along of the PCL with respect to the carbonyl carbon atom. Resonance **e** exhibits coupling to a ^{13}C NMR resonance at 41.6 ppm, **f'**, corresponding to the methine carbon atom of the PHEA backbone. The phasing of the **e-f'** coupling (red) corresponds to a methine environment, confirming that **e** corresponds to H_e (Fig. 3.2.2.1). The HSQC NMR spectrum (Fig. 3.15) shows that resonance **f** exhibits coupling to a ^{13}C NMR resonances at 59.9 ppm, **g'**, which corresponds to the ethylene carbon atom closest to the hydroxyl of the 2-hydroxyl ethyl moiety. Resonance **g** exhibits coupling to a ^{13}C NMR resonance at 64.0 ppm, **h'**; corresponding to the non-terminus fifth carbon atom along of the PCL with respect to the carbonyl carbon. Resonance **h** exhibits coupling to a ^{13}C NMR resonance at 66.4 ppm, **i**', which corresponds to the ethylene carbon atom of the 2-hydroxyl ethyl closest to the carbonyl.

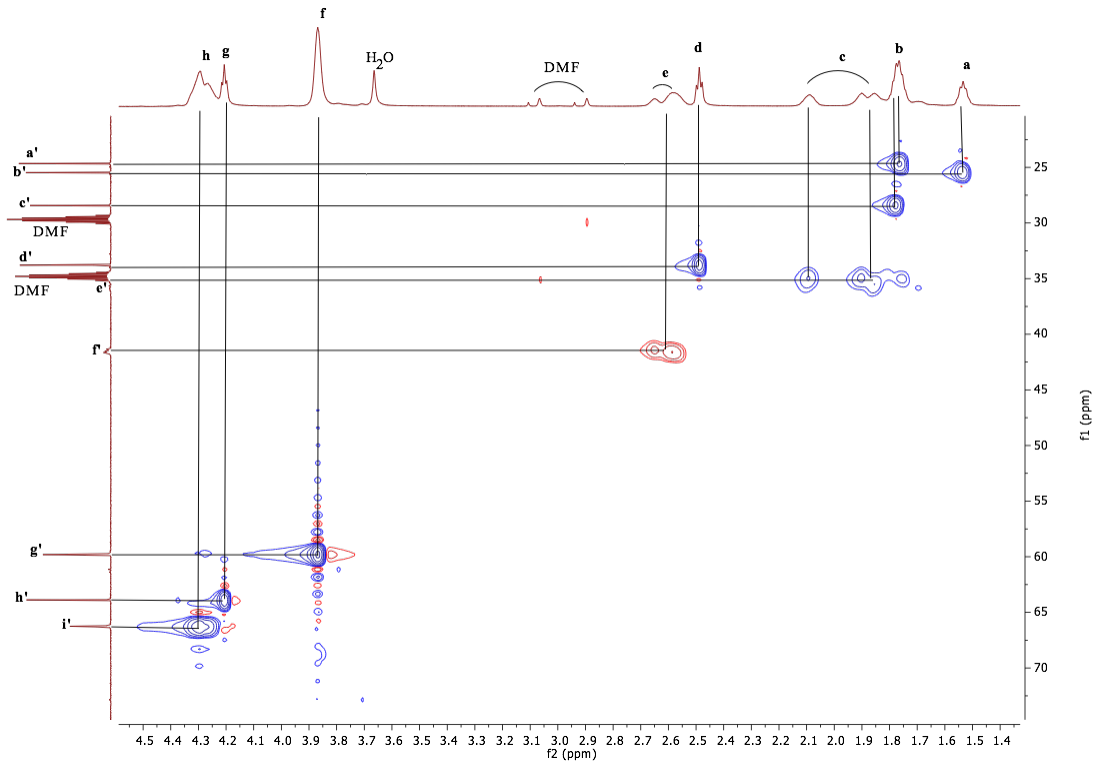

Figure 3.15. HSQC NMR spectrum of **10** in DMF-d7.

Due to the low concentration of calixarene core relative to PCL and PHEA only the aromatic protons could be observed *via* ^{1}H NMR, moreover, only limited carbon resonances could be observed in the ^{13}C NMR spectrum, shown in Figure 3.16.

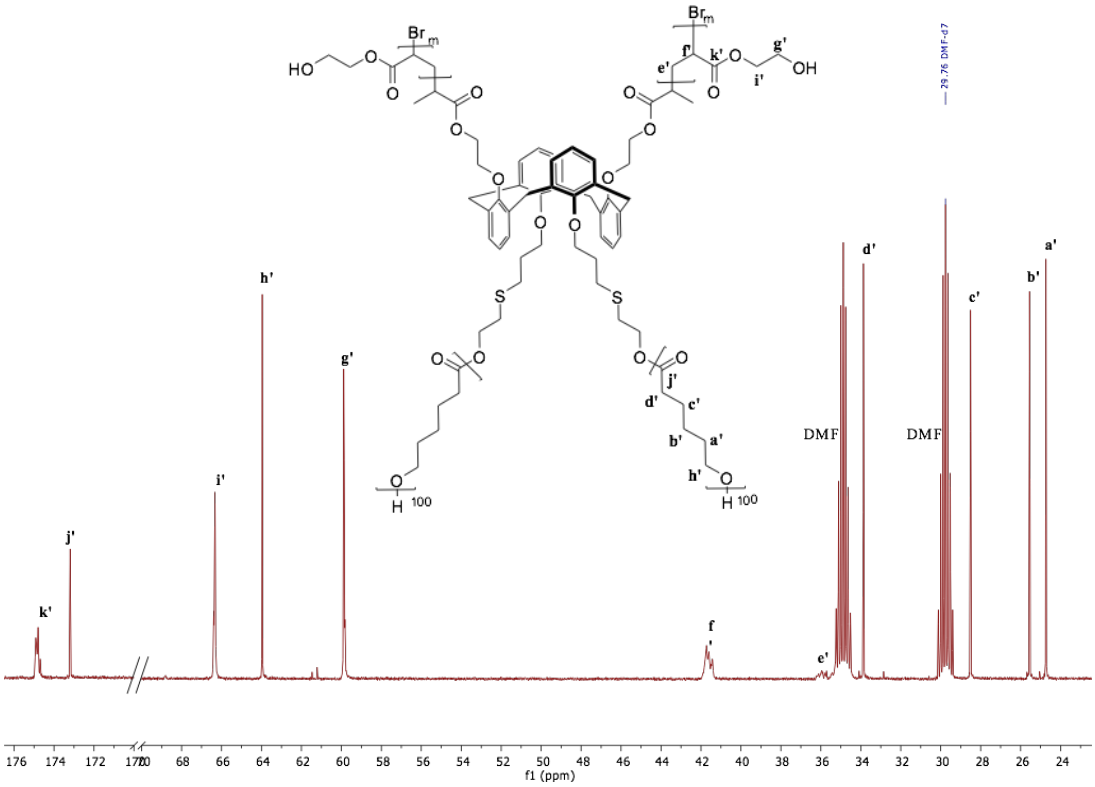

Figure 3.16. ^{13}C NMR spectrum of **10** in DMF-d7.

As expressed previously, various molecular weights of PHEA were targeted, 1.0 x 10^4 g mol^{-1}, 2.0 x 10^4 g mol^{-1} and 4.0 x 10^4 g mol^{-1}, corresponding to HEA **DP**'s of 50, 100 and 200 per arm, respectively. ^{1}H NMR resonances **j** and **h** (Fig. 3.12) had their integral values set to four and eigh, respectively, with the **DP** of the PHEA being determined with respect to these values. Figure 3.17 shows overlaid spectra corresponding to the three polymer systems, with the spectra being normalised with respect to resonance **a**. For the targeted molecular weight of 1.0 x 10^4 g mol^{-1}, an M_n of the PHEA of 1.8 x 10^4 g mol^{-1} was calculated from the ^{1}H NMR spectrum (Fig. 3.12) that lead to a total M_n of miktoarm polymer of 4.0 x 10^4 g mol^{-1}, **3**. The yield obtained for the reaction was 64%. For the targeted molecular weight of 2.0 x 10^4 g mol^{-1}, an M_n of the PHEA of 2.2 x 10^4 g mol^{-1} was calculated from the ^{1}H NMR (Fig. 3.12) that lead to a total molecular weight of miktoarm polymer of 4.4 x 10^4 g mol^{-1}, **4**. The yield obtained for the reaction was 75%. For the targeted molecular weight of 4.0 x 10^4 g mol^{-1}, an M_n of the PHEA was 6.1 x 10^4 g mol^{-1} was calculated from the ^{1}H NMR (Fig. 3.12) that lead to a total molecular weight of miktoarm polymer of 8.3 x 10^4 g mol^{-1}, **5**. The yield obtained for the reaction was 63%. In all

cases but most profoundly for **8** and **10**, there is a greater molecular weight and lower yield than expected, thus indicating a lack of control and a greater rate of propagation relative to that initiation.

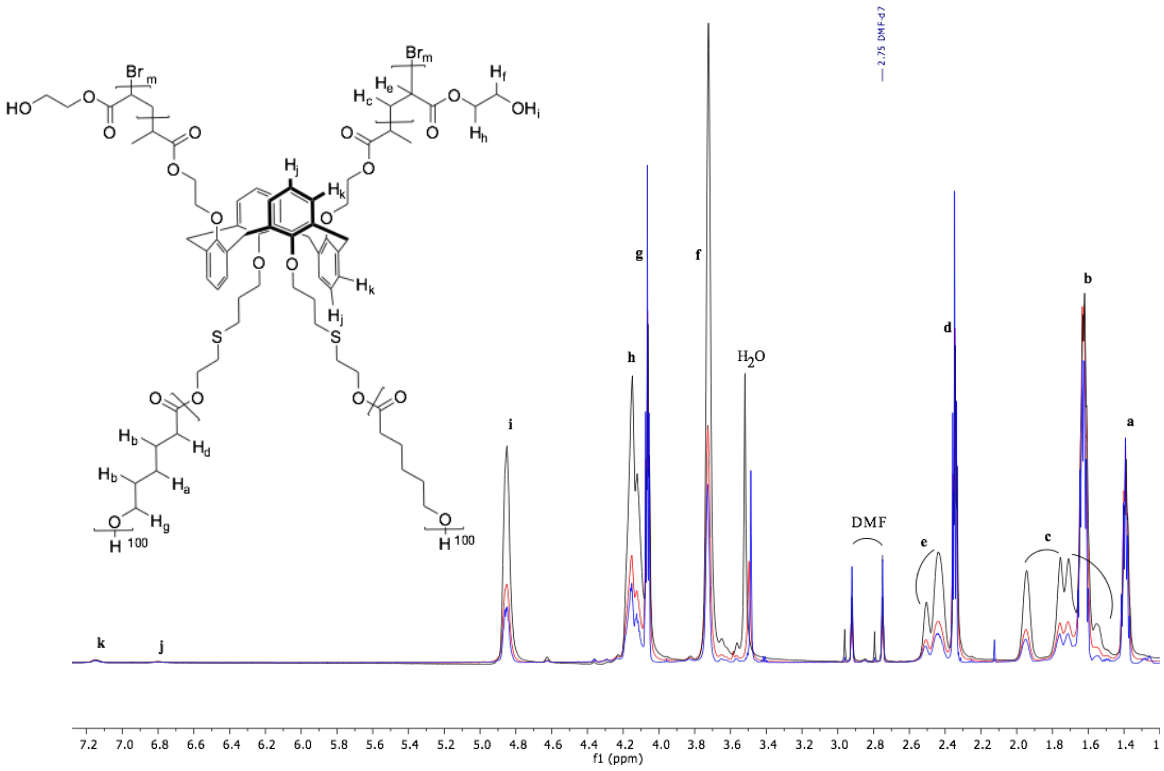

Figure 3.17. ^{1}H NMR overlaid spectra corresponding to various degrees of polymerisation of HEA, blue = **8**, red = **9** and black = **10,** in DMF-d7.

To further characterise the polymer systems **8** - **10** SEC was carried out. A chromatogram of the three miktoarm star polymers and the linear macro initiator, **7**, are shown in Figure 3.18.

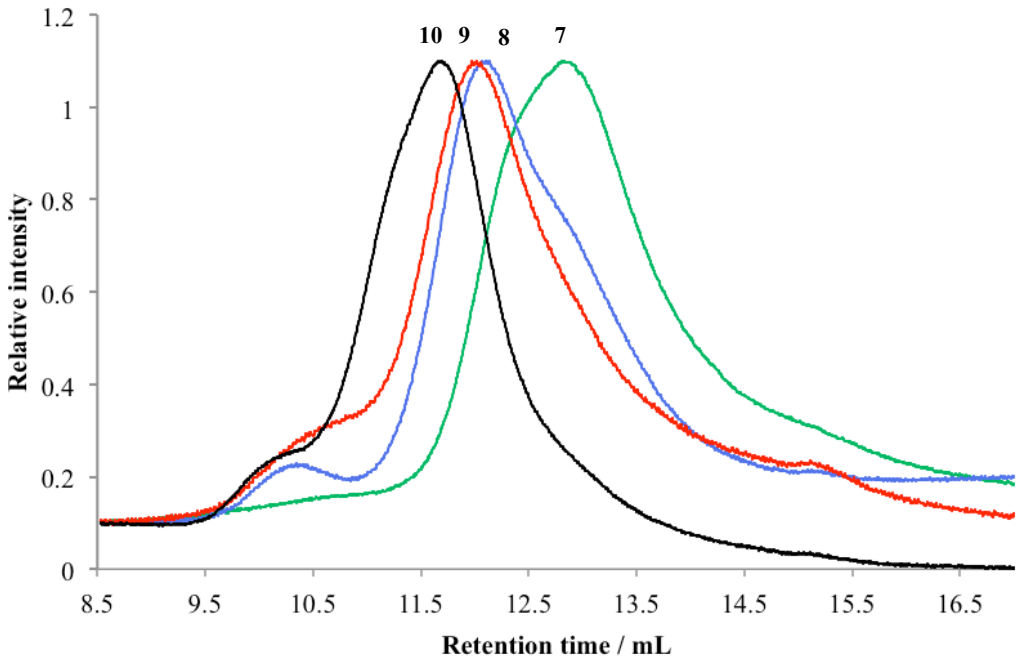

Figure 3.18. SEC chromatogram of green = **7**, red = **8**, blue = **9** and black = **10**, using DMF as the eluent at 1 mL min^{-1} and the molecular weights determined with respect to PEG standards.

The SEC chromatogram (Fig. 3.18) shows a slightly broad distribution at 12.8 mL (green), corresponding to **7** as discussed in section 3.2.1. A bimodal distribution is observed at 12.06 mL (blue), corresponding to **8**, which has a small shoulder at 12.80 mL and a high molecular weight (HMW) shoulder at 10.40 mL. The M_p of the main distribution and HMW shoulder are 3.7 x 10^4 g mol^{-1} and 8.6 x 10^4 g mol^{-1}, respectively. The value for the M_p of the HMW shoulder is approximately double that of the main distribution, suggesting dimerization of the star polymer has occurred, which would lead to loss of chain end fidelity. Using a conventional calibration method (polystyrene standards), the M_n and M_w were calculated to be 1.4 x 10^4 g mol^{-1} and 3.7 x 10^4 g mol^{-1}, respectively. The Đ was calculated to be 2.64. The high Đ indicates that there was a lack of control over the polymerisation and that the **DP** of each arm is not likely to be equal, further suggesting that the rate of initiation of the system is slower than the rate of propagation. A bimodal distribution is observed at 11.98 mL (red), corresponding to **9**, which has a HMW shoulder at 10.36 mL. The M_p of the main distribution and HMW shoulder are 4.2 x 10^4 g mol^{-1} and 8.1 x 10^4 g mol^{-1}, respectively. The value for the M_p of the HMW shoulder is approximately double that of the main distribution, suggesting dimerization of the star polymer has occurred, which would lead to loss of chain end fidelity. Using a

conventional calibration method (polystyrene standards), the M_n and M_w were calculated to be 3.1 x 10^4 g mol^{-1} and 5.6 x 10^4 g mol^{-1}, respectively. The Đ was calculated to be 1.81. The relatively high dispersity indicates that there was a lack of control over the polymerisation and that the **DP** of each arm is not likely to be equal, further suggesting that the rate of initiation of the system is slower than the rate of propagation. It must be noted that the Đ of **7** was 1.68, so relatively; the increase in Đ of **9** is not vast. A bimodal distribution is observed at 11.67 mL (black), corresponding to **10**, which has a HMW shoulder at 10.06 mL. The M_p of the main distribution and HMW shoulder are 5.9 x 10^4 g mol^{-1} and 9.5 x 10^4 g mol^{-1} respectively. The value for the M_p of the HMW shoulder is approximately double that of the main distribution, suggesting dimerization of the star polymer has occurred, which would lead to loss of chain end fidelity. Using a conventional calibration method (polystyrene standards), the M_n and M_w were calculated to be 4.1 x 10^4 g mol^{-1} and 8.3 x 10^4 g mol^{-1} respectively. The Đ was calculated to be 2.02. The high dispersity indicates that there was a lack of control over the polymerisation and that the **DP** of each arm is not likely to be equal, further suggesting that the rate of initiation of the system is slower than the rate of propagation. The increased Đ in all cases is likely to be a result of trapped active sites. The PCL chains are flexible, which could lead to the encapsulation of calixarene core active sites within the macroinitiator structure, away from the catalyst, thus the rate of propagation would be greater than initiation.[11,12] For all three samples, **8 - 10**, the M_n determination *via* SEC is greatly under estimated, which is common for star polymers, as the hydrodynamic volume does not increase greatly as branching occurs relative to linear polymers. Table 3.2 illustrates the theoretical and measured molecular weights and dispersity measured.

Table 3.2. Characterisation of polymers.

Sample	M_n(theo) g mol^{-1}	M_n(NMR) g mol^{-1}	M_n(SEC) g mol^{-1}	Đ
7	2.0 x 10^4	2.2 x 10^4	2.2 x 10^4	1.68
8	3.2 x 10^4	4.0 x 10^4	1.4 x 10^4	2.64
9	4.2 x 10^4	4.4 x 10^4	3.1 x 10^4	1.81
10	6.2 x 10^4	8.3 x 10^4	4.1 x 10^4	2.02

The miktoarm star polymers were further characterised by differential scanning calorimetry (DSC) and thermogravimetric analysis (TGA); the results are shown in Figures 3.19 and 3.20, respectively. The DSC traces (Fig. 3.19) show that as the percentage of PHEA increased so did the amorphous nature of the polymer system. Both **8** and **9** exhibited a T_m and T_c at 61.13 ^oC and 25.13 ^oC, and 57.21 ^oC and 25.43 ^oC, corresponding to calculated %crystallinities of 5.96% and 5.94% respectively. **10** exhibited no T_m or T_c, indicating the material is solely amorphous in nature. The large amount of PHEA has interrupted the packing of the PCL chain to such an extent that there is no order to the packing of the material.

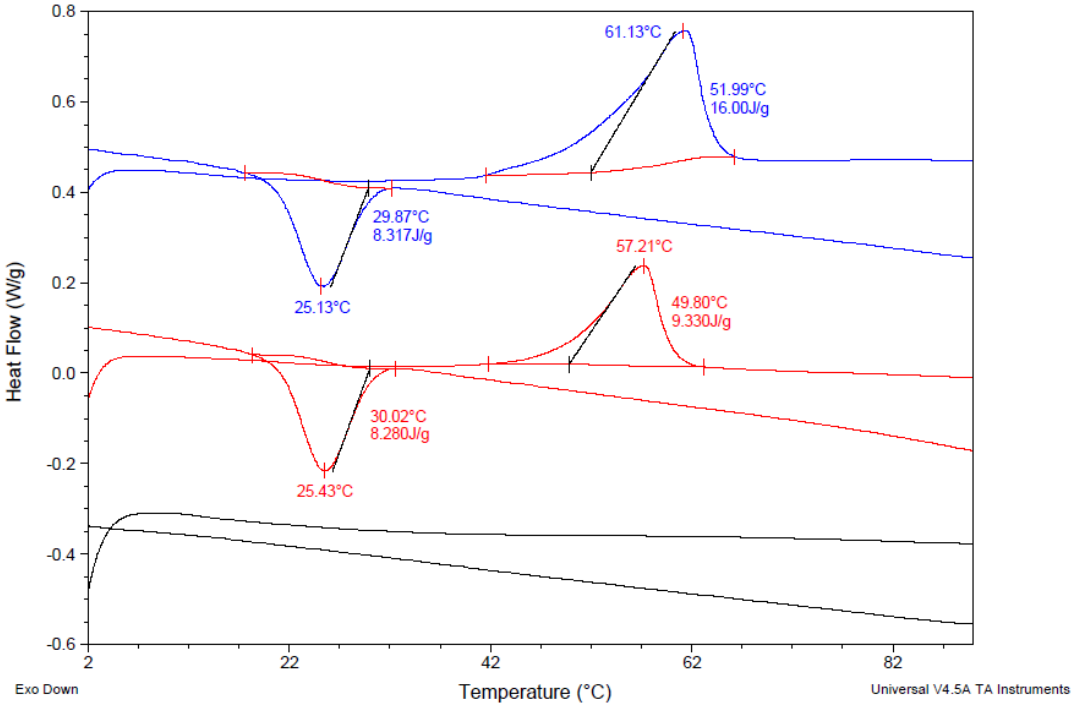

Figure 3.19. DSC of blue = **8**, red = **9** and black = **10**, run in N_2 gas, with a flow rate of 30 mL min^{-1} and a heating rate of 10 ^oC min^{-1}.

TGA analysis was further carried out on all three samples, with the traces shown in Figure 3.20.

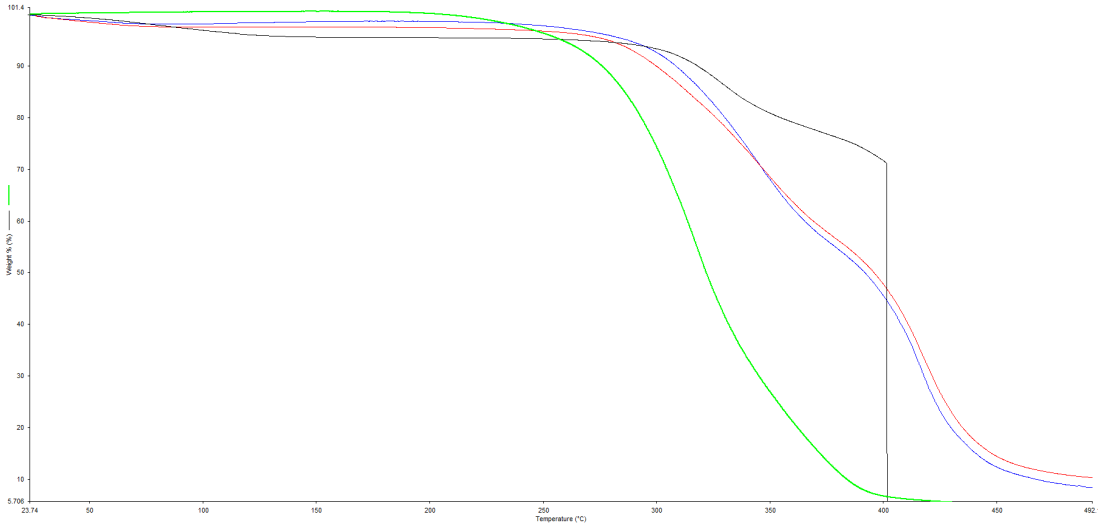

Figure 3.20. TGA of green = **7**, blue = **8**, red = **9** and black = **10**, run in N_2 gas with a heating rate of 10 ^{o}C min^{-1}.

The TGA thermogram (Fig. 3.20) shows **8** - **10** all exhibiting two distinct thermal events with the first thermal event (X_1) occurring at 286.65 ^{o}C, 297.31 ^{o}C and 302.52 ^{o}C and the second thermal event (X_2) occurring at 399.98 ^{o}C, 403.21 ^{o}C and 401.52 ^{o}C, respectively. The TGA thermogram (Fig. 3.2.2.9) showed that as the M_n of the incorporated PHEA increased the thermal stability of the system in turn increased as seen by the increasing X_1. With respect to X_2, the thermal stability increases relative to **7** (green), but increasing the amount of PHEA further does not appear to increase stability. The increased overall stability is likely to be brought about by hydrogen bonding between the PHEA hydroxyl moieties and the ester moieties of the PCL. It can be seen from the TGA (Fig. 3.20) that for **10** (black), where the M_n of PHEA is much greater than that of PCL, there is an abrupt mass loss at 401.52 ^{o}C. This abnormal behaviour was observed on repeated runs and we have not been able to come up with a reasonable explanation. For all three samples with the PHEA incorporated into the system there is a less distinctive thermal event occurring due to the loss of water from 22 ^{o}C to 100 ^{o}C, with the greater the M_n of PHEA the greater the mass loss.

3.3. Conclusion

Initiator **6** was used to synthesise a novel 2-armed PCL polymer with a calixarene core, **7**, which could be further used for copper(0) mediated polymerisation due to

the alkyl halide moieties remaining in the calixarene core. **7** was fully characterised *via* 1D and 2D NMR spectroscopy techniques, SEC chromatography, DSC and TGA. The M_n determined *via* ^{1}H NMR spectroscopy was 2.2 x 10^4 g mol^{-1}, indicating the **DP** of 193, which is equivalent to ~97 units per arm, which agreed with the calculated theoretical M_n. SEC calculated a M_n of 2.2 x 10^4 g mol^{-1}, which agreed with that calculated *via* ^{1}H NMR spectroscopy. The Đ calculated was 1.68 suggesting a lack of control over the polymerisation and that the **DP** of each arm is not likely to be equal, suggesting that the rate of initiation of the system is slower than the rate of propagation. From the DSC, a T_m and T_c were calculated to be 51.53 ^{o}C and 32.67 ^{o}C, respectively, and a %crystallinity of 31.43% was calculated. The TGA trace showed two distinct thermal events corresponding to the two mechanisms in which PCL degrades. The percentage of PCL (ΔY_1) and calixarene core (ΔY_2) was calculated to be 94.149% and 5.851%, respectively, which was in reasonable agreement with ^{1}H NMR spectroscopy.

Compound **7** was used as a macro-initiator for the SET-LRP of HEA leading to a amphiphilic A_2B_2 Miktoarm star polymer, **8 – 10**. **8 - 10** were fully characterised *via* 1D and 2D NMR spectroscopy techniques, SEC chromatography, DSC and TGA. The M_n, determined *via* ^{1}H NMR spectroscopy, was calculated to be 1.8 x 10^4 g mol^{-1}, 2.2 x 10^4 g mol^{-1} and 6.1 x 10^4 g mol^{-1} corresponding to 75, 100 and 270 HEA units per arm, respectively. The SEC showed that little control was maintained over the polymerisation with Đ ranging from 1.81 to 2.64. The lack of control was attributed to a greater rate of propagation than initiation. A plausible explanation is that the flexible PCL chains could lead to the encapsulation of calixarene core active sites within the macroinitiator structure, away from the catalyst, thus the rate of propagation would be greater than initiation. The DSC showed that as more PHEA was incorporated crystallinity was reduced, to a point where no exotherm was observed and the material was completely amorphous. The TGA for all three showed an increase in thermal stability, which was attributed to hydrogen bonding between the PHEA hydroxyl moieties and the ester moieties of the PCL.

3.4. References

(1) Inoue, K. *Prog. Poly. Sci.* **2000**, *25*, 453.
(2) Doganci, E.; Tasdelen, M. A.; Yilmaz, F. *Macromol. Chem. Phys.* **2015**, *216*, 1823.
(3) Kowalczuk-Bleja, A.; Sierocka, B.; Muszynski, J.; Trzebicka, B.; Dworak, A. *Polymer* **2005**, *46*, 8555.
(4) Liu, Y. Y.; Lan, S.; Xiao, L. Q. *Macromol. Chem. Phys.* **2015**, *216*, 749.
(5) Gao, H.; Matyjaszewski, K. *Chem. – A Eur. J.,l* **2009**, *15*, 6107.
(6) Gao, H.; Min, K.; Matyjaszewski, K. *Macromol. Chem. Phys.* **2007**, *208*, 1370.
(7) Leng, X. F.; Nguyen, N. H.; van Beusekom, B.; Wilson, D. A.; Percec, V. *Polymer Chemistry* **2013**, *4*, 2995.
(8) Wu, D.; Wu, L.; Sun, Y.; Zhang, M. *J. Poly.Sci. P. B-Poly. Phy.,* **2007**, *45*, 3137.
(9) Pitt, C. G.; Chasalow, F. I.; Hibionada, Y. M.; Klimas, D. M.; Schindler, A. *J. App. Poly. Sci.* **1981**, *26*, 3779.
(10) Persenaire, O.; Alexandre, M.; Degee, P.; Dubois, P. *Biomacromolecules* **2001**, *2*, 288.
(11) Perrier, S.; Haddleton, D. M. *Eur.Poly.J.* **2004**, *40*, 2277.
(12) Cole, D. P.; Khosravi, E.; Musa, O. M. *J. Poly. Sci. P. A: Poly. Chem.* **2015**, *54*, 3, 335.

Chapter 4

A_4B_4 Heterofunctional Initiator with Calix[4]arene Core

4.0. Introduction

Chapter 2 described the synthesis of a novel calix[4]arene A_2B_2 heterofunctional initiator, which employed initiating sites for both ROP and single electron transfer living radical polymerisation (SET-LRP) (Fig. 4.1).

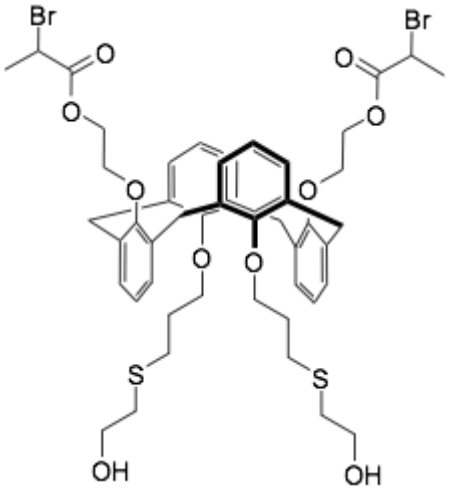

Figure. 4.1. Heterofunctional initiator.

The overview of this chapter is to illustrate the synthesis of several novel derivatised calix[4]arene compounds that led to synthesis of a novel A_4B_4 heterofunctional initiator. The lower and upper rim of the calix[4]arene were utilised. Traditional and cutting edge organic manipulations were used in the modification of compounds. The final A_4B_4 heterofunctional initiator incorporated primary hydroxyl moieties to allow for ROP of ε-caprolactone and alkyl-halogen moieties to facilitate SET-LRP.

The design of the synthetic strategy for an A_4B_4 heterofunctional initiator involved unsuccessful direct attachment of the alkyl-halogen moieties, i.e. 2-bromopropionyl bromide, to the phenolic hydroxyls of the calix[4]arene aromatics. It has previously been reported that two similar compounds have been attached.[1,2] However, in both cases low yields were obtained, even when using aggressive alkylating conditions, such as ^{n}BuLi in toluene and as discussed in Chapter 1 the nuclear magnetic resonance (NMR) data for both is unconvincing. The addition of 2-bromopropionyl bromide to calix[4]arene in this chapter was unsuccessful, even under the conditions reported as well as alternative synthetic conditions (Scheme 4.1).

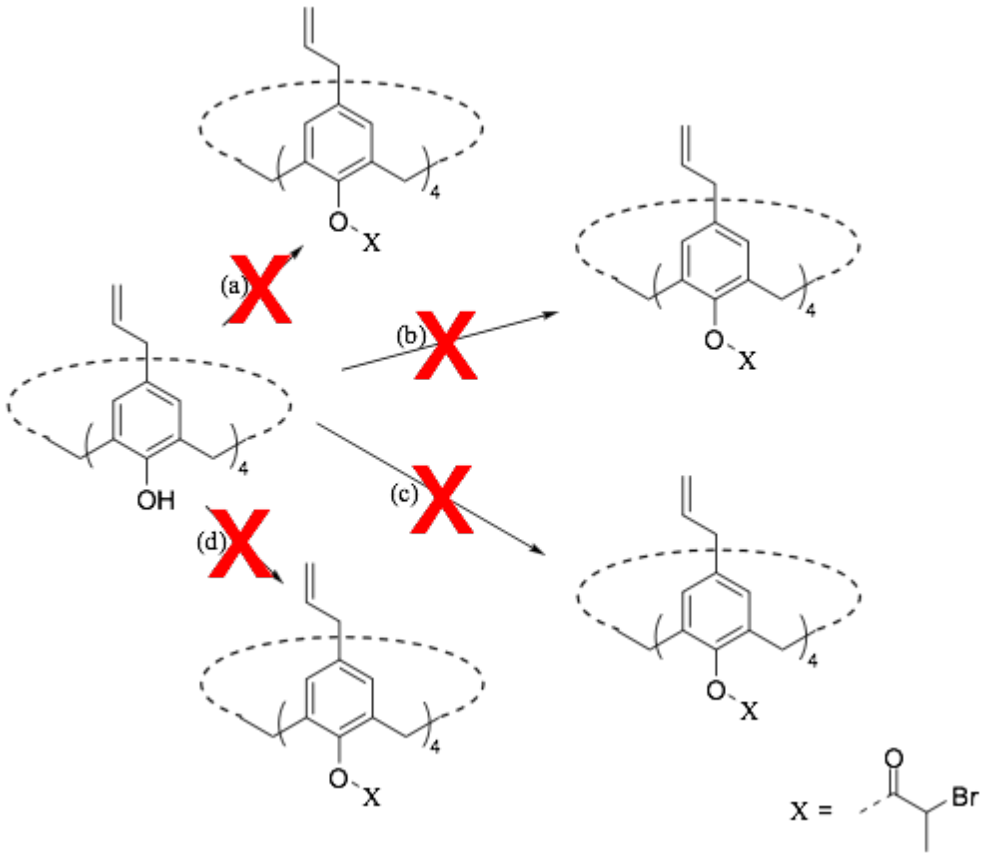

Scheme 4.1. Attempted Synthesis. (a) K_2CO_3, 2-bromopropionyl bromide, MeCN, reflux, (b) ^{n}BuLi, 2-bromopropionyl bromide, toluene, -78 ^{o}C, (c) NaH, 2-bromopropionyl bromide, DMF/THF. (d) NEt_3, 2-bromopropionyl bromide, dichloromethane.

Therefore, an alternative synthetic strategy was implemented to introduce the alkyl halide moiety, Scheme 4.2. The first step was a de-*tert*-butylation of the *p*-*tert*-butylcalix[4]arene starting material, **1**, an in-depth analysis of the first step is discussed in Chapter 2. The second step was to saturate the lower rim of **1** with allyl moieties, **11**. The Allyl moiety was selected as it can be re-arranged to reside in the *para* position of the calix[4]arene, which can then be further used to facilitate thiol-ene "click" reactions.

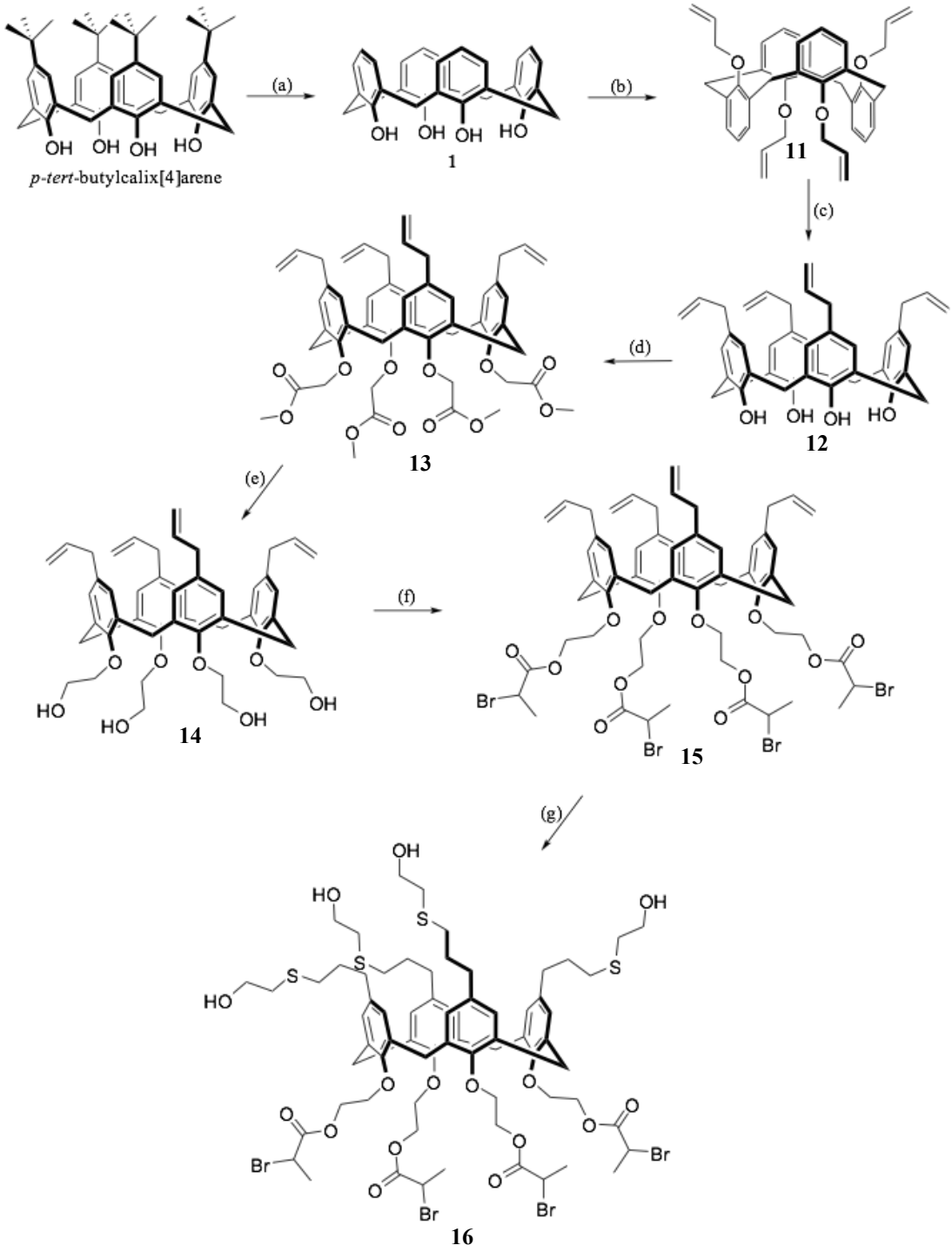

Scheme 4.2. Synthetic strategy employed for the synthesis of initiator 2. (a) $AlCl_3$, phenol, toluene. (b) allyl iodide, K_2CO_3, MeCN. (c) N,N-dimethylaniline. (d) Methyl chloroacetate, K_2CO_3, KI, MeCN. (e) $LiAlH_4$, THF. (f) 2-bromopropionyl bromide, TEA, dichloromethane. (g) 2-mercaptoethanol, dichloromethane, UV.

The third step was a Claisen rearrangement, which would rearrange the allyl moiety from the lower rim to the upper rim, **12**. The fourth step was introduction of an ester moiety *via* a Williamson ether synthesis of methyl chloroacetate to the lower rim, **13**. The alkyl ester moiety was selected as is could be reduced to a primary hydroxyl that

could facilitate the esterification of 2-bromopropionyl bromide. The fifth step was the reduction of **13**, with $LiAlH_4$ selected as the reducing agent to give **14**. The sixth step was the esterification of the primary hydroxyl of **14** with the acyl bromide of 2-bromopropionyl bromide, **15**. The seventh step was a photo initiated thiol-ene "click" reaction between **15** and 2-mercaptoethanol, to give **16**, which was selected as it would introduce a primary hydroxyl to facilitate ROP. The reaction conditions and an in depth analysis of all compounds synthesised is described herein.

4.1 Experimental

4.1.1. Materials

1 was synthesised according to the literature and is discussed in Chapter 2.[3] *p-tert*-butylcalix[4]arene, allyl iodide (98%), anhydrous potassium carbonate (>99%), N,N-dimethylaniline (99%), anhydrous potassium iodide (>99%), methyl chloroacetate (99%), lithium aluminium hydride pellets (95%), trimethylamine (>99.5%), 2-bromopropionyl bromide (97%), 2-mercaptoethanol (>99%) and magnesium sulfate were purchased from Sigma Aldrich and used without further purification. Chloroform, dichloromethane, hexane, ethyl acetate, methanol analytical grade solvents and hydrochloric acid (c.HCl, 37%) were purchased from Fisher Scientific and used without further purification. Dry acetonitrile (MeCN), Tetrahydrofuran (THF) and dichloromethane were obtained from the Durham University Chemistry Department Solvent Purification Service (SPS). Deuterated chloroform ($CDCl_3$) for NMR analysis was purchased from Apollo Scientific.

4.1.2. Instrumentation

^1H and ^{13}C NMR spectra were recorded using a Varian VNMRS 700 spectrometer operating at 700 MHz and 176 MHz respectively, with *J* values given in Hz. $CDCl_3$ was used as deuterated solvent for ^1H and ^{13}C NMR analysis and the spectra were referenced to the solvent traces at 7.26 ppm and 77.0 ppm respectively. The following abbreviations are used in describing NMR spectra: s = singlet, d = doublet, t = triplet, m = multiplet, , q = quartet, quin = quintet, b = broad, dd = doublet of

doublets, dq = doublet of quartets. Pure shift ^{1}H NMR spectroscopy was used when simplification and increased resolution of spectra was required, which is brought about from ^{1}H-^{1}H decoupling. 2D NMR experiments were also used to fully assign the proton and carbon environments in the products. ^{1}H-^{1}H Correlation Spectroscopy (COSY) demonstrated proton-proton correlations over two or three bonds. ^{1}H-^{13}C Heteronuclear Shift Correlation Spectroscopy (HSQC) demonstrated correlation between directly bonded proton and carbons atoms. ^{1}H-^{13}C Heteronuclear Multiple-Bond Correlation (HMBC) demonstrated the correlation between proton and carbon environments through several bonds.

Atmospheric Solids Analysis Probe Mass **S**pectrometry (ASAP MS) was carried out using a *LCT Premier XE* mass spectrometer and an Acquity UPLC (Waters Ltd, UK). A melting point tube was dipped into the sample solution (1 mg mL^{-1}). Samples were run isothermally at 350 °C. The sample was vaporised from the melting point tube enabling atmospheric pressure chemical ionisation (APCI) to occur.

Fourier transform-infra-red (FT-IR) spectroscopy was conducted using a Perkin Elmer 1600 series spectrometer.

Elemental analyses of small molecules were obtained using an Exeter CE-440 elemental analyser.

Thiol-ene reactions were conducted using a *Fusion UV LC6B Benchtop Conveyor*. The samples were placed in glass vials and dissolved in chloroform. The samples were passed under the UV source on a conveyer belt, with a UV exposure time of 15 seconds. The UV lamp was operating at 200 watt cm^{-2}.

4.1.3. Synthesis of 25,26,27,28-*tetrakis*(prop-2-en-1-yloxy)calix[4]arene, 11

To a 500 mL 2-necked round bottomed flask fitted with a septum, reflux condenser and stopper **1** (6.005 g, 14.20 mmol) and potassium carbonate (9.786 g, 70.8 mmol) were added. The flask was evacuated (0.5 h) then purged with dry argon (Ar). Under

Ar, dry MeCN (300 mL) was transferred in *via* cannula. Allyl iodide (6.48 mL, 70.80 mmol) was syringed into the reaction mixture leading to a cream/yellow coloured solution. The reaction mixture was refluxed for 48 h. A blue/green coloured solution resulted. The MeCN was reduced *in vacuo* resulting in a blue/green coloured residue. The residue was taken up in dichloromethane (250 mL) and HCl 10% (150 mL) and added to a separating funnel. The translucent pale red/orange organic phase was collected and further washed with brine (2 x 100 mL), then dried over magnesium sulphate and filtered. The volume of dichloromethane was reduced *in vacuo* to ~10 mL. Methanol (200 mL) was added and the remaining dichloromethane was removed *in vacuo* leading to the precipitation of a pale red solid. The pale red solid was collected under reduced pressure. The product was purified *via* column chromatography using hexane:ethyl acetate in a ratio of 100:1 on silica leading to a white solid. Mass = 6.289 g, yield = 76%. M.p. = 255-56 ºC.[1] ν_{max} (Perkin Elmer FT-IR, Diamond, cm^{-1}). 1638 (w, C=C). ^{1}H NMR (700 MHz, $CDCl_3$) δ: 3.61 (s, $8H_a$), 4.18 (m, $8H_b$), 5.17 (dq, $4H_c$, J_1 = 29.2 Hz, J_2 = 1.9 Hz), 5.19 (m, $4H_d$), 5.92 (m, $4H_e$), 6.69 (t, $4H_f$, J = 7.8 Hz), 7.00 (d, $8H_g$, J = 7.8 Hz). ^{13}C NMR (176 MHz, $CDCl_3$) δ: 36.9 (**a'**), 71.5 (**b'**), 115.9 (**c'**), 121.7 (**d'**), 131.0 (**e'**), 133.7 (**f'**), 134.0 (**g'**), 155.7 (**h'**). Mass spectrum (ASAP MS); *m/z* = 585.296, (100%) $[M]^+$.

(a) (b)

Figure 4.2. Labelling of the chemical environments in compound **11** (a) proton (b) carbon.

4.1.4. Synthesis of 5,11,17,23-*tetrakis*(prop-2-en-1-yloxy)-calix[4]arene, 12

To a 150 mL round bottomed flask fitted with reflux condenser, **11** (5.00 g, 8.60 mmol) was added. The flask was evacuated (0.5 h) then purged with dry Ar. Under

Ar, *N,N*-dimethylaniline (75 mL) was transferred in forming a translucent colourless solution. The solution was stirred at reflux (2 h) forming a dark brown solution. The solution was poured over ice (400 g) with the further addition of HCl 37% (150 mL) forming a white/pale green precipitate, which was collected by filtration. The precipitate was dissolved in dichloromethane (200 mL) and washed with HCl 10% (100 mL) in a separating funnel. The translucent pale green organic phase was further washed with brine (2 x 25 mL), then dried over magnesium sulphate and filtered. The volume of dichloromethane was reduced *in vacuo* leading to a white/pale green solid. The residue was purified *via* re-crystallisation from methanol leading to a white solid. Mass = 4.546 g, yield = 91%. ν_{max} (Perkin Elmer FT-IR, Diamond, cm^{-1}). 3158 (s, OH), 1638 (w, C=C). ^{1}H NMR (700 MHz, $CDCl_3$) δ: 3.22 (d, $8H_a$, J = 7.4 Hz), 3.48 (s, $4H_b$), 4.25 (s, $4H_c$), 5.07 (m, $4H_d$), 5.90 (m, $4H_e$), 6.87 (s, $8H_f$), 10.19 (s, $4H_g$). ^{13}C NMR (176 MHz, $CDCl_3$) δ: 31.9 (**a'**), 39.5 (**b'**), 115.7 (**c'**), 128.3 (**d'**), 129.1 (**e'**), 133.6 (**f'**), 137.7 (**g'**), 147.2 (**h'**). Mass spectrum (ASAP MS); *m/z* = 585.299, (100%) $[M+H]^+$.

(a) (b)

Figure 4.3. Labelling of the chemical environments in compound **12** (a) proton (b) carbon.

4.1.5. Synthesis of 5,11,17,23-*tetrakis*(prop-2-en-1-yloxy)-25,26,27,28-tetrakis(methyl acetateoxy)- calix[4]arene, 13

To a 250 mL 2-necked round bottomed flask fitted with a septum, reflux condenser and stopper, **12** (4.011 g, 6.90 mmol), potassium carbonate (4.776 g, 34.55 mmol) and potassium iodide (0.400 g, 2.41 mmol) were added. The flask was evacuated (0.5 h) then purged with dry Ar. Under Ar, dry MeCN (200 mL) was transferred in *via* cannula forming a pale blue suspension. Methyl chloroacetate (3.1 mL, 35.37

mmol) was syringed into the reaction mixture leading to a cream/pale blue opaque solution. The reaction mixture was refluxed for 48 h. A cream coloured opaque solution resulted. The MeCN was reduced *in vacuo* resulting in a cream coloured residue. The residue was taken up in dichloromethane (250 mL) and HCl 10% (100 mL) then added to a separating funnel. The translucent pale yellow organic phase was collected and further washed with brine (2 x 50 mL), dried over magnesium sulphate and filtered. The volume of dichloromethane was reduced *in vacuo* leading to a brown sticky residue. The residue was purified *via* column chromatography using hexane:ethyl acetate in a ratio of 5:1 on silica, a pale yellow solid was obtained. Mass = 3.468 g, yield = 58%. R.f = 0.326 (Hexane:ethylacetate, 2:1). ν_{max} (Perkin Elmer FT-IR, Diamond, cm^{-1}). 1760 (s, C=O), 1638 (w, C=C). ^{1}H NMR (700 MHz, $CDCl_3$) δ: 3.07 (d, $8H_a$, J = 6.5 Hz), 3.17 (d, $4H_b$, J = 13.6 Hz), 3.75 (s, $12H_c$), 4.75 (s, $8H_d$), 4.79 (d, $4H_e$, J = 13.3 Hz), 4.89 (dq, $4H_f$, J_1 = 17.0Hz, J_2 = 1.6 Hz), 4.96 (dq, $4H_g$, J_1 = 10.0 Hz, J_2 = 1.6 Hz) 5.79 (m, $4H_h$), 6.50 (s, $8H_i$). ^{13}C NMR 176 (176 MHz, $CDCl_3$) δ: 31.3 (**a'**), 39.3 (**b'**), 51.4 (**c'**), 71.1 (**d'**), 115.0 (**e'**), 128.7 (**f'**), 134.0 (**g'**), 134.2 (**h'**), 137.9 (**i'**), 154.0 (**j'**), 170.7 (**k'**). Mass spectrum (ASAP MS); *m/z* = 873.377, (100%) $[M+H]^+$. CHN expected = %C = 71.54, %H = 6.47, %N 0.00; measured %C = 71.56, %H = 6.48, %N 0.00.

(a) (b)

Figure 4.4. Labelling of the chemical environments in compound **13** (a) proton (b) carbon.

4.1.6. Synthesis of 5,11,17,23-*tetrakis*(prop-2-en-1-yl)25,26,27,28-*tetrakis*(ethanoloxy)-calix[4]arene, 14

To a 150 mL 2-necked round bottomed flask fitted with a septum and argon inlet, **13** (3.001 g, 5.13 mmol) was added. The flask was evacuated (0.5 h) then purged with dry Ar. Under Ar, dry THF (50 mL) was transferred in *via* cannula forming a translucent colourless solution. The translucent solution was transferred *via* cannula, drop wise, to a suspension of $LiAlH_4$ (0.584 g, 15.39 mmol) in dry THF (100 mL) under Ar. The solution was stirred at 23 ^oC for 0.5 h and then for a further 1.5 h at 50 ^oC. The reaction mixture was carefully quenched by the drop wise addition of water. The solvent was removed under reduced pressure leading to a white residue, which was collected in dichloromethane (100 mL) and HCl 10% (50 mL) and added to a separating funnel. The translucent pale yellow organic phase was collected and further washed with brine (2 x 25 mL), dried over magnesium sulphate and filtered. The volume of dichloromethane was reduced *in vacuo* leading to a pale yellow tacky residue. Mass = 1.876 g, yield = 92%. ν_{max} (Perkin Elmer FT-IR, Diamond, cm^{-1}). 3380 (s, OH), 1638 (w, C=C). ^1H NMR (700 MHz, $CDCl_3$) δ: 3.12 (bs, $8H_a$), 3.23 (bm, $4H_b$), 4.03 (bs, $16H_c$), 4.41 (bs, $4H_d$), 4.93 (bm, $4H_e$), 5.01 (bm, $4H_f$), 5.81 (bm, $4H_g$), 6.68 (bs, $8H_h$). ^{13}C NMR (176 MHz, $CDCl_3$) δ: 30.2 (**a'**), 39.5 (**b'**), 61.2 (**c'**), 77.9 (**d'**), 115.6 (**e'**), 129.0 (**f'**), 134.7 (**g'**), 137.5 (**h'**), 152.8 (**i'**). Mass spectrum (ASAP MS); *m/z* = 593.290, (100%) $[M]^+$. CHN expected = %C = 75.76, %H = 7.42, %N 0.00; measured %C = 76.03, %H = 7.56, %N 0.00.

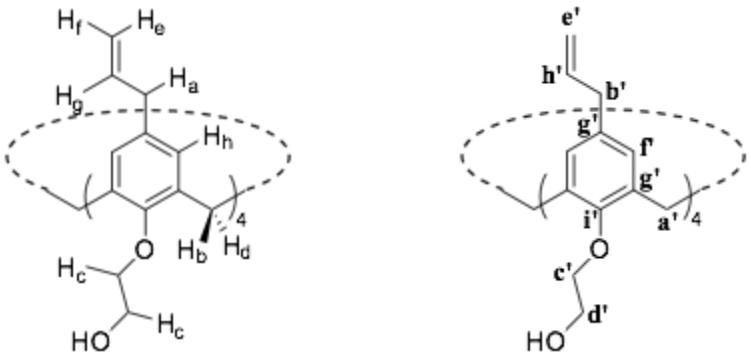

(a) (b)

Figure 4.5. Labelling of the chemical environments in compound **14** (a) proton (b) carbon.

4.1.7. Synthesis of 5,11,17,23-*tetrakis*(prop-2-en-1-yl)-25,26,27,28-*tetrakis*(ethoxyester-2-bromo-acetate)calix[4]arene, 15

To a 150 mL 2-necked round bottomed flask fitted with a septum and reflux condenser, **5** (1.602 g, 2.70 mmol) was added. The flask was evacuated (0.5 h) then purged with dry Ar. Under Ar, dry dichloromethane (50 mL) was transferred in *via* cannula forming a translucent pale yellow solution followed by the addition of NEt_3 (1.88 mL, 13.50 mmol). The solution was cooled *via* a salt ice bath and the temperature was maintained at ~-8 ^oC. 2-bromopropionyl bromide (1.41 mL, 13.50 mmol) was added drop wise over 0.5 h. The solution turned translucent brown and was allowed to warm to 23 ^oC, then left to stir at 23 ^oC for a further 3.5 h, the solution turned yellow over this period. The reaction mixture was collected in additional dichloromethane (50 mL) and washed with HCl 10% (30 mL) and with brine (2 x 25 mL), then dried over magnesium sulphate and filtered. The volume of dichloromethane was reduced *in vacuo* leading to a brown sticky residue. The residue was purified *via* column chromatography using hexane:ethyl acetate in a ratio of 10:1 on silica. A colourless sticky residue was obtained. Mass = 2.738 g, yield = 78%. R.f = 0.292 (heaxane:ethylacetate, 10:1). ν_{max} (Perkin Elmer FT-IR, Diamond, cm^{-1}). 2850-3100 (m, CH), 1739 (s, C=O), 1638 (m, C=C). ^1H NMR (700 MHz, $CDCl_3$) δ: 1.78 (dd, $12H_a$, J = 7.0 Hz), 1.85 (d, $4H_b$, J = 8.0 Hz), 3.06 (d, $8H_c$, J = 7.2 Hz), 3.15 (d, $4H_d$, J = 15.6 Hz), 4.19 (m, $8H_e$), 4.35 (m, $8H_{f,g}$), 4.40 (q, $4H_h$, J = 8 Hz), 4.64 (m, $4H_i$), 4.88 (dd, $4H_j$, J_1 = 19.9 Hz, J_2 = 1.4 Hz), 4.96 (dd, $4H_k$, J_1 = 11.9 Hz, J_2 = 1.4 Hz), 5.77 (m, $4H_l$), 6.50 (s, $8H_m$). ^{13}C NMR (176 MHz, $CDCl_3$) δ: 21.6 (**a'**), 21.7 (**b'**), 31.0 (**c'**), 39.4 (**d'**), 39.5 (**e'**), 40.0 (**f'**), 65.7 (**g'**), 72.2 (**h'**), 115.2 (**i'**), 128.8 (**j'**), 134.1 (**k'**), 134.3 (**l'**), 138.0 (**m'**), 154.1 (**n'**), 170.4 (**o'**), 174.8 (**p'**). Mass spectrum (ASAP MS); *m/z* = 1301.153, (31.96%) $[M+H]^+$. CHN expected = %C = 52.05, %H = 5.06, %N 0.00; measured %C = 52.61, %H = 5.37, %N 0.00.

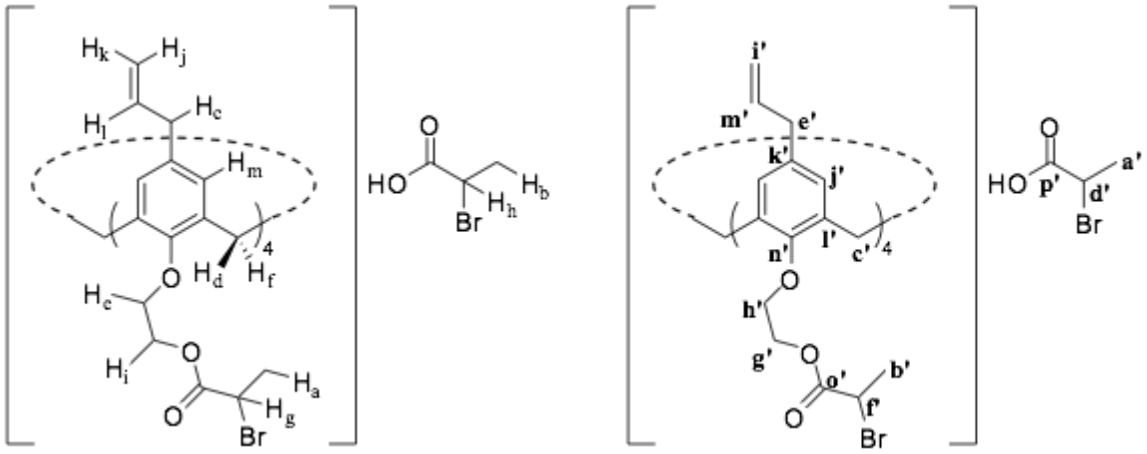

Figure 4.6. Labelling of the chemical environments in compound **15** (a) proton (b) carbon.

4.1.8. Synthesis of 5,11,17,23-*tetrakis*(3-(hydroxyethyl)thioether-propanyl)-25,26,27,28-*tetrakis*(ethoxyester-2-bromo-propanoate)-calix[4]arene, 16

To a 10 mL glass vial, **15** (0.350 g, 0.22 mmol) was added and dissolved in chloroform (3 mL) followed by the addition of 2-mercaptoethanol (0.16 mL, 2.27 mmol). The sample was irradiated with a broad wavelength UV lamp for 30 s, a colourless solution remained. The chloroform was removed *in vacuo* leaving a viscous colourless liquid, which was further purified *via* a silica plug. On silica, the sample was washed with pure ethyl acetate, and then to collect 7, pure methanol was passed through the silica. The methanol was removed *in vacuo* resulting in a tacky white residue. Mass = 0.387 g, yield = 89%. ν_{max} (Perkin Elmer FT-IR, Diamond, cm^{-1}). 3306 (s, OH), 2923 (s, CH), 1732 (s, C=O). ^{1}H NMR (700 MHz, $CDCl_3$) δ: 1.70 (quin, $8H_a$, J = 8.2 Hz) 1.78 (d, $12H_b$, J = 8.0 Hz), 2.40 (t, $8H_c$, J = 8.0 Hz), 2.47 (t, $8H_d$, J = 8.3 Hz), 2.72 (t, $8H_e$, J = 7.0 Hz), 3.13 (d, $4H_f$, J = 15.4 Hz), 3.72 (t, $8H_g$, J = 7.0 Hz), 4.18 (m, $8H_h$), 4.35 (m, $8H_{i,j}$), 4.63 (m, $8H_k$), 6.47 (s, $8H_l$) .^{13}C NMR (176 MHz, $CDCl_3$) δ: 21.7 (a'), 31.0 (b'), 31.3 (c'), 31.4 (d'), 34.1 (e'), 35.4 (f'), 40.1 (g'), 60.6 (h'), 65.6 (i'), 72.2 (j'), 128.5 (k'), 134.3 (l'), 135.6 (m'), 154.1 (n'), 170.4 (o'). CHN Expected = %C = 50.63, %H = 5.75, %N = 0.00; Measured %C = 50.98, %H = 5.79, %N = 0.00.

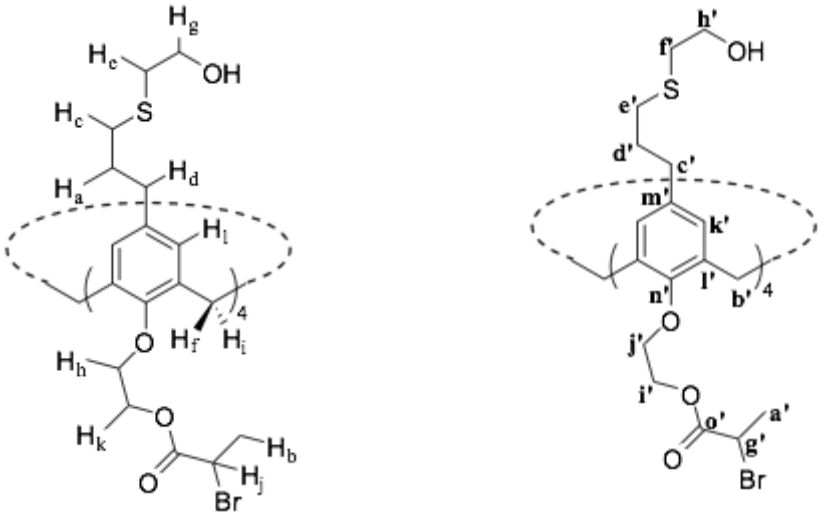

(a) (b)

Figure 4.7. Labelling of the chemical environments in compound **16** (a) proton (b) carbon.

4.2. Results and Discussion

4.2.1. 25,26,27,28-*tetrakis*(allyloxy)-calix[4]arene, 11

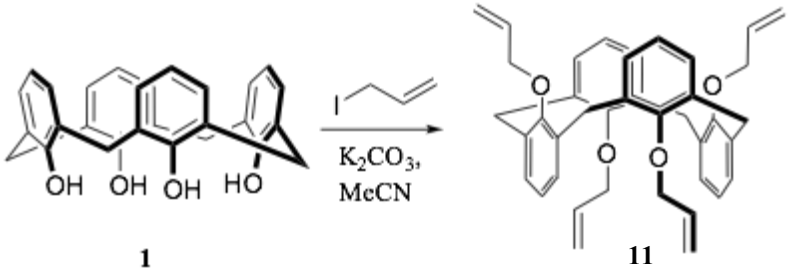

1 **11**

Scheme 4.3. Synthesis of **11**.

The known compound **11** was successfully synthesised, by treating calix[4]arene, **1**, with an excess of allyl iodide in the presence of excess potassium carbonate (Scheme 4.3).[3] A yield of 76% was achieved after refluxing for 48 h in MeCN. The product was purified *via* column chromatography, leading to a pure white powder. A complete and thorough analysis is discussed herein as previous characterisation was limited.[3]

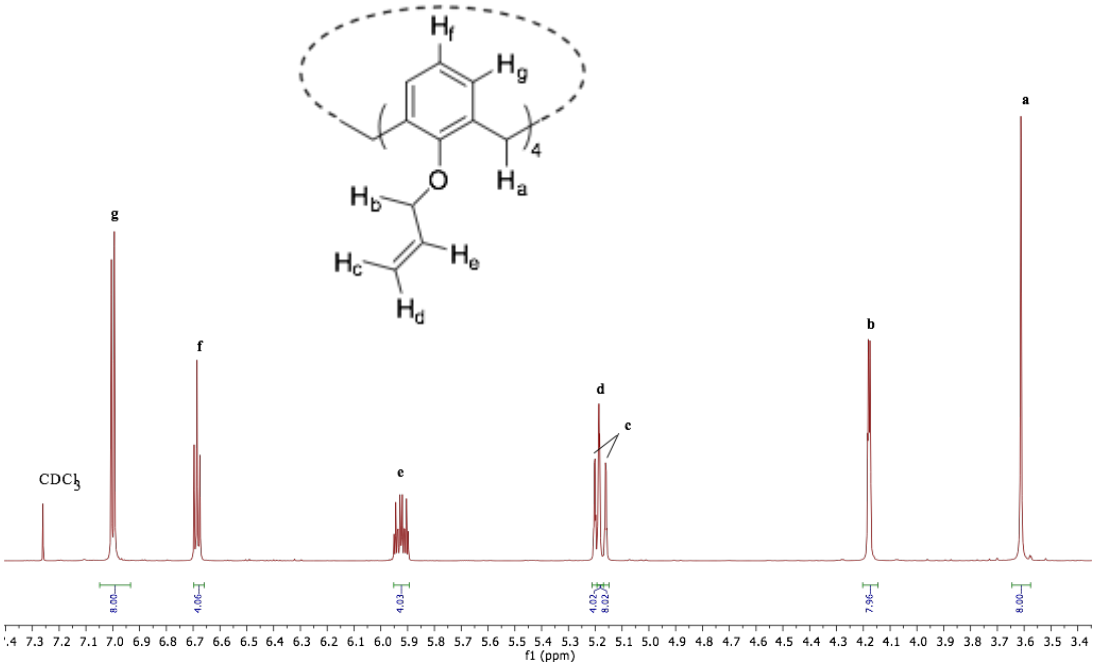

Figure 4.8. ^{1}H NMR spectrum of **11** in $CDCl_3$.

The ^{1}H NMR spectrum (Fig. 4.8) shows a singlet resonance with its integral set to eight at 3.61 ppm, **a**, which corresponds to the methylene protons that bridge the aromatics. The presence of a singlet resonance indicates that **2** exists in a 1,3-alternate conformation.[4] A multiplet resonance with an integral of eight is observed at 4.18 ppm, **b**, corresponding to the aliphatic protons of the allyl moiety, H_b.

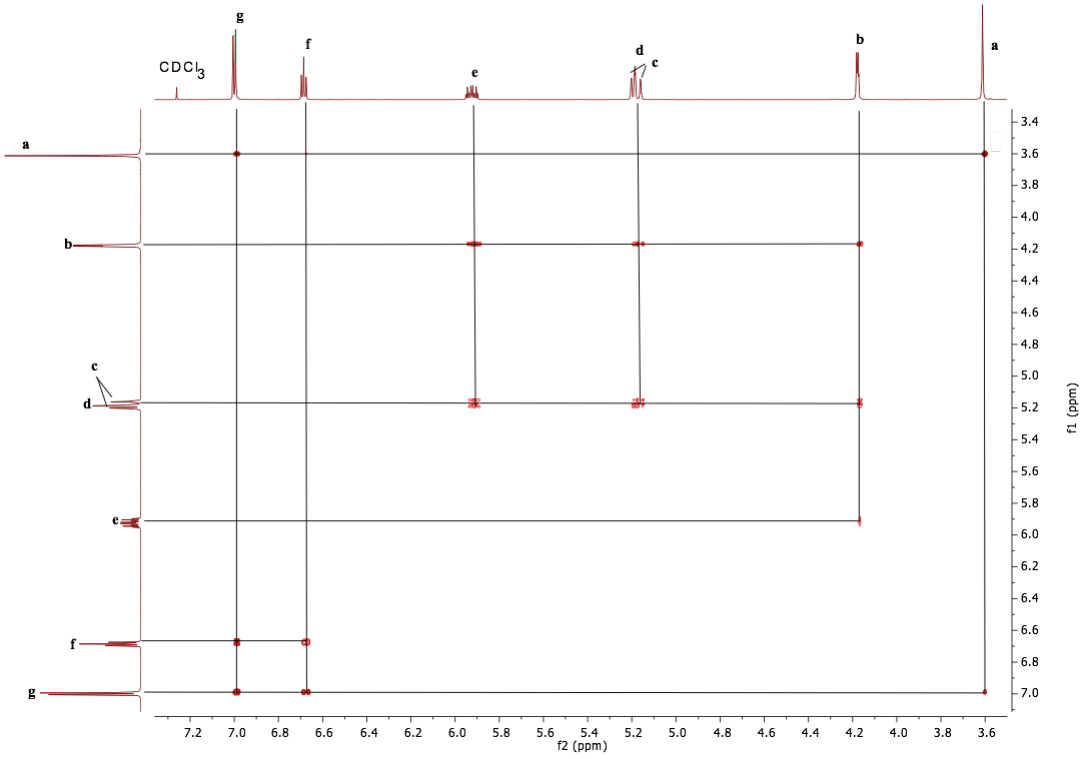

Figure 4.9. COSY NMR spectrum of **11** in $CDCl_3$.

The COSY NMR spectrum (Fig. 4.9) shows **b** exhibiting coupling to **c**, **d** and **e**. The ^{1}H NMR spectrum (Fig. 4.8) showed a multiplet resonance with an integral of four at 5.92 ppm, **e**, which corresponds to the non-terminus alkene proton of the allyl moiety, H_e. A doublet of quartets with an integral of four at 5.17 ppm, **c**, with a J_1 coupling of 29.2 Hz and a J_2 coupling of 1.2 Hz is observed. A multiplet with an integral of four is observed at 5.19 ppm, **d**. Both resonances **c** and **d** correspond to the terminus protons of the alkene of the allyl moiety, with **c** corresponding to the hydrogen atom in the *trans* position with respect to $H_{c,}$, and **d** corresponds to the hydrogen atom in the *cis* position, H_d. The doublet of quartet's multiplicity of **c** is brought about by coupling to H_e that leads to the doublet splitting and the J_1 value and the second coupling to H_g, which leads to the smaller coupling constant of J_2. **d** exhibits a multiplet multiplicity due the same coupling as **c,** but because of the closer

proximity of H_e, leads to a much smaller J_1 coupling constant; the doublet of quartet multiplicity coalesces. Confirmation that **c** and **d** are two distinct resonances come from the ^{1}H pure shift NMR experiment, where two distinct resonances are observed, shown in Figure 4.10.

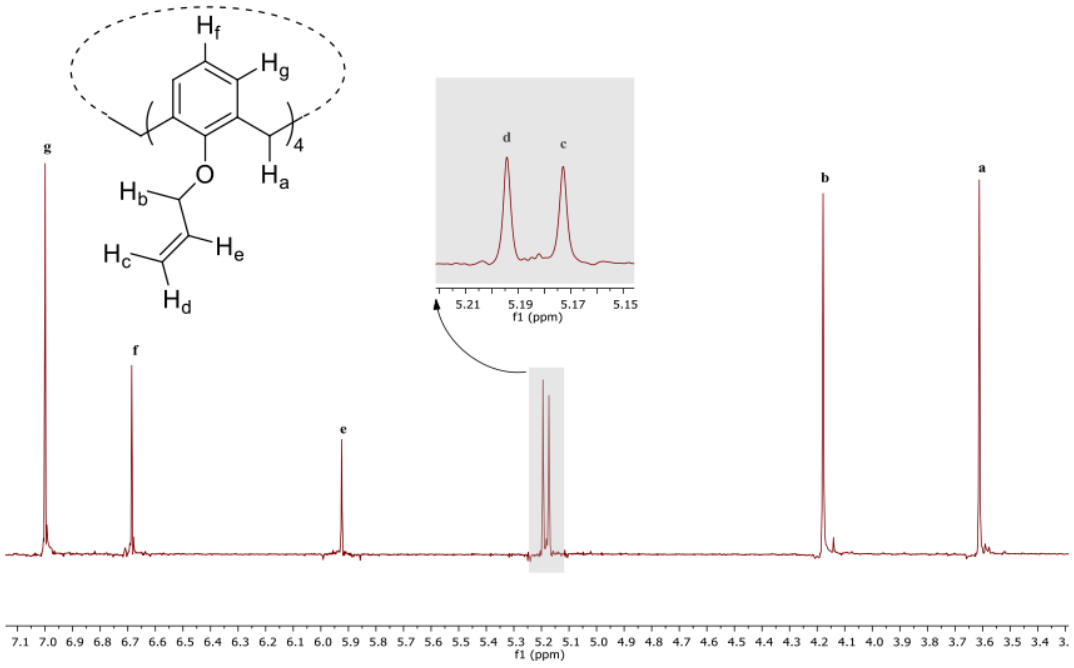

Figure 4.10. ^{1}H Pure Shift NMR spectrum of **11** in $CDCl_3$.

The ^{1}H NMR spectrum (Fig. 4.8) shows a triplet resonance with an integral of four at 6.69 ppm, **f**, corresponding to the hydrogen atoms in the *para* position of the aromatic with respect to the oxygen of the aryl ether moiety, H_f. The triplet multiplicity is brought about by coupling to hydrogen atoms, H_g, either side of H_f. A doublet resonance is observed at 7.00 ppm, **g**, corresponding in the hydrogen atoms in the *meta* position of the aromatics with respect to the oxygen of the aryl ether moiety, H_g. The doublet splitting multiplicity is brought about by coupling to the single hydrogen atom of H_f. The coupling between H_f and H_g is confirmed by COSY NMR spectroscopy and is highlighted in Figure 4.9. Furthermore, all assigned integrals are in agreement with the proposed structure. To assign the ^{13}C NMR spectrum, HSQC NMR and HMBC NMR spectroscopy were carried out. Using HSQC NMR spectroscopy the carbon atoms directly attached to hydrogen atoms could be easily assigned. The HSQC NMR spectrum (Fig. 4.11) shows **a** coupling to a ^{13}C NMR resonance at 36.9 ppm, **a'**, corresponding to the bridging methylene

carbon atom between the aromatics. The chemical shift of **a'** at 36.9 ppm indicates that the calixarene is in the 1,3-alternate conformation, which agrees with what is observed in the ^{1}H NMR spectrum.[5] **b** exhibits coupling to a ^{13}C NMR resonance at 71.5 ppm, **b'**, corresponding to the linking aliphatic methylene carbon atom of the allyl moiety. **c** and **d** both couple to a ^{13}C NMR resonance at 115.9 ppm, **c'**, corresponding to the terminus carbon atom of the alkene of the allyl moiety. **e** couples to a ^{13}C NMR resonance at 134.0 ppm, **g'**, corresponding to the non-terminus carbon atom of the alkene of the allyl moiety. **f** exhibits coupling to a ^{13}C NMR resonance at 121.7 ppm, **d'**, corresponding to the carbon atom in the *para* position of the aromatic with respect to the oxygen of the aryl ether moiety. **g** exhibits coupling to a ^{13}C NMR resonance at 131.0 ppm, **e'**, corresponding to the carbon atom in the *meta* position of the aromatic with respect to the oxygen of the aryl ether moiety.

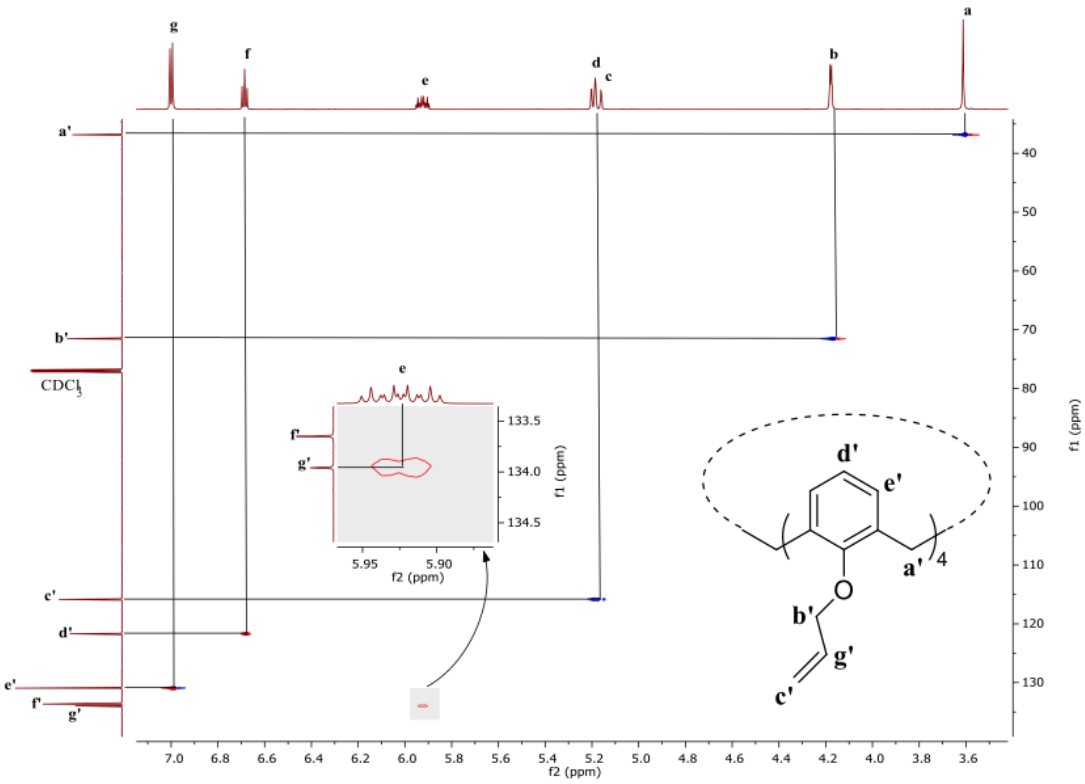

Figure 4.11. HSQC NMR spectrum of **11** in $CDCl_3$.

To assign the final ^{13}C NMR resonances that do not directly couple to any hydrogen atom, HMBC NMR spectroscopy was carried out and was fully analysed. The HMBC spectrum (Fig. 4.12) shows that a ^{13}C NMR resonance at 155.7 ppm, **h'**, exhibits coupling to **a**, **b**, **f** and **g**, with the most pronounced coming from the

coupling to **b**, which corresponds to H_b, therefore **h'** must correspond to the *ipso* carbon atom of the aromatic with respect to the oxygen of the aryl ether moiety. The ^{13}C NMR resonance at 133.7 ppm, **f'**, exhibits coupling to **a**, **f** and **g**, but significantly not **b**, therefore corresponds to the *ortho* carbon atom of the aromatic with respect to the oxygen of the aryl ether moiety. The full assignment of the ^{13}C NMR spectrum is shown in Figure 4.13.

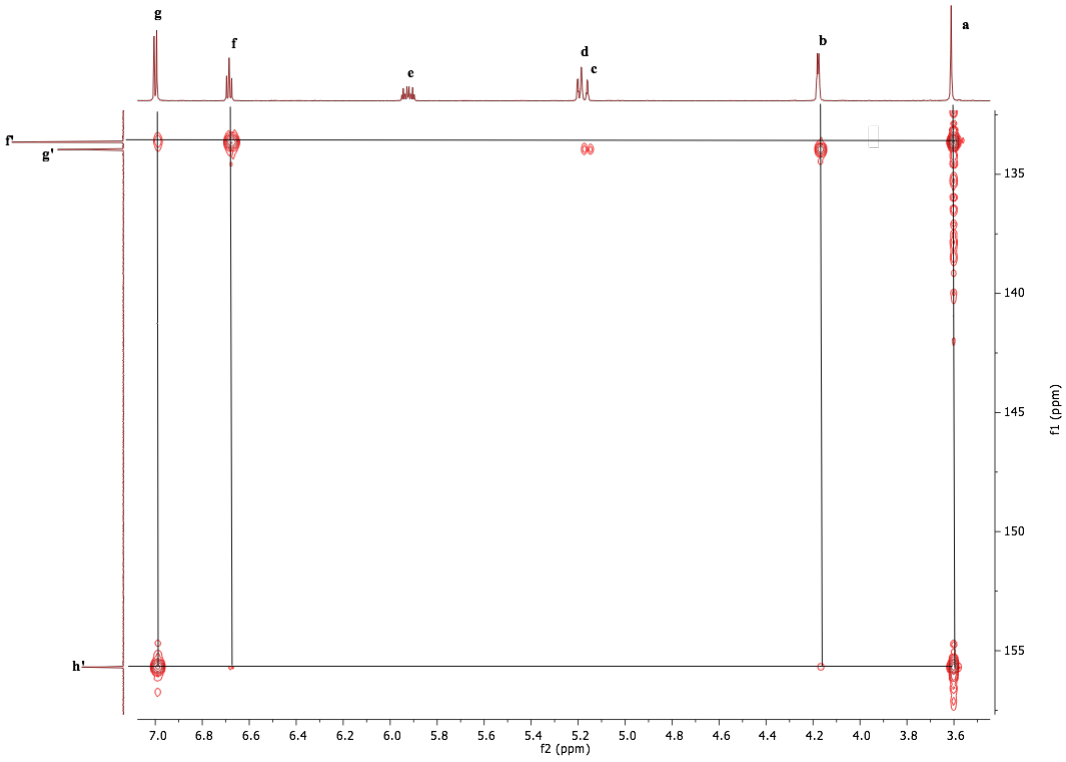

Figure 4.12. HMBC NMR spectrum of **11** in $CDCl_3$.

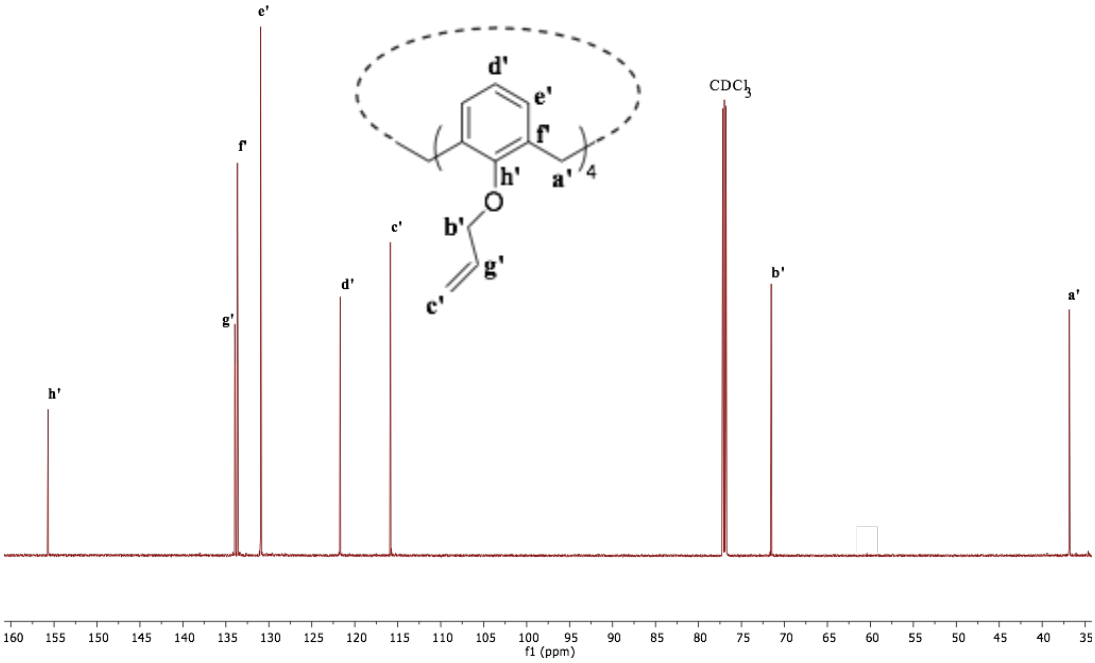

Figure 4.13. ^{13}C NMR spectrum of **11** in $CDCl_3$.

ASAP mass spectrometry was carried out and the molecular ion was seen at 585.296 Da (100%) (Fig. 4.14), which is consistent with the empirical formula $C_{40}H_{41}O_4^+$.

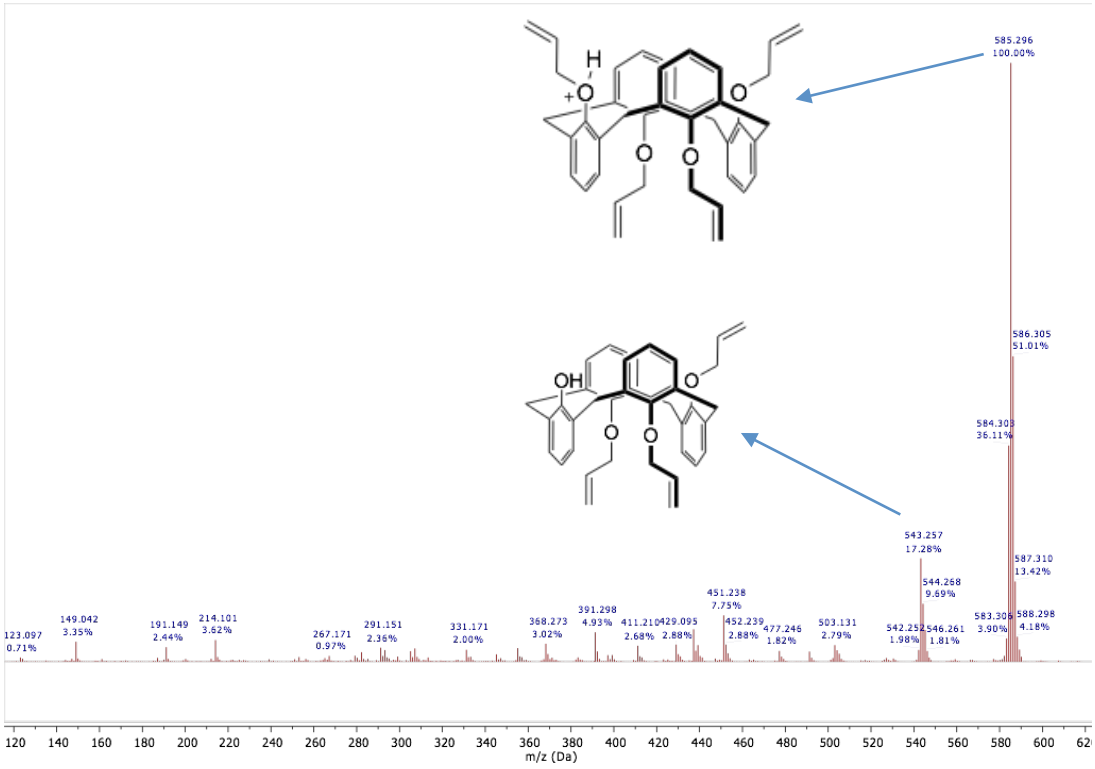

Figure 4.14. ASAP MS spectrum of **11**.

The ASAP MS spectrum (Fig. 4.14) showed fragmentation products, with the most abundant corresponding to the loss of one allyl moiety as depicted. Further confirmation that **2** had been successfully synthesised came from FT-IR spectroscopy, where there was complete loss of the OH stretch at 3120 cm^{-1}.

4.2.2. 5,11,17,23-*tetrakis*(prop-2-en-1-yl)-calix[4]arene, 12

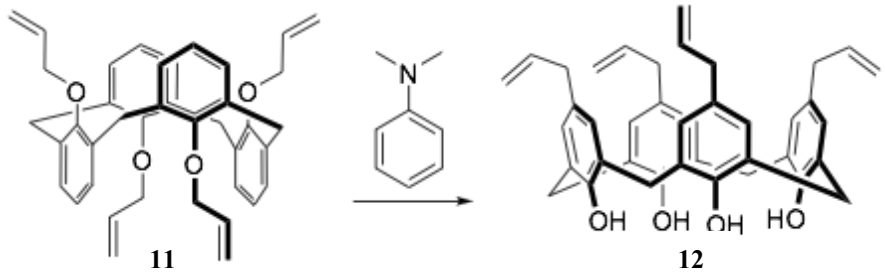

11 **12**

Scheme 4.4. Synthesis of **12**.

The known compound **12**, was successfully synthesised according to the literature (Scheme 4.4), using the high boiling N,N-dimethylaniline as a solvent to facilitate a sigmatropic reaction, in this case the Claisen rearrangement (Scheme 4.5).[3]

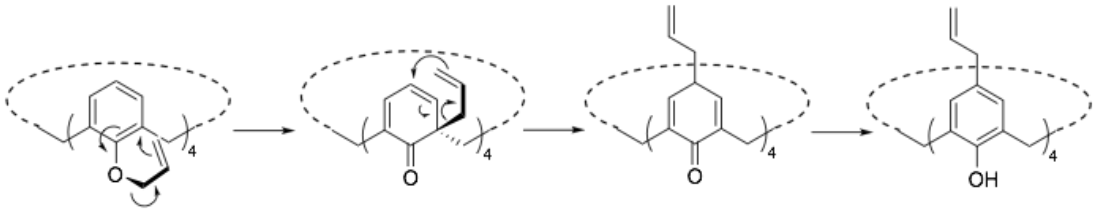

Scheme 4.5. Claisen rearrangement.

A yield of 91% was achieved. A complete analysis was carried out and is described below.

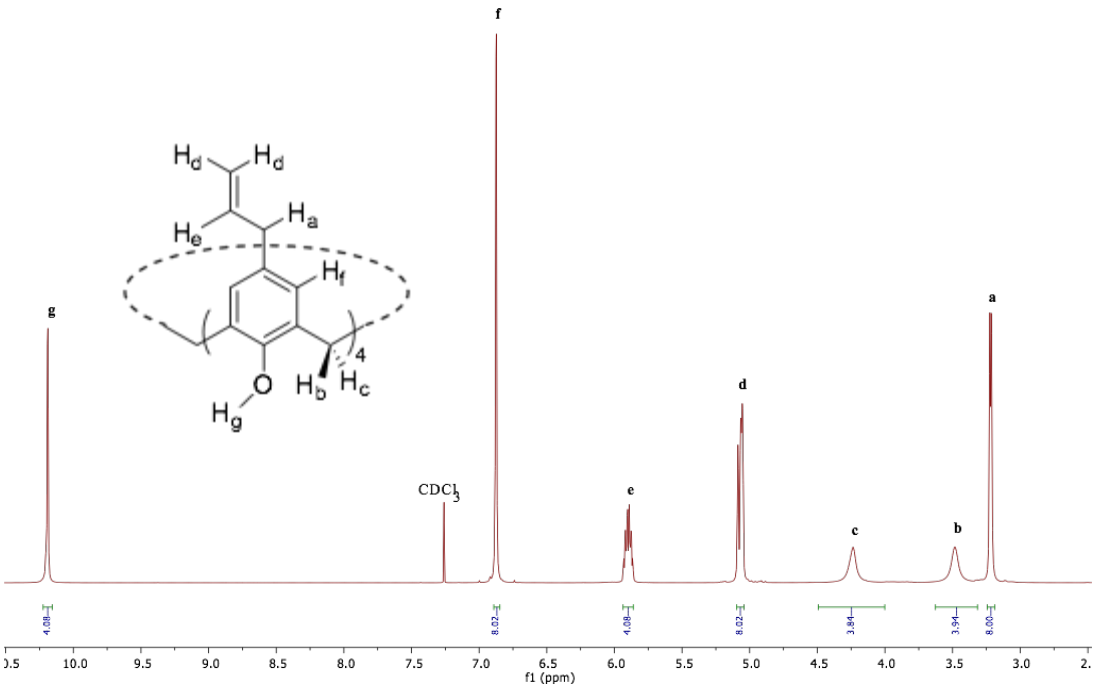

Figure 4.15. ^{1}H NMR spectrum of **12** in $CDCl_3$.

The ^{1}H NMR spectrum (Fig. 4.15) shows that **12** was synthesised. A doublet resonance with its integral set to eight was observed at 3.22 ppm, **a**, corresponding to the aliphatic protons of the allyl moiety, H_a. The COSY NMR spectrum (Fig. 4.16) shows that **a** exhibits coupling to resonances **d**, **e** and **f**. The ^{1}H NMR spectrum (Fig. 4.15) shows a multiplet resonance with an integral of eight at 5.07 ppm, **d**, corresponding to the terminal alkene protons of the allyl moiety, H_d. **d** appears as a multiplet due to overlapping signals from the *cis* and *trans* protons with respect to H_e, as shown by the COSY NMR spectrum (Fig. 4.16), where two coupling resonances are observed between **d** and **a**. The ^{1}H NMR spectrum (Fig. 4.15) shows a multiplet resonance with an integral of four at 5.90 ppm, **e**, corresponding to the non-terminus proton of the double bond of the allyl moiety, H_e. The multiplet multiplicity of **e** is brought about from coupling to the *cis* and *trans* H_d and the methylene H_a protons as shown by the COSY NMR (Fig 4.16).

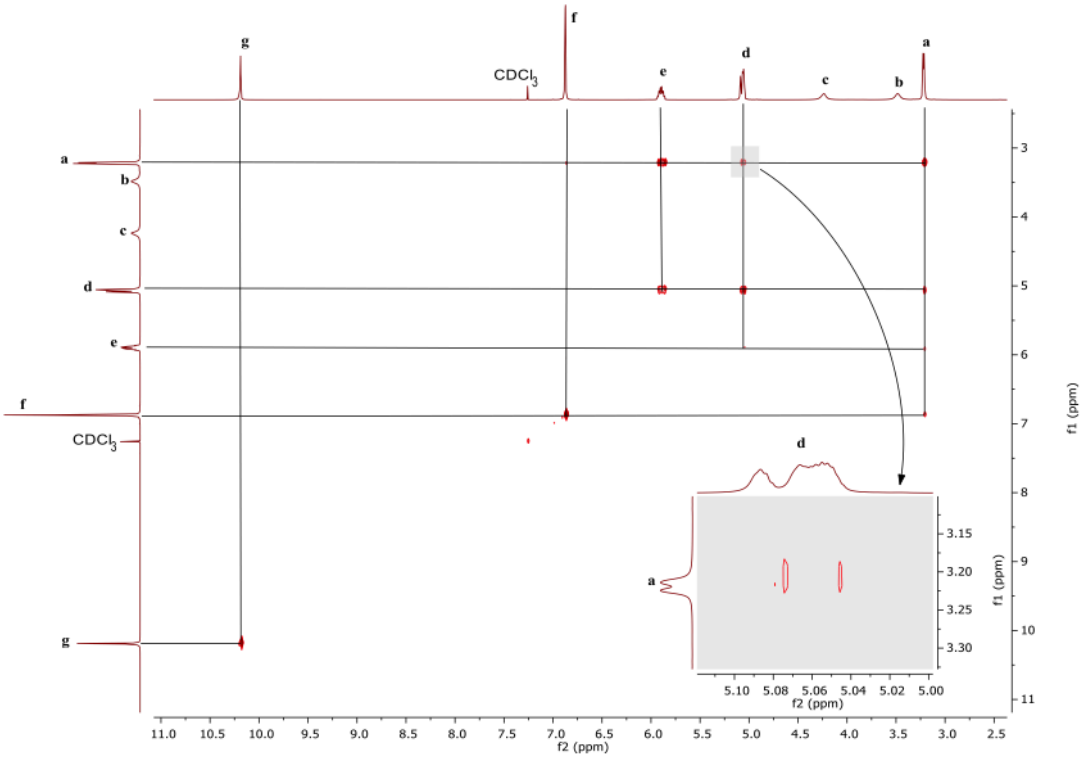

Figure 4.16. COSY NMR spectrum of **12** in $CDCl_3$.

The ^{1}H NMR spectrum (Fig. 4.15) shows a singlet resonance with an integral of eight at 6.87 ppm, **f**, which corresponds to the aromatic protons of the phenolic ring in the *meta* position with respect to the hydroxyl moiety, H_f. Two broad singlet resonances with integrals of four are observed at 3.48 ppm and 4.25 ppm, **c** and **d**, respectively, which correspond to the bridging methylene protons between the aromatic rings, H_b and H_c. The presence of two environments for the methylene bridging protons indicates that the calix[4]arene is in a cone conformation.[4] Resonance **b** corresponds to the protons pointing up with respect to the allyl moieties, whereas **c** corresponds to the protons pointing down to the oxo environment. A singlet resonance with an integral of four is observed at 10.19 ppm, **g**, which corresponds to the protons of the hydroxyl moiety, H_g. The sharpness and down field nature of resonance **g** is brought about by strong hydrogen bonding between the hydroxyl moieties. The strong hydrogen bonding is further observed *via* FT-IR spectroscopy, where a relatively sharp absorption band is observed at 3154 cm^{-1}. Furthermore, all assigned integrals are in agreement with the proposed structure. To assign the ^{13}C NMR spectrum, HSQC NMR and HMBC NMR spectroscopy were carried out. Using HSQC NMR spectroscopy the carbon atoms directly attached to hydrogen atoms could be easily assigned.

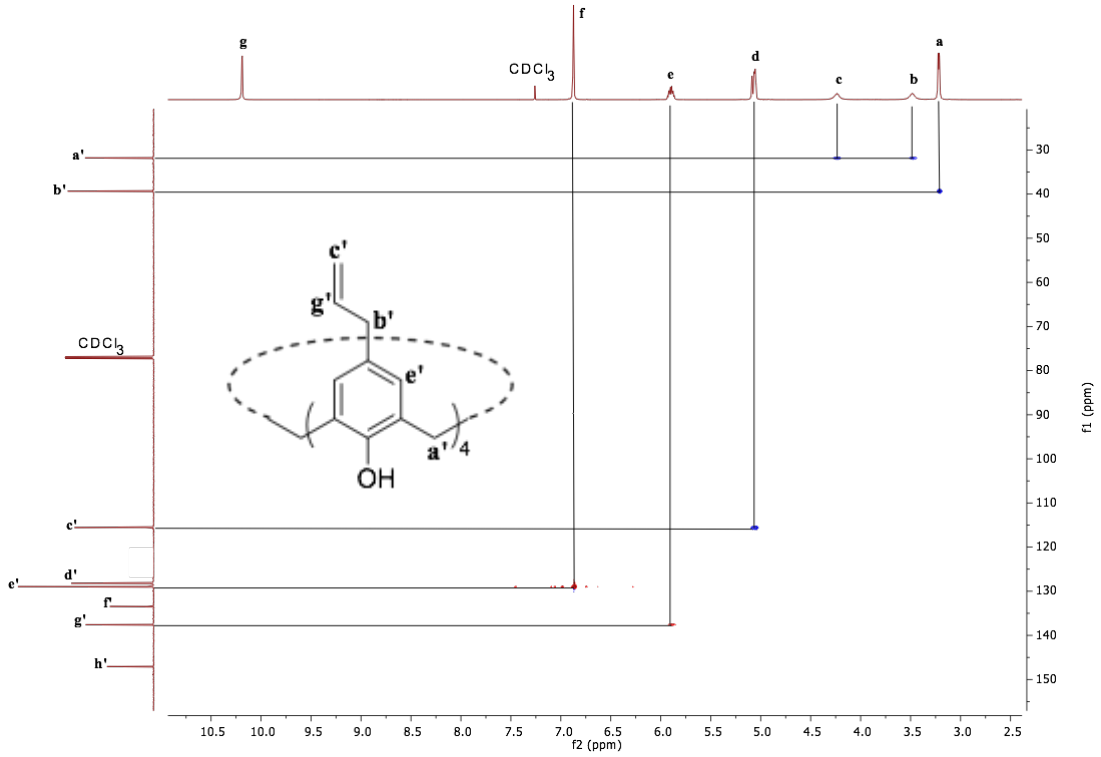

Figure 4.17. HSQC NMR spectrum of **12** in $CDCl_3$.

The HSQC NMR spectrum (Fig. 4.17) shows that **a** couples to a ^{13}C NMR resonance at 39.5 ppm, **b'**, which therefore corresponds to the ether linking allyl carbon atom. The coupling resonance between **a** and **b'** has a blue phasing indicating it is a methylene carbon atom. Both resonances, **b** and **c,** couple to a single ^{13}C NMR resonance at 31.9 ppm, **a'**, with the coupling resonance expressing blue phasing indicating it corresponds to a methylene moiety, therefore **a'** corresponds to the bridging methylene carbon atoms in-between aromatics. The fact that the bridging methylene carbon atom ^{13}C NMR resonance resides in the 31 ppm region is further indication that the calixarene exists in a cone conformation.[5] **d** couples to a ^{13}C NMR resonance at 115.7 ppm, **c'**, and has blue phasing indicating it is a methylene carbon atom environment, therefore corresponds to the terminus alkene carbon atom of the allyl moiety. **e** couples to a ^{13}C NMR resonance at 137.7 ppm, **g'**, and is observed as a red phase, indicating it corresponds to a methine or methyl moiety, therefore **g'** corresponds to the methine carbon atom of the non-terminus end of the alkene of the allyl moiety. **f** couples to a ^{13}C NMR resonance at 129.1 ppm, **e'**, and is observed as a red phase, therefore corresponds to the *meta* carbon atom with respect the hydroxyl moiety of the phenolic ring. To assign the quaternary carbon environments HMBC NMR spectroscopy was carried out and was fully analysed.

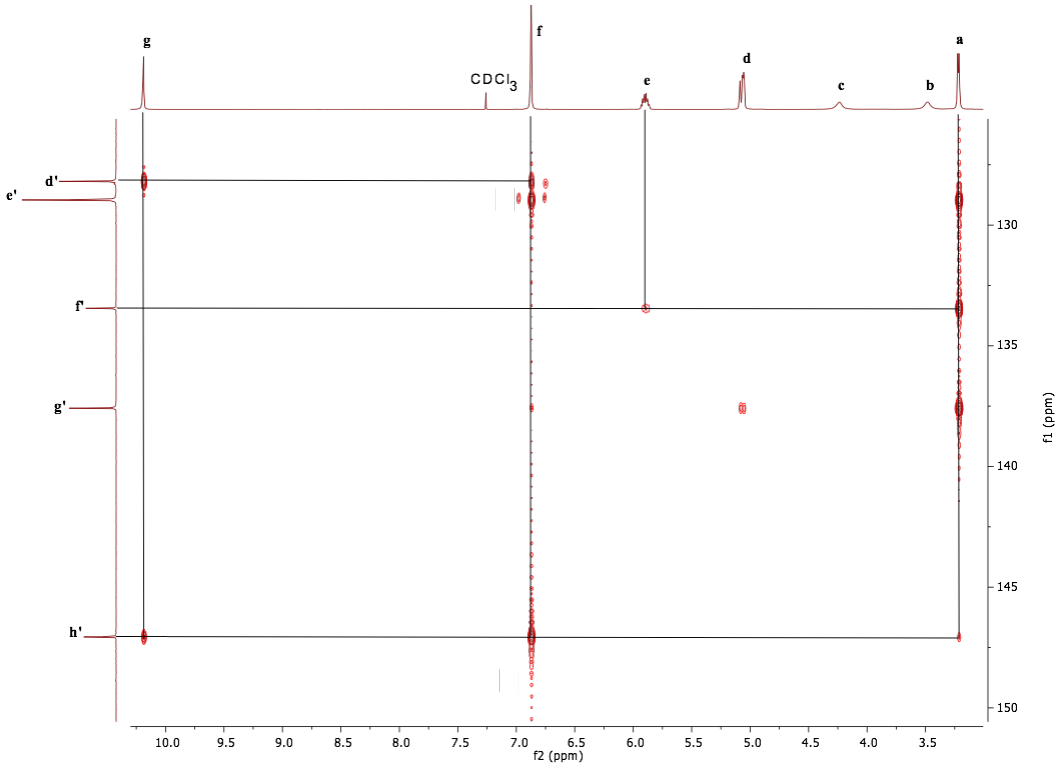

Figure 4.18. HMBC NMR spectrum of **12** in $CDCl_3$.

The HMBC NMR spectrum (Fig. 4.18) shows that there is a coupling between the hydroxyl proton, H_g, and a ^{13}C NMR resonance at 128.3 ppm and 147.2 ppm, **d'** and **h'** respectively. The ^{13}C NMR resonance **d'** exhibits coupling to **f**, H_f, whereas **h'** exhibits coupling to **f** and **a**, corresponding to H_f and H_a respectively, therefore **d'** must correspond to the *ipso* carbon atom of the phenolic ring with respect to the hydroxyl moiety and **h'** must therefore correspond to the *ortho* carbon atom of the phenolic ring with respect to the hydroxyl moiety. A ^{13}C NMR resonance at 133.6 ppm, **f'**, exhibits a coupling to ^{1}H NMR resonances **a** and **d**, corresponding to H_a and H_d, respectively, therefore corresponds to the *para* carbon atoms of the phenolic ring with respect to the hydroxyl moiety. The complete assignment of the ^{13}C NMR spectrum and structure are shown in Figure 4.19.

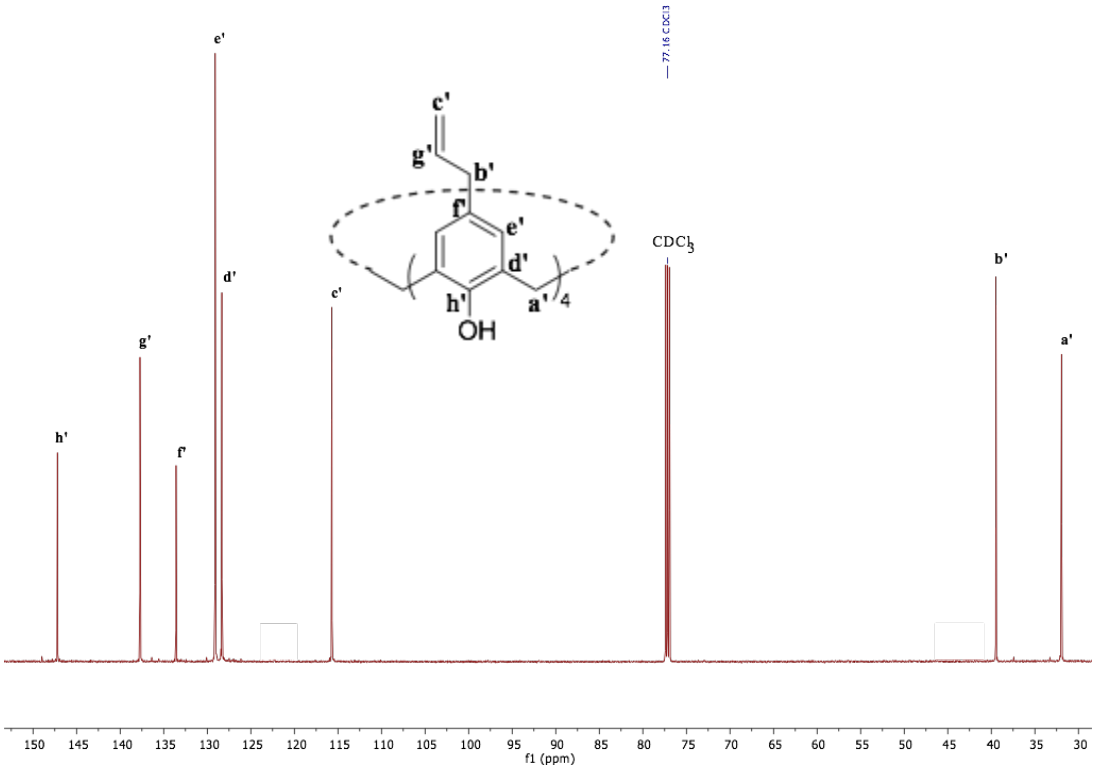

Figure 4.19. ^{13}C NMR spectrum of **12** in $CDCl_3$.

ASAP mass spectrometry was carried out and the molecular ion was seen at 585.296 Da (100%) (Fig. 4.20), which is consistent with the empirical formula $C_{40}H_{41}O_4^+$.

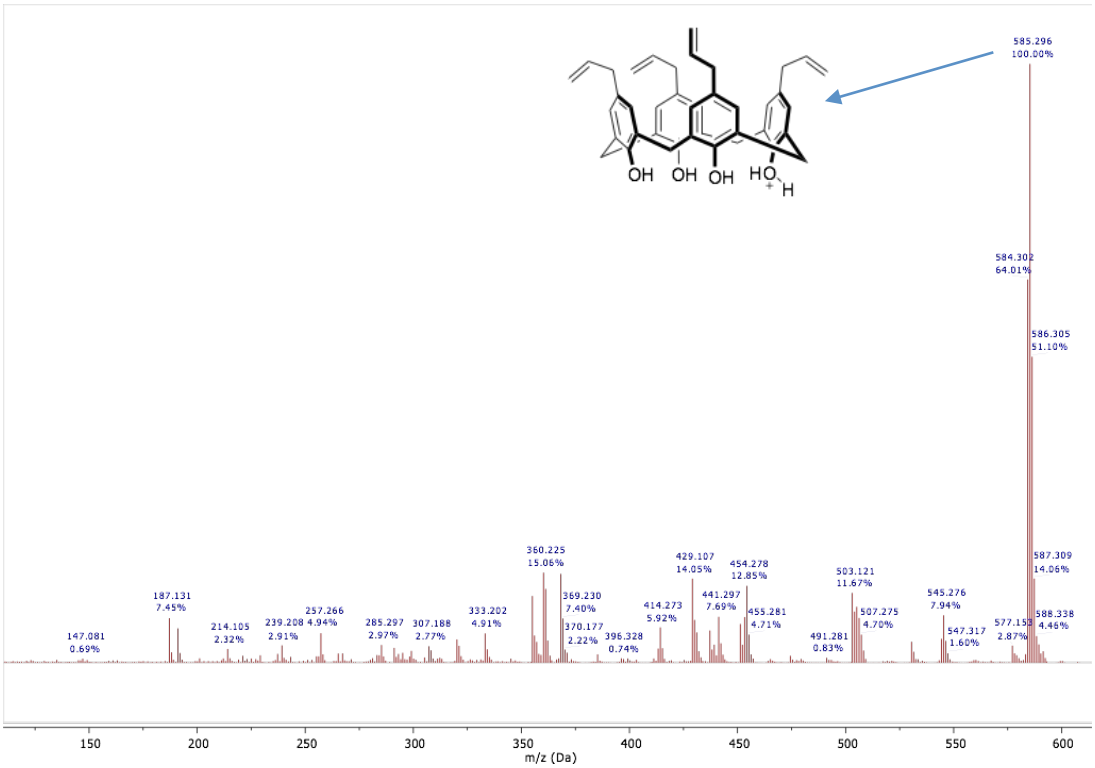

Figure 4.20. ASAP MS spectrum of **12**.

4.2.3. *5,11,17,23- tetrakis*(prop-2-en-1-yl)-25,26,27,28-*tetrakis*(methyl acetateoxy)-calix[4]arene, 13

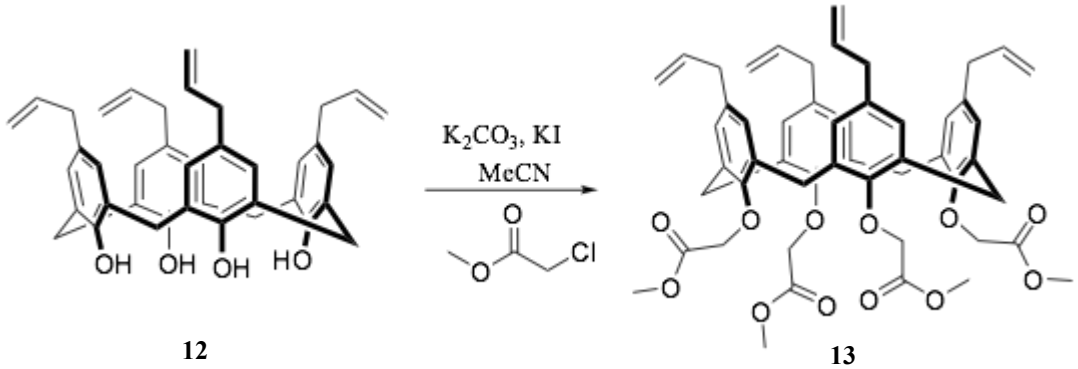

12 **13**

Scheme 4.6. Synthesis of **13**.

The novel compound **13**, was successfully synthesised using an excess of potassium carbonate in acetonitrile with a catalytic amount of potassium iodide (Scheme 4.6). The addition of potassium iodide leads to an exchange equilibrium between the halogen ions of Cl^- and I^-, known as the Finkelstein reaction (Scheme 4.7).[6] Iodide is a much better nucleofuge than that of chloride, therefore will lead to an increase in yield.

Scheme 4.7. Finkelstein reaction.

13 was obtained in a yield of 60%. An attempt at increasing the yield using the stronger base NaH in DMF/THF was attempted, but an increase in yield was not observed. A full characterisation is described below.

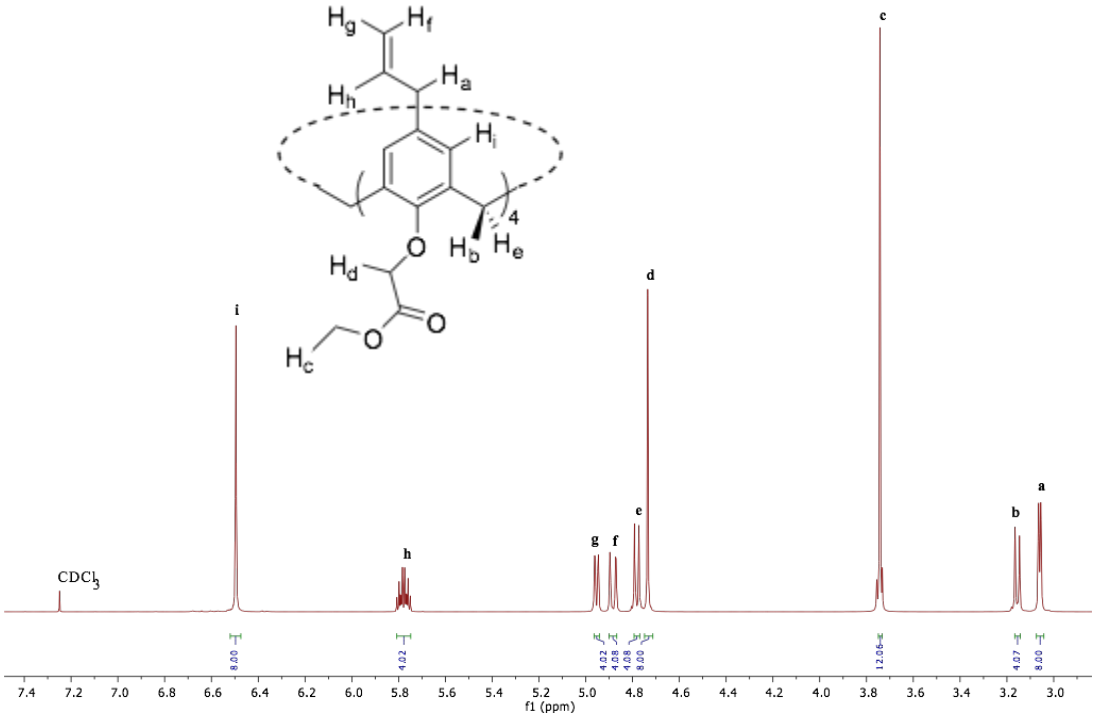

Figure 4.21. ^{1}H NMR spectrum of **13** in $CDCl_3$.

The ^{1}H NMR spectrum (Fig. 4.21) indicated that the **13** was synthesised. A doublet resonance with its integral set to eight is observed at 3.07 ppm, **a**, corresponding to the aliphatic protons of the allyl moiety, H_a. The COSY NMR spectrum (Fig. 4.22) showed that **a** exhibited coupling to resonances **f**, **g** and **h**. The ^{1}H NMR spectrum (Fig. 4.21) showed a multiplet resonance with an integral of four at 5.79 ppm, **h**, which corresponds to the non-terminus alkene proton of the allyl moiety, H_h. A doublet of quartets with an integral of four at 4.89 ppm, **f**, with J_1 and a J_2 coupling constants of 17.0 Hz and 1.6 Hz, respectively, is observed. A second set of doublet quartets with an integral of four are observed at 4.96 ppm, **g**, which has J_1 and J_2 coupling constants of 10 Hz and 1.6 Hz, respectively. Both resonances **f** and **g** correspond to the terminus protons of the alkene of the allyl moiety, with **f** corresponding to the hydrogen atom in the *trans* position with respect to H_n, $H_{f,}$, and **g** corresponds to the hydrogen atom in the *cis* position, H_g. The doublet of quartets multiplicity of **f** and **g** are brought about by the coupling to H_h that leads to the doublet splitting and the J_1 value and the second coupling to one another, which leads to the smaller coupling constant of J_2.

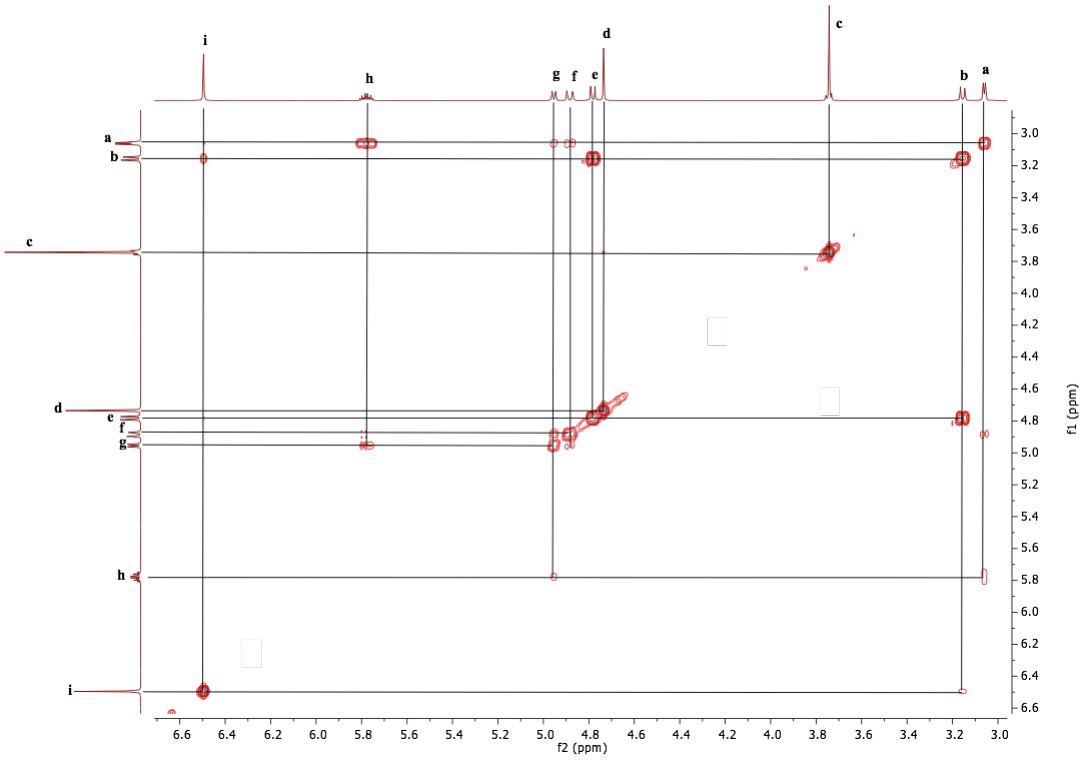

Figure 4.22. COSY NMR spectrum of **13** in $CDCl_3$.

The ^{1}H NMR spectrum (Fig. 4.21) shows a doublet resonance with an integral of four at 3.17 ppm, **b**, which has a J_1 coupling of 13.3 Hz and shows a coupling in the COSY NMR spectrum (Fig. 4.22) to a doublet resonance at 4.79 ppm, **e**. **e** has an integral of four and a J_1 coupling constant of 13.3 Hz. Both resonances **b** and **e** correspond to the methylene protons that bridge the aromatics, thus indicating that the compound exists in the cone conformation.[4] **b** is less deshileded relative to **e**, therefore corresponds to the proton pointing up to the aromatic region, H_b, and **e** corresponds to the proton pointing down to the oxo environment, H_e. The ^{1}H NMR spectrum (Fig. 4.21) shows a singlet resonance with an integral of 12 at 3.75 ppm, **c**, which corresponds to the methyl protons of the ester moiety, H_c. A second singlet resonance with an integral of eight is observed at 4.75 ppm, **d**. The resonance corresponds to the methylene protons of the oxo ethyl ester moiety, H_d. A third singlet resonance with an integral of eight is observed at 6.51 ppm, **i**, which corresponds to the aromatic protons in the *meta* position with respect to the oxygen of the aryl ether linkage, H_i. To assign the ^{13}C NMR spectrum, HSQC NMR and HMBC NMR spectroscopy were carried out. Using HSQC NMR spectroscopy the carbon atoms directly attached to hydrogen atoms could be easily assigned.

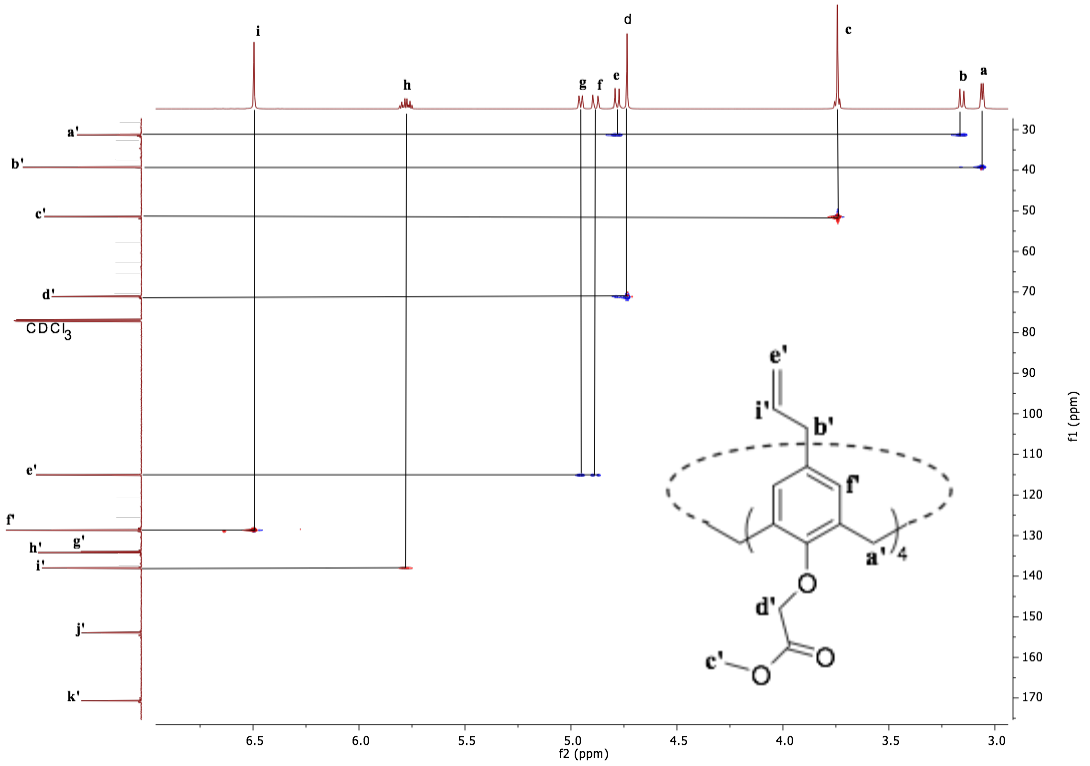

Figure 4.23. HSQC NMR spectrum of **13** in $CDCl_3$.

The HSQC NMR spectrum (Fig. 4.23) shows that **a** couples to a ^{13}C NMR resonance at 39.3 ppm, **b'**, which corresponds to the ether linking methylene carbon atom of the allyl moiety. Both **b** and **e** couple to a ^{13}C NMR resonance at 31.3 ppm, **a'**, which corresponds to the bridging methylene carbon atoms between aromatics. The fact that the bridging methylene carbon atoms resonance resides in the 31 ppm region is further indication that the calixarene exists in a cone conformation.[5] **c** couples to a ^{13}C NMR resonance at 51.4 ppm, **c',** which corresponds to the methyl carbon atom of the ester moiety. **d** couples to a ^{13}C NMR resonance at 71.1 ppm, **d'**, which corresponds to the methylene carbon atom of the oxo ethyl ester moiety. Resonances **f** and **g** both couple to a ^{13}C NMR resonance at 115.0 ppm, **e'**, which corresponds to the terminus carbon atom of the allyl moiety. **h** couples to a ^{13}C NMR resonance at 39.3 ppm, **b'**, which corresponds to the methylene carbon atom of the allyl moiety. **i** couples to a ^{13}C NMR resonance at 128.7 ppm, **f'**, which corresponds to the *meta* carbon atom of the aryl ether with respect to the oxygen of the ether linkage. To assign the ^{13}C NMR resonances corresponding to quaternary carbon atoms HMBC NMR spectroscopy was carried out and fully analysed.

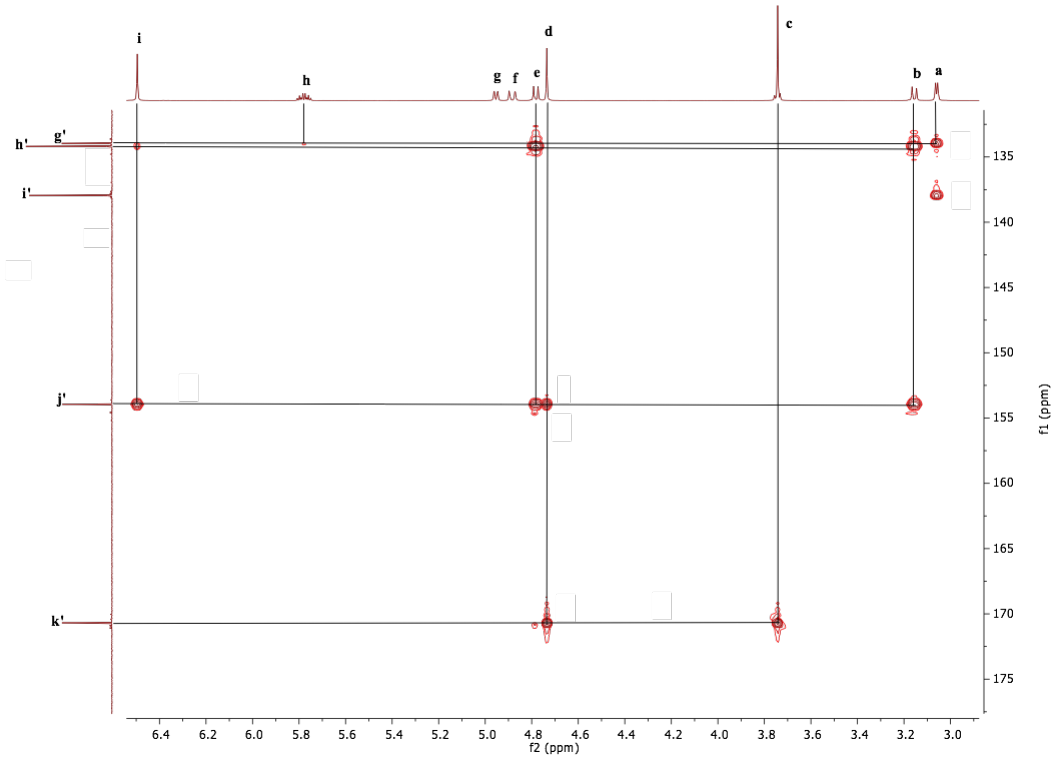

Figure 4.24. HMBC NMR spectrum of **13** in $CDCl_3$.

The HMBC NMR spectrum (Fig. 4.24) shows a ^{13}C NMR resonance at 170.7 ppm, **k'**, which exhibits a coupling to **c** and **d**, H_c and H_d respectively (Fig. 4.24), therefore corresponds to the carbonyl carbon atom of the ester moiety. The HMBC NMR spectrum (Fig. 4.24) shows that a ^{13}C NMR resonance at 134.0 ppm, **g'**, exhibits coupling to resonances **a**, **b**, **e** and **h**, H_e, H_b, H_e, and H_h respectively (Fig. 4.21), therefore as this is the only carbon resonances exhibiting a coupling to **h** it must correspond to the *para* carbon atom of the aromatic system with respect to the oxygen of the ether of the aryl ether. The HMBC NMR spectrum (Fig. 4.24) shows a ^{13}C NMR resonance at 154.0 ppm, **j'**, which exhibits coupling to the methylene protons corresponding to **a** and **e**, the aromatic protons corresponding to **f** and also the methylene protons of the ether ester, H_d (Fig. 4.21), therefore must correspond to the *ipso* carbon atom of the aromatic system with respect to the oxygen of the ether of the aryl ether. The HMBC NMR spectrum (Fig. 4.24) shows a ^{13}C NMR resonance at 134.2 ppm, **h'**, which exhibits a coupling to the methylene protons corresponding to **a** and **e**, and the aromatic protons corresponding to **f**, therefore must correspond to the *ortho* carbon atoms of the aromatic system with respect to the oxygen of the ether of the aryl ether. The complete characterisation of the ^{13}C NMR spectrum and structure are shown in Figure 4.25.

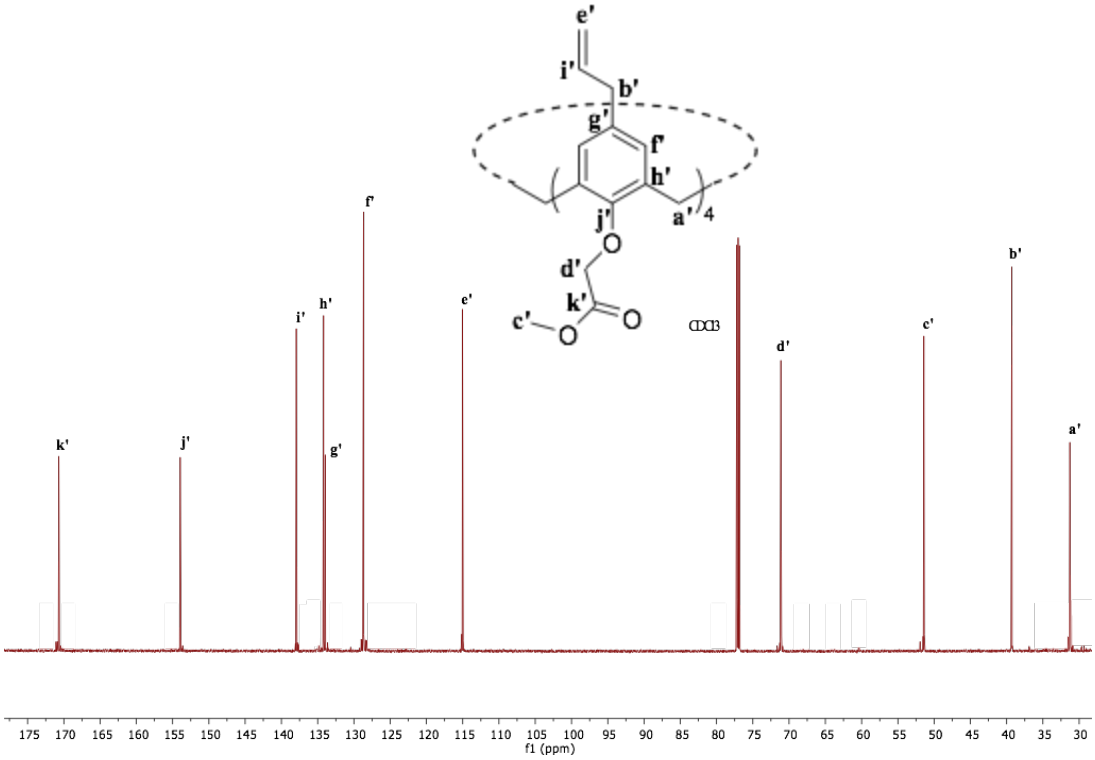

Figure 4.25. ^{13}C NMR spectrum of **13** in $CDCl_3$.

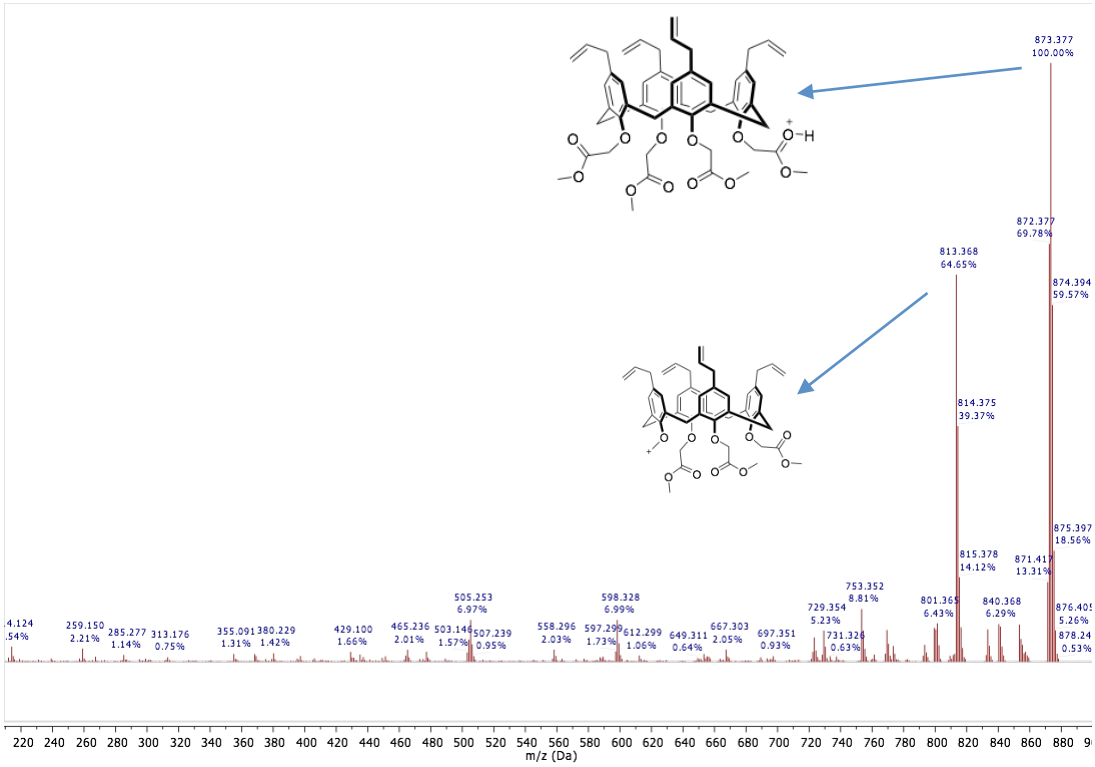

Figure 4.26. ASAP MS spectrum of **13**.

ASAP mass spectrometry was carried out and the molecular ion was seen at 873.377 Da (100%) (Fig. 4.26), which is consistent with the empirical formula $C_{52}H_{57}O_{12}^{+}$. A secondary fragment was observed at 813.368 Da (64.65%) (Fig. 4.2.3.6), which is consistent with the formula $C_{50}H_{53}O_{10}^{+}$. Further confirmation that **4** had been synthesised was through FT-IR spectroscopy, where there was the loss of the OH absorption band at 3154 cm^{-1} and the presence of a strong carbonyl absorption band at 1758 cm^{-1} were observed. Additionally, CHN analysis was carried out with the results closely matching the predicted values; CHN expected = %C = 71.54, %H = 6.47, %N 0.00; measured %C = 71.56, %H = 6.48, %N 0.00.

4.2.4. 5,11,17,23-*tetrakis*(prop-2-en-1-yl)-25,26,27,28-*tetrakis*(ethanoloxy)calix[4]arene, 14

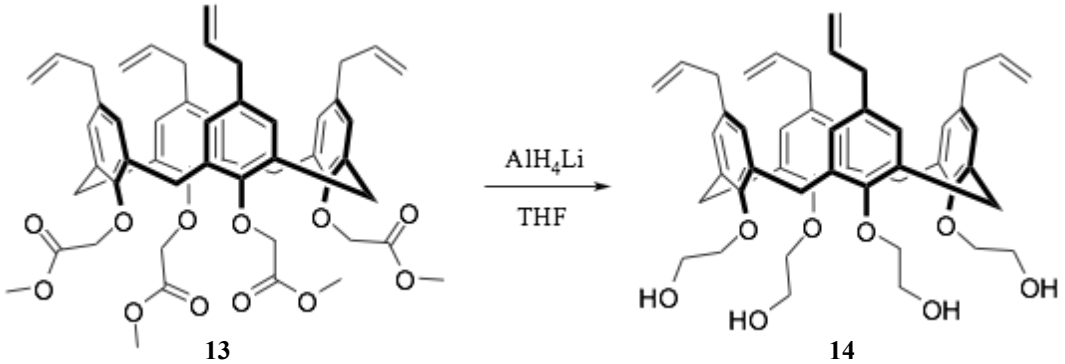

13 **14**

Scheme 4.8. Synthesis of **14**.

The novel compound **14**, was successfully synthesised, *via* the reduction of the ester moieties of **13** (Scheme 4.8). Compound **13**, was added to a suspension of excess $LiAlH_4$ in THF, leading to the complete reduction of ester functionality in a 92% yield. A full characterisation of **14** is described below. The ^{1}H NMR (Fig. 4.28) spectrum and ^{13}C NMR (Fig. 4.31) spectrum both exhibit broad resonances, which suggests on the NMR timescale the aromatics are rotating with respect to each other. The aromatics rotations are confined to the limits of the cone conformation as depicted in Figure 4.27. There is a rotational energy barrier that cannot be overcome to rotate the aromatics 180^{o} on the NMR timescale. The rotational freedom of the calixarene, on the NMR timescale, affects the resonance resolution as well as the coupling spin systems; leading to poor clarity of spectra within the 2D NMR

experiments, which therefore lead to difficulty when fully assigning the ^{13}C NMR spectra, thus is further discussed below.

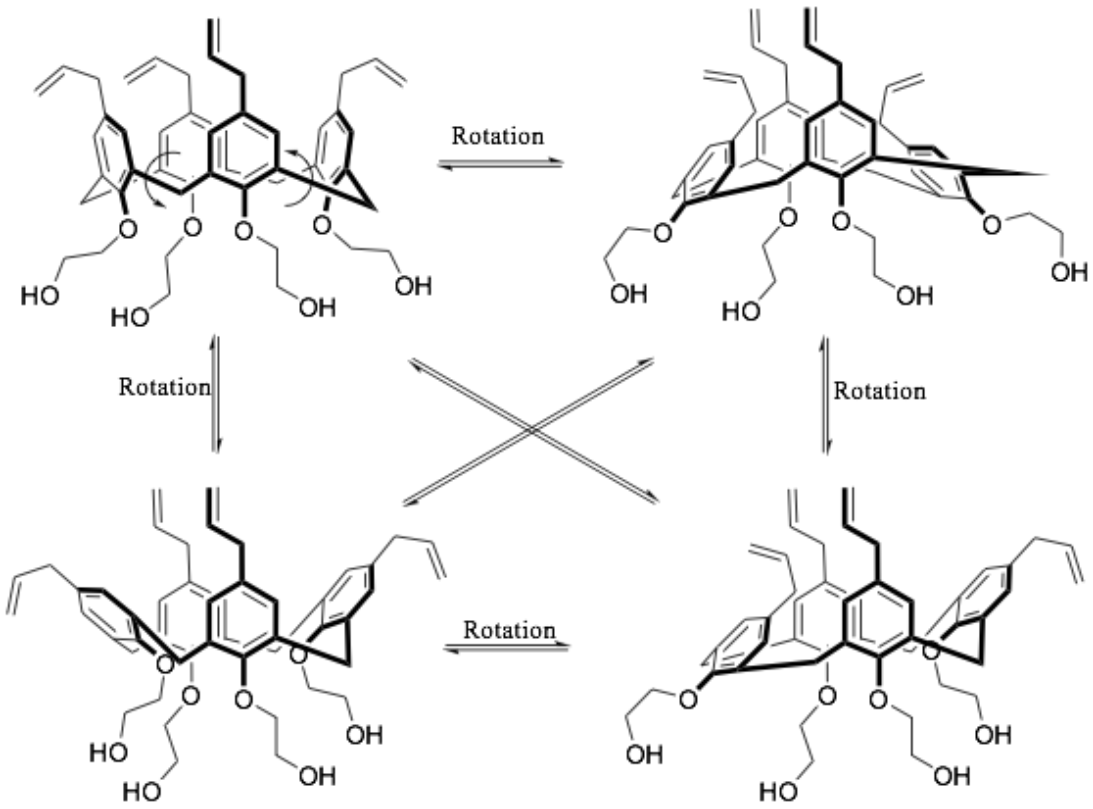

Figure 4.27. Conformational isomerisation of **14**, confined to the limits of the cone conformation.

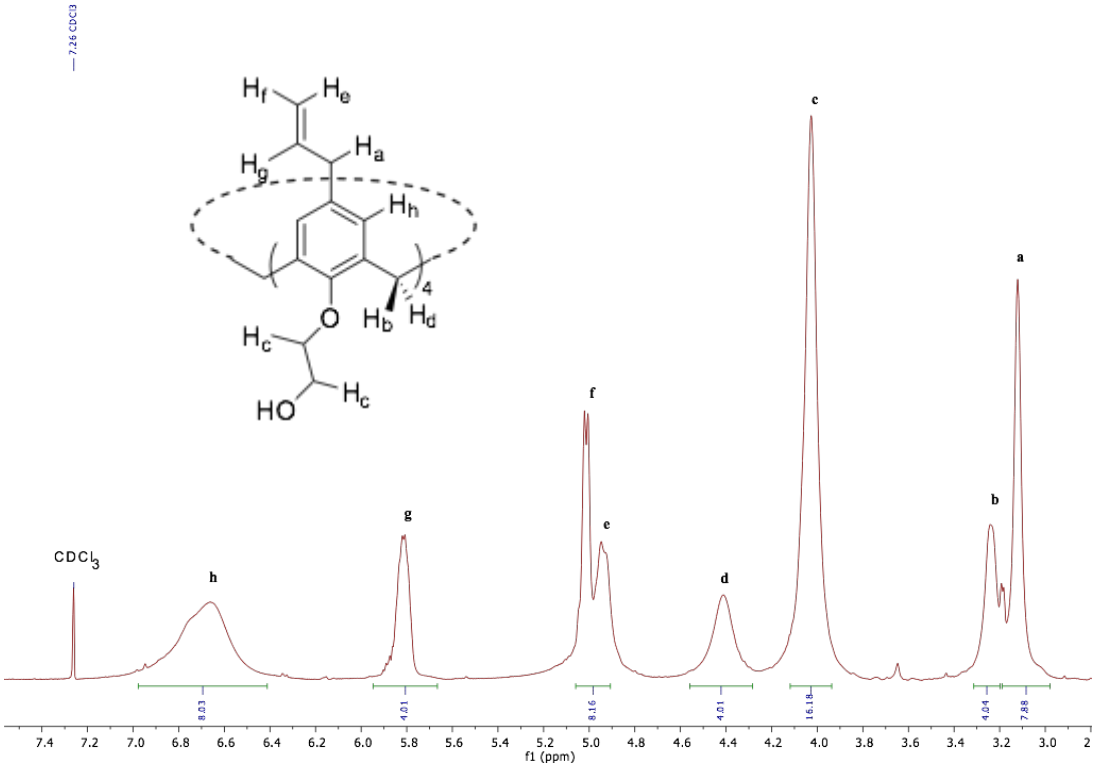

Figure 4.28. ^{1}H NMR spectrum of **14** in $CDCl_3$.

The ^{1}H NMR spectrum (Fig. 4.28) shows a broad singlet resonance at 3.12 ppm, **a**. The COSY NMR spectrum (Fig. 4.29) shows **a** exhibiting coupling to a resonances at 4.93, 5.01 and 5.81 ppm, **e**, **f** and **g**, respectively, therefore **a**, **e**, **f** and **g** correspond to the protons of the allyl moiety. **a** corresponds to the aliphatic protons of the allyl moiety, H_a (Fig. 4.28). **g** corresponds to the non-terminus alkene proton of the allyl moiety, H_g. **e** and **f** correspond to the terminus alkene protons of the allyl moiety, with **e** corresponding to the terminus proton in the *trans* position with respect to H_g, H_e; and **f** corresponds to the terminus proton in the *cis* position with respect to H_g, H_f.

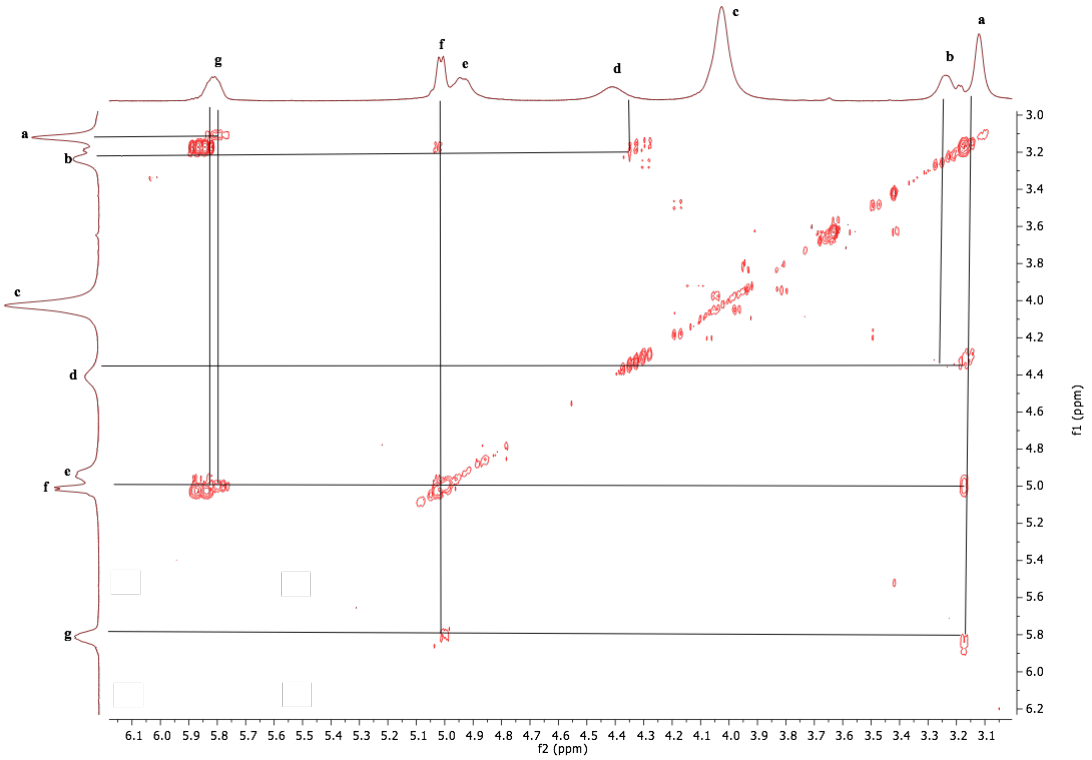

Figure 4.29. COSY NMR spectrum of **14** in $CDCl_3$.

The ^1H NMR spectrum (Fig. 4.28) shows two broad resonances with integrals of four each at 3.23 ppm and 4.41 ppm corresponding to **b** and **d**, respectively, which exhibit coupling in the COSY NMR spectrum (Fig. 4.29). **b** and **d** correspond to the bridging methylene protons between the aromatics, with **b** corresponding to the proton pointing up to the allyl moiety, H_b and **d** corresponding to the proton pointing down to the oxy environment, H_d (Fig. 4.28). The presence of two environments for the bridging methylene protons indicates that the calixarene exists in the cone conformation on the NMR timescale.[4] The ^1H NMR spectrum (Fig. 4.28) shows a broad singlet resonance with an integral of 16 at 4.03 ppm, **c**. **c** exhibits no coupling in the COSY NMR (Fig. 4.29), therefore, corresponds to the ethylene protons of the newly reduced esters, H_c. The ^1H NMR spectrum (Fig. 4.28) shows a broad resonance with an integral of eight at 6.68 ppm, **h**, which corresponds to the protons attached to the aromatic ring in the *meta* position with respect to the oxygen of the aryl ether, H_h. Using HSQC NMR spectroscopy the carbon atoms directly attached to hydrogen atoms could be easily assigned.

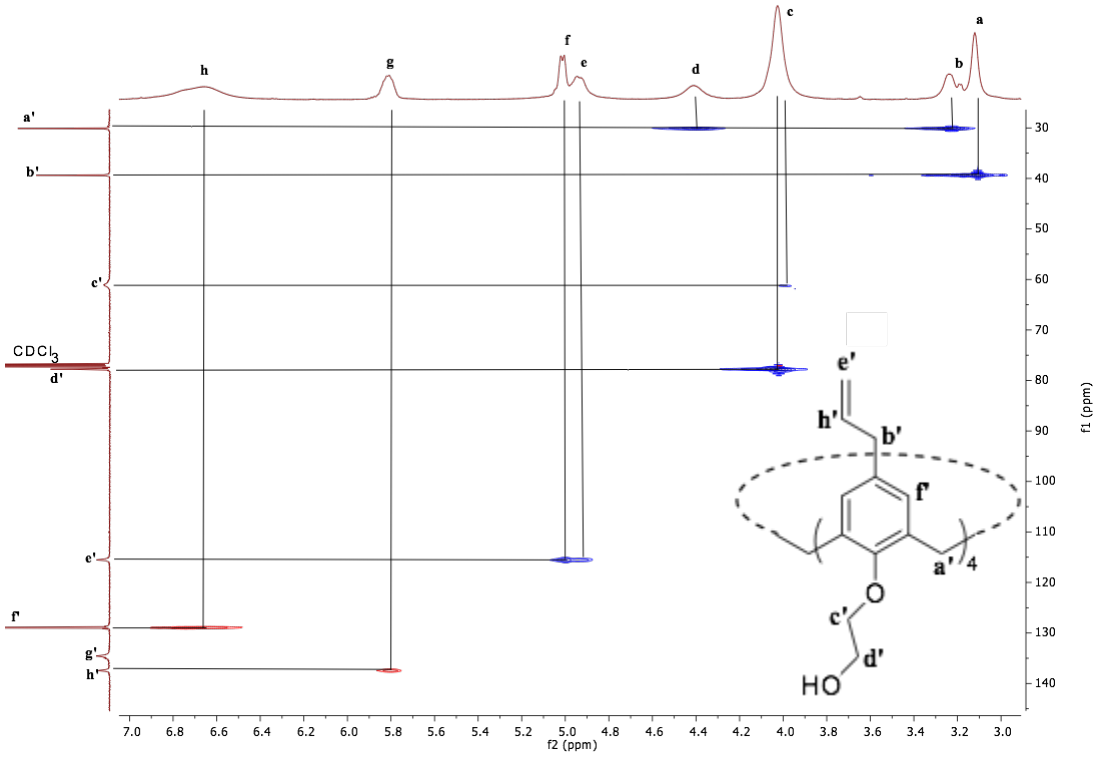

Figure 4.30. HSQC NMR spectrum of **14** in $CDCl_3$.

The HSQC NMR spectrum (Fig. 4.30) shows **a** coupling to a ^{13}C NMR resonance at 39.5 ppm, **b'**, which corresponds to the aliphatic carbon atom of the allyl moiety. **b** and **d** both couple to a ^{13}C NMR resonance at 30.2 ppm, **a'**, corresponding to the bridging methylene carbon atoms between aromatics. The fact that the bridging methylene carbon atom resonance resides in the ~31 ppm region is further indication that the calixarene exists in a cone conformation.[5] **c** couples to two ^{13}C NMR resonances, one at 61.2 ppm, **c'**, and a second at 77.9 ppm, **d'**. **c'** corresponds to the ether linking carbon atom of the ethylene carbon attached to the lower rim and **d'** corresponds to the ethylene carbon atom next to the hydroxyl moiety. Resonances **e** and **f** both couple to a ^{13}C NMR resonance at 115.6 ppm, **e'**, which corresponds to the terminus carbon atom of the allyl moiety. **g** exhibits coupling to a ^{13}C NMR resonance at 137.5 ppm, **h'**, which corresponds to the non-terminus alkene carbon atom of the allyl moiety. **h** couples to a ^{13}C NMR resonance at 129.0 ppm, **f'**, which corresponds to the *meta* carbon atom of the aromatic ring with respect to the oxygen of the aryl ether. The complete assignment of the ^{13}C NMR spectrum is shown below in Figure 4.31.

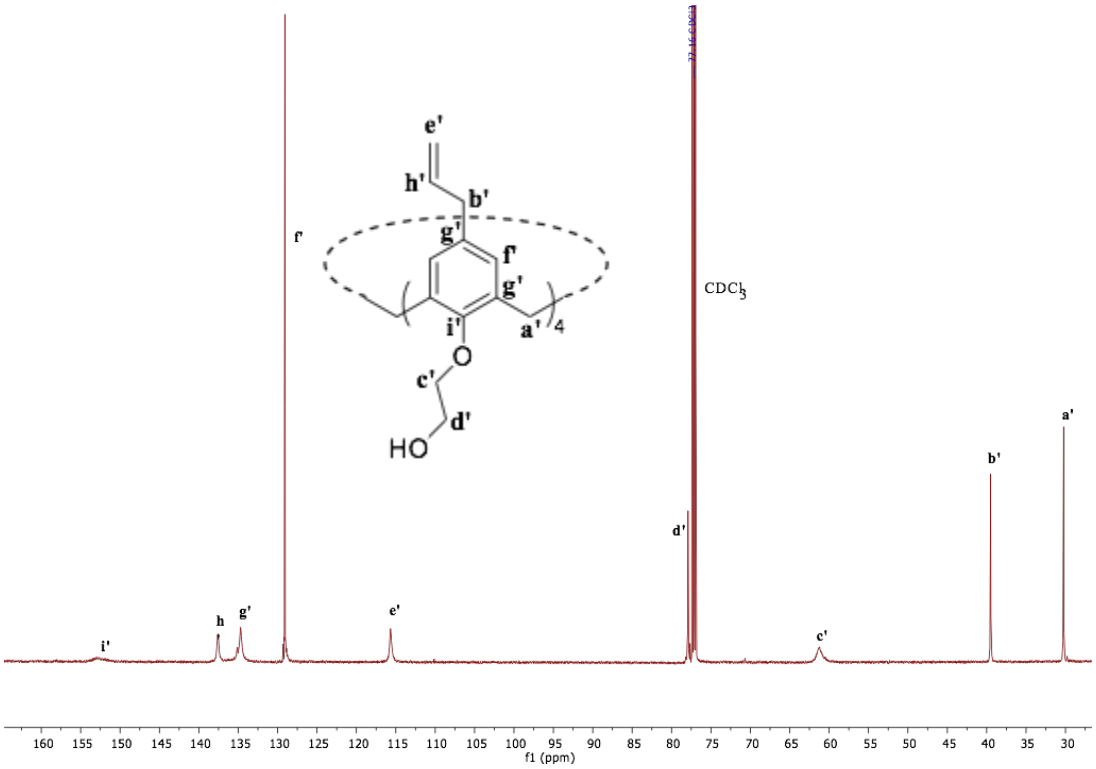

Figure 4.31. ^{13}C NMR spectrum of **14** in $CDCl_3$.

To complete the assignment of the ^{13}C NMR spectrum for **14**, resonances at 134.7 ppm and 152.8 ppm, corresponding to **g'** and **i'**, respectively, required identification. As expressed earlier, due to the rotational freedom of **5** on the NMR timescale 2D experiments proved challenging and no HMBC NMR spectrum was achieved, therefore conjecture was required to assign **g'** and **i'**. By comparing the chemical shifts of **14** to the previous compounds studied (**11**, **12** and **13**), **g'** and **i'** can be assigned with reasonable confidence, with **g'** at 134.7 ppm, corresponding to the *ortho* and *para* carbon atoms of the aromatic rings with respect to the oxygen of the aryl ether and **i'** at 152.8 ppm, corresponding to the *ipso* carbon atom of the aromatic rings with respect to the oxygen of the aryl ether. ASAP mass spectrometry was carried out and the molecular ion was seen at 760.293 Da (100%) (Fig. 4.32), which is consistent with the empirical formula $C_{48}H_{56}O_8^+$. A secondary fragment was observed at 716.276 Da (98.91%), which is consistent with the empirical formula $C_{46}H_{52}O_8^+$ (Fig. 4.32).

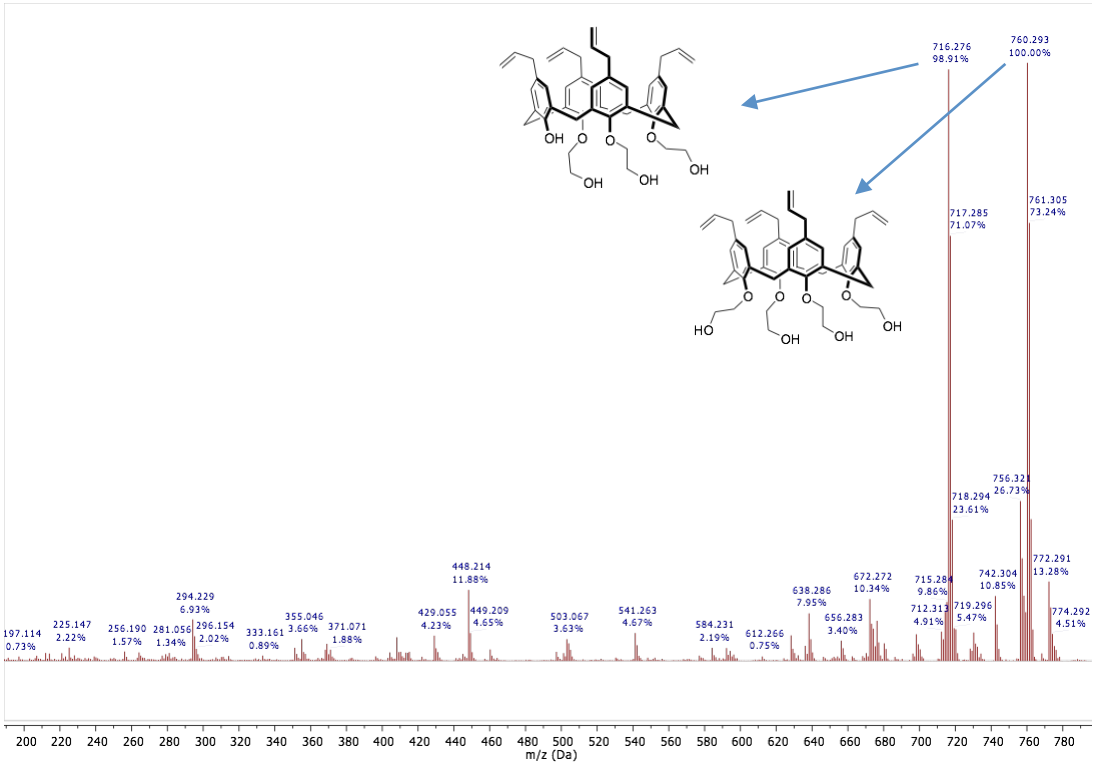

Figure 4.32. ASAP MS spectrum of **14**.

Further confirmation that **14** had been synthesised was through FT-IR spectroscopy, where there was the loss of the C=O absorption band at 1758 cm^{-1} and the presence of a OH absorption band at 3300 cm^{-1}. Additionally, CHN analysis was carried out with the results closely matching the predicted values; CHN expected = %C = 75.76, %H = 7.42, %N 0.00; measured %C = 76.03, %H = 7.56, %N 0.00.

A variable temperatue ^{1}H NMR spectroscopy experiment was carried out to assertain whether the calixarene, **14**, would become fixed into a single conformation, leading to a more resolved NMR spectrum. The results are shown in Figure 4.33.

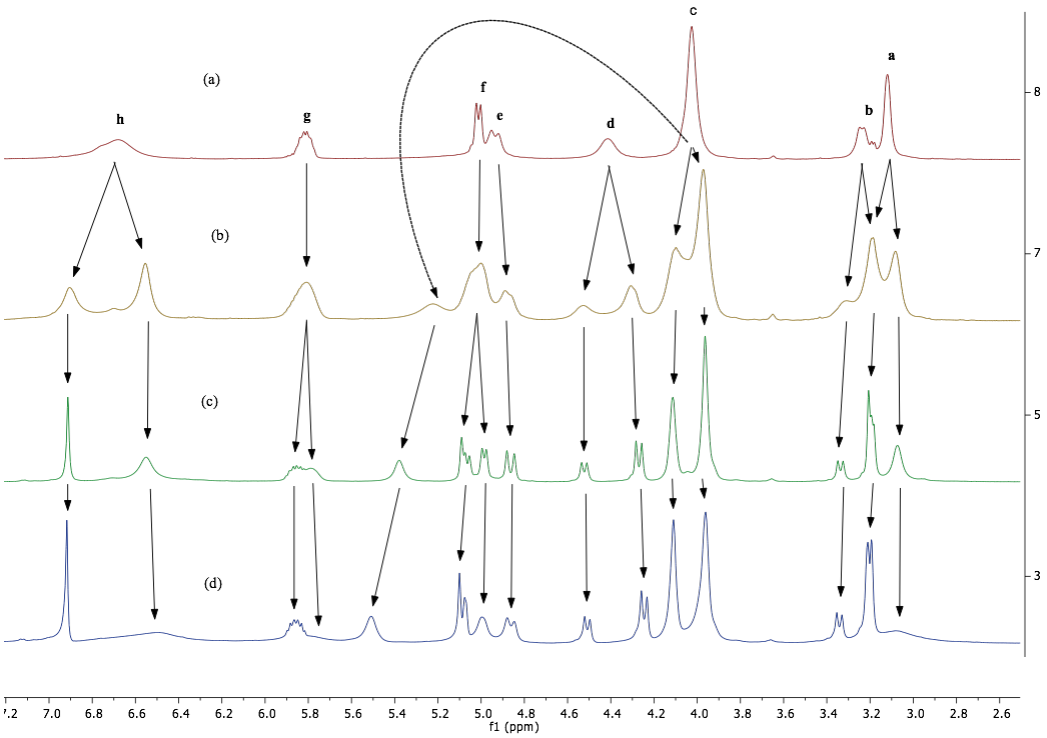

Figure 4.33. ^{1}H NMR variable temperature spectra of **14**, (a) 22 ^{o}C, (b) -1 ^{o}C, (c) -22 ^{o}C, (d) -44 ^{o}C, in $CDCl_3$.

The ^{1}H NMR spectra (Fig. 4.33) shows that from 22 ^{o}C to -1 ^{o}C two distinct conformational variations of the cone conformation become apparent, *via* resonances **d** and **h** (trace (a)) splitting into two (trace (b)). As the temperature is further lowered to -22 ^{o}C and -42 ^{o}C no further splitting is observed, but with one set of resonances becoming more resolved and the second set broadening, e.g. resonance **h** (trace (a) – (d)). This suggests that as the temperature is lowered one of the conformations with the sharp resonances resides in a potential well where there is not enough energy in the system to overcome rotation, whereas for the broad resonances there is enough energy in the system for rotational freedom. To identify the conformations and determine the energy of the conformations computational chemistry would be required, but for this body of work it was decided not to perform such a theoretical study. The rotational freedom observed for **14** on the NMR timescale but not for the previous compounds (**11**, **12**, and **13**) investigated is possibly due to the size and electronic nature of moiety attached to the lower rim. The precursor to **14**, **13**, exhibits no rotational conformation on the NMR timescale, and is possible due to the bulkiness of the ester moiety; inhibiting any rotation. The bulkiness of the ether ethanol lower rim moieties of **14** has been significantly reduced when compared to the precursor ester. Also, unlike **11**, where the bulkiness of the allyl moiety is

comparable to that of the ethanol moiety, hydroxyls are present that will lead to hydrogen bonding. There is likely to be an energy competition between the hydrogen bonding and rotating to a 1,3-alternate conformation.

4.2.5. 5,11,17,23- *tetrakis*(prop-2-en-1-yl)-25,26,27,28- *tetrakis*(ethoxyester-2-bromo-propanoate)calix[4]arene, 15

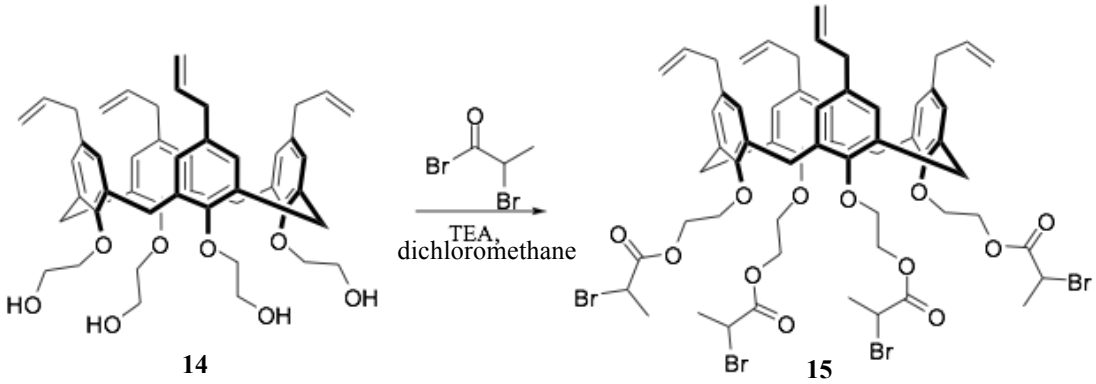

14 **15**

Scheme 4.9. Synthesis of **15**.

The novel compound **15** was successfully synthesised *via* performing an esterification of **14** with the acyl bromide, 2-bromopropionyl bromide, in the presence of TEA, used as a scavenger for the HBr side product (Scheme 4.9). A yield of 78% was achieved after column chromatography was carried out. Approximately one molecule of 2-bromopropionic acid was trapped within the calixarene, which could not be removed. Full analysis and characterisation is described below.

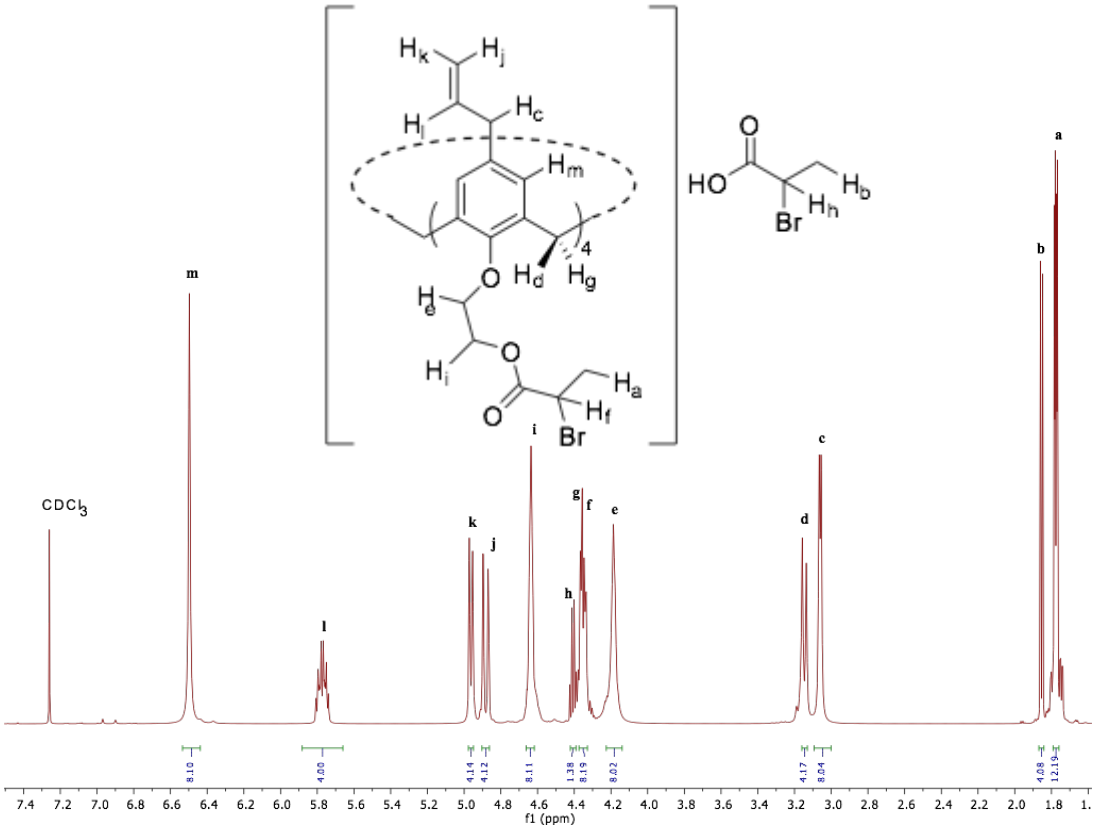

Figure 4.34. ^{1}H NMR spectrum of **15** in $CDCl_3$.

The ^{1}H NMR spectrum (Fig. 4.34) exhibits two overlapping sets of doublet resonances with an overall integral set to 12 at 1.78 ppm, **a**. **a** exhibits a COSY NMR (Fig. 4.36) coupling to a multiplet resonance at 4.35 ppm, **f/g**. The resonance of **a** (Fig. 4.34) corresponds to the methyl protons of the 2-bromopropanoate moiety, H_a, and **f** corresponds to the methine of the 2-bromopropanoate moiety, H_f. The appearance of an overlapping set of doublets with the overall integral of 12 and relatively equal intensities suggest that there are two possible environments for the methyl protons. Two environments could be resultant of steric interactions from the crowded lower rim of the calixarene, forcing the bulky ester moieties into two distinct conformations, resulting in the methyl protons of 1' and 1'' being non-equivalent (Fig. 4.35).

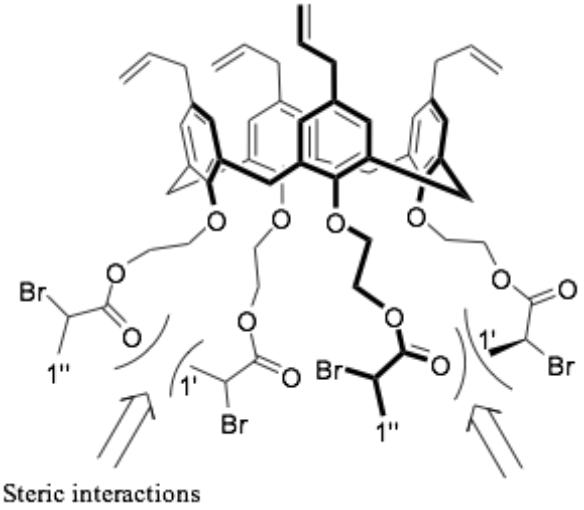

Figure 4.35. Possible steric interactions resulting in non-equivalent methyl protons, 1' and 1''.

The ^{1}H NMR spectrum (Fig. 4.34) shows a doublet resonance at 1.85 ppm, **b**, which has a *J* coupling constant of 8.0 Hz. The COSY NMR spectrum (Fig. 4.36) shows that **b** exhibits a coupling to a quartet resonance at 4.40 ppm, **h**, which also has a *J* coupling constant of 8 Hz. Resonances **b** and **h** exhibits no coupling to the calixarene core through HMBC NMR spectroscopy as discussed later, so corresponds to approximately one molecule of trapped 2-bromopropionic acid, with resonances **b** and **h** corresponding to H_b and H_h, respectively (Fig. 4.34). It has been well documented about calixarenes ability to act as host-guest complexes, trapping even large molecules such as chlorin e6.[7] The ^{1}H NMR spectrum (Fig. 4.34) shows a doublet resonance with an integral of eight at 3.06 ppm, **c**. The COSY NMR spectrum (Fig. 4.36) shows that **c** exhibits a coupling to a resonance at 4.88 ppm, 4.96 ppm and 5.77 ppm, corresponding to **j**, **k** and **l** respectively, with all corresponding to hydrogen atoms of the allyl moiety. **c** corresponds to the aliphatic methylene protons of the allyl moiety, H_c. Resonance **l** (Fig. 4.34) exists as a multiplet and has an integral of four, which corresponds to the non-terminus alkene proton of the allyl moiety, H_l. Resonances **j** and **k** (Fig. 4.34), which both have integrals of four and exist as a doublet of quartets, correspond to terminus protons of the alkene of the allyl moiety. Resonance **j** has a J_1 coupling constant of 19.9 Hz whereas **k** has a J_1 coupling constant of 11.9 Hz, therefore resonance **j** corresponds to the *trans* proton with respect to H_l, H_j and **k** corresponds to the *cis* proton, H_k.

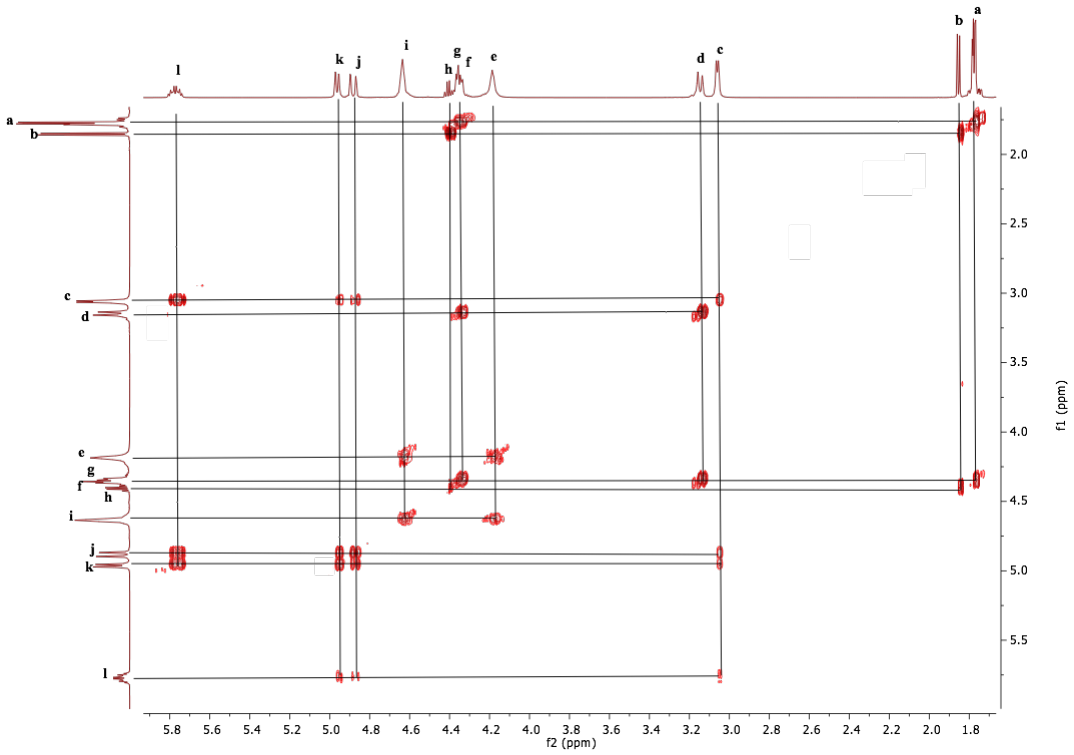

Figure 4.36. COSY NMR spectrum of **15** in $CDCl_3$.

The ^{1}H NMR spectrum (Fig. 4.34) shows a doublet resonance with an integral of four at 3.15 ppm, **d**. The COSY NMR spectrum (Fig. 4.36) shows that **d** exhibits coupling to the overlapped multiplet resonance **f/g**. **d** and **g** correspond to the methylene protons that bridge the aromatics, with **d** corresponding to the protons pointing up to the aromatic region, H_d, and **g** corresponding to the protons pointing down to the oxo environment, H_g. The splitting of the methylene protons indicated that the calixarene exists in a cone conformation.[4] The assignment of the multiplet resonance **f/g** is justified *via* a HMBC NMR experiment and is discussed later. The ^{1}H NMR spectrum (Fig. 4.34) shows a multiplet resonance at 4.19 ppm, **e**. **e** exhibits coupling to a resonance at 4.64 ppm, **i**, through COSY NMR spectroscopy (Fig. 4.36). Resonances **e** and **i** correspond to the ethylene protons of the ethyl ether 2-bromopropanoate moiety. To identify the exact position of the protons, i.e. next to the ester moiety or part of the ether linkage the HMBC spectrum must be referred to, which is discussed later. The ^{1}H NMR spectrum (Fig. 4.34) shows a singlet resonance at 6.50 ppm, **m**, which corresponds to the aromatic protons in the *meta* position with respect to the oxygen of the aryl ether, H_m. To assign the ^{13}C NMR spectrum, HSQC NMR and HMBC NMR spectroscopy were carried out. Using

HSQC NMR spectroscopy the carbon atoms directly attached to hydrogen atoms could be easily assigned.

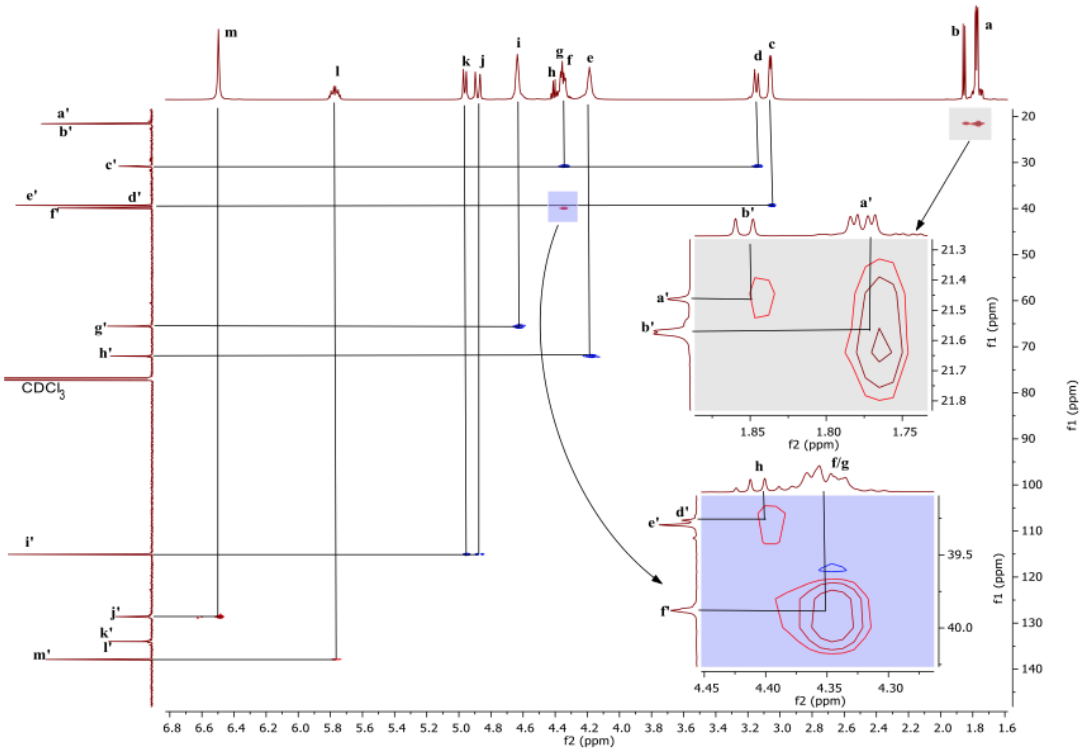

Figure 4.37. HSQC NMR spectrum of **15** in $CDCl_3$.

The HSQC spectrum (Fig 4.37) shows that **a** couples to a ^{13}C NMR resonance at 21.7 ppm, **b'**, which corresponds to the methyl carbon atom of the 2-bromopropanoate moiety. As observed in the ^{1}H NMR spectrum, with two overlapping doublets corresponding to H_a, there are two ^{13}C NMR resonances, **b'**, in very close proximity, explicitly shown in Figure 4.39. The two ^{13}C NMR resonances corresponding to **b'** are due to there being two methyl environments that are very similar but not identical as discussed previously, and is depicted in Figure 4.35. The HSQC NMR spectrum (Fig 4.37) shows that **b** couples to a ^{13}C NMR resonance at 21.6 ppm, **a'**, which corresponds to the methyl carbon atom of the trapped 2-bromopropionic acid. **c** couples to a ^{13}C NMR resonance at 39.5 ppm, **e'**, which corresponds to the methylene ether linkage of the allyl moiety. Both **d** and **f/g** couple to a ^{13}C NMR resonance at 31.0 ppm, **c'**, which corresponds to the methylene carbon atoms that bridge the aromatics. The fact that the bridging methylene carbon atom resonance resides in the 31 ppm region is further indication that the calixarene exists in a cone conformation.[5] The **f/g** resonance exhibits a coupling to two ^{13}C NMR

resonances, 31.0 ppm and 40.0 ppm, **c'** and **f'**, respectively, and as described above, **c'** corresponds to the bridging methylene carbon atom between the aromatic, therefore **f'** corresponds to the methine carbon of the attached 2-bromopropanoate moiety. Further differentiation of the **f** and **g** is ascertained from the difference in phasing of the coupled signals, with blue referring to a methylene carbon environment and red to a methyl or methine environment. **e** couples to a ^{13}C NMR resonance at 72.2 ppm, **h'**, which corresponds to one of the ethylene carbon atoms of the ethyl ether 2-bromopropanoate moiety, with the exact assignment requiring the HMBC NMR experiment, and is described later. **h** couples to a ^{13}C NMR resonance at 39.4 ppm, **d'**, which corresponds to the methine carbon atom of the trapped 2-bromopropanoate moiety. **i** couples to a ^{13}C NMR resonance at 65.7 ppm, **h'**, and corresponds to one of the ethylene carbon atoms of the ethyl ether 2-bromopropanoate moiety, with the exact assignment requiring the HMBC NMR experiment, and is described later. **j** and **k** both couple to a ^{13}C NMR resonance at 115.2 ppm, **i'**, which corresponds to the terminus alkene carbon atom of the allyl moiety. **l** exhibits coupling to a ^{13}C NMR resonance at 138.0 ppm, **m'**, which corresponds to the methylene ether linkage carbon atom of the allyl moiety. **m** couples to a ^{13}C NMR resonance at 128.8 ppm , **j'**, which corresponds to the *meta* carbon of the aryl ether moieties with respect to the ether oxygen. To assign the final ^{13}C NMR resonances that do not directly couple to a hydrogen atom HMBC NMR spectroscopy was carried out and is fully analysed.

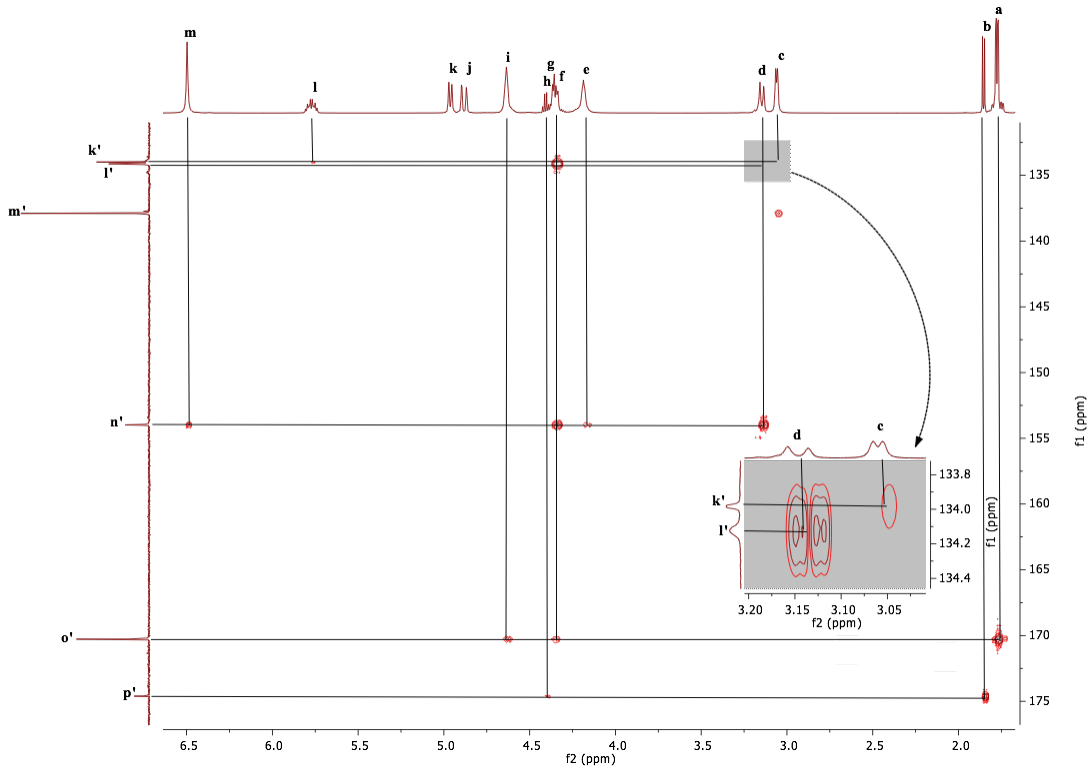

Figure 4.38. HMBC NMR spectrum of **15** in $CDCl_3$.

The HMBC NMR spectrum (Fig. 4.38) shows that there are two resonances at 170.4 and 174.8 ppm, **o'** and **p'**, respectively, which correspond to carbonyl carbon atoms. **o'** exhibits coupling to **a**, **e** and **i**, therefore corresponds to the carbonyl of the attached 2-bromopropanoate moiety. **p'** only exhibits coupling to **b**, therefore corresponds to the carbonyl carbon atom of the trapped 2-bromopropionic acid. The HMBC NMR spectrum (Fig. 4.38) shows that **k'** exhibits coupling to **c** and **l** of the allyl moiety, therefore must correspond to the *para* carbon atom of the aryl ether unit with respect to the ether oxygen. **l'** exhibits coupling to the protons of the bridging methylene unit, H_e and H_g, therefore corresponds to the *ortho* carbon atom of the aryl ether unit with respect to the ether oxygen. **n'** exhibits coupling to **e** and **g**, which correspond to H_e and H_g, respectively. **e** corresponds to one of the pairs of ethylene protons of ethylene ether 2-bromopropanoate moiety, and **m**, corresponds to the aromatic protons, H_m, therefore **n'** corresponds to the *ipso* carbon atom of the aryl ether unit with respect to the ether oxygen. The fact that **n'** couples to **e** and not **i**, indicates that **e** corresponds to the ether linkage protons of the ethylene ether 2-bromopropanoate moiety, H_e (Fig. 4.34) and in turn **h'** corresponds to the carbon atom of this ethylene unit (Fig. 4.39). **i** must therefore correspond to the protons of the ethylene unit closest to the ester unit of the ethylene ether 2-bromopropanoate

moiety, H_i (Fig. 4.34) and in turn **g'** corresponds to the carbon atom of this ethylene unit (Fig. 4.39). The complete assignment of the ^{13}C NMR spectrum is shown below in Figure 4.39.

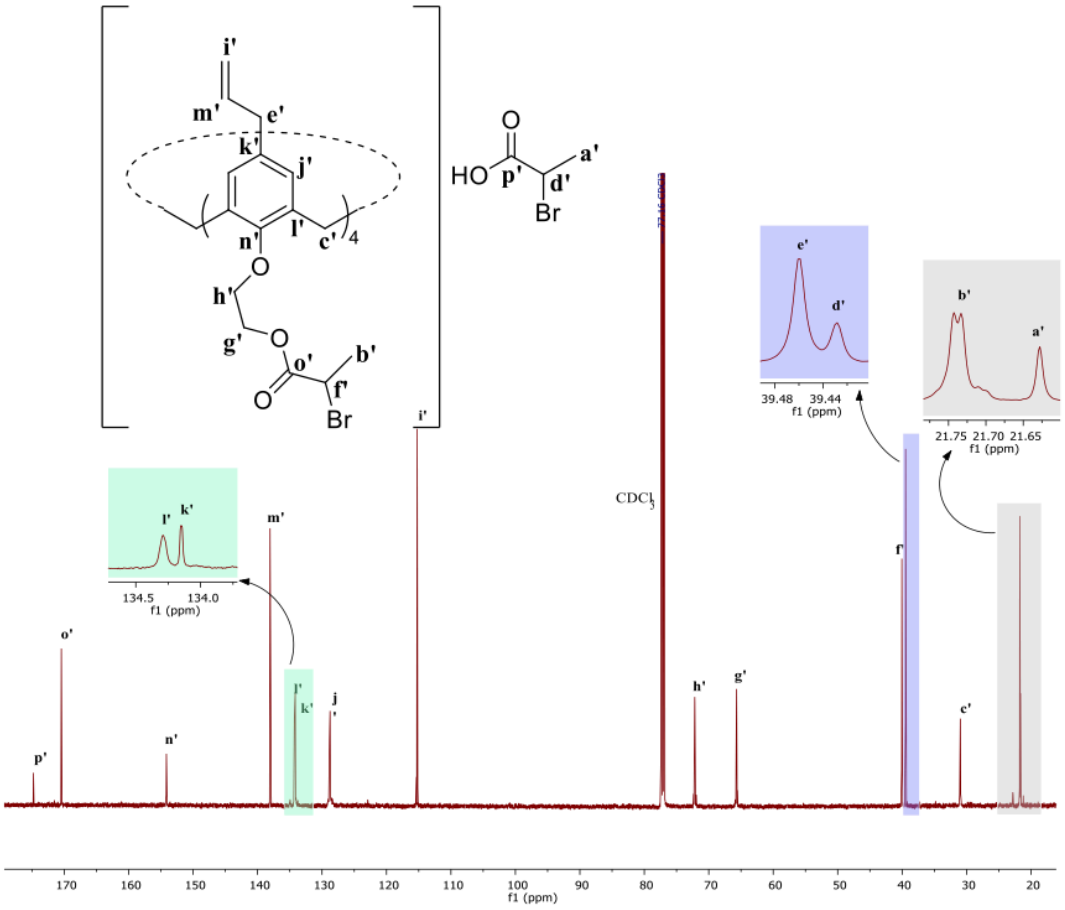

Figure 4.39. ^{13}C NMR spectrum of **15** in $CDCl_3$.

ASAP mass spectrometry was carried out and the molecular ion was seen at 1301.153 Da (31.96%) (Fig. 4.40), which is consistent with the empirical formula $C_{60}H_{69}O_{12}^{+}$. A secondary fragment was observed at 1122.184 Da (58.72%), which is consistent with the empirical formula $C_{55}H_{61}Br_3O_{10}^{+}$ (Fig. 4.40). The secondary fragment corresponded to **15** but with loss of one ethyl 2-bromopropanoate moiety; the ethyl 2-bromoproanoate ion is observed at 180.973 Da (100%).

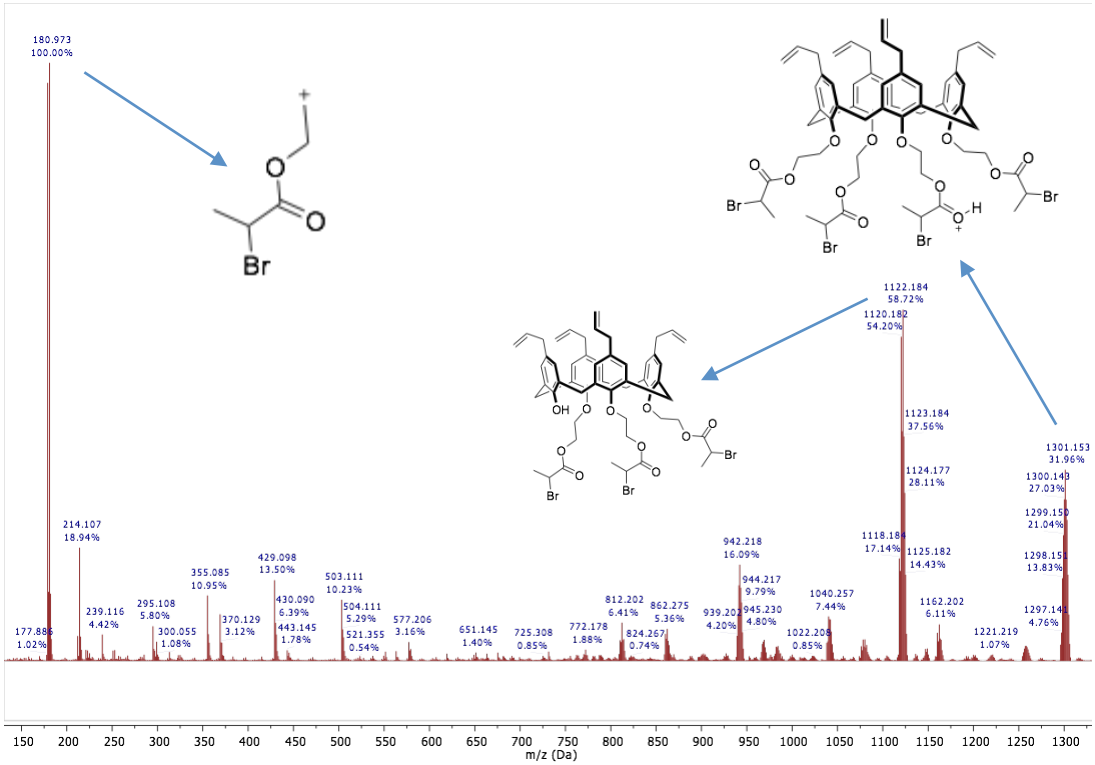

Figure 4.40. ASAP MS spectrum of **15**.

Further confirmation that **15** was synthesised was through FT-IR spectroscopy, where the was the loss of the OH absorption band at 3300 cm^{-1} and the presence of a strong carbonyl absorption band at 1739 cm^{-1} were observed. The trapped 2-bromopropanoic acid exhibited a small OH stretch at 3200 cm^{-1}. Additionally, CHN analysis was carried out with the results closely matching the predicted values; CHN expected = %C = 52.05, %H = 5.06, %N 0.00; measured %C = 52.61, %H = 5.37, %N 0.00.

4.2.6 5,11,17,23-*tetrakis*(3-(hydroxyethyl)thioether-propanyl)-25,26,27,28-*tetrakis*(ethoxyester-2-bromo-propanoate)calix[4]arene, 16

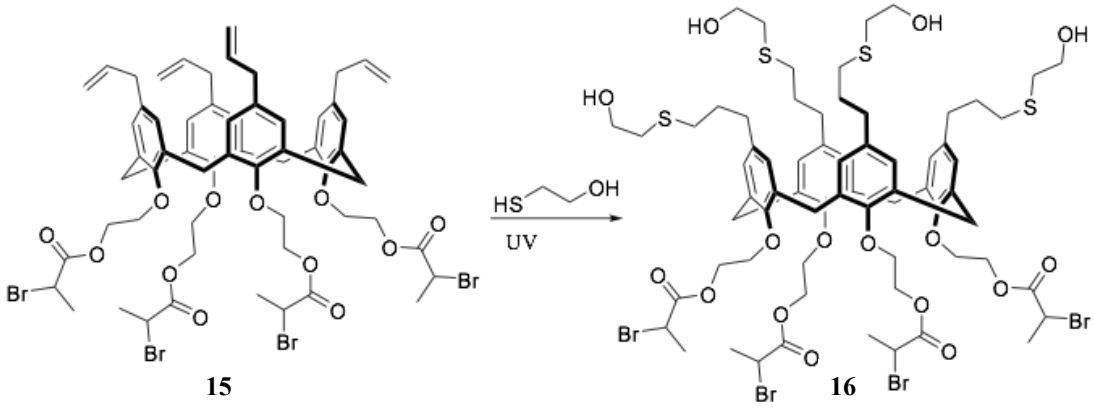

15 **16**

Scheme 4.10. Synthesis of **16**.

The novel compound **16** was successfully synthesised *via* performing photo initiated thiol-ene "click" chemistry on the double bonds of the allyl moiety (Scheme 4.10). Compound **15** was exposed to 30 seconds of a wide emission UV spectrum at an intensity of 200 W cm^{-2} in the presence of an excess of 2-mercaptoethanol. A yield of 89% was achieved after carrying out flash column chromatography. **16** adhered to the silica, therefore was washed with pure ethyl acetate to remove the excess 2-mercaptoethanol, then was removed from the silica *via* flushing the column with methanol, which strips off the silica hydroxyls releasing the compound. Full analysis and characterisation is described below.

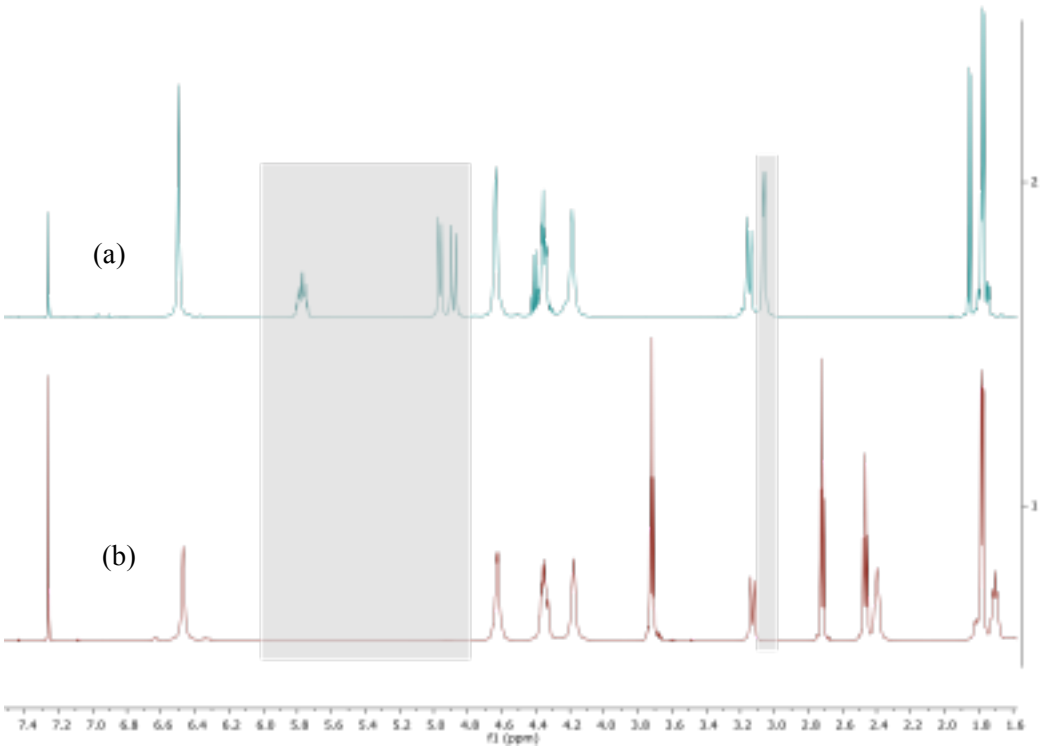

Figure 4.41. ^{1}H NMR spectra comparing **15** (a) and **16** (b)**,** showing the loss of the alkene resonance of the allyl moiety in $CDCl_3$.

The stacked ^{1}H NMR spectra (Fig. 4.41) showed that the resonance for the allyl moiety of **15** had disappeared. A full analysis of the spectra of **16** is discussed.

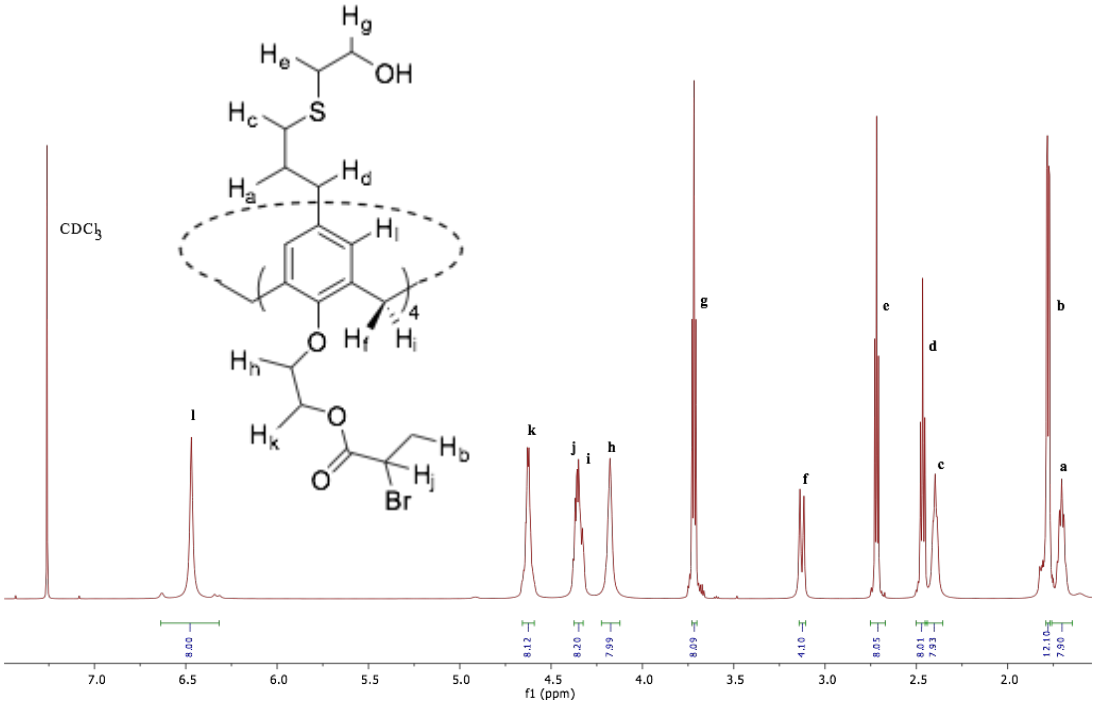

Figure 4.42. ^{1}H NMR spectrum of **16** in $CDCl_3$.

The ^{1}H NMR spectrum (Fig. 4.42) exhibits a quintet resonance with an integral set to eight at 1.70 ppm, **a**. The COSY NMR spectrum (Fig. 4.43) shows that **a** couples to two resonances, one at 2.40 ppm and a second at 2.47 ppm, **c** and **d**, respectively. The ^{1}H NMR spectrum (Fig. 4.42) shows that resonance **c** has a triplet multiplicity and an integral of eight with **d** also having a triplet multiplicity with an integral of eight. Resonance **a** corresponds to the hydrogen atoms on the second carbon atom along of the propylene unit of the *tetrakis(*3-hydroxyethyl)thioether-propanyl moiety with respect to the aromatic ring, H_a. The quintet resonance corresponding to H_a is a result of coupling to two methylene units on either side. Resonance **c** corresponds to the hydrogen atoms on the third carbon atom along of the propylene unit of the *tetrakis(*3-hydroxyethyl)thioether-propanyl moiety with respect to the aromatic ring, H_c. Resonance **d** corresponds to the hydrogen atoms on the first carbon atom along of the propylene unit of the *tetrakis(*3-hydroxyethyl)thioether-propanyl moiety with respect to the aromatic ring, H_d. The ^{1}H NMR spectrum (Fig. 4.42) exhibits an overlapped doublet resonance with an integral of 12 at 1.78 ppm, **b**. The COSY NMR spectrum (Fig. 4.43) shows that **b** couples to a resonance at 4.35 ppm, **j**. The resonance of **b** (Fig. 4.42) corresponds to the methyl protons of the 2-bromoproanoate moiety, H_b, and **j** corresponds to the methine of the 2-

bromoproanoate moiety, H_j. The appearance of an overlapping set of doublets with the overall integral of 12 with relatively equal intensities suggests that there are two environments for the methyl protons, which could be resultant of steric interactions from the crowded lower rim of the calixarene, forcing the bulky ester moieties into two distinct conformations, as discussed for **6** (Fig. 4.35), resulting in the methyl protons of 1' and 1'' being non-equivalent. The ^{1}H NMR spectrum (Fig. 4.42) exhibits a triplet resonance with an integral of eight at 2.72 ppm, **e**, and also has a J_1 coupling constant of 7.0 Hz.

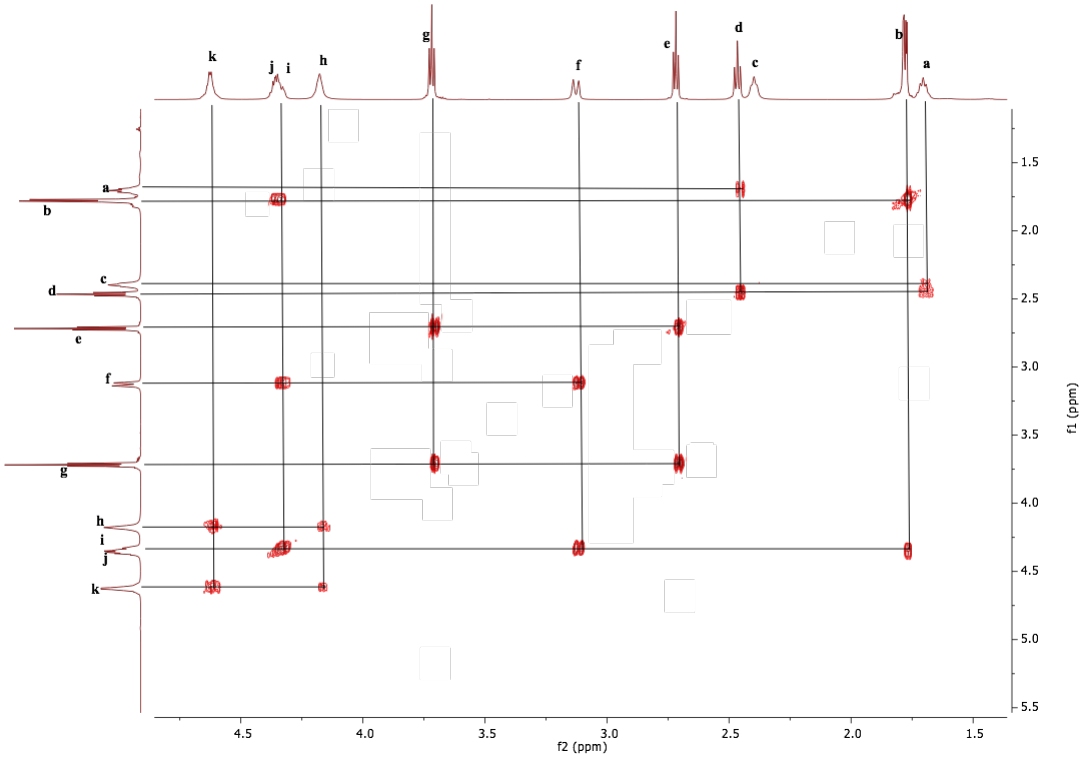

Figure 4.43. COSY NMR spectrum of **16** in $CDCl_3$.

The COSY NMR spectrum (Fig. 4.43) shows that **e** couples to a resonance at 3.72 ppm, **g**, which has an integral of eight and a J_1 coupling constant of 7.0 Hz. Resonances **e** and **g** correspond to the ethylene protons of the thio ether ethylene hydroxyl moiety, with **e** corresponding to the hydrogen atoms closest to the sulfur and **g** corresponding to the hydrogen atoms adjacent to the hydroxyl moiety, H_e and H_g, respectively. The assignment was achieved by the fact that sulfur is less electron withdrawing than oxygen, so will therefore pull less electron density away from the adjacent carbon atom, thus the protons will be less deshielded. The ^{1}H NMR spectrum (Fig. 4.42) exhibits a doublet resonance at 3.13 ppm, **f**. The COSY NMR

spectrum (Fig. 4.43) shows that **f** couples to a resonance at 4.35 ppm, **i**. **f** and **i** correspond to the methylene protons that bridge the aromatics, with **f** corresponding to the protons pointing up to the aromatic region, H_f, and **i** corresponding to the protons pointing down to the oxo environment, H_i, indicating that the calixarene is in a cone conformation.[4] The ^{1}H NMR spectrum (Fig. 4.42) exhibits a multiplet resonance with an integral of eight at 4.18 ppm, **h**. The COSY NMR spectrum (Fig. 4.43) shows that **h** couples to a resonance at 4.63 ppm, **k**, which has an integral of eight. Resonances **h** and **k** correspond to the ethylene protons of the ethyl ether 2-bromoproanoate moiety, but to accurately assign the position the hydrogen atoms the HMBC NMR spectrum must be referred to and is discussed later. The ^{1}H NMR spectrum (Fig. 4.42) exhibits a singlet resonance with an integral of eight at 6.47 ppm, **l**, which corresponds to the aromatic hydrogen atoms attached to the carbon atom of the aryl ether ring in the *meta* position with respect to the aryl ether oxygen. To assign the ^{13}C NMR spectrum, HSQC NMR and HMBC NMR spectroscopy were carried out. Using HSQC NMR spectroscopy the carbon atoms directly attached to hydrogen atoms could be easily assigned.

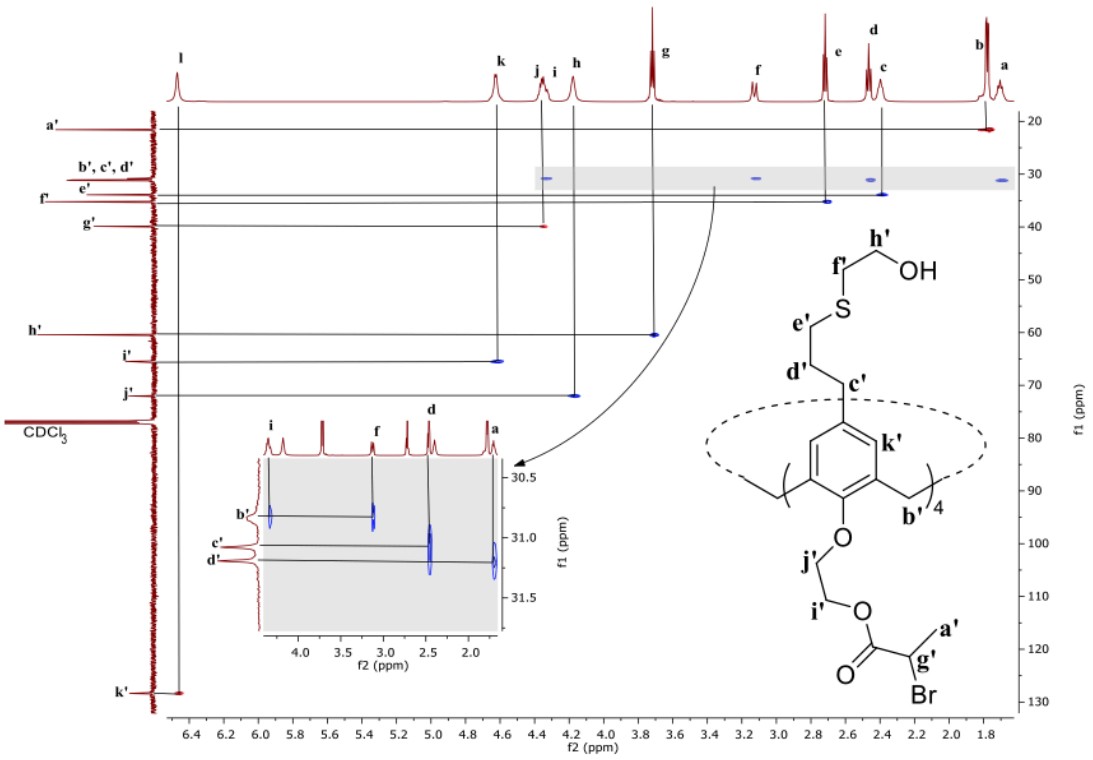

Figure 4.44. HSQC NMR spectrum of **16** in $CDCl_3$.

The HSQC NMR spectrum (Fig. 4.44) shows that **a** couples to a ^{13}C NMR resonance at 31.4 ppm, **d'**, which corresponds to the second carbon atom along of the propylene unit of the *tetra(*3-hydroxyethyl)thioehter-propanyl moiety with respect to the aromatic ring. **b** exhibits a coupling to a ^{13}C NMR resonance at 21.7 ppm, **a'**, which corresponds to the methyl carbon of the 2-bromopropanoate moiety. **c** couples to a ^{13}C NMR resonance at 34.1 ppm, **e'**, which corresponds to the third carbon atom along of the propylene unit of the *tetrakis(*3-hydroxyethyl)thioether-propanyl moiety with respect to the aromatic ring. **d** couples to a ^{13}C NMR resonance at 31.3 ppm, **c'**, which corresponds to the first carbon atom along of the propylene unit of the *tetrakis(*3-hydroxyethyl)thioether-propanyl moiety with respect to the aromatic ring. **e** couples to a ^{13}C NMR resonance at 35.4 ppm, **f'**, which corresponds to the carbon atom adjacent to the sulfur of the thio ether ethylene hydroxyl moiety. **f** and **i** both couple to a ^{13}C NMR resonance at 31.0 ppm, **b'**, which corresponds to the bridging methylene carbon atoms between aromatic rings. The fact that the bridging methylene carbon atoms resonance resides in the 31 ppm region is further indication that the calixarene exists in a cone conformation.[5] **g** couples to a ^{13}C NMR resonance at 60.6 ppm, **h'**, which corresponds to the carbon atom adjacent to the hydroxyl of the thio ether ethylene hydroxyl moiety. **h** couples to a ^{13}C NMR resonance at 72.2 ppm, **j'**, which corresponds to one of the ethylene carbon atoms of the ethyl ether 2-bromopropanoate moiety, with the exact characterisation requiring the HMBC NMR experiment, and is described later. **j** couples to a ^{13}C NMR resonance at 40.1 ppm, **g'**, which corresponds to the methine carbon atom of the 2-bromopropanoate moiety. **k** couples to a ^{13}C NMR resonance at 65.6 ppm, **i'**, which corresponds to one of the ethylene carbon atoms of the ethyl ether 2-bromopropanoate moiety, with the exact characterisation requiring the HMBC NMR experiment, and is described later. To assign the ^{13}C NMR resonances that do not directly couple to a hydrogen atom HMBC NMR spectroscopy was carried out and was fully analysed.

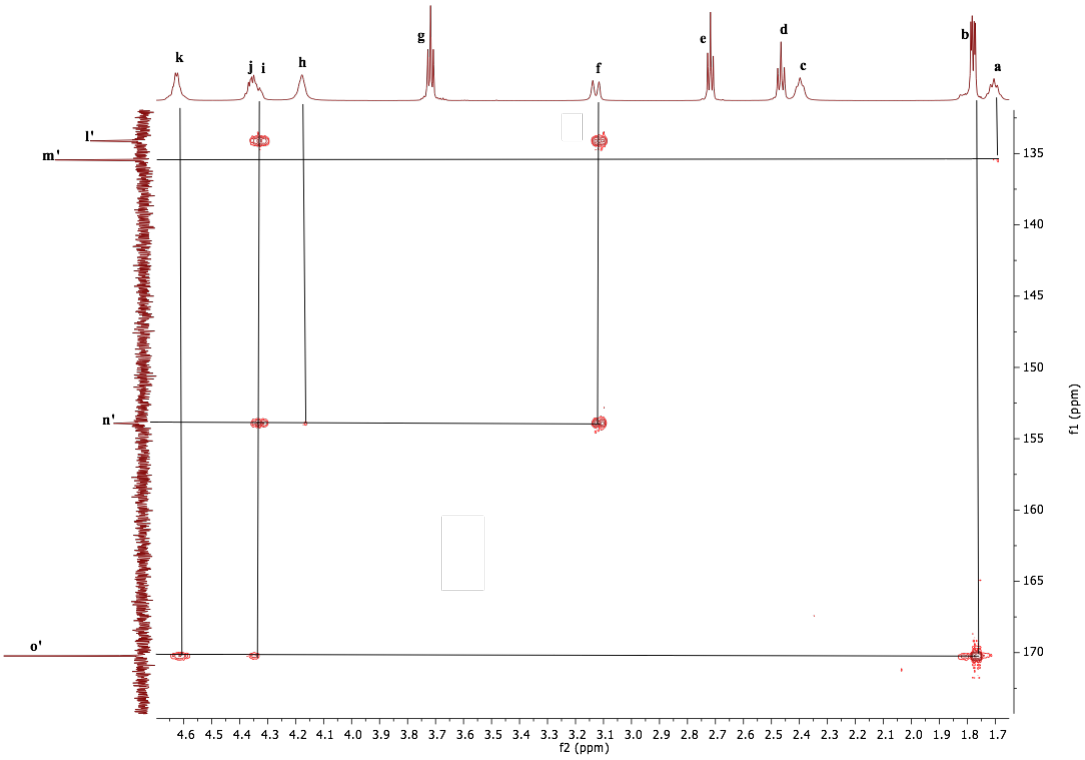

Figure 4.45. HMBC NMR spectrum of **16** in $CDCl_3$.

The HMBC NMR spectrum (Fig. 4.45) shows that there is a ^{13}C NMR resonance at 170.4 ppm, **o'**, which corresponds to the carbonyl carbon atom of the 2-bromoproanoate moiety. **o'** exhibits coupling to **b**, **i** and **k**, with resonances **b** and **i** corresponding to H_b and H_i, respectively (Fig. 4.42). **k** corresponds to one pair of the ethylene protons of the ethyl ether 2-bromopranoate moiety as discussed previously. The coupling between **o'** and **k** indicates that **k** corresponds to the ethylene protons closest to the carbonyl, H_k (Fig. 4.42). The HMBC NMR spectrum (Fig. 4.45) shows that there is a ^{13}C NMR resonance at 154.1 ppm, **n'**, which exhibits coupling to the resonances **f** and **j** corresponding to the bridging methylene protons, H_f and H_j, respectively (Fig. 4.42), and **h**, which as discussed previously corresponds to one pair of the ethylene protons of the ethyl ether 2-bromopropanoate moiety. **n'** therefore corresponds to the *ipso* carbon atom of the aryl ether with respect to the aryl ether oxygen and **h** corresponds to the methylene ether linker protons of the ethyl ether 2-bromopropanoate moiety, H_h (Fig. 4.42). The HMBC NMR spectrum (Fig. 4.45) shows that there is a ^{13}C NMR resonance at 135.6 ppm, **m'**, which exhibits coupling to **a** (H_a, Fig. 4.42), therefore corresponds to the *para* carbon atom of the aryl ether with respect to the aryl ether oxygen. The complete assignment of the ^{13}C NMR spectrum is shown in Figure 4.46.

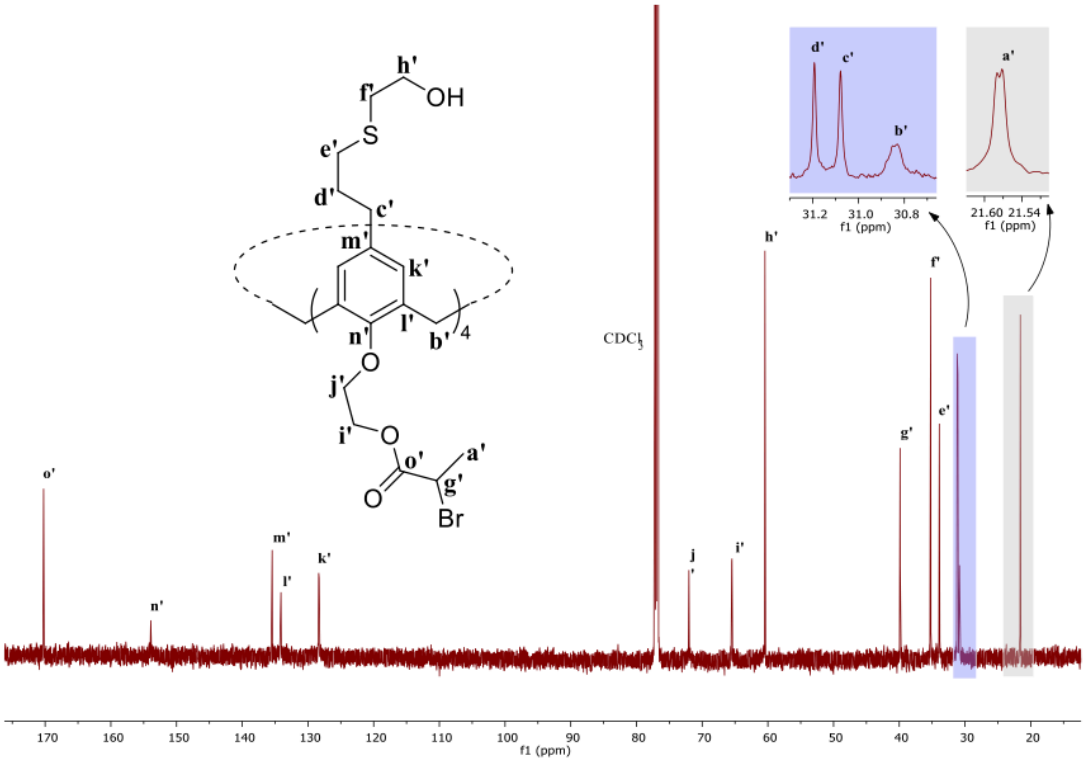

Figure 4.46. ^{13}C NMR spectrum of **16** in $CDCl_3$.

Compound **16** was unstable to ASAP MS. CHN analysis was carried out on **16**, with the results obtained closely matching the predicted values; CHN Expected = %C = 50.63, %H = 5.75, %N = 0.00; Measured %C = 50.98, %H = 5.79, %N = 0.00. Further indication that **16** (blue trace) was synthesised was through FT-IR spectroscopy, where there was loss of the C=C absorption band at 1638 cm^{-1} and the presence of a strong OH absorption band at 3307 cm^{-1} were observed (Fig. 4.47).

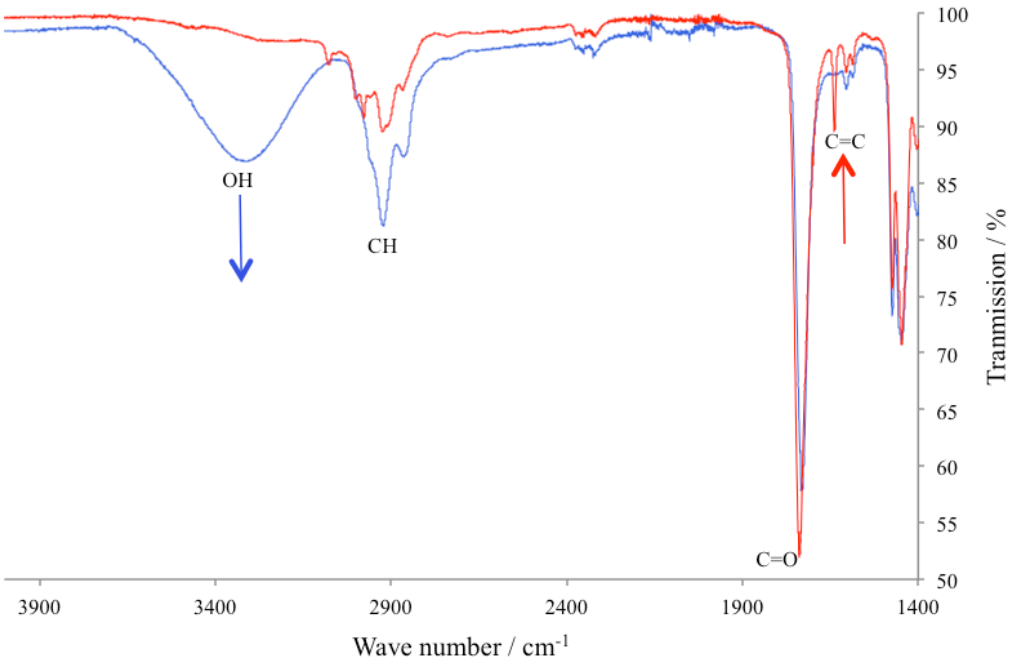

Figure 4.47. Stacked FT-IR spectra of, red = **15** and blue = **16**.

4.3. Conclusion

This chapter described the synthetic strategy employed for the synthesis of a novel A_4B_4 heterofunctional initiator that incorporated an alkyl halogen moiety required for SET-LRP and a primary hydroxyl moiety required for ROP. The known compound of 25,26,27,28-*tetrakis*(allyloxy)calix[4]arene, **11**, and 5,11,17,23-*tetrakis*(prop-2-en-1-yl)calix[4]arene, **12**, were synthesised according to the literature.[3] A full characterisation was carried out on both **11** and **12** as little characterisation had been carried out previously. The novel compound 5,11,17,23-*tetrakis*(prop-2-en-1-yl)-25,26,27,28-*tetrakis*(methylacetateoxy)calix[4]arene, **13**, was successfully synthesised *via* a Williamson ether synthesis between **12** and methyl chloroacetate and was fully characterised. **13** was taken forward and used as the precursor for the novel compound 5,11,17,23-*tetrakis*(prop-2-en-1-yl)-25,26,27,28-*tetrakis*(ethanoloxy)calix[4]arene, **14**, which was synthesised *via* an ester reduction of **13**. The novel compound *5*,11,17,23-*tetrakis*(prop-2-en-1-yl)-25,26,27,28-*tetrakis*(ethoxyester-2-bromo-propanoate)calix[4]arene, **15**, was successfully synthesised *via* an esterification reaction with 2-bromopropionyl bromide; a full characterisation was carried out. It was noted that ~1 molecule of 2-

bromopropanoic acid was trapped within the calixarene, which could not be removed. The final step was to incorporate a primary hydroxyl moiety, which was achieved *via* a photo initiated thiol-ene click reaction with the allyl moieties of **15** and 2-mercaptoethanol, resulting in the successful synthesis of the novel compound 5,11,17,23-*tetrakis*((3-hydroxyethyl)thioether-propanyl*)*-25,26,27,28-*tetrakis*(ethoxyester-2-bromo-propanoate)calix[4]arene, **16**. The full characterisation of **16** was carried out.

4.4. References

(1) Ueda, J.; Kamigaito, M.; Sawamoto, M. *Macromolecules* **1998**, *31*, 6762.
(2) Angot, S.; Murthy, K. S.; Taton, D.; Gnanou, Y. *Macromolecules* **2000**, *33*, 7261.
(3) Gutsche, C. D.; Levine, J. A.; Sujeeth, P. K. *J. Org. Chem.* **1985**, *50*, 5802.
(4) Gou, P. F.; Zu, W. P.; Shen, Z. Q. *Acta Polym. Sin.* **2007**, 967.
(5) Jaime, C.; Demendoza, J.; Prados, P.; Nieto, P. M.; Sanchez, C. *J. Org. Chem.* **1991**, *56*, 3372.
(6) Streitwieser, A. *Chem. Rev.* **1956**, *56*, 571.
(7) Tu, C. L.; Zhu, L. J.; Li, P. P.; Chen, Y.; Su, Y.; Yan, D. Y.; Zhu, X. Y.; Zhou, G. Y. *Chem. Commun.* **2011**, *47*, 6063.

Chapter 5

Amphiphilic A_4B_4 Miktoarm Star Polymer with Calix[4]arene Core

5.0. Introduction

This chapter describes the synthesis of a novel amphiphilic A_4B_4 miktoarm star polymer, which employs the "core first" strategy. The multifunctional core encompasses four primary hydroxyls, which facilitate ring opening polymerisation (ROP) and four alkyl bromo moieties, which facilitate single electron transfer living radical polymerisation (SET-LRP). The monomer selected for ROP was ε-caprolactone due to its biocompatibility and hydrophobic nature in its polymer form (poly(ε-caprolactone), PCL). To introduce an amphiphilic nature to the polymer system the monomer selected for SET-LRP was 2-hydroxylethyl acrylate (HEA) that forms poly(2-hydroxylethyl-acrylate) (PHEA), which is a hydrophilic polymer. The combination of hydrophilic and hydrophobic arms attached to a central core will lead to interesting properties, such as self-assembly in certain solvents.

5.1. Experimental

5.1.1. Materials

5,11,17,23-*tetrakis*((3-hydroxyethyl)thioether-propanyl*)*-25,26,27,28-*tetrakis*(ethoxyester-2-bromo-propanoate)-calix[4]arene, **16**, was synthesised according to Chapter 4. Tin(II) 2-ethylhexanoate (92.5 – 100%) and Tris[2-(dimethylamino)ethyl]amine (Me_6TREN) were purchased from Sigma Aldrich and used without further purification. ε-caprolactone (97%) was purchased from Sigma Aldrich and distilled before use. HEA (96%) was purchased from Sigma Aldrich and purified as follows: HEA was added to water (20% v/v) and washed with hexane ten times to remove the unwanted ethylene glycol diacrylate. The HEA monomer was collected *via* extraction with diethyl ether (five times), which was dried over magnesium sulfate and filtered. Hydroquinone (0.05%) was further added.[1] Bare copper wire (24 standard wire gauge, diameter = 0.559 mm) was purchased from Fisher Scientific and was activated prior to use *via* dipping in concentrated nitric acid and then washing with water and drying. Chloroform, methanol, anhydrous dimethylformamide (DMF) and diethyl ether analytical grade solvents and concentrated nitric acid (~37%) were purchased from Fisher Scientific and used without further purification. Dry toluene was obtained from the Durham University Chemistry Department Solvent Purification Service (SPS). Deuterated chloroform ($CDCl_3$) and deuterated DMF (DMF-d_7) for NMR analysis was purchased from Apollo Scientific.

5.1.2. Instrumentation

^{1}H and ^{13}C NMR spectra were recorded using a Varian VNMRS 700 spectrometer operating at 700 MHz and 176 MHz, respectively, with *J* values given in Hz. $CDCl_3$ or DMF-d_7 was used as deuterated solvent for ^{1}H and ^{13}C NMR analysis and the spectra were referenced to the solvent traces at 7.26 ppm, 77.0 ppm and 8.03 ppm, 163.15 ppm, respectively. The following abbreviations are used in describing NMR spectra: s = singlet, d = doublet, t = triplet, q = quartet, quin = quintet, s = sextet, m = multiplet, b = broad, o = overlapped, dd = doublet of doublets, dq = doublet of quartets. 2D NMR experiments were also used to fully assign the proton and carbon environments in the products. ^{1}H-^{1}H Correlation Spectroscopy (COSY)

demonstrated proton-proton correlations over two or three bonds. ^{1}H-^{13}C Heteronuclear Shift Correlation Spectroscopy (HSQC) demonstrated correlation between directly bonded proton and carbons atoms. ^{1}H-^{13}C Heteronuclear Multiple-Bond Correlation (HMBC) demonstrated the correlation between proton and carbon environments through several bonds.

Fourier transform-infra-red (FT-IR) spectroscopy was conducted using a Perkin Elmer 1600 series spectrometer.

Measurements of molecular weight (M_n and M_w, corresponding to the number average and weight average molecular weight respectively), and dispersity (Đ) of polymers synthesised were carried out *via* Size Exclusion Chromatography (SEC) on a Viscotek TDA 302 with triple detectors: refractive index, light scattering and viscosity. The columns used were PLgel 2 x 300 mm 5 μm mixed C, which have a linear range of molecular weights from 2.0 x 10^2 – 2.0 x 10^6 g mol^{-1}. The solvent used was THF or DMF at flow rates and temperatures at 1.0 mL min^{-1}, 35 ^{o}C and 1.0 mL min^{-1}, 70 ^{o}C respectively. The detectors were calibrated using narrow molecular weight distribution linear polystyrene or polyethylene glycol standards.

Differential scanning calorimetry (DSC) was carried out using a *TA Instrument Q1000 DSC*, ran in N_2 gas, with a flow rate of 30 mL min^{-1} and a heating rate of 10 ^{o}C min^{-1}.

Thermogravimetric analysis (TGA) was carried out using a *Perkin Elmer Pyris 1 TGA* connected to a *HIDEM HPR20 MS*, ran in N_2 gas with a heating rate of 10 ^{o}C min^{-1}.

5.1.3. Synthesis of Calixarene-starPCL_{20}, 17

To a Schlenk vessel, **16** (0.150 g, 0.09 mmol) was added. The flask was evacuated for 3 h, then purged with dry argon (Ar), this process was repeated a second time. ε-caprolactone (0.750 mL, 6.77 mmol) was then injected, forming a colourless solution. A stock solution of $Sn(Oct)_2$ in dry toluene (0.23 M, 0.063 mL) was further injected in. The system was heated to 120 ^{o}C and left to stir for 24 h, forming a pale

brown translucent viscous liquid. The viscous liquid was dissolved in a small volume of chloroform and precipitated into a cold solution of methanol; the precipitation process was repeated three times. The white precipitate was collected and dried under vacuum resulting in a white powdery material. Mass = 0.89 g, yield = 99%. ν_{max} (Perkin Elmer FT-IR, Diamond, cm^{-1}). 3441 (w, OH), 2850-2990 (s, CH), 1721 (s, C=O). ^{1}H NMR (700 MHz, $CDCl_3$) δ: 1.33 (quin, 153H_a, J = 7.6 Hz), 1.60 (m, 310H_b), 1.75 (dd, 12H_c, J = 6.9 Hz), 1.88 (bm, 8H_d), 2.26 (t, 154H_e, J =7.6 Hz), 2.42 (m, 8H_f), 2.54 (m, 8H_g), 2.67 (m, 8H_h), 3.08 (d, 4H_i, J = 14.9 Hz), 3.59 (t, 8H_j, J = 6.6 Hz), 4.01 (t, 150H_k, J = 6.7 Hz), 4.12 (m, 8H_l), 4.16 (m, 8H_m), 4.28 (m, 4H_n), 4.32 (m, 4H_o), 4.58 (m, 8H_p), 6.00-6.87 (m, 8H_q).^{13}C NMR (176 MHz, $CDCl_3$) δ: 21.6 (**a'**), 24.6 (**b'**), 25.5 (**c'**), 28.3 (**d'**), 30.4 (**e'**), 31.0 (**f'**), 31.4 (**g'**), 31.6 (**h'**), 32.3 (**i'**), 34.1 (**j'**), 40.0 (**k'**), 62.5 (**l'**), 63.3 (**m'**), 64.2 (**n'**), 65.7 (**o'**), 72.0 (**p'**), 128.3 (**q'**), 134.8 (**r'**), 154.4 (**s'**), 170.2 (**t'**), 173.5 (**u'**). SEC (THF): M_n = 4.4 x10^3 g mol^{-1}, M_w = 5.5 x 10^3, Đ = 1.25. DSC: T_m = 50.27 ^oC, T_c = 24.40 ^oC, %crystallinity = 19.65%. TGA: Onset X_1 = 253.47 ^oC, Onset X_2 = 344.64 ^oC, ΔY_1 = 84.715%, ΔY_2 = 15.262%.

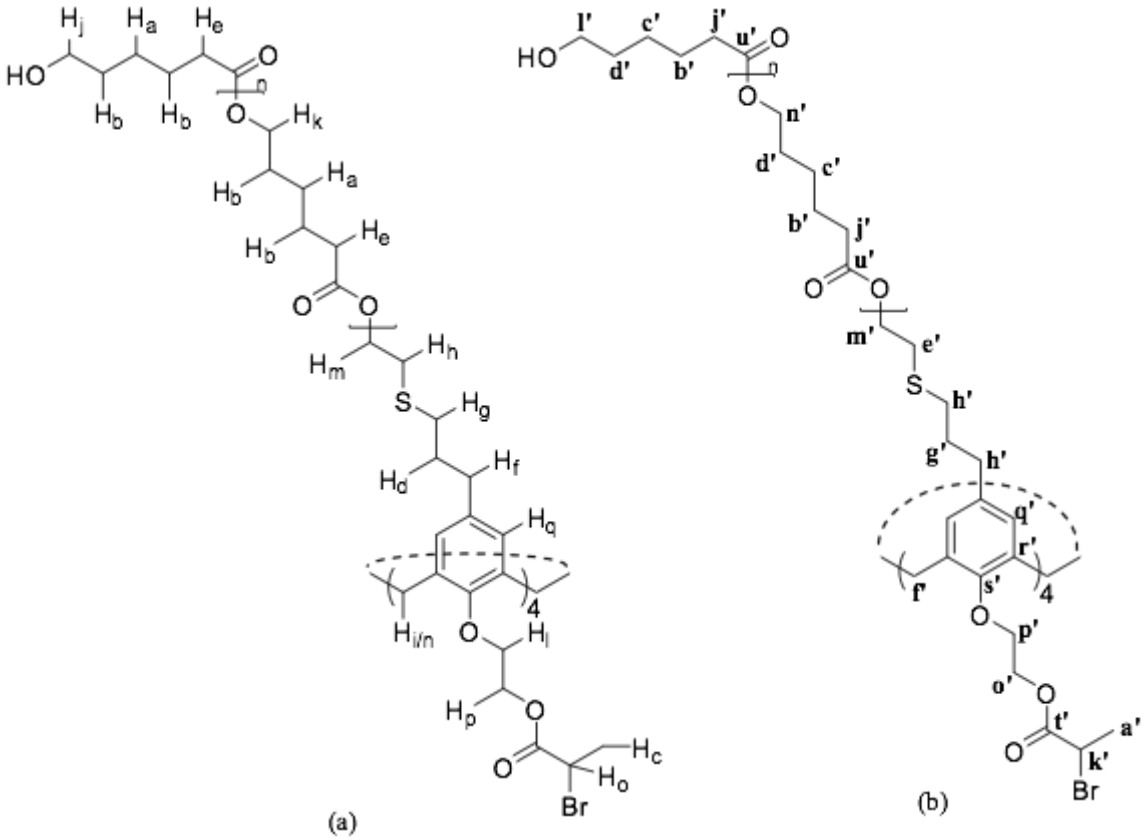

Figure 5.1. Labelling of the chemical environments in **2** (a) proton (b) carbon.

5.1.4. Synthesis of Calixarene-star$PCL_{20}PHEA_m$ using SET-LRP, 18 - 20

To a Schlenk vessel charged with a magnetic stirrer, **17** (0.100 g, 0.0012 mmol) and activated copper wire (2 cm, activated using nitric acid) were added. The system was evacuated and purged with dry Ar. $CuBr_2$ in dry DMF (0.03 mL, 0.01915 M), further dry DMF (if required) and HEA (appropriate amount for desired M_n) was added *via* a syringe. The pale white/colourless solution was deoxygenated with dry Ar for 0.5 h. To initiate the polymerisation a deoxygenated stock solution of Me_6TREN in DMF (0.03 mL, 0.02518 M) was injected in, the solution remained colourless. The reaction mixture was stirred at 25 ^oC for 16 h, leading to a very pale blue translucent viscous solution. Further DMF (appropriate amount) was added to the reaction vessel; the free flowing solution was precipitated into diethyl ether, the precipitation process was carried out a further two times. The white precipitate was collected and further washed with diethyl ether and chloroform resulting in a tacky white material. Yields = 84-88%, conversion (HEA to PHEA) = 92-96%. ν_{max} (Perkin Elmer FT-IR, Diamond, cm^{-1}). 3441 (s, OH), 2850-2990 (s, CH), 1721 (s, C=O). ^1H NMR (700 MHz, d-DMF) δ: 1.39 (quin, $155H_a$, J = 7.6 Hz), 1.49 (m, $8H_b$), 1.62 (m, $340H_c$), 1.54-2.00 (m, $300H_d$), 2.34 (t, $153H_e$, J = 7.4 Hz), 2.38 – 2.55 (m, $190H_f$), 2.81 (bs, $11H_f$), 3.50 (m, $10H_h$), 3.56 (m, $8H_i$), 3.65 (m, $8H_j$), 3.73 (s, $383H_k$), 4.06 (t, $154H_l$, J = 6.6 Hz), 4.14 (m, $370H_m$), 4.23 (m, $9H_n$), 4.38 (t, $8H_o$, J = 5.0 Hz), 4.63 (m, $4H_p$), 4.86 (bs, $190H_q$), 6.46-6.92 (bm, $8H_r$). ^{13}C NMR (176 MHz, d_6-DMF) δ: 24.5 (**a'**), 26.3 (**b'**), 29.3 (**c'**), 30.9 (**d'**), 33.6 (**e'**), 34.6 (**f'**), 36.6 (**g'**), 42.3 (**h'**), 60.7 (**i'**), 62.0 (**j'**), 62.2 (**k'**), 64.3 (**l'**), 64.8 (**m'**), 67.1 (**n'**), 73.7 (**o'**), 174.0 (**p'**), 176.0 (**q'**). M_{nNMR} = 5.0 x10^3 g mol^{-1} – 2.2 x10^4 g mol^{-1}. SEC (DMF): M_n = 1.3 – 2.0 x 10^4 g mol^{-1}, Đ = 1.23-1.45. DSC: T_m = 50.27 ^oC, T_c = 24.40 ^oC. TGA: Onset X_1 = ~292 ^oC, Onset X_2 = 395-412 ^oC , ΔY_1 = ~89%, ΔY_2 = ~11%.

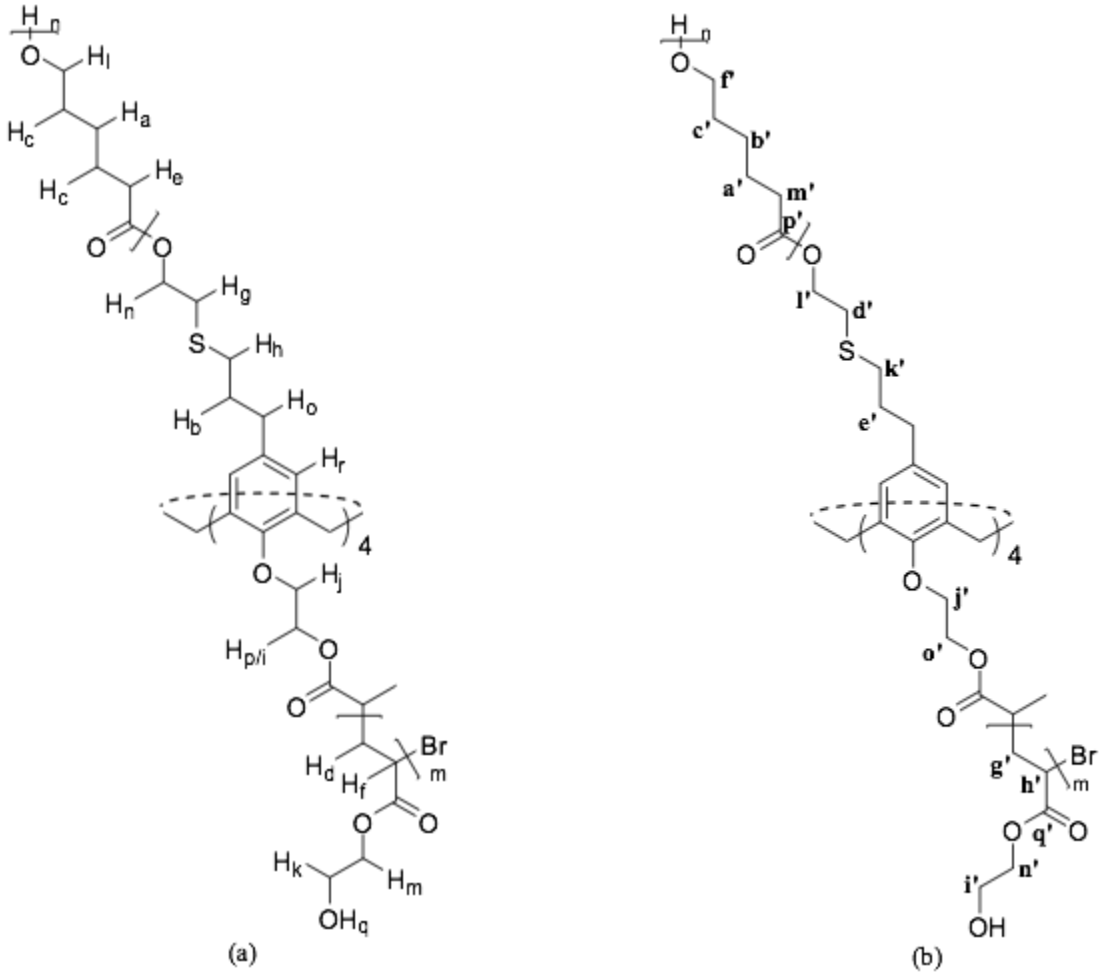

Figure 5.2. Labelling of the chemical environments in **18 - 20** (a) proton (b) carbon.

5.2. Results and discussion

5.2.1. Ring opening polymerisation of ε-caprolactone using A_4B_4 heterofunctional initiator, 16

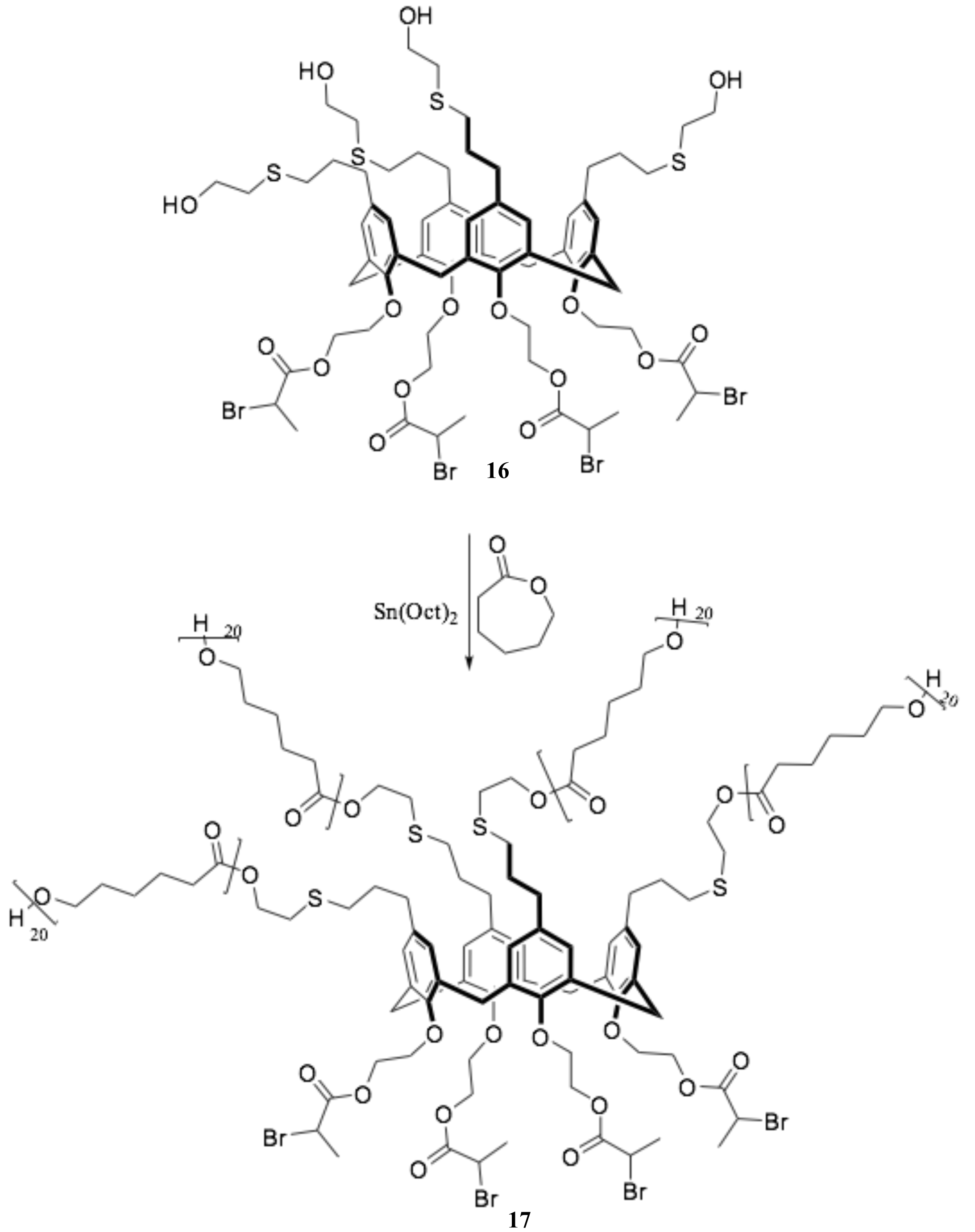

Scheme 5.1. Ring opening polymerisation of ε-caprolactone using **16**.

ε-Caprolactone was ring opened off the primary hydroxyls of **16** using tin octoate, with the reaction run in bulk, leading to a star poly(ε-caprolactone) (PCL) with a

calix[4]arene core (Scheme 5.1). A monomer to initiator to catalyst ratio of 80:1:0.05 was used to target a molecular weight of 9.2 x 10^4 g mol^{-1}, therefore a degree of polymerisation (**DP**) of 20 per arm. The polymer has been fully analysed and the results are discussed below.

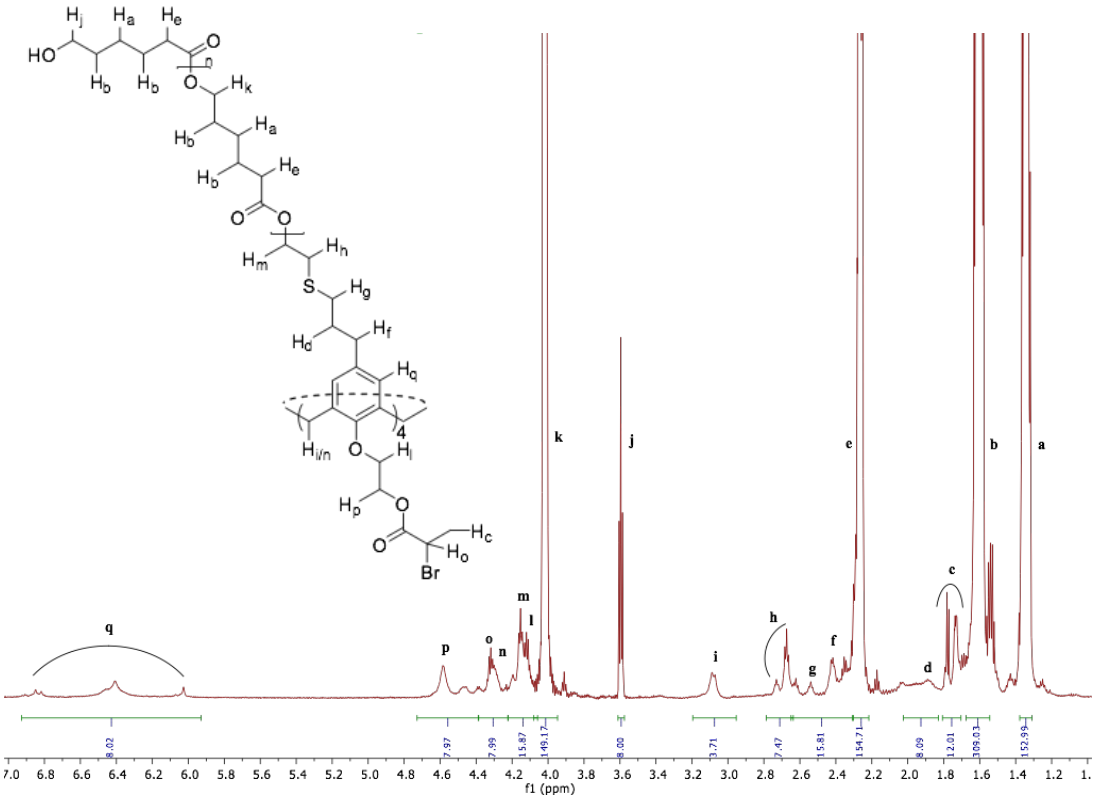

Figure 5.3. ^{1}H NMR spectrum of **17**, in $CDCl_3$.

The ^{1}H NMR spectrum (Fig. 5.3) shows the resonances of the calixarene core aromatic protons, with several broad resonances observed at 6.00-6.87 ppm, **q**, corresponding to H_q. The various broad resonances are observed due to the many different rotational conformations of the calixarene core present. Resonance **q** had its integral value set to eight, with the **DP** of the PCL being determined with respect to this value. The ^{1}H NMR spectrum (Fig. 5.3) shows the resonances for the PCL backbone protons **a**, **b**, **e**, **j** and **k**. A quintet resonance with an integral of 153 is observed at 1.33 ppm, **a**, corresponding to the hydrogen atoms of the PCL on the third carbon atom with respect to the carbonyl carbon atom, H_a. A sextet resonance with an integral of 310 is observed at 1.60 ppm, **b**, corresponding to the methylene hydrogen atoms of the PCL on the second and fourth carbon atoms with respect to the carbonyl carbon, H_b. A triplet resonance with an integral of 154 is observed at

2.26 ppm, **e**, corresponding to the methylene hydrogen atoms of the PCL on the first carbon atom with respect to the carbonyl carbon, H_e. A triplet resonance with an integral of 150 is observed at 4.01 ppm, **k**, corresponding to the methylene hydrogen atoms of the PCL backbone on the fifth carbon atom with respect to the carbonyl carbon, H_k. A triplet resonance with an integral of eight is observed at 3.59 ppm, **j**, corresponding to the PCL methylene protons conjoint with the hydroxyl group on the fifth carbon atom of the end chain, H_j. To assign the proton signals from the calixarene core initiator and assign the ^{13}C NMR spectrum, COSY NMR, HSQC NMR and HMBC NMR spectroscopy were carried out, with the results discussed below.

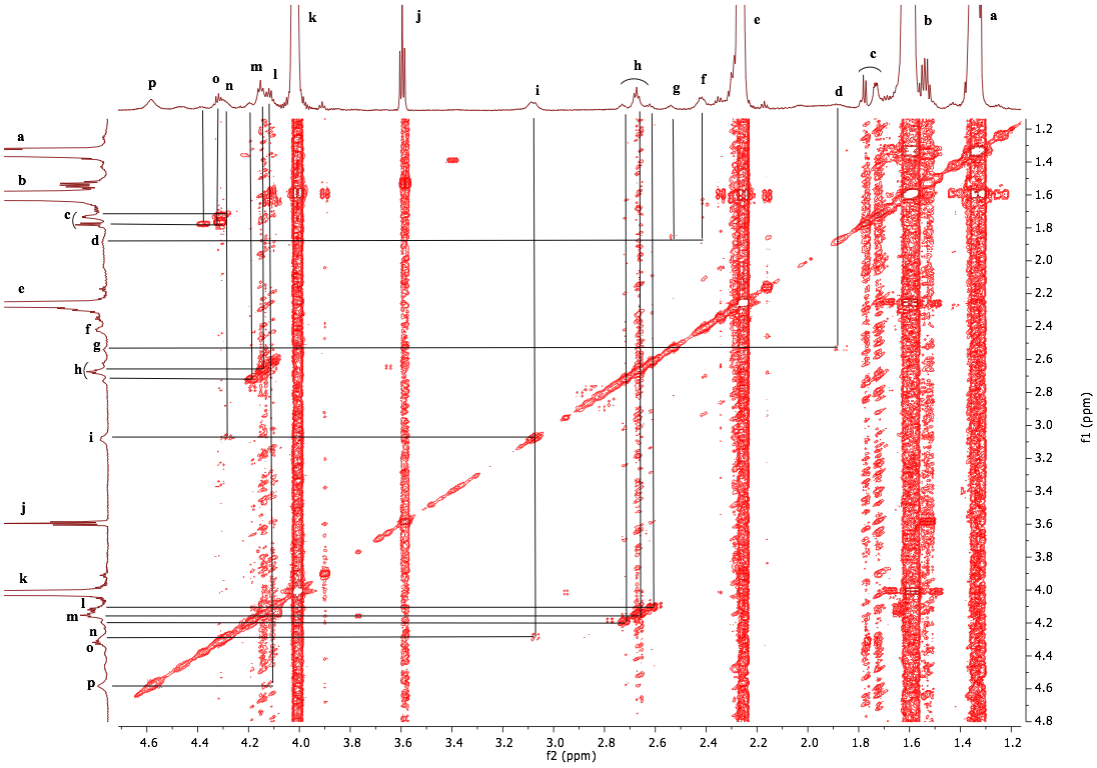

Figure 5.4. COSY NMR spectrum of **17**, in $CDCl_3$.

The COSY NMR spectrum (Fig. 5.4) exhibits two sets of doublets with an overall integral of 12 at 1.75 ppm, **c**, which exhibits coupling to an overlapped quartet signal at 4.32 ppm, **o**. **c** corresponds to the methyl protons of the bromopropanoate moiety, H_c and **o** corresponds to the methine protons of the bromopropanoate moieties, H_o (Fig. 5.3). Two sets of doublets are observed for H_c due to the four bromopropanoate moieties of the calixarene core being forced into various distinct conformations, which was previously observed (Section 4.5). The COSY NMR spectrum (Fig. 5.4)

shows a broad multiplet at 1.88 ppm, **d**, which exhibits coupling to resonances at 2.42 ppm and 2.54 ppm, **f** and **g**, respectively. **d** corresponds to the protons on the second carbon atom along of the propylene unit of the *tetra(*3-oxyetherethyl)thioether-propanyl moiety with respect to the aromatic ring, H_d, whereas **f** and **g** correspond to the protons on the first and third carbon atoms along of the propylene unit of the *tetrakis(*3-oxyetherethyl)thioether-propanyl moiety with respect to the aromatic ring, H_f and H_g, respectively (Fig. 5.3). The COSY NMR spectrum (Fig. 5.4) shows a multiplet of resonances at 2.67 ppm, **h**, which exhibits coupling to a multiplet resonance at 4.16 ppm, **m**. Resonances **h** and **m** correspond to the ethylene protons of the ethylene unit of the *tetrakis(*3-oxyetherethyl)thioether-propanyl moiety, with **m** corresponding to the protons adjacent to the oxygen and **h** corresponding to the protons next to the sulfur, H_m and H_h respectively (Fig. 5.3). The assignment was confirmed *via* an HMBC experiment (Fig. 5.5), which shows the resonance of H_m exhibiting coupling to the carbonyl carbon of the PCL back bone, **u'**. This coupling additionally confirms that the ROP was initiated *via* the primary hydroxyls of the calixarene initiator, **16**.

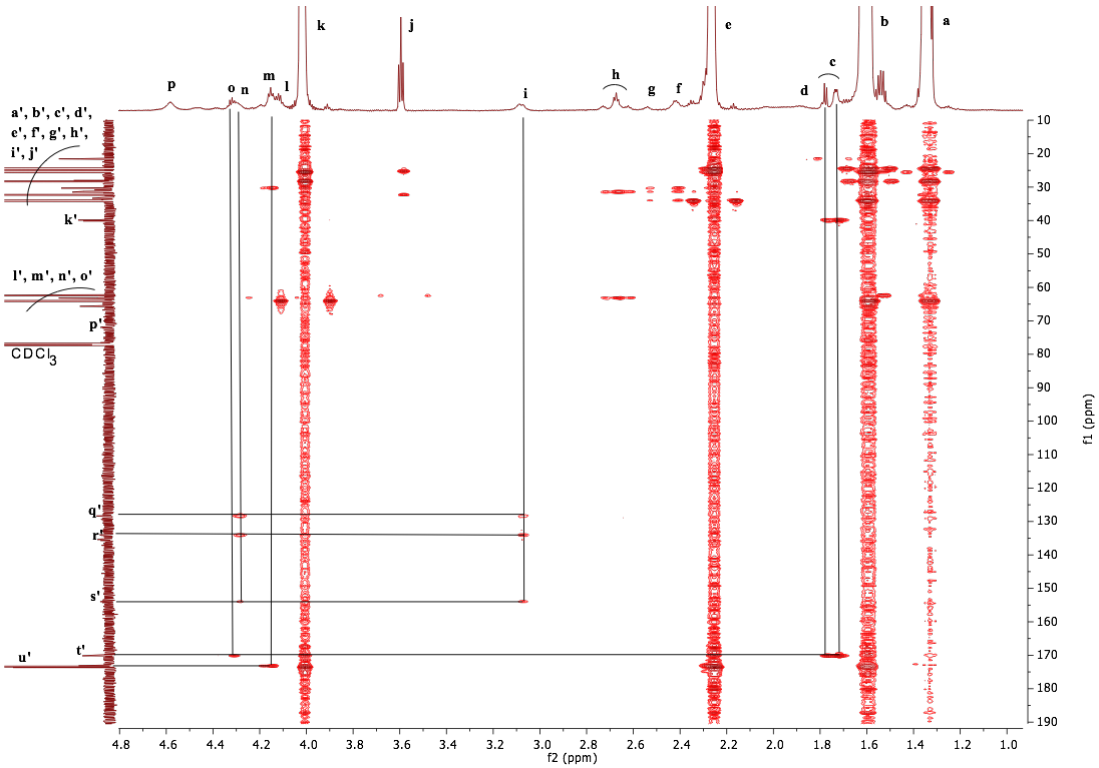

Figure 5.5. HMBC NMR spectrum of **17**, in $CDCl_3$.

The COSY NMR spectrum (Fig. 5.4) shows a broad doublet resonance with an integral of four at 3.08 ppm, **i**, which exhibits coupling to a broad resonance at 4.28

ppm, **n**. Resonances **i** and **n** correspond to the methylene protons that bridge the aromatics, H_i and H_n (Fig. 5.3), respectively. The presence of two sets of resonances corresponding to the bridging methylene protons indicates that the calixarene core is predominantly in the *cone* conformation.[2] The COSY NMR spectrum (Fig. 5.4) shows a overlapped multiplet resonance at 4.12 ppm, **l**, which exhibits coupling to a broad resonance at 4.58 ppm, **p**. Resonances **l** and **p** correspond to the ethylene protons of the ethyl ether 2-bromoproanoate moiety, H_l and H_p respectively (Fig. 5.3). Using HSQC NMR spectroscopy the carbon atoms directly attached to hydrogen atoms could be easily assigned.

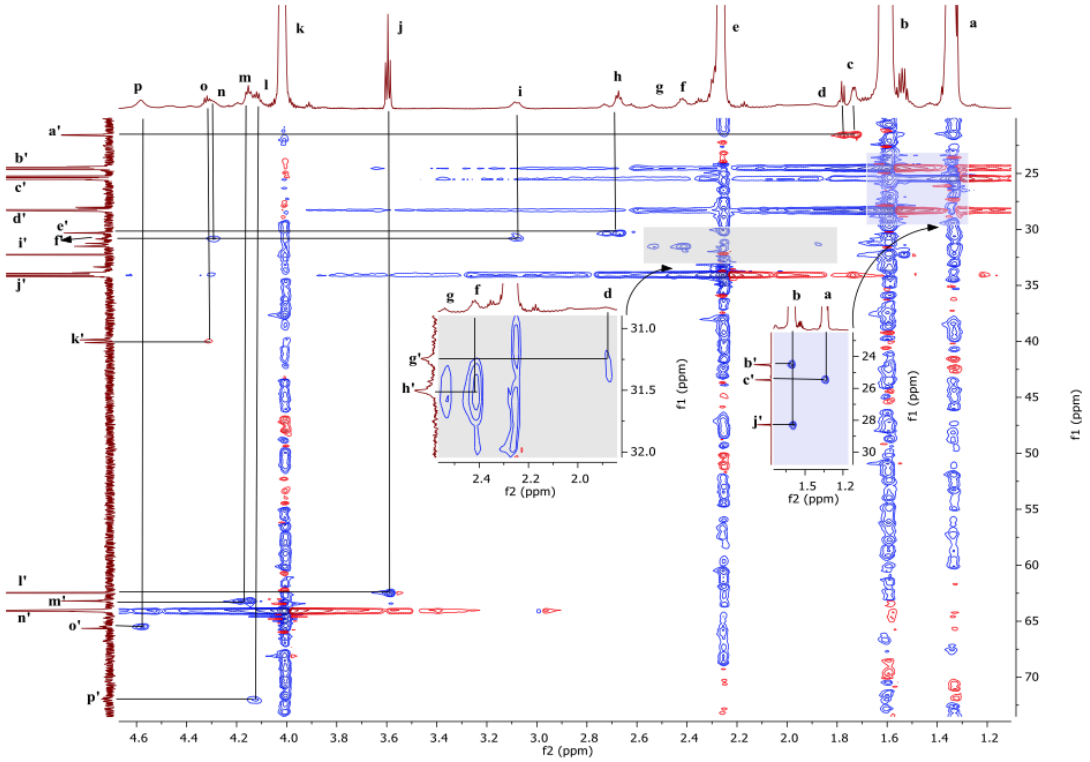

Figure 5.6. HSQC NMR spectrum of **17**, in $CDCl_3$.

The HSQC NMR spectrum (Fig. 5.6) shows **a** couples to a ^{13}C NMR resonance at 25.6 ppm, **c'**, corresponding to the third carbon atom along of the PCL with respect to the carbonyl carbon atom. Resonance **b** exhibits coupling to two ^{13}C NMR resonances at 24.6 ppm, **b'**; and 34.2 ppm, **d'**; corresponding to the second and fourth carbon atoms along of the PCL with respect to the carbonyl carbon atom, respectively. Resonance **c** exhibits coupling to a ^{13}C NMR resonances at 21.6 ppm, **a'**, corresponding to the methyl carbon atom of the bromopropanoate moiety. Resonance **d** exhibits coupling to a ^{13}C NMR resonance at 31.4 ppm, **g'**, corresponding to the second carbon atom along of the propylene unit of the *tetra(*3-

oxyetherethyl)thioether-propanyl moiety with respect to the aromatic ring. Resonance **e** exhibits coupling to a ^{13}C resonance at 34.1 ppm, **j'**, corresponding to the first carbon atom along of the PCL with respect to the carbonyl carbon. Resonances **f** and **g** both exhibit coupling to a broad ^{13}C NMR resonance at 31.4 ppm, **h'**, corresponding to the first and third carbon atoms along of the propylene unit of the *tetra(*3-oxyetherethyl)thioether-propanyl moiety with respect to the aromatic ring. Resonance **h** exhibits coupling to a ^{13}C NMR resonance at 30.4 ppm, **e'**, corresponding to the carbon atom adjacent to the sulfur of the ethylene unit of the *tetra(*3-oxyetherethyl)thioether-propanyl moiety. Resonances **i** and **n** both couple to a ^{13}C NMR resonance at 31.0 ppm, **f'**, corresponding to the methylene carbon atom that bridges the aromatics of the calixarene core. The fact that the bridging methylene carbon atom resonance resides in the 31 ppm region is further indication that the calixarene exists in a cone conformation.[3] Resonance **j** exhibits coupling to a ^{13}C NMR resonance at 62.5 ppm, **l'**, corresponding to the methylene carbon atom next to the terminus PCL hydroxyl moiety. Resonance **k** exhibits coupling to a ^{13}C NMR resonance at 64.2 ppm, **n'**, corresponding to the non-terminus methylene carbon atom of the PCL backbone on the fifth carbon atom along with respect to the carbonyl carbon. Resonance **l** exhibits coupling to a ^{13}C NMR resonance at 72.0 ppm, **p'**, corresponding to the ethylene carbon atom of the ethyl ether 2-bromopropanoate moiety adjacent to the ether oxygen. Resonance **m** exhibits coupling to a ^{13}C NMR resonance at 63.1 ppm, **m'**, corresponding to the carbon atom adjacent to the oxygen of the ethylene unit of the *tetra(*3-oxyetherethyl)thioether-propanyl moiety. Resonance **o** exhibits coupling to a ^{13}C NMR resonance at 40.0 ppm, **k'**, corresponding to the methine carbon atom of the bromopropanoate moieties. Resonance **p** exhibits coupling to a ^{13}C NMR resonance at 65.7 ppm, **o'**, corresponding to the ethylene carbon atom of the ethyl ether 2-bromopropanoate moiety adjacent to the ester oxygen. Resonance **i'** corresponds to a satellite peak of the PCL backbone. Resonance **q'**, at 128.3 ppm, corresponds to the *meta* carbon atoms of the aromatic ring of the calixarene core. Resonance **r'**, at 134.8 ppm corresponds to the *ortho* carbon atom of the aromatic and resonance **s'** at 154.4 ppm corresponds to the *ipso* carbon atom of the aromatics of the calixarene core. The complete assignment of the ^{13}C NMR spectrum is shown in Figure 5.7.

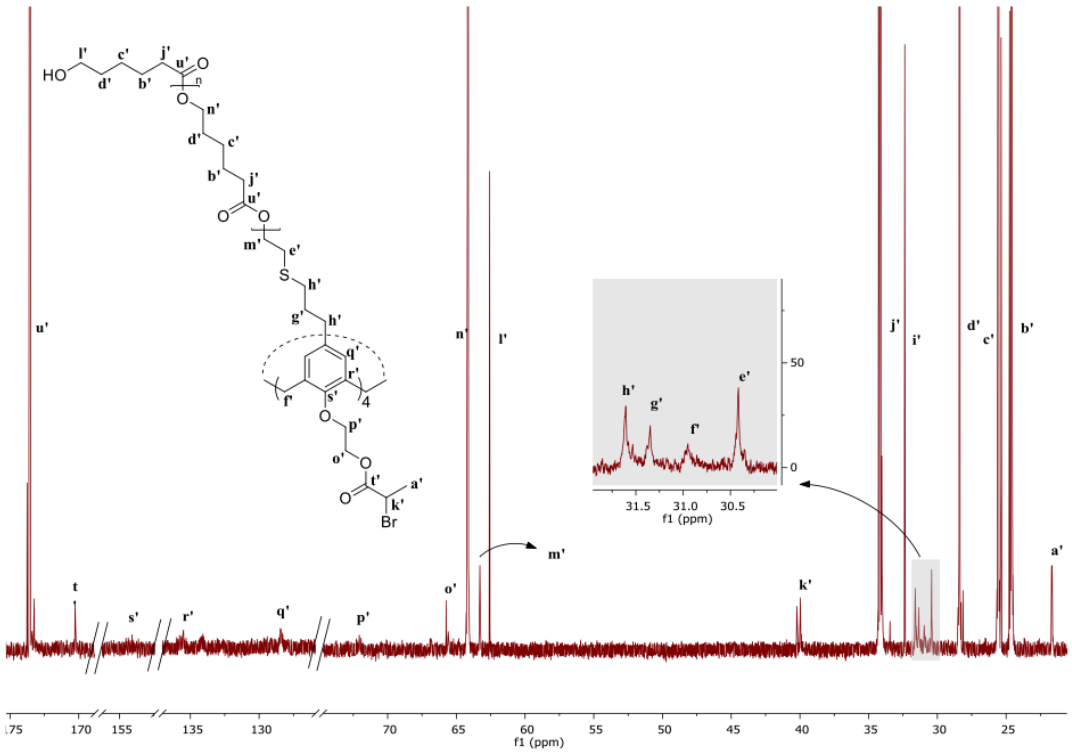

Figure 5.7. ^{13}C NMR spectrum of **17**, in $CDCl_3$.

As expressed previously, from the ^{1}H NMR spectrum (Fig. 5.3), resonance **q** had its integral set to eight, with the **DP** of the PCL being determined with respect to this value. From the ^{1}H NMR (Fig. 5.3), comparing the integrals of resonance **q** to **a**, the M_n was calculated to be 8.7 x 10^3 g mol^{-1}. Each ε-caprolactone unit has a molecular weight of 114.14 g mol^{-1}, therefore the total number of units in the PCL is 76, thus if the length of each arm was equal, 76 total units corresponds to a **DP** of 19 per arm. To further characterise **17**, size exclusion chromatography (SEC) was performed. The chromatogram is shown in Figure 5.8.

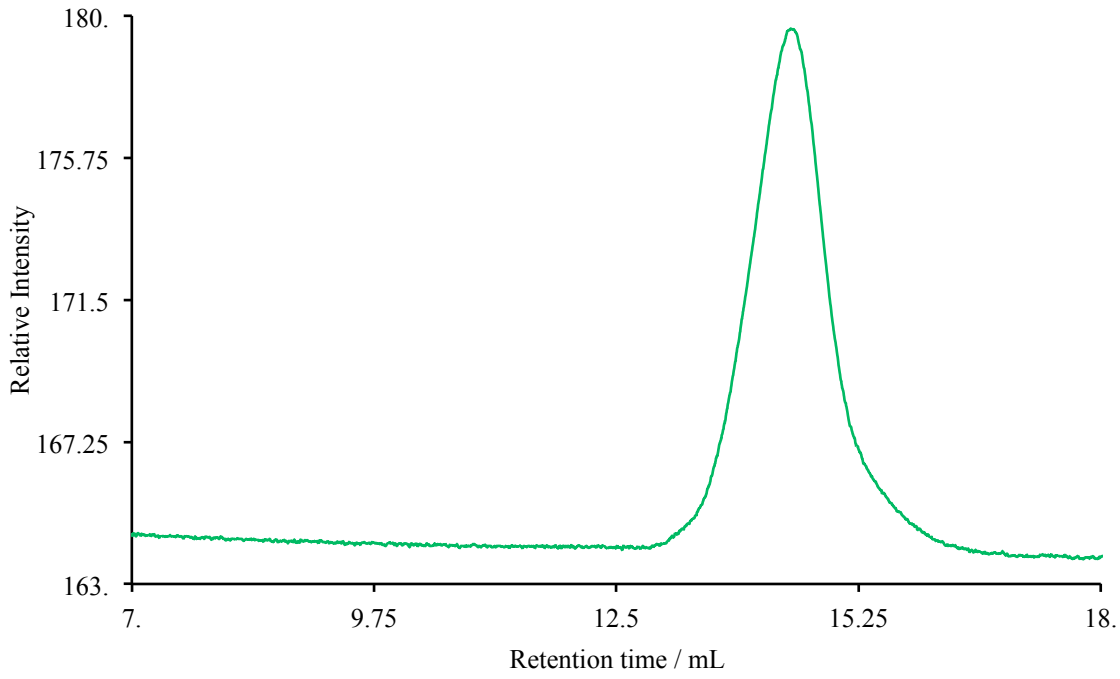

Figure 5.8. SEC chromatogram of **17**, using THF as the eluent at 1 mL min^{-1} and the molecular weights determined with respect to polystyrene standards.

The SEC chromatogram (Fig. 5.8) shows a uniform distribution at 14.42 mL. Using a conventional calibration method (polystyrene standards), the M_n and a M_w were calculated to be 4.4 x 10^3 g mol^{-1} and 5.5 x 10^3 g mol^{-1}, respectively. The M_n calculated from the SEC is approximately half of what was calculated through ^{1}H NMR spectroscopy. The large discrepancy is due to SEC's inability to measure the molecular weight of star polymers using a conventional calibration accurately. The hydrodynamic volume of a star polymer is less than that of a linear polymer with the same molecular weight, thus the molecular weight of a star polymer is underestimated. The dispersity, Đ, was calculated to be 1.25. The relatively low Đ indicates that there was good control over the polymerisation and that the **DP** of each arm is likely to be equal, ~19 units per arm. Table 5.1 illustrates the theoretical and measured molecular weights and dispersity measured.

Table 5.1. Characterisation of **17**.

Sample	**M_n(theo) g mol^{-1}**	**M_n(NMR) g mol^{-1}**	**M_n(SEC) g mol^{-1}**	**Đ**
17	9.2 x 10^3	8.7 x 10^4	4.4 x 10^3	1.25

17 was further characterised by differential scanning calorimetry (DSC) and thermogravimetric analysis (TGA); the results are shown in Figures 5.9 and 5.10 respectively. The DSC (Fig. 5.9) shows that **2** exhibited an endotherm (melting transition, T_m) and an exotherm (crystallisation transition, T_c) at 50.27 ^oC and 24.40 ^oC, respectively. The degree of crystallinity (%X) was calculated according to equation 1.[4]

$$\%X = 100(\Delta H_c / \Delta H_{co}) \qquad (1)$$

Where ΔH_c is the enthalpy of crystallinity and ΔH_{co} is the standard enthalpy of crystallinity for PCL, which is 139.5 J g^{-1}.[5] %X was calculated to be 19.65%. It is reported that neat linear PCL has a %X of 46.72%.[4] Thus, the star architecture of **2** has reduced the crystallinity of PCL, which is likely to be a resultant of the packing fashion of the PCL, as not all the arms can line up in an orderly fashion, and additionally the calixarene core will have an effect on the packing of the material.

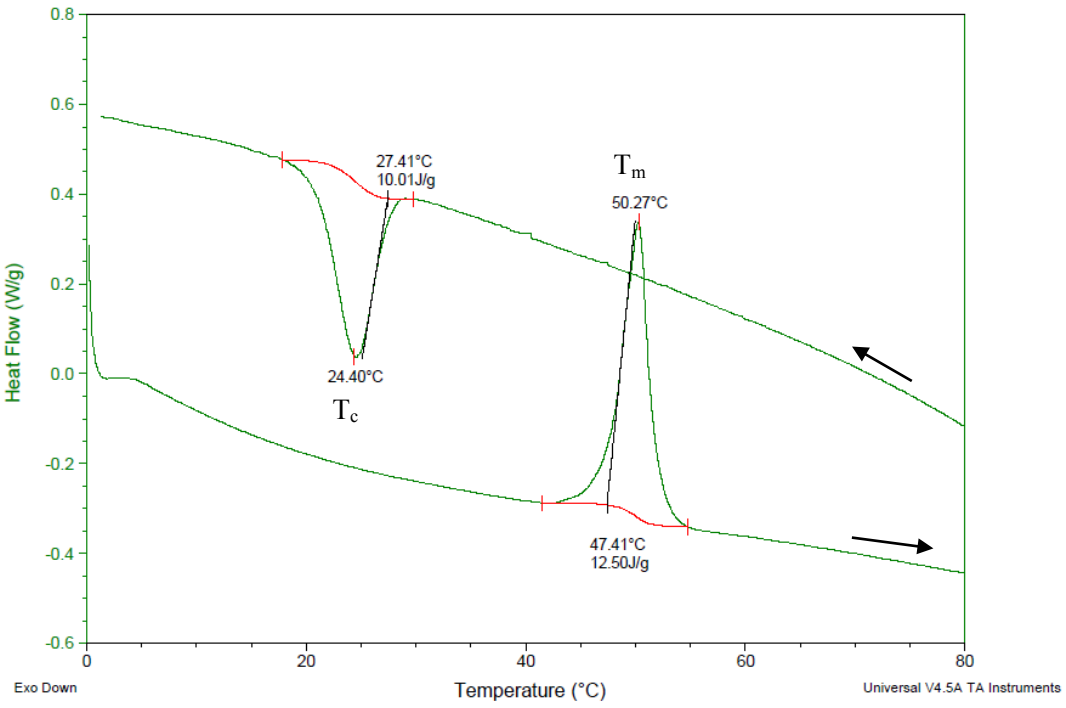

Figure 5.9. DSC of **17**, run in N_2 gas, with a flow rate of 30 mL min^{-1} and a heating rate of 10 ^oC min^{-1}.

The TGA thermogram (Fig. 5.10) shows **17** has two distinct thermal events corresponding to the decomposition of PCL.

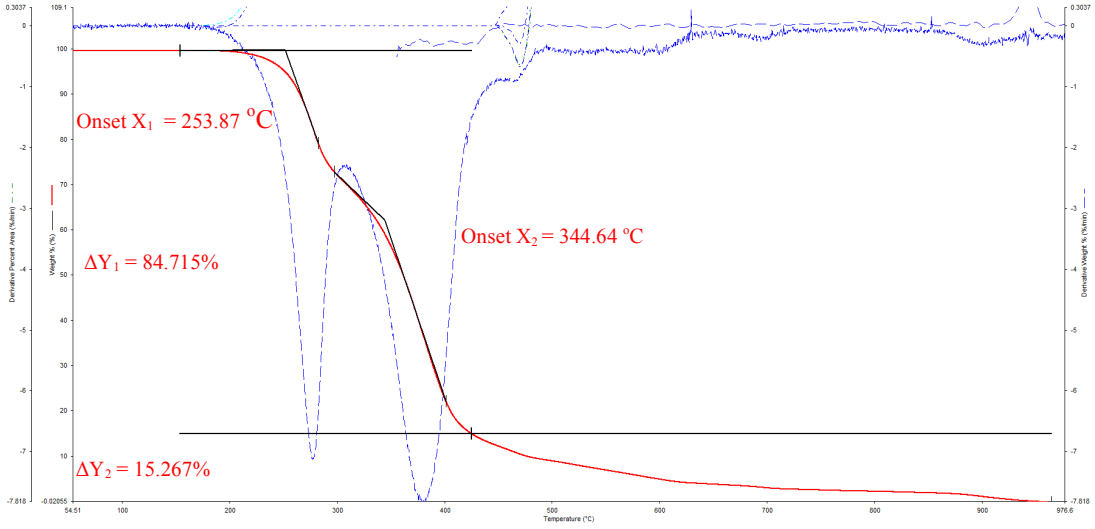

Figure 5.10. TGA of **17**, run in N_2 gas with a heating rate of 10 °C min^{-1}. Red line = TGA trace, blue dashed line = first derivative.

The first (X_1) and second (X_2) thermal events of the decomposition of PCL had onsets of 253.87 °C and 344.64 °C, respectively. As discussed previously in section 3.2, two distinct thermal events are observed due to a thermal degradation that involves a double mechanism.[6] The first degradation process implies a statistical rupture of the PCL chains *via* ester pyrolysis reaction. The produced products of the ester pyrolysis are H_2O, CO_2 and 5-hexenoic acid. A first derivative was calculated (blue dashed line, Fig. 5.10), which indicates the point of the greatest rate of change; two inflection points were observed, clearly showing the two degradation processes for PCL. The percentage of PCL was calculated to be 84.715% (ΔY_1). A ΔY_2 was calculated to be 15.267%, starting from 425.14 °C, which corresponds to the percentage of calixarene. The calixarene exhibited a gradual degradation from 424.14 °C up to 951.70 °C. The first derivative shows there is no clear single inflection point for the degradation of calixarene core. The ^{1}H NMR spectrum (Fig. 5.3) indicates that there are 76 units to the PCL per calixarene core, therefore a M_n ratio of 8700:1612, which corresponds to 84.67% PCL and 15.64% calixarene core. From TGA, looking at ΔY_1 and ΔY_2, the percentages of PCL and calixarene core were calculated to be 84.715% and 15.267% respectively, which is in good agreement with what is calculated from ^{1}H NMR.

5.2.2. Amphiphilic A4B4 Miktoarm Star polymer, 18 - 20

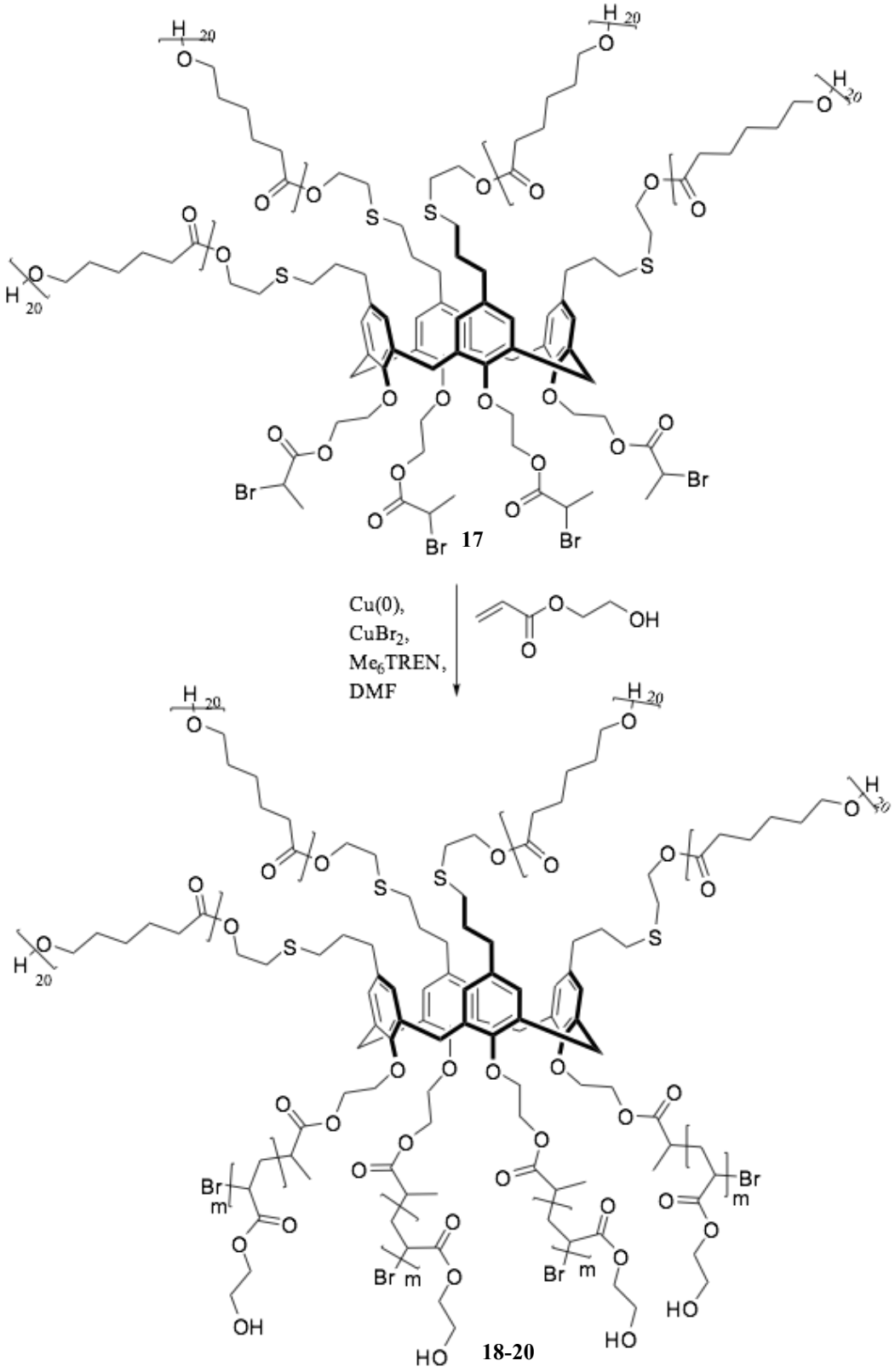

Scheme 5.2. SET-LRP of HEA using **17**.

The synthesis of an amphiphilic A_4B_4 Miktoarm star polymer was carried out *via* a copper(0) mediated radical polymerisation, SET-LRP, using **17** macroinitiator (Scheme 5.2). The hydrophilic monomer utilised was 2-hydroxylethyl acrylate (HEA). The reaction used activated copper wire in the presence of the multidentate amine ligand, Me_6TREN, in the aprotic polar solvent DMF. 5% of $CuBr_2$ was added to the reaction system to give control at the early stages of the reaction due to Cu(II) ability to act as a deactivator as discussed in the introduction (Chapter 1). A monomer (X) to initiator to $CuBr_2$ to ligand ratio of X:1:0.05:0.18 was used to target various PHEA molecular weights of 4.2 x 10^3 g mol^{-1} to 17.6 x 10^4 g mol^{-1}, therefore a **DP** of 9 - 38 HEA per arm. The various polymers have been fully analysed and the results are discussed below.

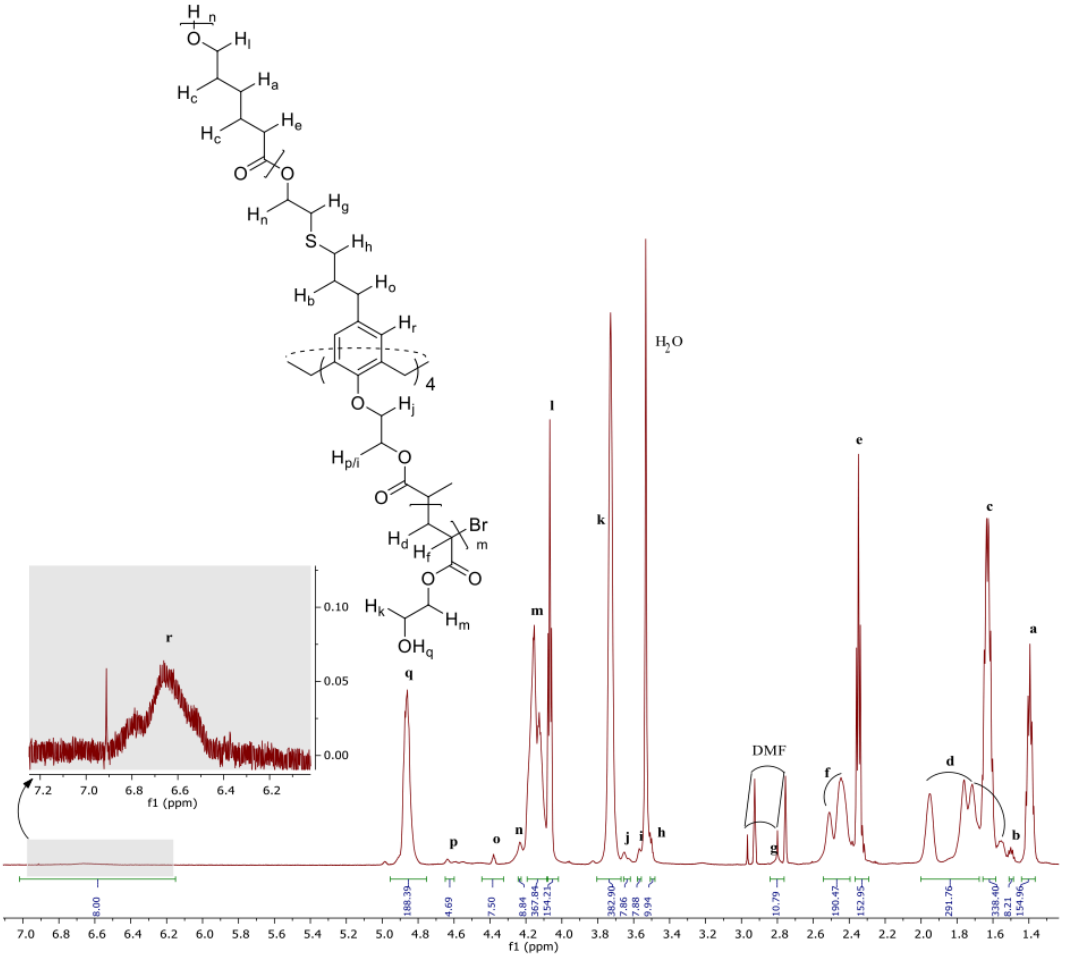

Figure 5.11. ^{1}H NMR spectrum of **20**, in DMF-d_7.

The ^{1}H NMR spectrum (Fig. 5.11) shows the resonances of the calixarene initiator aromatic CH protons, with a multiplet observed at 6.41-6.95, **r**, corresponding to H_r.

The multiplet multiplicity is observed due to the many different rotational conformations of the calixarene core present. **r** had its integral value set to eight, with the **DP** of the PHEA being determined with respect to this value. Additionally, the **DP** of the PHEA could be determined from comparing its integral with respect to **a**, corresponding to H_a of the PCL, as the chain length is known as discussed in 5.2.1. The ^{1}H NMR spectrum (Fig. 5.11) shows the resonances for the PCL backbone protons **a**, **c**, **e** and **l**. A quintet resonance with an integral of 155 is observed at 1.39 ppm, **a**, corresponding to the hydrogen atoms of the PCL on the third carbon atom with respect to the carbonyl carbon, H_a. A multiplet resonance is observed at 1.62 ppm, **c**, corresponding to the methylene hydrogen atoms of the PCL on the second and fourth carbon atoms with respect to the carbonyl carbon, H_c. A triplet resonance with an integral of 153 is observed at 2.34 ppm, **e**, corresponding to the methylene hydrogen atoms of the PCL on the first carbon atom with respect to the carbonyl carbon, H_e. A triplet resonance with an integral of 154 is observed at 4.06 ppm, **l**, corresponding to the methylene hydrogen atoms of the PCL backbone on the fifth carbon atom with respect to the carbonyl carbon, H_l. The remaining unassigned resonances were assigned using a combination of 1D and 2D NMR spectroscopy techniques and are explained herein. The ^{1}H NMR spectrum (Fig. 5.11) shows a multiplet resonance at 1.49 ppm, **b**. The COSY NMR spectrum (Fig. 5.12) shows **b** exhibiting a coupling with a multiplet resonance at 3.50 ppm, **h**, and in turn **h** exhibits coupling to a resonance at 4.38 ppm, **o**. Resonances **b**, **h** and **o** correspond to the hydrogen atoms of the *tetra(*3-oxyetherethyl)thioether-propanyl moiety, with **b** corresponding to the protons on the second carbon atom along of the propylene unit of the *tetra(*3-oxyetherethyl)thioether-propanyl moiety with respect to the aromatic ring, H_b, whereas **o** and **h** correspond to the protons on the first and third carbon atoms along of the propylene unit of the *tetra(*3-oxyetherethyl)thioether-propanyl moiety with respect to the aromatic ring, H_o and H_h, respectively (Fig. 5.11). The ^{1}H NMR spectrum (Fig. 5.11) shows a multiplet resonance between 1.54 – 2.00 ppm, **d**. The COSY NMR spectrum (Fig. 5.12) shows **d** exhibiting a coupling with a multiplet between 2.38 – 2.54 ppm, **f**. Resonances **d** and **f** correspond to the methine and methylene protons of the PHEA backbone. To ascertain which protons belong to which resonance the HSQC NMR spectrum must be referred too, and is discussed later. The ^{1}H NMR spectrum (Fig. 5.11) shows a broad resonance, which is overlapped by a DMF satellite resonance at 2.81 ppm, **g**. The COSY NMR

spectrum (Fig. 5.12) shows **g** exhibiting coupling to a resonance at 4.23 ppm, **n**, and in turn the HMBC spectrum (Fig. 5.14) shows **n** exhibiting coupling to the ^{13}C NMR carbonyl resonance of the PCL backbone at 174.0 ppm, **p'**, therefore ^{1}H NMR resonances **g** and **n** correspond to the ethylene protons of the ethylene unit of the *tetra(*3-oxyetherethyl)thioether-propanyl moiety, with **n** corresponding to the protons adjacent to the oxygen and **g** corresponding to the protons next to the sulfur, H_n and H_g respectively (Fig. 5.11). The ^{1}H NMR spectrum (Fig. 5.11) shows a resonance at 3.56 ppm, **i**.

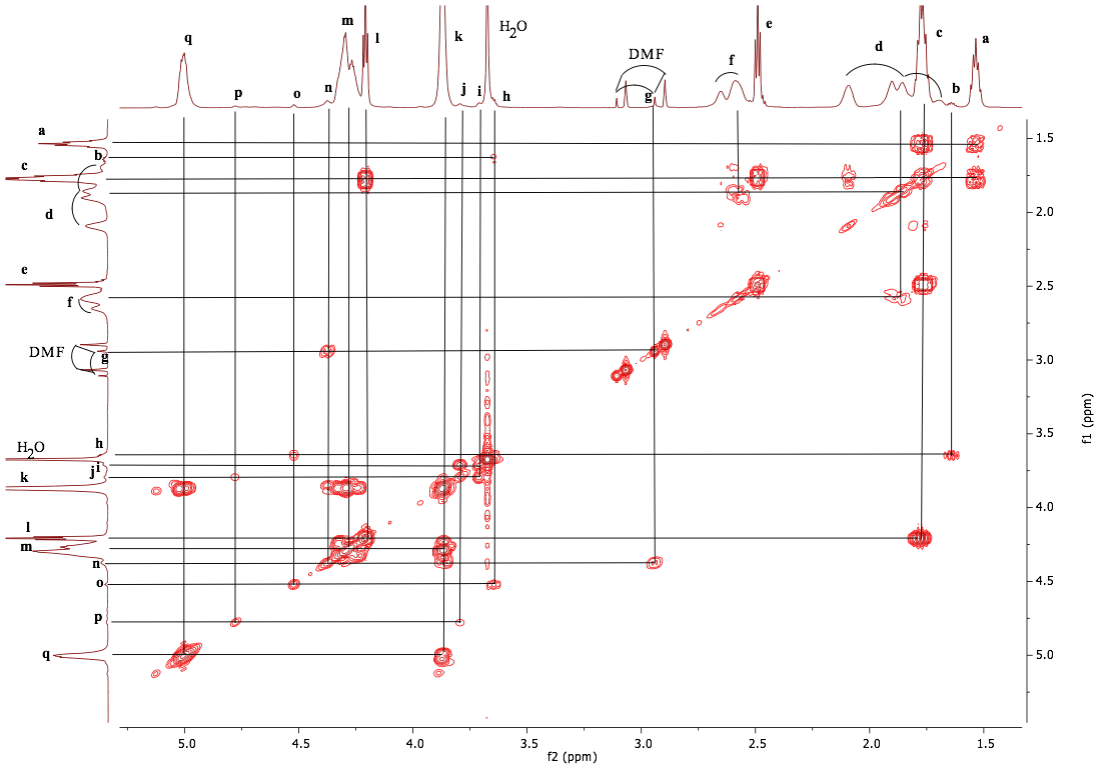

Figure 5.12. COSY NMR spectrum of **20**, in DMF-d7.

The COSY NMR spectrum (Fig. 5.12) shows resonances **i** exhibiting a coupling with a resonance at 3.65 ppm, **j**. **j** additionally exhibits coupling to a resonance at 4.63 ppm, **p**. **j** corresponds to one set of ethylene protons of the ethyl ether 2-bromopropanoate moiety, H_j, and **i** and **p** correspond to the same set of protons of the ethyl ether 2-bromopropanoate moiety, $H_{i/p}$. Two different resonances are observed corresponding to $H_{i/p,}$ which are likely to be due to various conformations present of the same functional group brought about by the size of the polymers and additionally the conformational freedom of the calixarene core. The hydrogen atoms corresponding to $H_{i/p}$ are likely to be split due to the different conformations of the

calixarene core as well as the position of the polymer chain with respect to the calixarene core, which in turn alter the electronics of the environment as depicted in Figure 5.13.[7]

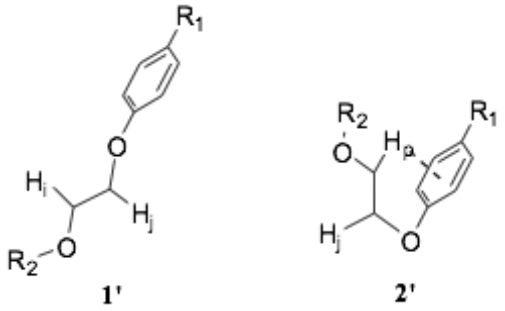

Figure 5.13. Possible interactions leading to different chemical environments, therefore resonances **i**, **1'**, and **p**, **2'**,are observed in the ^{1}H NMR spectrum (Fig. 5.11).

The ^{1}H NMR spectrum (Fig. 5.11) shows a broad singlet resonance with an integral of 382 at 3.73 ppm, **k**. The COSY NMR spectrum (Fig. 5.12) shows **k** exhibiting coupling with a multiplet resonance at 4.14 ppm, **m**, and a singlet at 4.86 ppm, **i**. **k** has an integral of 382 and **q** has an integral of 190, therefore **q** corresponds to the proton of the hydroxyl moieties of the PHEA, H_q, and **k** and **m** correspond to the ethylene protons of the ethylene ether hydroxyl moiety of the PHEA. To determine the exact assignment of resonances **k** and **m** the HMBC spectrum must be referred to.

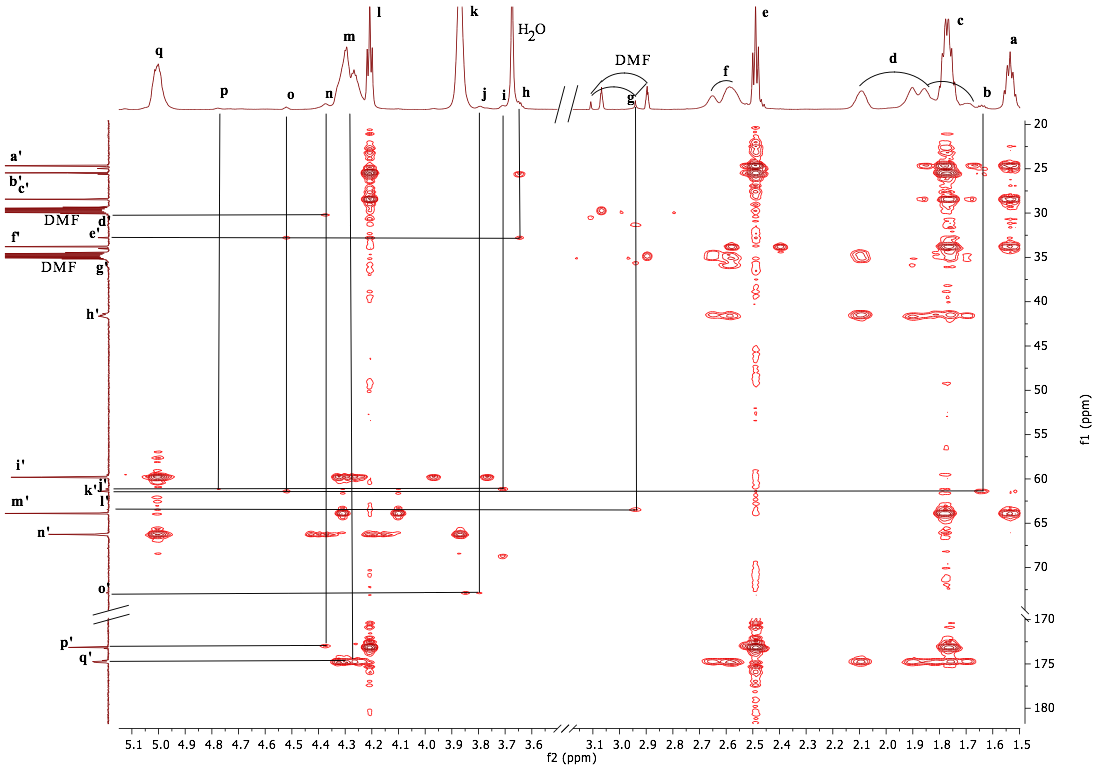

Figure 5.14. HMBC NMR spectrum of **20**, in DMF-d7.

The HMBC NMR spectrum (Fig. 5.14) shows **m** coupling to a ^{13}C NMR resonance at 176.0 ppm, **q'**, where **q'** corresponds to the carbon atom of the carbonyl of the PHEA, therefore **m** corresponds to the ethylene protons of the 2-hydroxyl ethyl closest to the carbonyl, H_m (Fig. 5.11) and **k** must correspond to the ethylene protons closest to the hydroxyl moiety, H_k (Fig. 5.11). Using HSQC NMR spectroscopy the carbon atoms directly attached to hydrogen atoms could be easily assigned, although, due to the low concentration of calixarene core, not all ^{13}C NMR resonances were observed.

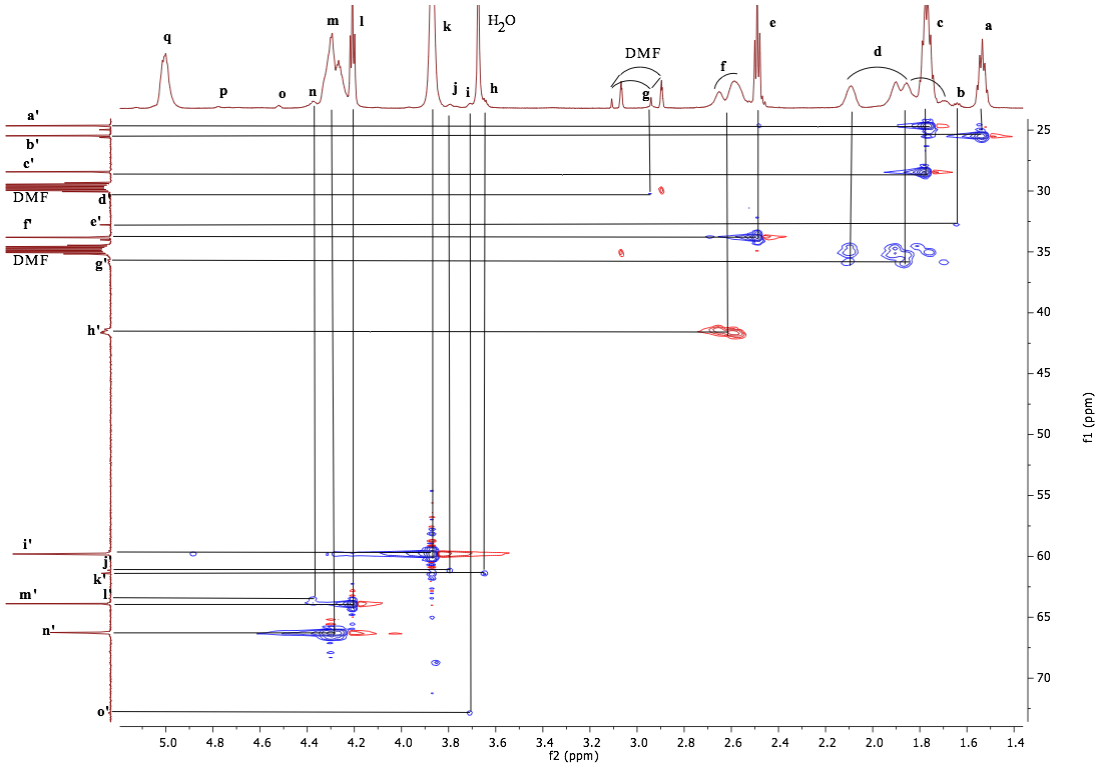

Figure 5.15. HSQC NMR spectrum of **20**, in DMF-d_7.

The HSQC NMR spectrum (Fig. 5.15) shows **a** coupling to a ^{13}C NMR resonance at 26.3 ppm, **b'**, corresponding to the third carbon atom along the PCL chain with respect to the carbonyl carbon atom. Resonance **b** exhibits coupling to a ^{13}C NMR resonance at 33.6 ppm, **e'**, corresponding to the second carbon atom along of the propylene unit of the *tetra*(3-oxyetherethyl)thioether-propanyl moiety with respect to the aromatic ring. Resonance **c** exhibits coupling to two ^{13}C NMR resonances at 24.5 ppm, **a'**; and 29.3 ppm, **c'**; corresponding to the second and fourth carbon atoms along of the PCL chain with respect to the carbonyl carbon atom, respectively. Resonance **d** exhibits coupling to a ^{13}C NMR resonance at 36.6 ppm, **g'**, corresponding to the methylene carbon atom of the PHEA backbone. The phasing of the **d-g'** coupling (blue) corresponds to a methylene environment, confirming that **c** corresponds to H_d (Fig. 5.11). The HSQC NMR spectrum (Fig. 5.15) shows resonance **e** coupling to a ^{13}C NMR resonance at 34.6 ppm, **f'**, corresponding to the methylene carbon atom of the PCL of the first carbon atom with respect to the carbonyl carbon. Resonance **f** exhibits coupling to a ^{13}C NMR resonance at 42.3 ppm, **h'**, corresponding to the methine carbon atom of the PHEA backbone. The phasing of the **f-h'** coupling (red) corresponds to a methine environment, confirming that **f** corresponds to H_f (Fig. 5.11). The HSQC NMR spectrum (Fig. 5.15) shows

resonance **g** coupling to a ^{13}C NMR resonance at 30.9 ppm, **d'**, corresponding to the carbon atom next to the sulfur of the *tetra*(3-oxyetherethyl)thioether-propanyl moiety. Resonance **h** exhibits coupling to a ^{13}C NMR resonance at 62.2 ppm, **k'**, corresponding to the third carbon atom along of the propylene unit of the *tetra*(3-oxyetherethyl)thioether-propanyl moiety with respect to the aromatic ring. Resonance **i** exhibits coupling to a ^{13}C NMR resonance at 73.7 ppm, **o'**, corresponding to the ethylene carbon atom next to the ester of the ethyl ether 2-bromoproanoate moiety. Resonance **j** exhibits coupling to a ^{13}C resonance at 62.0 ppm, **j'**, corresponding to the ethylene ether linker carbon atom of the ethyl ether 2-bromoproanoate moiety. Resonance **k** exhibits coupling to a ^{13}C NMR resonance at 60.7 ppm, **i'**, corresponding to the ethylene carbon atoms of the PHEA closest to the hydroxyl moiety. Resonance **l** exhibits coupling to a ^{13}C NMR resonance at 64.8 ppm, **m'**, corresponding to the fifth methylene carbon atom along of the PCL backbone with respect to the carbonyl carbon. Resonance **m** exhibits coupling to a ^{13}C NMR resonance at 67.1 ppm, **n'**, corresponding to the ethylene carbon atom of the PHEA of the 2-hydroxyl ethyl moiety closest to the carbonyl. Resonance **n** exhibits coupling to a ^{13}C NMR resonance at 64.3 ppm, **l'**, corresponding to the carbon atom adjacent to the oxygen of the ethylene unit of the *tetra(*3-oxyetherethyl)thioether-propanyl moiety. Resonances **o** and **p** exhibit no coupling in the HSQC spectrum. As expressed earlier, due to low concentration of calixarene core relative to PCL and PHEA, the complete characterisation of the ^{13}C NMR spectra could not be completed, but what could be assigned is shown in Figure 5.16.

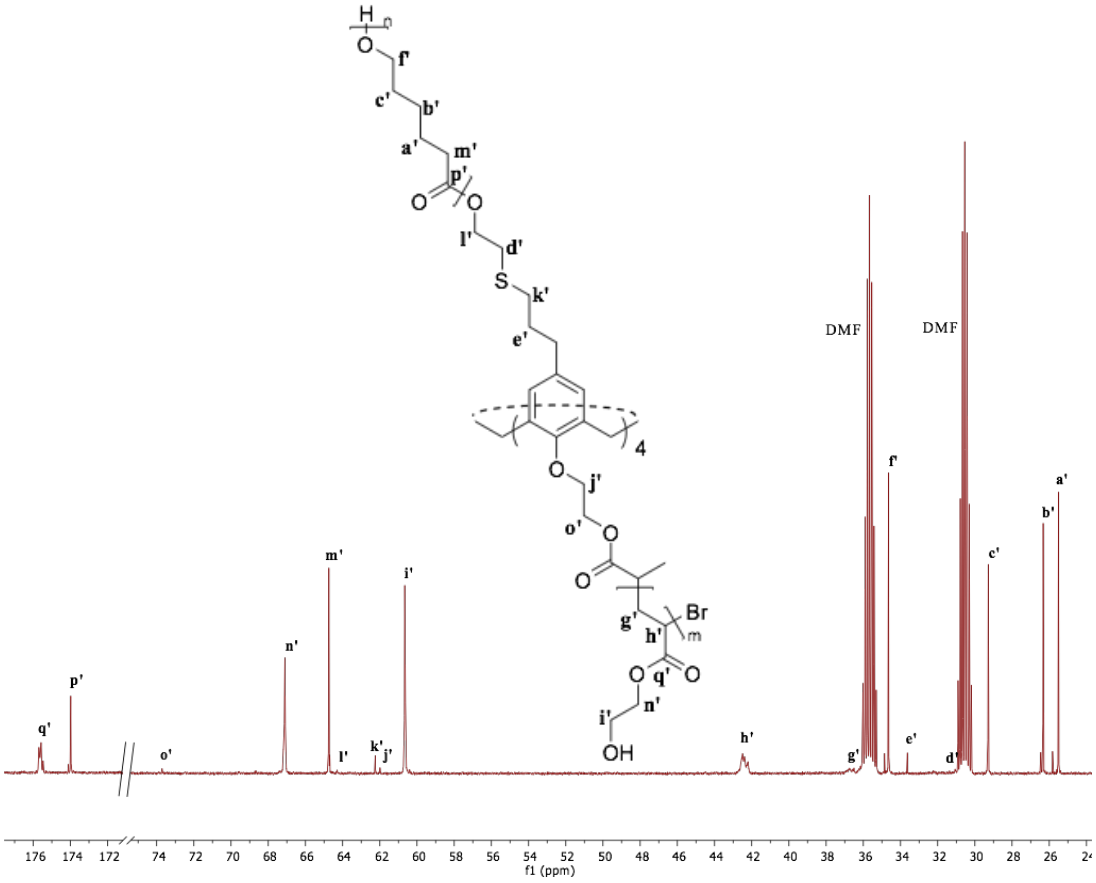

Figure 5.16. ^{13}C NMR spectrum **20**, in DMF-d_7.

As expressed previously, various molecular weights of PHEA were targeted, 4.2 x 10^3 g mol^{-1}, 8.8 x 10^3 g mol^{-1} and 17.6 x 10^4 g mol^{-1}, corresponding to **DP** of 9, 19 and 38 HEA per arm respectively. Resonance **r** (Fig. 5.11) had its integral value set to eight, with the **DP** of the PHEA being determined with respect to this value. Figure 5.17 shows overlaid ^{1}H NMR spectra corresponding to the three polymer systems, with the spectra being normalised with respect to resonance **a** (Fig. 5.17). For the targeted molecular weight of 4.2 x 10^3 g mol^{-1}, the M_n of the PHEA of 5.0 x 10^3 g mol^{-1} was calculated from the ^{1}H NMR (Fig. 5.11), which corresponds to a **DP** of ~11 units per arm. The total molecular weight of miktoarm star polymer was calculated to be 13.7 x 10^4 g mol^{-1}, **18**. The conversion obtained for the reaction was 92%. For the targeted molecular weight of 8.8 x 10^3 g mol^{-1}, the M_n of the PHEA of 1.2 x 10^4 g mol^{-1} was calculated from the ^{1}H NMR (Fig. 5.11), which corresponds to a **DP** of ~25 units per arm. The total molecular weight of miktoarm star polymer was calculated to be 2.1 x 10^4 g mol^{-1}, **19**. The conversion obtained for the reaction was 95%. For the targeted molecular weight of 1.8 x 10^4 g mol^{-1}, the M_n of the PHEA of 2.2 x 10^4 g mol^{-1} was calculated from the ^{1}H NMR (Fig. 5.11), which corresponds to a **DP** of ~48 units per arm. The total molecular weight of miktoarm star polymer was

calculated to be 3.1 x 10^4 g mol^{-1}, **20**. The conversion obtained for the reaction was 96%.

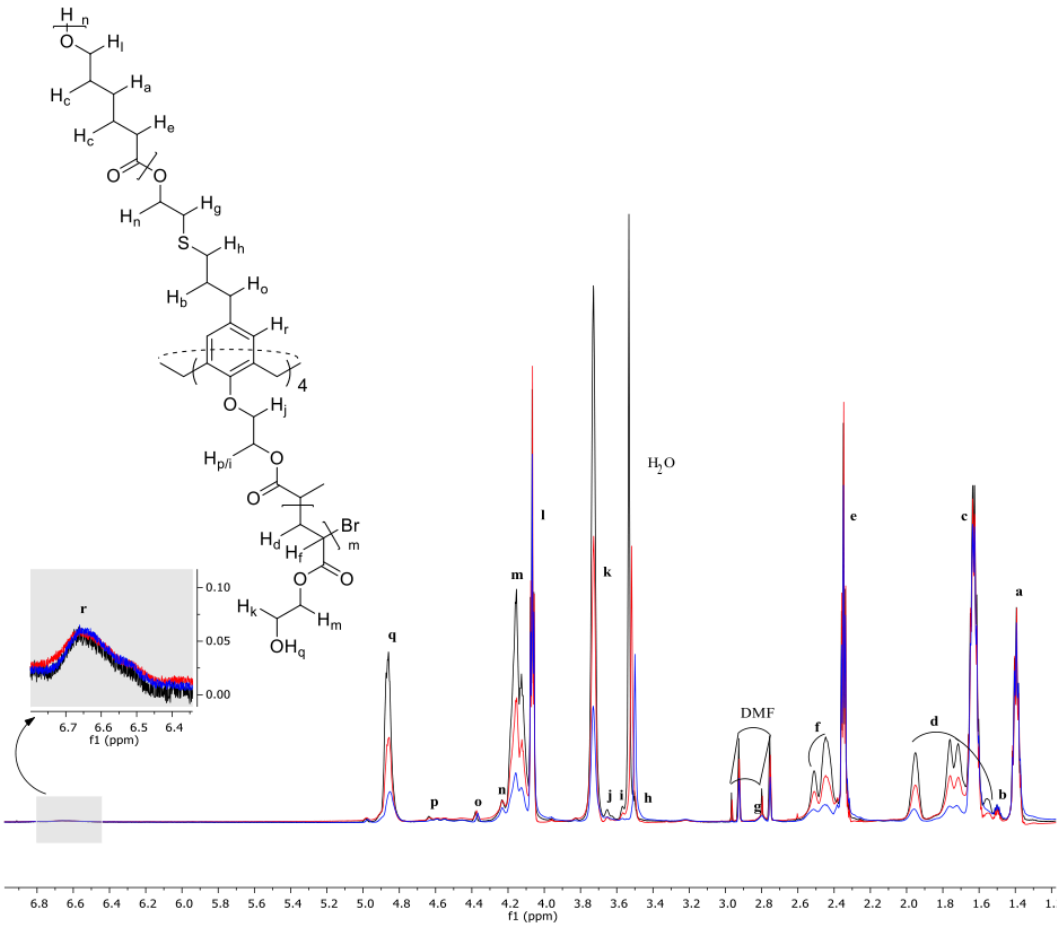

Figure 5.17. ^{1}H NMR overlaid spectra corresponding to various of HEA, blue = **18**, red = **19** and black = **20**, in DMF-d7.

To further characterise the polymer systems, **18**, **19** and **20**, SEC was carried out. A chromatogram of the three miktoarm star polymers and the linear calixarene PCL initiator**,** **17**, is shown in Figure 5.18.

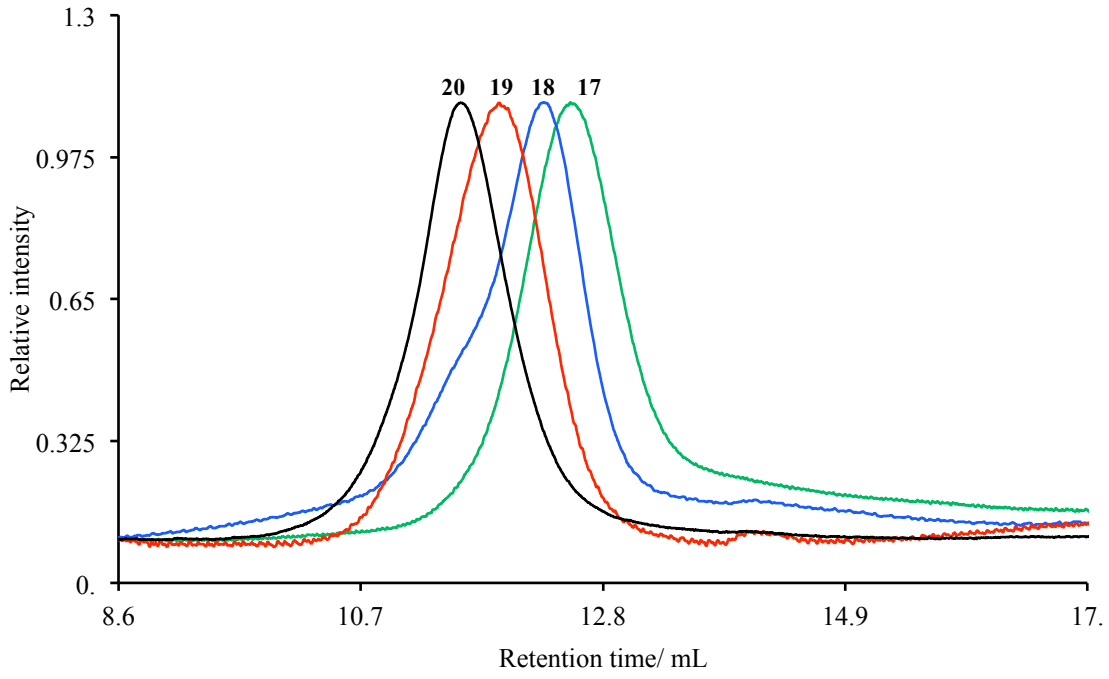

Figure 5.18. SEC chromatogram of green = **17**, blue = **18**, red = **19** and black = **20**, using DMF as the eluent at 1 mL min^{-1} and the molecular weights determined with respect to PEG standards.

The SEC chromatogram (Fig. 5.18) shows a uniform distribution at 12.53 mL (green), corresponding to the **17** initiator as discussed in section 5.2. A relatively uniformed distribution is observed at 12.28 mL (blue), corresponding to **18**, which has a shoulder at the lower retention volume of 11.62 mL. Using a conventional calibration method (polyethylene glycol), the M_n and M_w were calculated to be 1.3 x 10^4 g mol^{-1} and 1.6 x 10^4 g mol^{-1}, respectively. The Đ was calculated to be 1.23. The low dispersity indicates that there was good control over the polymerisation and that the **DP** of each arm is likely to be equal. A uniformed distribution is observed at 11.92 mL (red), corresponding to **19**. Using a conventional calibration method (polyethylene glycol), the M_n and M_w were calculated to be 1.6 x 10^4 g mol^{-1} and 2.1 x 10^4 g mol^{-1} respectively. The Đ was calculated to be 1.32. The low dispersity indicates that there was good control over the polymerisation and that the **DP** of each arm is likely to be equal. A uniformed distribution is observed at 11.56 mL (black), corresponding to **20**. Using a conventional calibration method (polyethylene glycol), the M_n and M_w were calculated to be 2.0 x 10^4 g mol^{-1} and 2.9 x 10^4 g mol^{-1} respectively. The Đ was calculated to be 1.45. The Đ indicates that there was reasonable control over the polymerisation and that the **DP** of each arm is likely to be approximately equal. It is observed that as the **DP** increases so does Đ. The

increased Đ is likely to be a result of trapped active sites. The PCL chains are flexible, which could lead to the encapsulation of calixarene core active sites within the macroinitiator structure, away from the catalyst, thus the rate of propagation would be greater than initiation.[8,9] In each sample, the M_n calculated *via* SEC is approximately half to two thirds of that calculated *via* ^{1}H NMR spectroscopy. The large discrepancy is attributed to the hydrodynamic volume of the star polymer, which is much less than that of an analogous linear polymer, thus SEC greatly underestimates the size of star polymers. Table 5.2 illustrates the theoretical and measured molecular weights and dispersities measured.

Table 5.2. Characterisation of polymers.

Sample	M_n(theo) g mol^{-1}	M_n(NMR) g mol^{-1}	M_n(SEC) g mol^{-1}	Đ
17	9.2 x 10^3	8.7 x 10^4	4.4 x 10^3	1.25
18	1.3 x 10^4	1.4 x 10^4	1.3 x 10^4	1.23
19	1.8 x 10^4	2.1 x 10^4	1.6 x 10^4	1.32
20	2.7 x 10^4	3.1 x 10^4	2.0 x 10^4	1.45

DSC analysis was carried out with the traces shown in Figure 5.19.

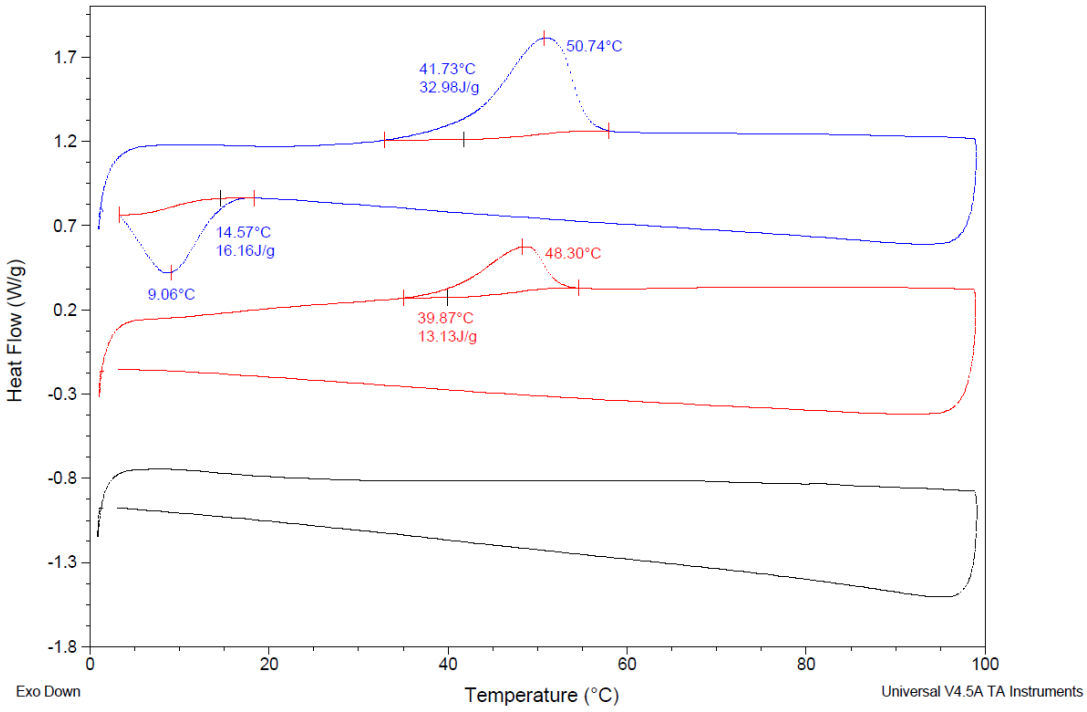

Figure 5.19. DSC of blue = **18**, red = **19** and black = **20**, run in N_2 gas, with a flow rate of 30 mL min^{-1} and a heating rate of 10 ^oC min^{-1}.

The DSC traces (Fig. 5.19) show that as the percentage of PHEA increased, so did the amorphous nature of the polymer system. Only **18** exhibited a T_m and T_c, with the %X calculated to be 11.68%, which is approximately half of that calculated for the **17** (Fig. 5.9). **19** exhibited a T_m at 48.30 ^oC but no T_c. A DSC of **19** was carried out again to a lower temperature, but no T_c was observed. A plausible explanation is that there is not significant time during the cooling process (10^oC min^{-1}) for chains to orientate themselves in order to crystallise. **20** exhibited no exo- or endo-therm, indicating the material is solely amorphous in nature. The large amount of PHEA has interrupted the packing of the PCL chain to such an extent that there is no order to the packing of the material. TGA analysis was further carried out on all three samples, with the traces shown in Figure 5.10.

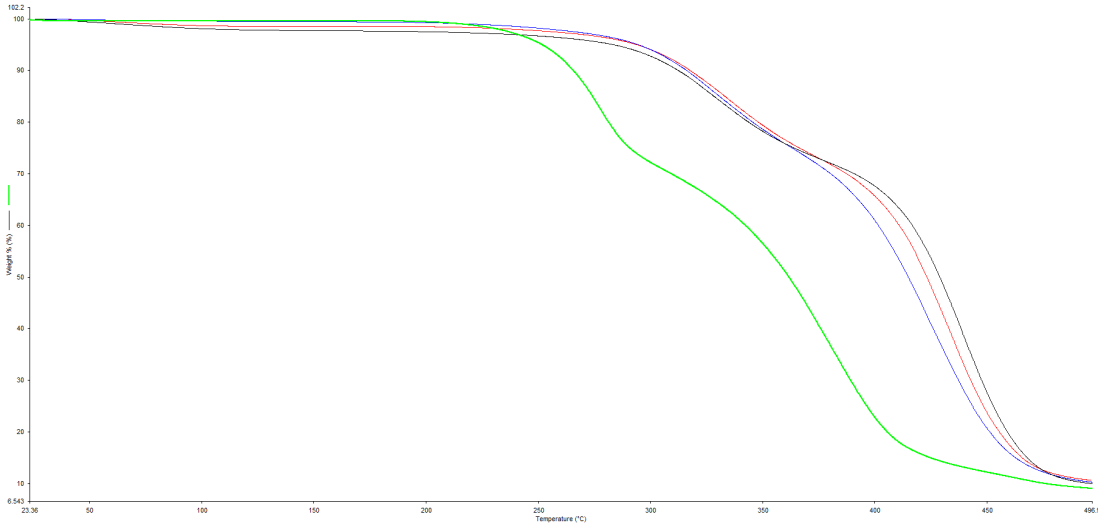

Figure 5.20. TGA of green = **17**, blue = **18**, red = **19** and black = **20**, run in N_2 gas with a heating rate of 10 ^oC min^{-1}.

The TGA thermogram (Fig. 5.20) shows **18** (blue), **19** (red) and **20** (black) all exhibiting two distinct thermal events with the first thermal event (X_1) occurring at 292.16 ^oC, 292.47 ^oC and 293.11 ^oC and the second thermal event (X_2) occurring at 396.09 ^oC, 405.82 ^oC and 412.30 ^oC, respectively. The TGA thermogram (Fig. 5. 20) showed that incorporation of PHEA significantly increased the thermal stability of the system, with the first onset of decomposition occurring at an increase of 35 ^oC relative to **17** (green). Once the PHEA is incorporated into the system the X_1 does not increase, but the X_2 does increase as the M_n of PHEA increases. TGA-MS was carried out and the ions produced matched what is reported in the literature, indicating the thermal stability of the PCL has increased.[6] The increased stability is likely to be brought about by hydrogen bonding between the PHEA hydroxyl moieties and the ester moieties of the PCL. For all three samples with the PHEA incorporated into the system there is a less distinctive thermal event occurring from the loss of water from 22 ^oC to 100 ^oC, with the greater M_n of PHEA the greater the mass loss. In all three cases the ΔY_1 was calculated to be ~89%, thus suggesting the ΔY_2 was ~11%, and further to this the weight loss percentage did not go to 0% up to the temperature limit of 1000 ^oC. The ^1H NMR spectrum (Fig. 5.11) indicated that for **18** there were 76 units of PCL and 44 units of HEA per calixarene core, therefore a M_n ratio of 13,700:1612, which corresponds to 89.47% polymer and 10.52% calixarene core. For **19** and **20** the M_n ratio from ^1H NMR was calculated to be 21,000:1612 and 31,000:1612, which corresponds to 92.87% and 95.01% polymer

and 7.13% and 4.94% calixarene core, respectively. What is calculated from ^{1}H NMR does not agree with the percentages obtained through TGA. The TGA of the miktoarm system appears to be inadequate to give the exact ratio of calixarene core to polymer.

5.3. Conclusion

Compound **16** was used to synthesise a novel 4-armed PCL star polymer with a calixarene core, **17**, which could be further used as a macroinitiator for copper(0) mediated polymerisation due to the alkyl halide moieties remaining in the calixarene core. **17** was fully characterised *via* 1D and 2D NMR spectroscopy techniques, SEC chromatography, DSC and TGA. The M_n determined *via* ^{1}H NMR spectroscopy was 8.7 x 10^3 g mol^{-1}, indicating the **DP** was 76, which is equivalent to 19 units per arm, which agreed with the calculated theoretical M_n. SEC calculated a M_n of 4.4 x 10^3 g mol^{-1}, which is approximately half of that calculated *via* ^{1}H NMR spectroscopy. The large discrepancy is due to the hydrodynamic volume of star polymers being much less than their linear analogue, which is not taken into account when using SEC with a conventional calibration method. The Đ calculated was 1.25 suggesting there was good control over the polymerisation. From the DSC, a T_m and T_c were calculated to be 50.27 ^{o}C and 24.40 ^{o}C respectively, and a % crystallinity of 19.65% was calculated. The TGA trace showed two distinct thermal events corresponding to the two mechanisms in which PCL degrades. The percentage of PCL (ΔY_1) and calixarene core (ΔY_2) was calculated to be 84.715% and 15.267% respectively, which was in agreement with ^{1}H NMR spectroscopy.

Compound **17** was used as a macro-initiator for the SET-LRP of HEA leading to a amphiphilic A_4B_4 Miktoarm star polymer, **18**, **19** and **20**. Compounds **18**, **19** and **20** were fully characterised *via* 1D and 2D NMR spectroscopy techniques, SEC chromatography, DSC and TGA. The M_n determined *via* ^{1}H NMR spectroscopy calculated to be 5.0 x 10^3 g mol^{-1}, 1.2 x 10^4 g mol^{-1} and 2.2 x 10^4 g mol^{-1} corresponding to 11, 25 and 48 HEA units per arm, respectively. The SEC showed good control was maintained over the polymerisation with Đ ranging from 1.23 to

1.45. The DSC showed that as more PHEA was incorporated crystallinity was reduced, to a point where no exotherm was observed and the material was completely amorphous. The TGA for all three samples were similar and showed an increase in thermal stability, which was attributed to hydrogen bonding between the PHEA hydroxyl moieties and the ester moieties of the PCL.

5.4. References

(1) Leng, X. F.; Nguyen, N. H.; van Beusekom, B.; Wilson, D. A.; Percec, V. *Poly. Chem..,* **2013**, *4*, 2995.
(2) Gou, P. F.; Zu, W. P.; Shen, Z. Q. *Acta Polym. Sin.* **2007**, 967.
(3) Jaime, C.; Demendoza, J.; Prados, P.; Nieto, P. M.; Sanchez, C. *J. Org. Chem.* **1991**, *56*, 3372.
(4) Wu, D.; Wu, L.; Sun, Y.; Zhang, M. *J. Poly. Sci. P. B-Poly. Phy.,* **2007**, *45*, 3137.
(5) Pitt, C. G.; Chasalow, F. I.; Hibionada, Y. M.; Klimas, D. M.; Schindler, A. *J Appl. Poly. Sci.,* **1981**, *26*, 3779.
(6) Persenaire, O.; Alexandre, M.; Degee, P.; Dubois, P. *Biomacromolecules* **2001**, *2*, 288.
(7) Inukai, M.; Fukushima, T.; Hijikata, Y.; Ogiwara, N.; Horike, S.; Kitagawa, S. *J. Am. Chem. Soc.* **2015**, *137*, 12183.
(8) Perrier, S.; Haddleton, D. M. *Eur.Poly. J.,* **2004**, *40*, 2277.
(9) Cole, D. P.; Khosravi, E.; Musa, O. M. *J. Poly. Sci. Part A: Poly. Chem.* **2015**, *54*, 3, 335.

Chapter 6

Self-assembly of Amphiphilic A_2B_2 and A_4B_4 Miktoarm Star Polymers

6.0. Introduction

The self-assembly of amphiphilic block copolymers in solution has attracted a vast amount of attention over the past decade due to the resulting structures having a great potential in in a variety of fields: cosmetics, catalysis, separation and most profoundly, drug delivery.[1,2] The self-assembly of amphiphilic polymeric systems can lead to a variety of aggregate morphologies including spheres, cylinders, lamellae and bicontinuous structures.[3] Spherical self-assemblies are known as micelles; they are the most studied morphology due to their ability to provide a platform for drug delivery.[4] In the formation of micelles in aqueous solutions the hydrophobic polymer chains aggregate, forming a core, with the hydrophilic polymer chains extended out to the aqueous environment. The hydrophobic core is shielded by the hydrophilic chains, which reduces the interfacial free energy of the water/polymer system. The driving force of micelle formation is minimizing the interfacial free energy.[5] The minimum concentration of polymer at which micellisation occurs is known as the critical micelle concentration (CMC) (Fig. 6.1).

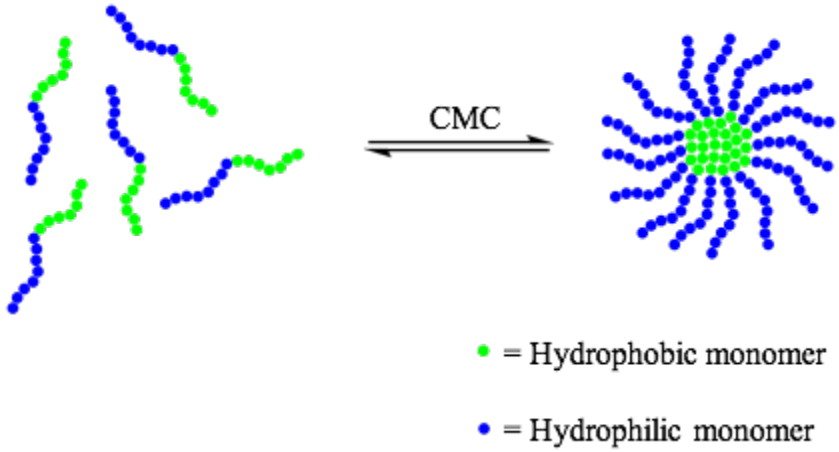

Figure 6.1. Micellisation of amphiphilic polymeric material.

The thermodynamic stability of a polymeric system can be characterised by the CMC. The CMC is related to the thermal energy and the effective interaction energy between the bulk solution and the polymer, with the lower the thermal energy the greater the stability.[6] Polymeric micelles have greater stability relative to their surfactant counterparts due to the many more points of interaction within the chains.

This chapter reports on the self-assembly of A_2B_2 and A_4B_4 amphiphilic miktoarm star polymers **calixarene-A_2B_2starPCL$_{100}$PHEA$_m$**, **8 - 10** (a), where m = 75, 100 and 270, respectively and **calixarene-A_4B_4starPCL$_{20}$PHEA$_m$** , **18 – 20** (b), where m = 10, 25 and 48, respectively (Fig. 6.2) in water.

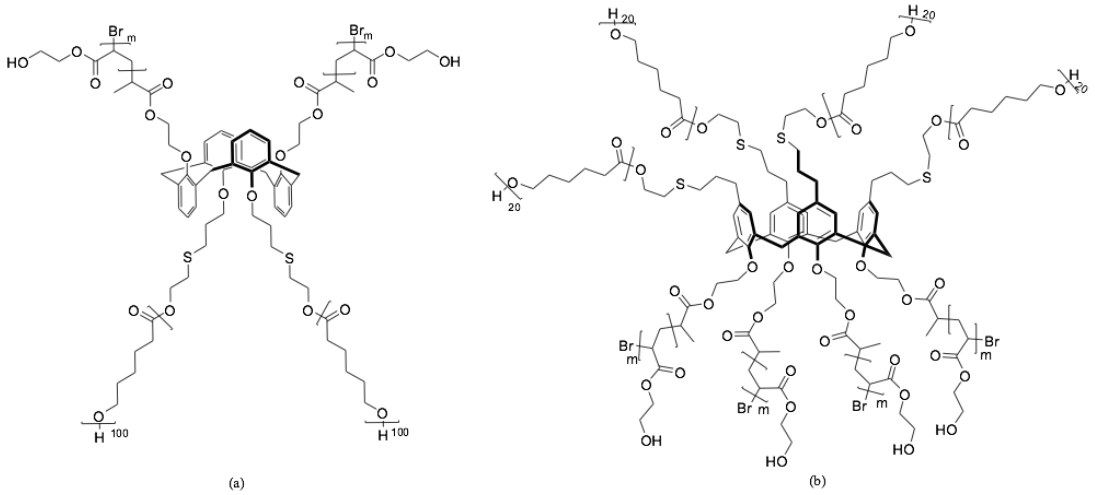

Figure 6.2. A_2B_2 and A_4B_4 amphiphilic miktoarm star polymers (a) **8 -10** and (b) **18 - 20**, respectively.

The morphologies of the polymeric systems are analysed *via* transmission electron microscopy (TEM), which will give evidence for self-assembly and the structure and size of structure produced. TEM is a form of microscopy that involves a thin beam of electrons. Depending on the density, the electrons pass through, scatter or are absorbed as they come into contact with the sample. The electrons that pass through the sample hit a fluorescent screen, which leads to a shadow image of the specimen.[7] TEM is a common technique used to image polymer nanoparticles due to the relative ease by which it can be performed.[8,9] Additionally, the CMC is determined *via* fluorescence spectroscopy by the introduction of the fluorescent probe pyrene.

6.1. Experimental

6.1.1. Materials

The synthesis of A_2B_2, **8 – 10**, and A_4B_4, **18 – 20**, amphiphilic miktoarm star polymers is discussed in sections 3 and 5, respectively. The pyrene probe was purchased from Sigma Aldrich and used without further purification. HPLC grade acetone was purchased from Fischer Scientific and used without further purification.

High-purity (R=18.2 MΩ) water was obtained from Durham University High Purity Water service.

6.1.2. Instrumentation

Transmission electron microscopy (TEM) was carried out using a JEOL 2100F field emission gun TEM (FEG TEM) operating at 200 kV.

All fluorescence measurements were taken at ambient temperature using a HORIBA Jobin-Yvon Fluoromax 2 spectrofluorometer using a quartz cuvette supported on a riser. Prior to any CMC determination experiments, working solutions (1.0 mg mL^{-1}) of miktoarm star polymers were checked for autofluorescence by excitation at 335 nm and monitoring from 350-500 nm in the absence of pyrene.

6.1.3. TEM

Compounds **8 - 10** and **18 – 20**, in high-purity (R=18.2 MΩ) water, at a concentration of 1 mg mL^{-1}, was deposited on a holey carbon grid and blotched with filter paper to remove excess water, then examined in a JEOL 2100F field emission gun TEM (FEG TEM) operating at 200 kV.

6.1.4. CMC spectroscopic measurements

For CMC measurements, stock solutions (1.0 mg mL^{-1}) of **8 - 10** and **18 – 20** were serially diluted across at least two orders of magnitude in high-purity (R=18.2 MΩ) water. Aliquots of these polymer solutions (1.7 cm^3) were transferred into sample vials that had previously been charged with a solution of pyrene (17 μL, 10^{-5}mol dm^{-3} in acetone) that had been allowed to evaporate to give a final concentration of approximately 10^{-7} mol dm^{-3} pyrene in each polymer solution. Solutions were then excited at 335 nm and the emission response measured from 350-500 nm (ex/em slit width= 2nm/2nm). The emission maximum nearest 370 nm was assigned as band 1 (I_1) and that nearest 380 nm as band 3 (I_3). The corrected emission intensity of band 1 was divided by that of band 3 to give the I_1/I_3 value at each concentration.

6.2. Results and Discussion

6.2.1. Calixarene-A_2B_2starPCL$_{100}$PHEA$_m$, 8 - 10

6.2.1.1. TEM Studies

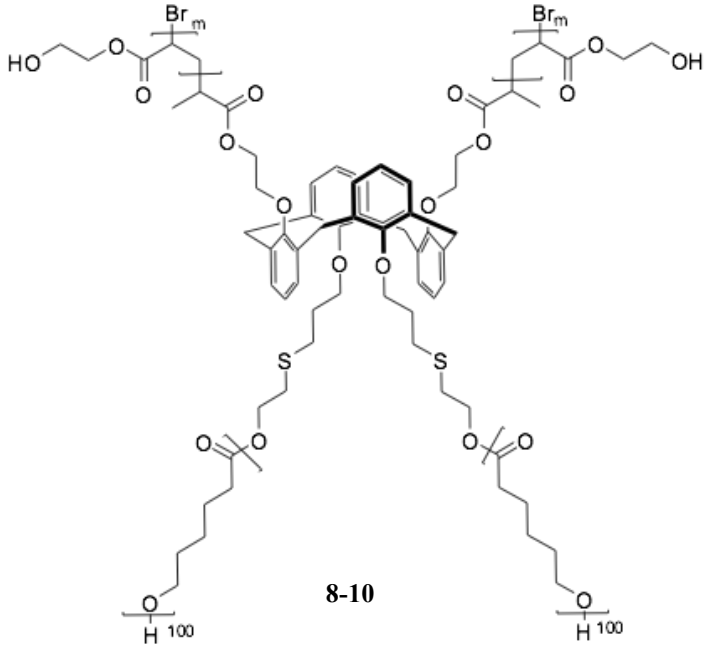

Figure 6.3. Generic structure of **8 - 10**.

Polymer solutions (Fig. 6.3) in high purity water (R=18.2 MΩ) at a concentration of 1 mg mL^{-1} were sonicated for two hours then left to stand overnight. The samples were deposited on a holey carbon grid and blotched with filter paper to remove excess water. The samples were introduced to the TEM and analysed with the results shown in Figure 6.4.

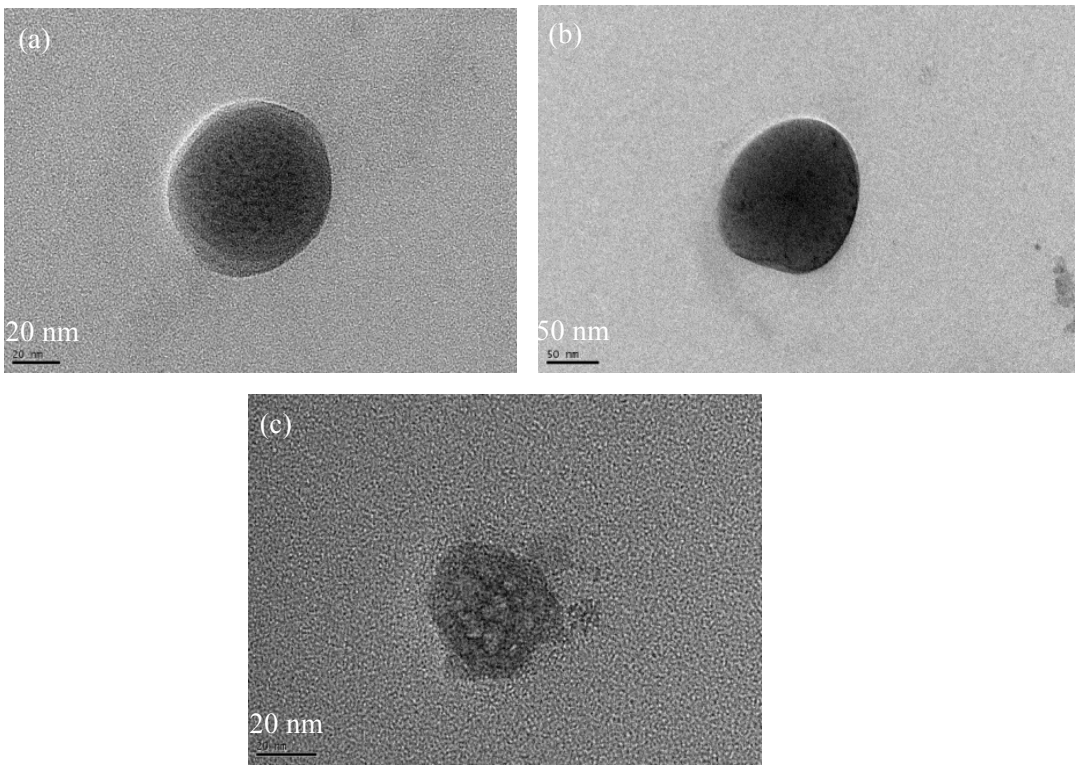

Figure 6.4. TEM images of (a) **8**, (b) **9** and (c) **10** in high purity water (R=18.2 MΩ) at a concentration of 1 mg mL^{-1} deposited on a holey carbon grid.

As can be seen in Figure 6.4, spherical aggregates (micelles) were produced. **8** produced micelles with uniform structures in the range of 90-110 nm (Fig. 6.4, (a)). **9** produced micelles with relatively uniform structures in the range of 82-100 nm (Fig. 6.4, (b)). **10** produced much smaller micelles with relatively uniformed structures, which were in the range of 30-40 nm (Fig. 6.4, (c)). Table 6.1 illustrates the size of micelles corresponding to each polymer.

Table 6.1. Table illustrating the size of the micelles for each polymer sample as determined through TEM.

Polymer sample	PCL DP per arm	PHEA DP per arm	Micelle Size (nm)
8	100	75	90-110
9	100	100	82-100
10	100	270	30-40

It can be concluded from the TEM data that as the proportion of poly(2-hydroxylethyl acrylate) (PHEA) is increased as the size of the micelles decreased,

which is attributed to the enhanced ability of the polymer to shield the nanoparticle core as the hydrophilic nature increased. A greater proportion of hydrophilic polymer will increase the solubility of the polymer as well as lower the polymer diffusion coefficients. This would be expected to increase the particle size, but the fact that in increasing hydrophilic polymer chain length permits each polymer to sterically screen a larger area of the particle surface out ways the other two parameters, i.e. solubility and diffusion coefficients.[10]

6.2.1.2. CMC determination

The CMC can be determined by measuring sharp changes in physical parameters that occur at the CMC. Fluorescence spectroscopy is a very sensitive technique that can measure CMC onsets of ~1 ppm. A fluorescent probe (pyrene, Fig. 6.5) is introduced into the system, which has a tendency to associate into the hydrophobic core of a micelle rather than in the water phase, in doing so the emission spectra changes indicating the encapsulation of the probe.[11]

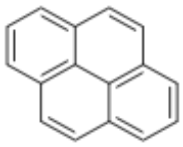

Figure 6.5. Pyrene.

While other fluorescent probes and methods are described in the literature, especially for monomeric surfactants, determination of the molal CMC values for each polymer system was chosen to be through monitoring the intensity of the solvent-sensitive pyrene emission bands as a function of concentration of polymer.[12,13,14] Figure 6.6 illustrates how the pyrene emission bands change as the concentration of amphiphilic polymer increases, thus more pyrene is incorporated into a hydrophobic domain.

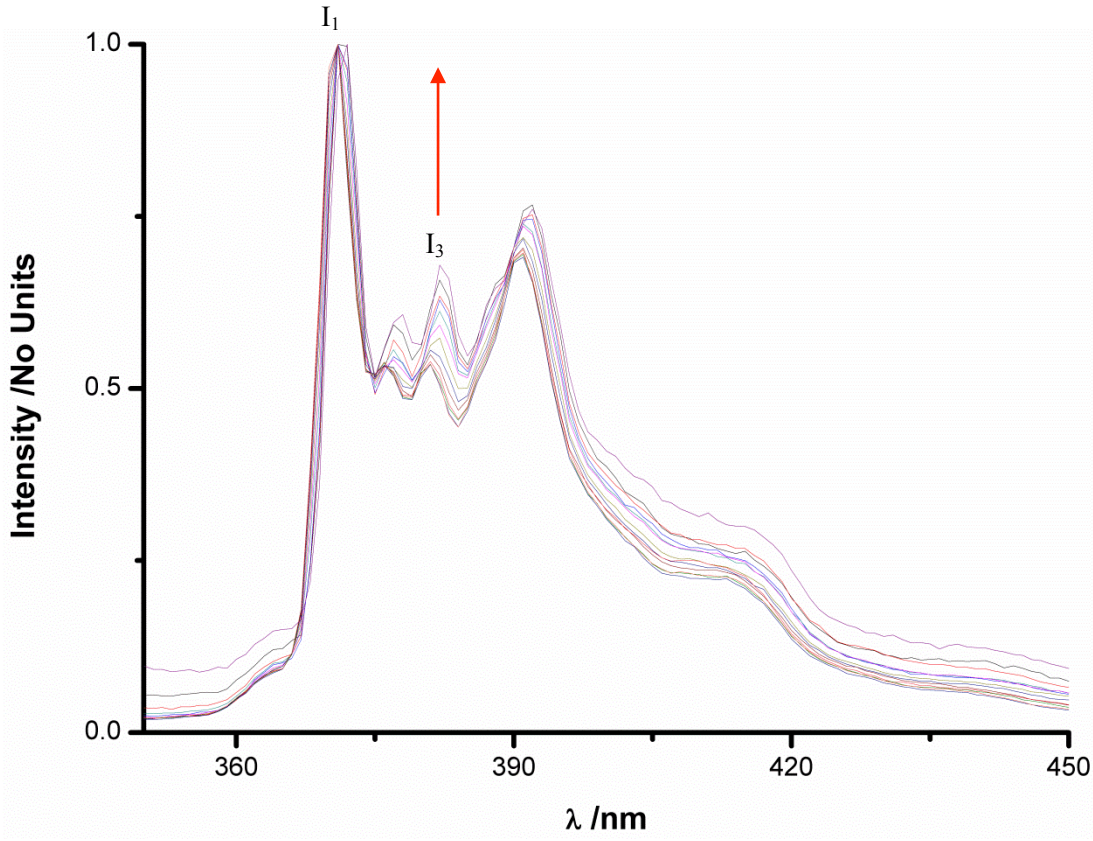

Figure 6.6. Pyrene emission bands on incorporation into a hydrophobic core.

It can been seen from Figure 6.6 that an increase in intensity bands at 379 nm and 383 nm are observed as the amphiphilic polymer concentration is increased indicating the onset of micellisation. To determine the CMC, the relationship of the intensity ratios at 373 nm (I_1) and 383 nm (I_3) are plotted as a function of polymer concentration. The plots of fluorescence intensity ratio I_1/I_3 from pyrene excitation spectra as a function of log concentration of A_2B_2 amphiphilic polymers **8 - 10** are plotted in Figure 6.7.

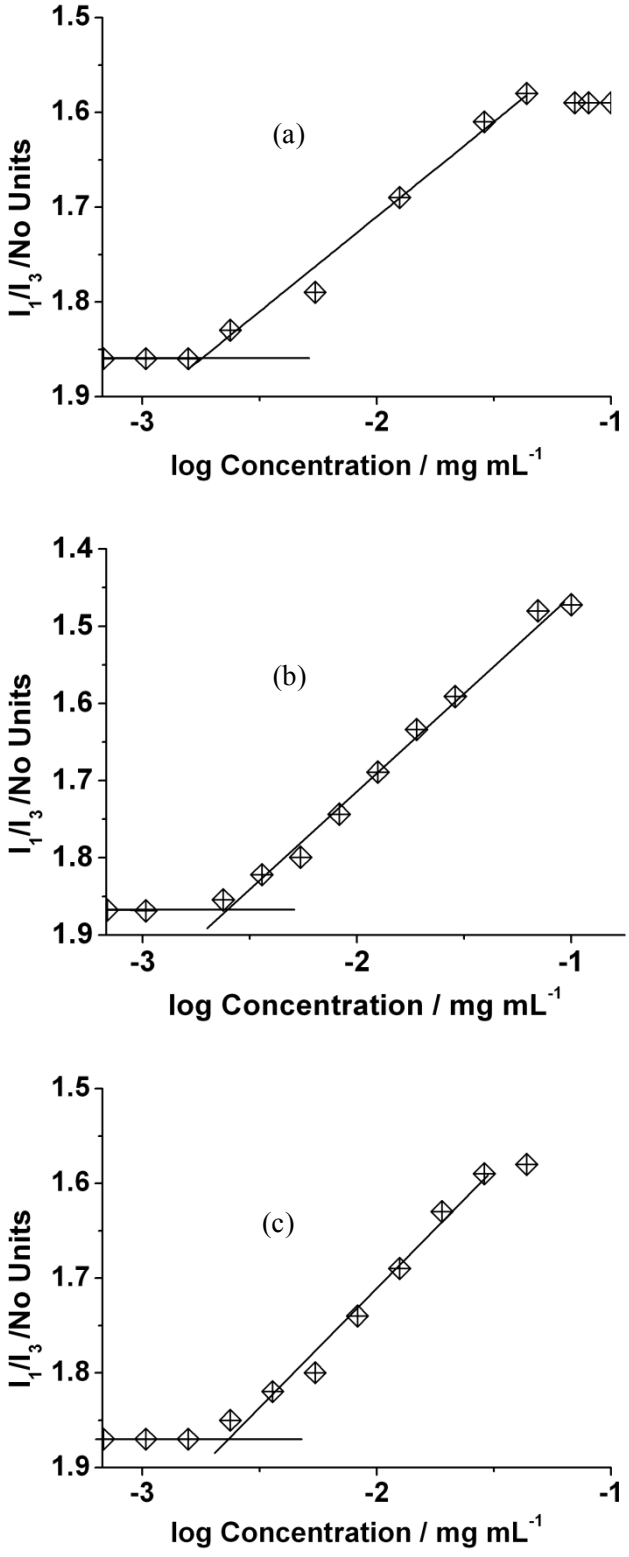

Figure 6.7. Plots of fluorescence intensity ratio I_1/I_3 from pyrene excitation spectra as a function of log concentration of A_2B_2 amphiphilic polymers (a) **8**, (b) **9** and (c) **10**.

Different approaches in the literature implemented for interpreting similar plots were critically assessed to reduce the element of subjectivity.[15,16] It was concluded that breaking the data down into two straight lines, one with a shallow gradient

corresponding to concentration of polymer ([P])<CMC and the other with steeper gradient corresponding to [P]>CMC (Fig 6.7). Plateauing of the I_1/I_3 ratio at high concentration was ignored for the fit. Using a least squares fit, the equations of the lines were determined and then solved *via* a pair of simultaneous equations. The results are presented in Table 6.2.

Table 6.2.CMC values for polymers **8** - **10** (a) corresponds to the pre-aggregated (shallow gradient) component and (b) corresponds to the aggregated (steep gradient) component.

Polymer	Equation 1 (a)	Equation 2 (b)	log(CAC)c	CMC mg L^{-1}
8	$y = 1.86$	$y = -0.200x + 1.31$	-2.75	1.8
9	$y = 0.0055x + 1.89$	$y = -0.252x + 1.21$	-2.64	2.3
10	$y = 1.07e^{-15}x + 1.87$	$y = -0.251x + 1.21$	-2.63	2.3

Table 6.2 shows that the CMC's measured are low and comparable to what is reported in the literature for star polymers (1.35 – 6.53 mg L^{-1}), indicating good thermodynamic stability of micelle produced.[17,18] The three CMC's measured are similar in value indicating that the length of the hydrophilic polymer chain has had little effect on the CMC.

6.2.3. Calixarene-A_4B_4starPCL$_{20}$PHEA$_m$, 18 - 20

6.2.3.1. TEM Studies

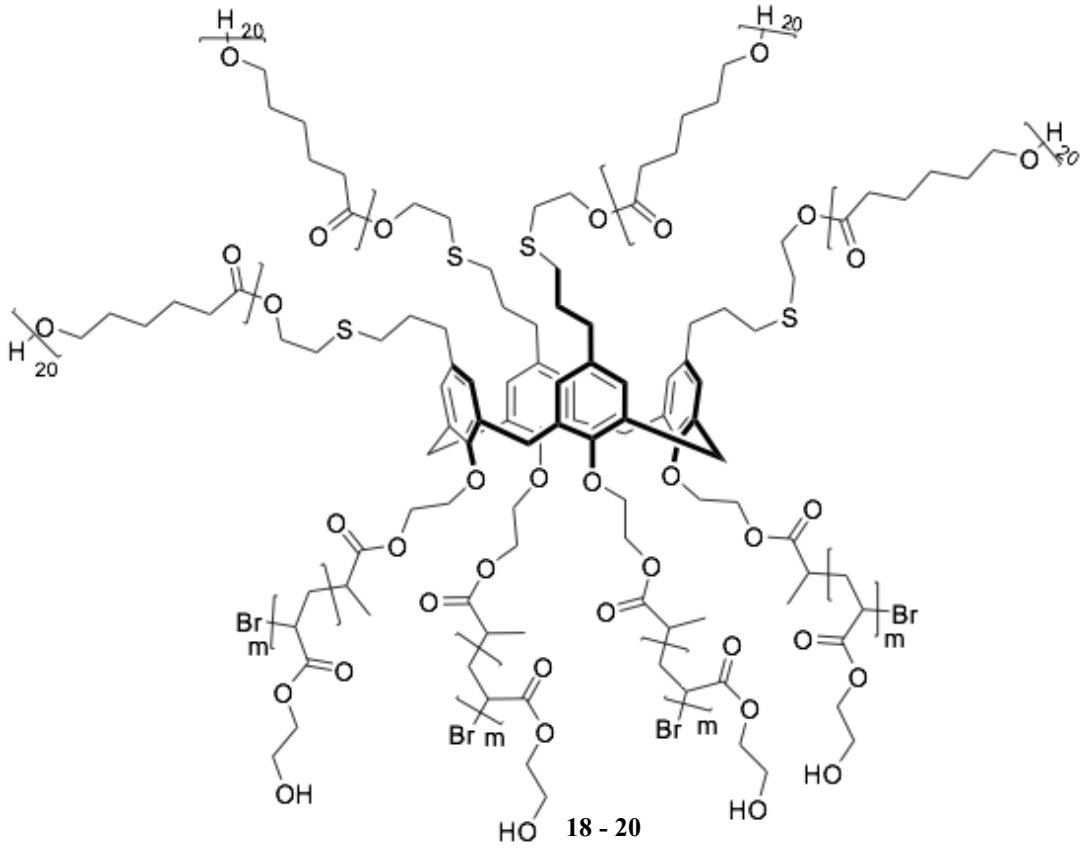

Figure 6.8. Generic structure of 1**8 - 20**.

Polymer solutions (**18** – **20**) in high purity water (R=18.2 MΩ) at a concentration of 1 mg mL^{-1} were sonicated for two hours then left to stand overnight. The samples were deposited on a holey carbon grid and blotched with filter paper to remove excess water. The samples were introduced to the TEM and analysed with the results shown in Figure 6.9.

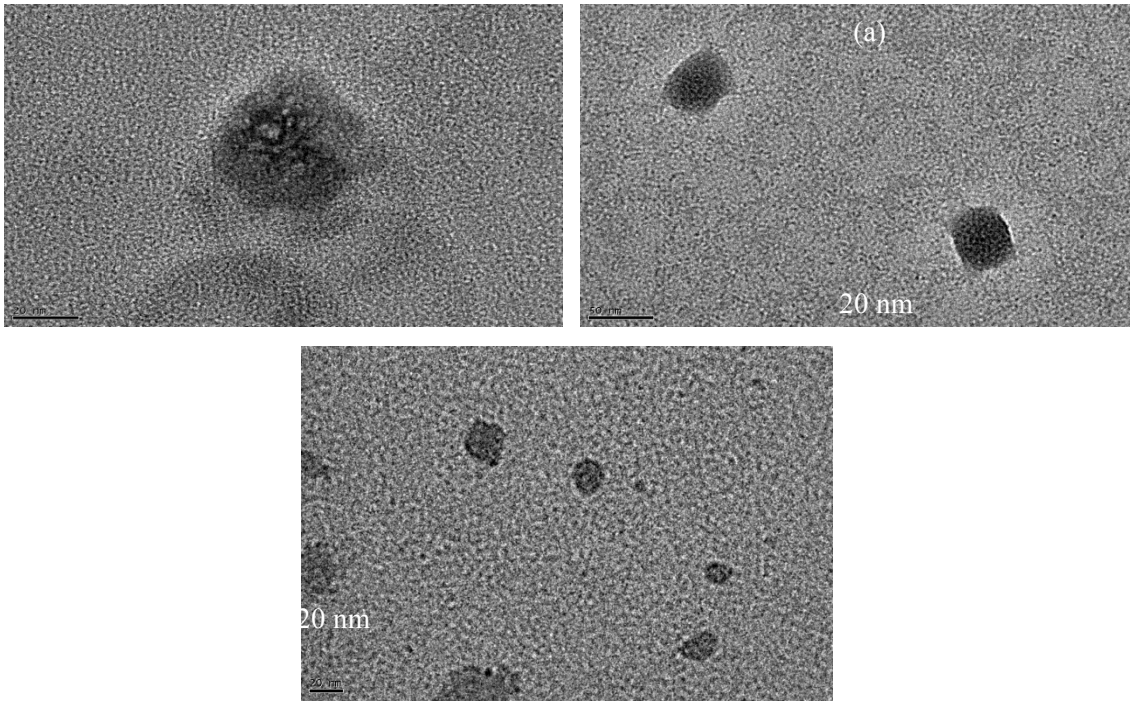

Figure 6.9. TEM images of (a) **18**, (b) **19** and (c) **20** in high purity water (R=18.2 MΩ) at a concentration of 1 mg mL^{-1} deposited on a holey carbon grid.

As it can be seen in Figure 6.9 spherical aggregates (micelles) were produced. **18** produced micelles with relatively uniform structures in the range of 55-68 nm (Fig. 6.9, (a)). **19** produced micelles with relatively uniform structures in the range of 48-55 nm (Fig. 6.9, (b)). **20** produced much smaller micelles with relatively uniform structures but over a greater range of 8-35 nm (Fig. 6.9, (c)). Table 6.3 illustrates the size of micelles corresponding to each polymer.

Table 6.3. Table illustrating the size of the micelles for each polymer sample as determined through TEM.

Polymer sample	PCL DP per arm	PHEA DP per arm	Micelle Size (nm)
18	20	10	55-68
19	20	25	48-55
20	20	48	8-35

As discussed previously it can be concluded from the TEM data that as the proportion of PHEA is increased the size of the micelles decrease, which is attributed to the enhanced ability of the polymer to shield the nanoparticle core as the hydrophilic nature in increased.[10]

6.2.3.2. CMC determination

To determine the CMC, the relationship of the intensity ratios at 373 nm (I_1) and 383 nm (I_3) are plotted as a function of polymer concentration. The plots of fluorescence intensity ratio I_1/I_3 from pyrene excitation spectra as a function of log concentration of A_4B_4 amphiphilic polymers **18 - 20** are plotted in Figure 6.10.

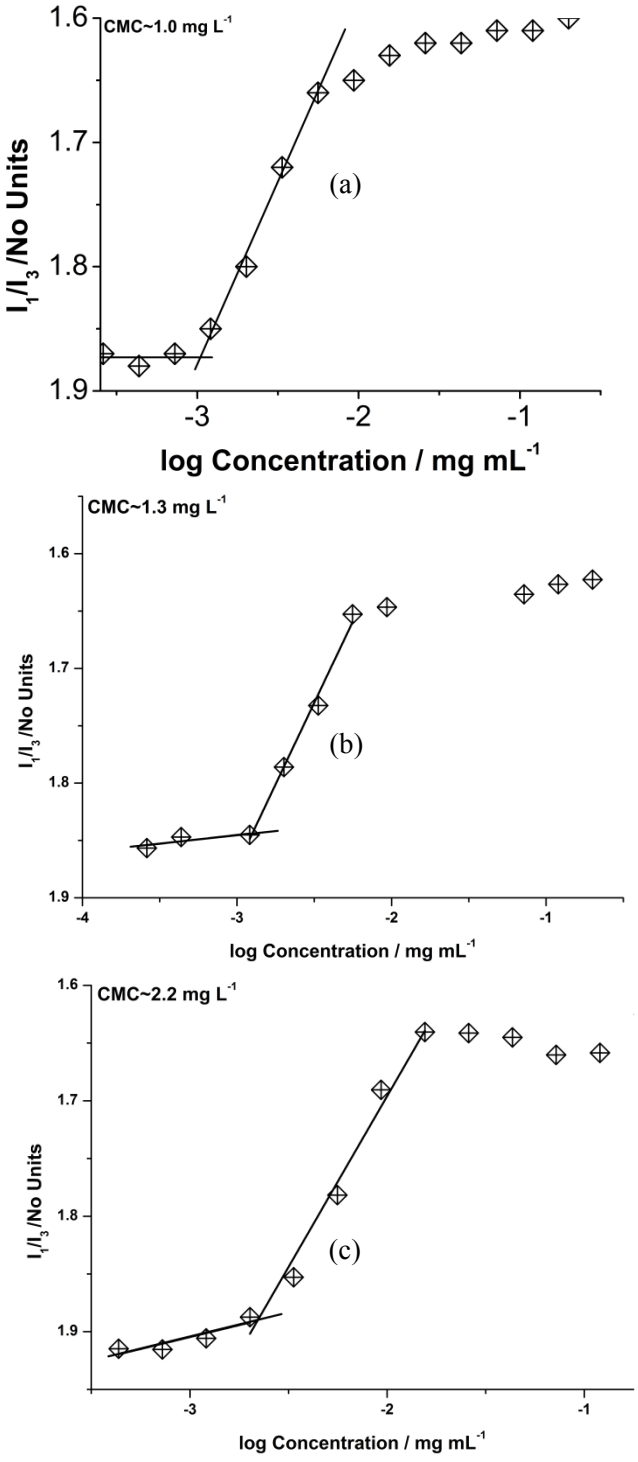

Figure 6.10. Plots of fluorescence intensity ratio I_1/I_3 from pyrene excitation spectra as a function of log concentration of A_2B_2 amphiphilic polymers (a) **18**, (b) **19** and (c) **20**.

Table 6.4. CMC values for polymers **18** – **20** (a) corresponds to the pre-aggregated (shallow gradient) component and (b) corresponds to the aggregated (steep gradient) component

Polymer	Equation 1 (a)	Equation 2 (b)	log(CAC)c	CMC mg L^{-1}
18	$y = 1.8733$	$y = -0.29299x + 1.00021$	-2.98	1.0
19	$y = -0.28449x + 1.01875$	$y = -0.01532x + 1.179929$	-2.90	1.3
20	$y = -0.04142x + 1.78043$	$y = -0.29585x + 1.10435$	-2.66	2.2

Table 6.4 shows that the CMC's measured are low and comparable to what is produced in the literature for star polymers (1.35 – 6.53 mg L^{-1}), indicating good thermodynamic stability of micelle produced.[17,18] The data suggests that as the amount of hydrophilic polymer chain increases (PHEA) so does the CMC. It has previously been reported that the nature and percentage of hydrophobic polymer primarily determines the micalization onset. In the case of **18, 19** and **20** as the length of PHEA increases, the percentage of PCL decreases, thus the CMC in turn increases.[19,20]

6.3. Conclusion

From TEM, for both types of star polymer system, **8 - 10** and **18 - 20**, spherical micelles were produced, with the size of the micelle decreasing as the proportion of hydrophilic PHEA increased. A greater proportion of hydrophilic polymer will increase the solubility of the polymer as well as lower the polymer diffusion coefficients, which would be expected to increase the particle size, but the fact that increasing the hydrophilic polymer length permits each polymer to sterically screen a larger area of the particle surface out weighs the other two parameters.

From the CMC determinations the length of the hydrophilic chain does not appear to have a significant effect on the CMC for **8 - 10**, which contradicts what has been previously published.[17,18] The lack of effect of hydrophilic chain length is attributed to the high dispersity of the polymer chains. For **18 - 20**, the CMC increases as the length of the hydrophilic polymer increases, this is in agreement with the literature.[19,20] For both polymeric systems **8 - 10** and **18 - 20**, low CMC values were determined, which indicates excellent thermodynamic stability of micelle produced. The novel polymeric systems studied have a potential in medical applications, as they form micelles in the range of 5 to 110 nm and have the ability to encapsulate highly hydrophobic material, such as the fluorescent probe pyrene.

6.4. References

(1) Mai, Y. Y.; Eisenberg, A. *Chem. Soc. Rev.,* **2012**, *41*, 5969.
(2) Wang, L.; Liu, G. H.; Wang, X. R.; Hu, J. M.; Zhang, G. Y.; Liu, S. Y. *Macromolecules* **2015**, *48*, 7262.
(3) Park, C.; Yoon, J.; Thomas, E. L. *Polymer* **2003**, *44*, 6725.
(4) Owen, S. C.; Chan, D. P. Y.; Shoichet, M. S. *Nan.Tod.,* **2012**, *7*, 53.
(5) Tados, T. F. *Applied Surfactants: Principles and Applications*; WILEY-VCH Verlag GmbH & Co: Weinheim, 2006.
(6) Zana, R. *Langmuir* **1996**, *12*, 1208.
(7) Michler, G. H. *Electron Microscopy of Polymers*; Springer-Verlag Berlin Heidelberg: Heidelberg, 2008.
(8) Luo, J.; Sun, J.; Huang, J.; Liu, X. Y. *Chem. Eng. J.,* **2016**, *283*, 1118.
(9) Zhang, L. F.; Eisenberg, A. *J. Am. Chem. Soc.* **1996**, *118*, 3168.
(10) Spaeth, J. R.; Kevrekidis, I. G.; Panagiotopoulos, A. Z. *The J. Chem. Phy.* **2011**, *135*, 184903.
(11) Torchilin, V. P. *J. Cont. Rel.,* **2001**, *73*, 137.
(12) Nakahara, Y.; Kida, T.; Nakatsuji, Y.; Akashi, M. *Langmuir* **2005**, *21*, 6688.
(13) Ray, G. B.; Chakraborty, I.; Moulik, S. P. *J. Coll. Inter. Sci.,* **2006**, *294*, 248.
(14) Hira, S. K.; Ramesh, K.; Gupta, U.; Mitra, K.; Misra, N.; Ray, B.; Manna, P. P. *Acs App. Mater. Inter.,***2015**, *7*, 20021.
(15) Aguiar, J.; Carpena, P.; Molina-Bolivar, J. A.; Ruiz, C. C. *J. Col. Inter. Sci.,* **2003**, *258*, 116.
(16) Khan, A. M.; Shah, S. S. *J. Chem. Soc. Pak.,* **2008**, *30*, 186.
(17) Gou, P. F.; Zhu, W. P.; Shen, Z. Q. *Biomacromolecules* **2010**, *11*, 934.
(18) Li, C.; Wang, B.; Liu, Y.; cao, J.; Feng, T.; Chen, Y.; Luo, X. *J. Bio. Sci, Poly Ed.,* **2013**, *24*, 741.
(19) Sezgin, Z.; Yuksel, N.; Baykara, T.; *Eur. J. Pharma. Bio*., **2006**, *3*, 261.
(20) Kim, S. Y.; Shin, L. G.; Lee, Y. M.; Cho, C. S.; Sung, Y. K., *J. Cont. Rel*. **1998**, *51*, 13.

Chapter 7

Summary, Conclusions and Future Work

7.0. Summary and Conclusions

This project involved the development of several novel heterofunctional initiators with a calix[4]arene centre that can facilitate a "core" first method for the synthesis of miktoarm star polymers. *p-tert*-butylcalix[4]arene was selected as a base compound due to its low toxicity, relatively low cost and its ability to facilitate selective functionalisation on both the upper and lower rims of the macrocycle.

Chapter 1 gave an introduction to calixarenes, their synthesis, functionalisation and uses in polymer chemistry. An in-depth analysis of the literature into SET-LRP and ROP of ε-caprolactone was reported.

Chapter 2 described the synthetic strategy employed for the synthesis of a novel A_2B_2 heterofunctional initiator that incorporated an alkyl halogen moiety required for SET-LRP and a primary hydroxyl moiety required for ROP. Calix[4]arene, **1**, and 25,27-*bis*(prop-2-en-1-yloxy)calix[4]arene, **2**, were synthesised according to the literature.[1,2] A full characterisation was performed on both, as little characterisation had been reported previously. 25,27-*bis*(prop-2-en-1-yloxy)-26,28-*bis*(ethyleneacetate)-calix[4]arene, **3**, was successfully synthesised *via* a Williamson ether synthesis between **2** and methyl chloroacetate and was fully characterised. Compound **3** was used as the precursor for synthesising 25,27-*bis*(prop-2-en-1-yloxy)-26,28-*bis*(ethanolxy)calix[4]arene, **4**, *via* an ester reduction. 25,27-*bis*(prop-2-en-1-yloxy)-26,28-*bis*(ethoxyester-2-bromo-acetate)calix[4]arene, **5**, was successfully synthesised *via* an esterification reaction with 2-bromopropionyl bromide; and fully characterised. The final step of incorporating a primary hydroxyl moiety was achieved *via* a photo initiated thiol-ene click reaction with the allyl moieties of **5** and 2-mercaptoethanol. This resulted in the successful synthesis of 25,27-*bis*(3-(hydroxyethyl)thioether-propan-1-yloxy)-26,28-*bis*(ethoxyester-2-bromo-acetate)calix[4]arene, **6**; which was fully characterised.

Chapter 3 described how 25,27-*bis*(3-(hydroxyethyl)thioether-propan-1-yloxy)-26,28-*bis*(ethoxyester-2-bromo-acetate)calix[4]arene, **6**, was used to synthesise a novel 2-armed PCL polymer centred around a calixarene core, **calixarene-starPCL$_{100}$**, **7**. This could be further used for copper(0) mediated polymerisation due to the alkyl halide moieties remaining at the calixarene core. Compound **7** was fully characterised *via* 1D and 2D NMR spectroscopy techniques, SEC chromatography, DSC and TGA. The M_n determined *via* ^{1}H NMR spectroscopy was 2.2 x 10^4 g mol^{-1}, indicating the **DP** was 193, which is equivalent to ~97 units per arm, which agreed with the calculated theoretical M_n. SEC analysis showed an M_n of 2.2 x 10^4 g mol^{-1}, which agreed with that obtained *via* ^{1}H NMR spectroscopy. The Đ obtained from SEC analysis was 1.68 suggesting the lack of good control over the polymerisation and the **DP** of each arm. This could suggest that the rate of initiation of the system is slower than the rate of propagation. From the DSC analysis, showed a T_m and T_c of 51.53 ^{o}C and 32.67 ^{o}C, respectively, and a %crystallinity of 31.43%. The TGA trace showed two distinct thermal events corresponding to the two mechanisms in which PCL degrades. The percentage of PCL (ΔY_1) and calixarene core (ΔY_2) was calculated to be 94 % and 6%, respectively, which was in reasonable agreement with ^{1}H NMR spectroscopy. Compound **7** was used then as a macro-initiator for the SET-LRP of HEA leading to a amphiphilic A_2B_2 Miktoarm star polymer, **calicarene-A$_2$B$_2$starPCL$_{100}$PHEA$_{75}$, 8**, **calixarene-A$_2$B$_2$starPCL$_{100}$PHEA$_{100}$, 9** and **calixarene-A$_2$B$_2$StarPCL$_{100}$PHEA$_{270}$, 10**. Polymers **8**, **9** and **10** were fully characterised *via* 1D and 2D NMR spectroscopy techniques, SEC chromatography, DSC and TGA. Three *M*n were targeted, with the M_n determined for **8 - 10** *via* ^{1}H NMR spectroscopy calculated to be 1.8 x 10^4 g mol^{-1}, 2.2 x 10^4 g mol^{-1} and 6.1 x 10^4 g mol^{-1} corresponding to 75, 100 and 270 HEA units per arm respectively. The SEC gave a Đ ranging from 1.81 to 2.64, indicating a lack of control over the polymerisation, attributed to a greater rate of propagation than initiation, possibly as a result of trapped active sites. The PCL chains are flexible and could lead to the encapsulation of calixarene core active sites within the macroinitiator structure, thus reducing the rate of initiation. The DSC showed that as more PHEA was incorporated crystallinity was reduced, to a point where no exotherm was observed and the material was completely amorphous. The large amount of PHEA has interrupted the packing of the PCL chain to such an extent that there is no order to the packing of the material. The TGA for all three showed an increase in thermal

stability, which was attributed to hydrogen bonding between the PHEA hydroxyl moieties and the ester moieties of the PCL.

Chapter 4 described the synthetic strategy employed for the synthesis of a novel A_4B_4 heterofunctional initiator that incorporated an alkyl halogen moiety required for SET-LRP and a primary hydroxyl moiety required for ROP. 25,26,27,28-*tetrakis*(allyloxy)calix[4]arene, **11**, and 5,11,17,23-*tetrakis*(prop-2-en-1-yl)calix[4]arene, **12**, were synthesised according to the literature.[2] A full characterisation was performed on both as little characterisation had been reported previously. 5,11,17,23-*tetrakis*(prop-2-en-1-yl)-25,26,27,28-*tetrakis*(methylacetateoxy)calix[4]arene, **13**, was successfully synthesised *via* a Williamson ether synthesis between **12** and methyl chloroacetate and fully characterised. 4 was taken forward and used as the precursor for 5,11,17,23-*tetrakis*(prop-2-en-1-yl)-25,26,27,28-tetra*kis*(ethanoloxy)calix[4]arene, **14**, which was synthesised *via* an ester reduction. *5*,11,17,23-*tetrakis*(prop-2-en-1-yl)-25,26,27,28-*tetrakis*(ethoxyester-2-bromo-propanoate)calix[4]arene, **15**, was successfully synthesised *via* an esterification reaction with 2-bromopropionyl bromide, and fully characterised. It was noted that ~1 molecule of 2-bromopropanoic acid was trapped within the calixarene, which could not be removed. The final step of incorporating a primary hydroxyl moiety was achieved *via* a photo initiated thiol-ene click reaction with the allyl moieties and 2-mercaptoethanol. This resulted in the successful synthesis of 5,11,17,23-*tetrakis*((3-hydroxyethyl)thioether-propanyl*)*-25,26,27,28-*tetrakis*(ethoxyester-2-bromo-propanoate)calix[4]arene, **16**, which was fully characterised.

Chapter 5 described how 5,11,17,23-*tetrakis*((3-hydroxyethyl)thioether-propanyl)-25,26,27,28-*tetrakis*(ethoxyester-2-bromo-propanoate)calix[4]arene, **16**, was used to synthesise a novel 4-armed PCL star polymer centred around a calixarene core, **calixarene-starPCL$_{20}$**, **17**. Compound **17** could be further used for copper(0) mediated polymerisation due to the alkyl halide moieties remaining in the calixarene core. Compound **17** was fully characterised *via* 1D and 2D NMR spectroscopy techniques, SEC chromatography, DSC and TGA. The M_n determined *via* ^{1}H NMR

spectroscopy was 8.7 x 10^3 g mol^{-1}, indicating the **DP** was 76, which is equivalent to 19 units per arm, which agreed with the calculated theoretical M_n. SEC analysis gave a M_n of 4.4 x 10^3 g mol^{-1}, which is approximately half of that calculated *via* ^{1}H NMR spectroscopy. The large discrepancy is due to the hydrodynamic volume of star polymers being much less than their linear analogue, which is not taken into account when using SEC with a conventional calibration method. The Đ obtained from SEC analysis was 1.25, suggesting there was good control over the polymerisation. The DSC analysis showed a T_m and T_c of 50.27 ^oC and 24.40 ^oC, respectively, and a %crystallinity of 19.65%. The TGA trace showed two distinct thermal events corresponding to the two mechanisms in which PCL degrades. The percentage of PCL (ΔY_1) and calixarene core (ΔY_2) was calculated to be 85% and 15%, respectively, which was in agreement with ^{1}H NMR spectroscopy.

Compound **17** was used as a macro-initiator for the SET-LRP of HEA leading to a amphiphilic A_4B_4 Miktoarm star polymer, **calixarene-A_4B_4StarPCL$_{20}$PHEA$_{10}$**, **18**, **calixarene-A_4B_4starPCL$_{20}$PHEA$_{25}$**, **19**, and **calixarene-A_4B_4starPCL$_{20}$PHEA$_{48}$**, **20**. Polymers **18**, **19** and **20** were fully characterised *via* 1D and 2D NMR spectroscopy techniques, SEC chromatography, DSC and TGA. The M_n determined *via* ^{1}H NMR spectroscopy were 5.0 x 10^3 g mol^{-1}, 1.2 x 10^4 g mol^{-1} and 2.2 x 10^4 g mol^{-1} corresponding to 11, 25 and 48 HEA units per arm, respectively. The SEC gave Đ ranging from 1.23 to 1.45, indicating good control was maintained over the polymerisation. The DSC showed that as more PHEA was incorporated crystallinity was reduced, to a point where no exotherm was observed and the material was completely amorphous. The large amount of PHEA has interrupted the packing of the PCL chain to such an extent that there is no order to the packing of the material. The TGA for all three samples were similar and showed an increase in thermal stability, which was attributed to hydrogen bonding between the PHEA hydroxyl moieties and the ester moieties of the PCL.

Chapter 6 describes the self-assembly of A_2B_2 and A_4B_4 amphiphilic miktoarm star polymers **calixarene-A_2B_2starPCL$_{100}$PHEA$_m$**, **8**, **9** and **10**, where m = 75, 100 and 270, respectively and **calixarene-A_4B_4starPCL$_{20}$PHEA$_m$**, **18**, **19** and **20** where m =

10, 25 and 48, respectively). The TEM analysis on polymer systems **8 - 10** and **18 - 20**, revealed spherical micelles, with the size of the micelle decreasing as the proportion of hydrophilic PHEA increased. A greater proportion of hydrophilic polymer will increase the solubility of the polymer as well as lower the polymer diffusion coefficients. This would be expected to increase the particle size, but the fact that in increasing hydrophilic polymer length permits each polymer to sterically screen a larger area of the particle surface out ways the solubility and diffusion coefficients.

The CMC determinations for polymers **8 – 10** revealed that the length of the hydrophilic chain does not appear to have a significant effect on the CMC. This contradicts what has been previously reported. The lack of effect of hydrophilic chain length is attributed to the high dispersity of polymer chains. For polymers **18 – 20**, the CMC increases as the length of the hydrophilic polymer chain increases; this is in agreement with the literature. For both polymeric systems **8 - 10** and **18 - 20**, low CMC values were calculated, which indicates excellent thermodynamic stability of micelle produced. This work showed the synthesis of novel polymeric systems that have a potential in medical applications, with their ability to form micelles in the range of 5 to 110 nm and have the ability to encapsulate highly hydrophobic material, such as the fluorescent probe pyrene.

7.1. Future work

With the proof of concept that the calixarene based initiators are capable of producing novel polymeric materials, further materials centred around the calixarebe heterofunctional initiators could be developed. It would be interesting to synthesise some well-defined linear polymers using RAFT. The trithiocarbamate moiety could be cleaved to leave a thiol that could potentially be thiol-ene clicked onto the allyl moieties of the calixarene initiator using an “arm first” strategy. A second polymer could be grown from the alkyl bromide unit using copper(0) mediated polymerisation (Fig. 7.1).

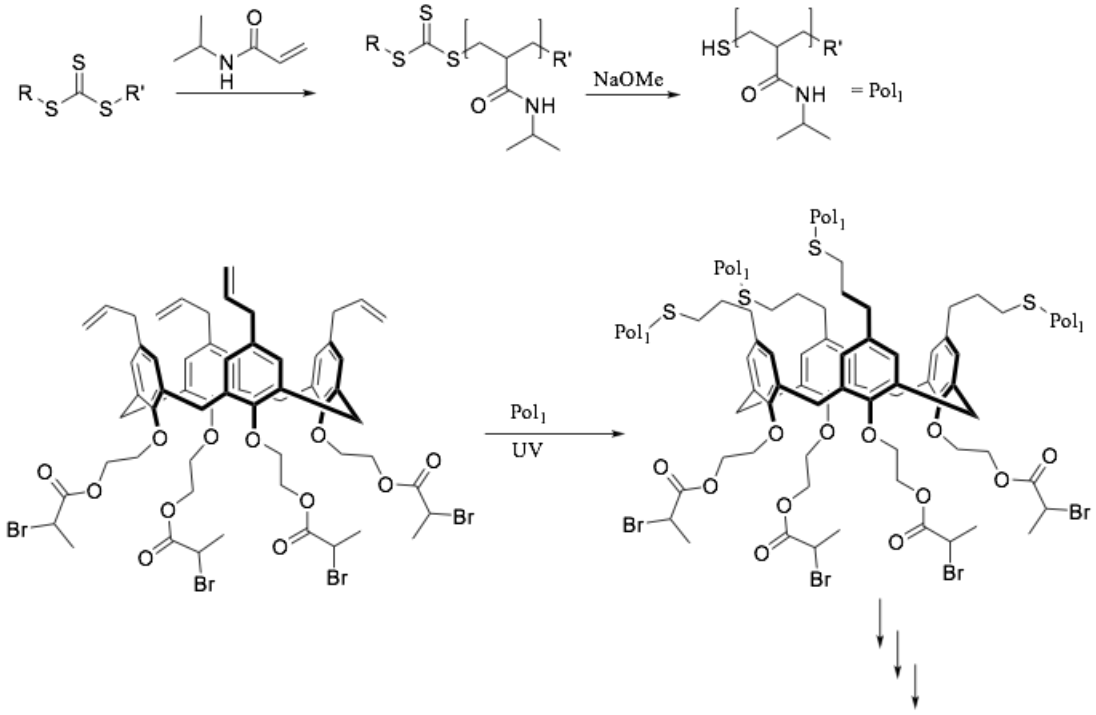

Figure 7.1. RAFT of NIPAM followed by cleavage of the trithiocarbamate moiety leading to thiol-ene click chemistry onto the calixarene based heterofunctional polymer initiator.

Although, it must be noted that attempts at thiol-ene clicking thiol-methyl-PEG onto the calixarene initiators described in Chapter 2 and 4 were unsuccessful, so development of the thiol-ene click chemistry of large polymers onto the allyls of the calixarene core would be required.

The synthesis of the calix[4]arene based heterofunctional initiators could be expanded to the calix[6]arene and calix[8]arene macrocycles, which would lead to A_6B_6 and A_8B_8 miktoarm star polymers, respectively.

7.2. References

(1) Parker, D. *Macrocycle Synthesis: A Practical Approach*; Oxford University Press: United States, 1996.
(2) Gutsche, C. D.; Levine, J. A.; Sujeeth, P. K. *J. Org. Chem.* **1985**, *50*, 5802.